APPLICATION OF THE BOUNDARY ELEMENT METHOD TO PARABOLIC TYPE EQUATIONS

A THESIS SUBMITTED TO
THE GRADUATE SCHOOL OF NATURAL AND APPLIED SCIENCES
OF
MIDDLE EAST TECHNICAL UNIVERSITY

BY

NURAY BOZKAYA

IN PARTIAL FULFILLMENT OF THE REQUIREMENTS
FOR
THE DEGREE OF DOCTOR OF PHILOSOPHY
IN
MATHEMATICS

JUNE 2010

Approval of the thesis:

APPLICATION OF THE BOUNDARY ELEMENT METHOD TO PARABOLIC TYPE EQUATIONS

submitted by **NURAY BOZKAYA** in partial fulfillment of the requirements for the degree of
Doctor of Philosophy in Mathematics Department, Middle East Technical University by,

Prof. Dr. Canan Özgen
Dean, Graduate School of **Natural and Applied Sciences** ______________

Prof. Dr. Zafer Nurlu
Head of Department, **Mathematics** ______________

Prof. Dr. Münevver Tezer-Sezgin
Supervisor, **Department of Mathematics, METU** ______________

Examining Committee Members:

Prof. Dr. Tanıl Ergenç
Mathematics Department, Atılım University ______________

Prof. Dr. Münevver Tezer-Sezgin
Mathematics Department, METU ______________

Assoc. Prof. Dr. İsmail Aydın
Civil Engineering, METU ______________

Assoc. Prof. Dr. Songül Kaya Merdan
Mathematics Department, METU ______________

Prof. Dr. Nevzat Güneri Gençer
Electrical and Electronics Engineering, METU ______________

Date: ______________

I hereby declare that all information in this document has been obtained and presented in accordance with academic rules and ethical conduct. I also declare that, as required by these rules and conduct, I have fully cited and referenced all material and results that are not original to this work.

Name, Last Name: NURAY BOZKAYA

Signature :

ABSTRACT

APPLICATION OF THE BOUNDARY ELEMENT METHOD TO PARABOLIC TYPE EQUATIONS

Bozkaya, Nuray
Ph.D., Department of Mathematics
Supervisor : Prof. Dr. Münevver Tezer-Sezgin

June 2010, 165 pages

In this thesis, the two-dimensional initial and boundary value problems governed by unsteady partial differential equations are solved by making use of boundary element techniques. The boundary element method (BEM) with time-dependent fundamental solution is presented as an efficient procedure for the solution of diffusion, wave and convection-diffusion equations. It interpenetrates the equations in such a way that the boundary solution is advanced to all time levels, simultaneously. The solution at a required interior point can then be obtained by using the computed boundary solution. Then, the coupled system of nonlinear reaction-diffusion equations and the magneto-hydrodynamic (MHD) flow equations in a duct are solved by using the time-domain BEM. The numerical approach is based on the iteration between the equations of the system. The advantage of time-domain BEM are still made use of utilizing large time increments. Mainly, MHD flow equations in a duct having variable wall conductivities are solved successfully for large values of Hartmann number. Variable conductivity on the walls produces coupled boundary conditions which causes difficulties in numerical treatment of the problem by the usual BEM. Thus, a new time-domain

BEM approach is derived in order to solve these equations as a whole despite the coupled boundary conditions, which is one of the main contributions of this thesis.

Further, the full MHD equations in stream function-vorticity-magnetic induction-current density form are solved. The dual reciprocity boundary element method (DRBEM), producing only boundary integrals, is used due to the nonlinear convection terms in the equations. In addition, the missing boundary conditions for vorticity and current density are derived with the help of coordinate functions in DRBEM. The resulting ordinary differential equations are discretized in time by using unconditionally stable Gear's scheme so that large time increments can be used. The Navier-Stokes equations are solved in a square cavity up to Reynolds number 2000. Then, the solution of full MHD flow in a lid-driven cavity and a backward facing step is obtained for different values of Reynolds, magnetic Reynolds and Hartmann numbers. The solution procedure is quite efficient to capture the well known characteristics of MHD flow.

Keywords: BEM, time-dependent fundamental solution, MHD, nonlinear reaction-diffusion, DRBEM

ÖZ

SINIR ELEMANLAR YÖNTEMİNİN PARABOLİK DENKLEMLERE UYGULANIŞI

Bozkaya, Nuray
Ph.D., Matematik Bölümü
Tez Yöneticisi : Prof. Dr. Münevver Tezer -Sezgin

Haziran 2010, 165 sayfa

Bu tezde, zaman bağımlı kısmi diferansiyel denklemlerle tanımlanmış iki-boyutlu başlangıç ve sınır değer problemleri, sınır elemanlar yöntemi ile çözülmüştür. Zamana bağlı temel çözümlü sınır elemanlar yöntemi, difüzyon, dalga ve konveksiyon-difüzyon denklemlerinin çözümü için etkin bir yöntem olarak sunulmuştur. Bu yöntem, denklemlerin bütününe nüfuz ederek, sınırdaki çözümü bütün zaman seviyelerine eş zamanlı olarak ilerletmektedir. Bundan sonra, içerideki bir noktada istenen çözüm, sınırda hesaplanmış değerler kullanılarak elde edilebilmektedir. Daha sonra, birbirine bağlı, doğrusal olmayan reaksiyon-difüzyon denklem sistemi ve kanal içerisinde tanımlı magnetohidrodinamik akış denklemleri zaman-bölge bağımlı sınır elemanlar yöntemi ile çözülmüştür. Bu sayısal yaklaşım yöntemi, denklemler arasındaki iterasyona dayanmaktadır. Zaman-bölge bağımlı sınır elemanlar yönteminin avantajları, bu uygulamalarda büyük zaman adımları kullanılabilmesi olarak görülmektedir. Genel olarak, duvar iletkenliği değişken olan kanal içerisinde tanımlı magnetohidrodinamik akış denklemleri büyük Hartmann sayıları için başarılı bir şekilde çözülmüştür. Duvarlardaki değişken iletkenliğin, birbirine bağlı sınır koşulları üretmesi, standart sınır

elemanlar yönteminin probleme uygulanışında zorluklara sebep olmaktadır. Bu nedenle, bu denklemleri bir bütün olarak çözecek yeni bir zaman-bölge bağımlı sınır elemanlar yönteminin türetilmiş olması, tezin temel katkılarından biridir.

Bununla birlikte, tüm magnetohidrodinamik denklemler, stream fonksiyonu-vortisity-manyetik indüksiyon-akım yoğunluğu formunda çözülmüştür. Denklemlerdeki doğrusal olmayan konveksiyon terimleri nedeniyle, sadece sınır integralleri üreten karşılıklı sınır elemanlar yöntemine ihtiyaç duyulmuştur. Buna ek olarak, vortisity ve akım yoğunluğu için bilinmeyen sınır koşulları, karşılıklı sınır elemanlar yöntemine ait olan koordinat fonksiyonları yardımıyla türetilmiştir. Elde edilen adi diferansiyel denklemler, zaman yönünde koşulsuz kararlı Gear yöntemiyle ayrıklaştırılmıştır. Böylece, büyük zaman adımları kullanılabilir. Kare kesitli kanal içerisindeki Navier-Stokes denklemleri Reynolds sayısı 2000'e kadar çözülmüştür. Ayrıca, gerek üst kapağı hareketli gerekse geriye doğru basamaklı kanallar içerisinde tanımlı tüm magnetohidrodinamik akış denklemlerinin çözümü farklı Reynolds, manyetik Reynolds ve Hartmann değerleri için elde edilmiştir. Bu çözüm yöntemi, magnetohidrodinamik akış problemlerinin tipik özelliklerini gösteren etkin bir yöntemdir.

Anahtar Kelimeler: Sınır elemanlar yöntemi, zaman bağımlı temel çözüm, magnetohidrodinamik, doğrusal olmayan reaksiyon-difüzyon, karşılıklı sınır elemanlar yöntemi

To my parents Şerife and Ahmet,
my sisters Nurhan and Canan,
my brothers Emre and Alparslan,
and my lovely niece Ayşe and nephew Mehmet

ACKNOWLEDGMENTS

It is a great pleasure having this opportunity to thank all the people who made this thesis possible.

First of all, I wish to express my heartfelt gratitude to my supervisor Münevver Tezer for her encouragement and support during this research period. She has been more than an academic supervisor to me all the time. I shall never forget her sincere friendship, helpful advices not only for academic research but also for social life. I have to say that without her supervision this thesis would not have been completed.

I would also like to offer many thanks to the members of my thesis defense committee, Assoc. Prof. Dr. İsmail Aydın, Assoc. Prof. Dr. Songül Kaya Merdan, Prof. Dr. Nevzat Güneri Gençer and Prof. Dr. Tanıl Ergenç for their guidance and understandings.

I am also very thankful for the financial support of The Scientific and Technical Research Council of Turkey (TÜBİTAK).

I deeply thank to my friend Hakan Tor for always caring about me, my laptop and my car. My hearty special thanks go to my lovely roommate Zeynep Kayar. The life would be really miserable and meaningless without her. I would like to acknowledge her contribution to translation of the abstract of this thesis with her nice Turkish.

The last but not the least, I want to show my deepest gratitude to my family, especially my mother and my sister Canan for their patience, encouragements and supports while this thesis is being written. They were always with me and never let me to give up during this period.

TABLE OF CONTENTS

LIST OF TABLES

TABLES

LIST OF FIGURES

FIGURES

LIST OF SYMBOLS

Ω	two-dimensional domain
Γ	boundary of Ω
u^*	fundamental Solution
q^*	normal derivative of fundamental solution
H	Heaviside function
$\boldsymbol{\xi}$	source point
$\boldsymbol{x}$	field point
θ_ξ	the internal angle at $\boldsymbol{\xi}$
$\boldsymbol{H}, \boldsymbol{G}$	BEM Matrices
$\delta(\boldsymbol{x})$	Kronecker delta function
$\Delta(\boldsymbol{x})$	Dirac delta function
r	radial distance
κ	diffusivity constant
c	wave velocity
Pe	Péclet number
N	number of boundary elements
IP	number of interior points
M	number of time blocks
ρ	density
Re	Reynolds number

p, p'	nondimensional and dimensional pressure
τ	maximum time level
Δt	time increment
$\mathbf{v}$	nondimensional velocity field
$\boldsymbol{n}$	outward normal of the boundary
Ha	Hartmann number
λ	conductivity parameter
ϕ_k	coordinate functions in DRBEM
$\boldsymbol{F}$	coordinate matrix in DRBEM
B_0	external imposed magnetic field
V_0	characteristic velocity (in Chapter 3)
L_0	characteristic length (in Chapter 3)
B_z	induced magnetic field (in Chapter 3)
V	nondimensional velocity (in Chapter 3)
B	nondimensional induced magnetic field (in Chapter 3)
ν	kinematic viscosity
U'	characteristic velocity
L'	characteristic length
B'	intensity of external magnetic field
ψ	stream-function
ω	vorticity
$\boldsymbol{E}$	electric field
$\boldsymbol{B}$	magnetic field
$\boldsymbol{b}$	nondimensional induced magnetic field
$\boldsymbol{H}_s$	magnetic field strength

$\boldsymbol{D}$ displacement

μ magnetic permeability

ϵ electric permittivity

$\boldsymbol{J}$ current density

j nondimensional current density

Re_m magnetic Reynolds number

σ electric conductivity

Al Alfvén number

S_t Stuart number

CHAPTER 1

INTRODUCTION

A great majority of problems arising in scientific and engineering applications can only be treated by numerical methods. A numerical approach basically contains two structures: modeling and solving with computational features. Actually, many situations in mathematical physics and mechanics can be mathematically modeled as boundary value problems. A boundary value problem in two or more dimensions is a partial differential equation or a set of partial differential equations (PDE) with additional restrictions called as boundary conditions. Excepting very simple cases, these equations are solved by using numerical techniques which connect them into matrix equations. Then, the need of the computational features involving geometry generation and meshing process, come into use for the solution of the resulting algebraic equations. The type of the numerical approximation used is very important since it affects the accuracy and economy of the solution. *Finite difference method* (FDM) and *finite element method* (FEM) are the most popular ones of the numerical techniques available in the literature. They are widely used to solve the potential problems of continuum mechanics, elastostatics, fluid dynamics and structural engineering problems. A common feature of these classical methods is that they are domain-type methods. This means that discretization of the whole domain is necessary when using these techniques. The type of domain discretization used in finite differences is a grid while is a series of elements in the case of finite element method.

Finite difference method approximates the derivatives in governing equations, by using equivalent difference equations (quotients). These quotients are obtained by using truncated Taylor polynomials. This way directly connects the governing equations to a set of algebraic equations since the difference equations provide a straightforward discretization over all the problem domain. Additionally, FDM is computationally economical due to the simplicity of matrix generation and manipulation. However, the application of the method may be very difficult especially when faced with more general geometries, like curved boundaries, and the boundary conditions involving derivative expressions. Recent developments in FDM for fluid dynamic problems can be found in [1, 2, 3].

For many years a huge number of finite element analysis is performed in engineering. Still, it preserves its popularity in the modeling of real world problems [4, 5, 6, 7] and give rise to the development of the structural and elastodynamic problems [8, 9]. The finite element method is a better choice for solving partial differential equations over complicated domains like cars and oil pipelines [10, 11, 12]. The technique is based on integral formulations generated by the *method of weighted residuals* (MWR) [13]. The domain of the solution is divided into a finite number of simple subdomains called as *finite elements*. Each element is studied in its own material and geometric properties independent to the others. They are joined together by nodes and inter-element boundaries. Thus, the solution over each individual elements are approximated in terms of polynomial functions (shape functions) and this leads influence (element) matrices for each individual elements. Then, the assembly procedure generates a global matrix describing the behavior of the body as a whole. Thus, the implementation of the general types of boundary conditions can then be handled by evaluating boundary integrals over each element giving more accurate approximation compared to FDM (which needs the use of a lower order Taylor expansion or external points for approximating the boundary conditions involving derivatives). Nevertheless, FEM has some drawbacks. Mainly, it requires domain discretization by using triangles or rectangles, and thus produces a large number of data which increases the computational cost and may cause to give inaccurate results. There are also difficulties when modeling infinite regions and moving boundary problems.

Thus, the *boundary element method* (BEM) [14], has emerged as a versatile and powerful tool for the solution of engineering problems as an alternative to the more widely used FDM and FEM. Integral equations can be seen as the starting point of the boundary element method as in FEM. Somigliana was the first person who established the integral equations for the potential problems in 1885. Later many others studied with integral equations of potential problems and theory of elasticity [15, 16]. Among these works Jaswon and Symm [15], performed direct boundary integral equation methods by discretizing the boundary into small segments (elements) for the solution of potential problems in 1963. They also developed a more general numerical technique for the solution of the Cauchy boundary value problems subject to mixed type boundary conditions. Then, based on the approach used in the works of Jaswon and Symm, Rizzo and Cruse [16] presented a boundary integral formulation for the solution of transient elastodynamic problems by using Laplace transform. A very important contribution for the development of the boundary element method is introduced by Lachat and Watson [17]. In their work, they give the boundary integral formulation for three dimensional elastostatic problems by using subregions involving quadrilateral and triangular elements. They also describe the algorithms for the computation of the singular integrals appearing in the boundary integral equations. Soon after the first book on the boundary element method appeared in 1978 by Brebbia [14]. After this book the method became very popular and many other significant applications for a wide range of engineering problems are performed. The publications by Banerjee and Butterfield [18], Brebbia et. al. [13], Banerjee [19], Brebbia and Dominguez [20], Kythe [21], Pozrikidis [22] and Gaul et. al. [23] can be counted as the most visible ones among these works. Application of the boundary element method to the boundary value problems generally consists of converting the original differential equation into an equivalent integral equation on the boundary, and to solve this integral equation using discretization procedures. In many cases this equation contains only boundary integrals and only boundary needs to be discretized. Therefore, after the discretization process and substitution of the boundary conditions a system of algebraic equations is obtained. Solution of this system generates all unknowns along the boundary. Thus, solution at internal nodes if needed is obtained by simple matrix operations, and making use of just the known boundary values.

When compared with FEM and FDM, the boundary element method has many attractions. The main comparative advantage of the boundary element method is its boundary-only discretization nature. Since only the boundary is discretized, the dimensionality of the problem is reduced by one, and hence the input data is reduced considerably and data preparation becomes quite fast. The resulting matrix equations to be solved are much smaller than those in domain methods which minimizes computational cost. Moreover, the required values at any point in the domain can be obtained directly by using computed boundary values. The final matrix is fully populated with lots of scattered zeros and shows no special form, and thus the system must be solved as a whole for obtaining the solution. This is the main disadvantage of the BEM which can not produce sparse systems as in FEM. However, the solution is much accurate even by using constant elements since the fundamental solution already satisfies the differential equation exactly and only the boundary conditions are approximated. Additionally, the method is quite ideal for problems with infinite domains due to its boundary-only nature [24, 25, 26]. For anisotropic medium and nonhomogeneous diffusivity problems the BEM application is difficult due to the absence of corresponding fundamental solutions.

The BEM is originally developed by method of weighted residuals which is a general method for most of the numerical techniques. Basically, in MWR, the unknown solution of the governing equation is expanded in a set of approximating functions which are specified in order to give the best solution to the differential equation. Since the solution is replaced with approximating functions, errors (residuals) occur. Then, these residuals are minimized by orthogonalizing them using weighting functions. These weighting functions can be chosen in many ways and each choice corresponds to a different feature of the technique. For example in collocation method the weighting functions are chosen to be the displaced Dirac delta function, while they are chosen to be the trial functions in Galerkin method [22]. Particularly, the boundary element method uses the fundamental solution of the governing equation as the weighting functions. Then, making use of Green's identities a boundary integral model can be derived and a discretization process results in matrix equations. Thus, the fundamental solution plays a very important role in the BEM applications. Especially, when dealing with time-dependent problems, a direct application of the boundary element method can only be performed by using corresponding time-dependent fundamental solution of the governing equation. This produces a time-domain BEM formulation which usually does not need another time integration scheme, thus allows to use large time increments. However, the main drawback of BEM and time-domain BEM occurs in problems with body forces, time dependent effects or nonlinearities. In these cases, the domain integrals appearing in the BEM formulations are usually computed by cell integrations. This is also very efficient but destroys the boundary-only nature of the boundary element techniques. Thus, many different approaches have been developed to deal with these domain integrals. Analytical integration, the use of Fourier expansions, Galerkin vector technique, the multiple reciprocity and the dual reciprocity methods are the most important ones [24]. In this thesis, the dual reciprocity boundary element method (DRBEM) is studied in Chapter 4 as an alternative to the time-domain BEM (Chapter 2 and 3).

1.1 Fundamental Solutions

A basic feature of all boundary element methods is the use of fundamental solutions. The invention of fundamental solutions for differential operators dates back to 1950s. Laurent Scwartz [27], who is the creator of the distribution theory, was the first to define a fundamental solution. A fundamental solution is an analytical free space solution of the governing differential equation for a point source. Now, let $\mathcal{L}$ be a differential operator for any distribution u leading the differential equation

$$\mathcal{L} u = 0. \tag{1.1}$$

Then, a fundamental solution u^* is described mathematically by

$$\mathcal{L} u^* = -\Delta(\boldsymbol{x} - \boldsymbol{\xi}) \tag{1.2}$$

which is an exact solution of (1.1) in Dirac delta distribution from the load point $\boldsymbol{\xi}$ to field point $\boldsymbol{x}$. Dirac delta is a generalized function that has zero value everywhere except $\boldsymbol{x} = \boldsymbol{\xi}$ where the total integral value in the latter case becomes 1, i.e.,

$$\Delta(\boldsymbol{x} - \boldsymbol{\xi}) = \begin{cases} +\infty, & \boldsymbol{x} = \boldsymbol{\xi} \\ 0, & \boldsymbol{x} \neq \boldsymbol{\xi}, \end{cases} \tag{1.3}$$

$$\int_{-\infty}^{\infty} \Delta(\boldsymbol{x} - \boldsymbol{\xi}) d\boldsymbol{x} = 1\,, \tag{1.4}$$

and for all continuous compactly supported functions f, the Dirac delta has the property below

$$\int_{-\infty}^{\infty} f(\boldsymbol{x})\, \Delta(\boldsymbol{x} - \boldsymbol{\xi}) d\boldsymbol{x} = f(\boldsymbol{\xi})\,. \tag{1.5}$$

The fundamental solutions coincide with Green functions which are introduced by George Green in 1818. When the boundary conditions for a boundary value problem are also approximated by an appropriate fundamental solution, as well as the governing equation itself, the fundamental solution becomes a Green's function. Thus, the approximate solution of a PDE is weighted by its fundamental solution and then, the resulting domain integrals are transformed into boundary integrals by using Green's identities.

1.1.1 Time-dependent fundamental solutions

The fundamental solution of Laplace equation is widely used in BEM applications. It is quite suitable for steady-state potential problems governed by Laplace or Poisson equations. But when the boundary value problem is defined by PDEs including time derivatives, the need of a time integration scheme takes into place. In this thesis, we mainly deal with the boundary element method solution of unsteady partial differential equations. As an alternative to the standard BEM, we aim to approximate the solution of the problem directly by using the corresponding time-dependent fundamental solutions as weighting functions. This way one can take the advantage of treating the time-dependent partial differential equations as a whole. Thus, there is no need to use a time integration scheme for BEM discretized equations and this procedure is called as *time-domain boundary element method*. Next two chapters (Chapter 2 and 3) involve the time-domain BEM solutions of the boundary value problems governed by time-dependent partial differential equations occurring in many branches of science and engineering. The important representative transient problems are the well known diffusion, scalar wave and convection-diffusion equations supplied by proper initial and boundary conditions.

Most of the numerical schemes based on the BEM treat the time derivative term either by using Laplace transform or finite difference method. The dual reciprocity boundary element method also requires a time integration scheme to advance the solution in time direction. The Laplace transform method needs the inverse transform to recover the solution. The finite difference scheme requires very small time increments due to the stability problems for solving the resulting system of ordinary differential equations which is computationally expensive. In 1970 Rizzo and Shippy [28] proposed a direct boundary element method formulation using Laplace transform for the solution of heat conduction problems for the first time. By making use of inverse Laplace transform they are able to remove the time dependence of the problem temporarily and thus an elliptic PDE is solved rather than the original parabolic form of the heat equation. Singh and Kalra [29] presented a comprehensive comparative study on the time integrators in the context of the DRBEM formulation of transient diffusion problems. In their work, a one step least squares algorithm was concluded the most accurate and efficient technique among all methods assessed. The DRBEM in space and the differential quadrature method (DQM) in time combination is applied to diffusion and elastodynamic problems by Tanaka and Chen [30, 31]. The DQM time integration scheme in their study, although it is known as an unconditionally stable method, results in Lyapunov matrix system which is solved by the special Bartel-Stewart algorithm. This needs large memory space and enormous computational time.

The time-domain BEM based numerical algorithms are presented for the solutions of several physical problems, involving heat conduction problems, elastodynamic problems, wave propagation problems, and the problems described by convection-diffusion type equations. Chang et. al. [32] were the first to give a direct method using the time-dependent fundamental solutions for the solution of heat conduction in isotropic and anisotropic media. For the discretization of the resulting boundary integral equation they used piecewise constant elements in space and time direction. A similar approach featured with analytical rather than numerical aspects was introduced by Shaw [33] for the solution of three-dimensional diffusion problems. All previously studied numerical schemes for heat conduction are collected in the book of Brebbia et. al. [13], particularly, the numerical implementation of the BEM with time-dependent fundamental solution is given in detailed form in this book. Recently, Qiao [34] performs a fully transient mold cooling analysis formulation using the time-domain BEM for heat conduction equation.

Carslaw and Jaeger provide foundation of the time-dependent fundamental solution of homogeneous convection-diffusion type equations [35]. The time-domain BEM applications of the time-dependent convection-diffusion problems are due to Grigoriev and Dargush [36, 37, 38]. In these studies, they have used time-dependent fundamental solution together with higher order boundary elements. Linear, quadratic and quartic time interpolation functions are introduced for exact integrations which make the computations quite complex. Although, the efficiency of their BEM solutions increases with the increase of the Péclet number of the flow, they need to use small time steps. DeSilva et. al. [39] have been attempted to develop a BEM formulation for transient conduction-convection problems involving spatially varying convective velocities. The fundamental solution corresponding to a transient conduction-convective problem with a constant velocity is utilized. The variable part of the convective velocity goes to the domain integral in their formulation. Currently, the time-domain BEM is applied successfully to the convection-diffusion type equations by Bozkaya and Tezer-Sezgin [40].

For the scalar wave equation the mathematical and numerical handling is more difficult then in the diffusion-type equations. One reason for this is the singularity associated with the delay of wave propagation. The DRBEM analysis of elastodynamic problems (containing first and second order time derivatives) are due to Nardini and Brebbia [41], Mansur and Brebbia [42], and Loeffler and Mansur [43]. Wave propagation analysis in time-domain requires careful modeling and representation of physical phenomenon. The first time-domain BEM applications are produced for acoustics by Friedman and Shaw [44] in 1962. Carrer and Mansur [45] have been used the concept of finite part of an integral to obtain space and time derivatives in time-domain BEM modeling of the scalar wave equation. Contributions due to the initial conditions have also been included. Benmansour, Ouazar and Wrobel [46] presented a wave equation formulation for one-dimensional free surface open channel flow. The numerical solution of the wave continuity equation was carried out by the BEM using a one-dimensional time-dependent fundamental solution. Mansur, Carrer and Siqueira [47] extended the traditional BEM formulation for time-domain scalar wave propagation analysis in which linear time variations for both the potential and flux (traction in elastodynamics) were considered. Linear boundary elements are taken in the boundary discretization and the domain discretization employs triangular linear cells. Telles et. al. [48] give a time-domain BEM solution for transient dynamic elasto-plastic problems. In their work linear time variation is assumed for the displacements and constant variation is assumed for the tractions. Carrer and Mansur [49] described a time-domain two-dimensional BEM formulation, which employs the fundamental solution corresponding to a time constant concentrated source. The numerical solution procedure employed linear boundary elements and linear triangular cells, respectively, for the boundary and domain discretization. In [50], scalar wave equation is solved by making use of BEM with time-dependent fundamental solution. Rizos and Zhou [51] present a direct time-domain BEM for the solution of the 3D wave propagation problems. A higher order B-spline time-dependent fundamental solution is derived in their solution procedure.

1.1.2 Time marching schemes

In this thesis, referring all previously studied numerical schemes, we first introduce the time-domain BEM solutions of the boundary value problems governed by typical PDEs as diffusion, convection-diffusion and scalar wave equations, subject to boundary conditions of Dirichlet or Neumann type. First, the weighted residual statement is obtained by weighting the governing equation and boundary conditions using the corresponding time-dependent fundamental solution. Thus, the resulting integral equation involves time integrals as well as boundary integrals due to time-dependence. Since the time variations of the solution and its normal derivative are not known priori, a time stepping technique, unlike the technique used in finite difference, is required for the numerical solution of the problem. Two different time-marching schemes [13] can be employed in this time-domain BEM for obtaining numerical solution.

- **Scheme 1**: This scheme treats each time block as a new problem. Soon after obtaining the boundary solutions, at the end of each step the interior solutions are computed wherever needed, and then they are all used to be initial values for the next step.

- **Scheme 2**: In this scheme, the time integration process always restarts from the initial time $t = t_0$, and so despite the increasing number of intermediate steps in the time progresses, the solution at interior nodes needs not to be recomputed.

Both of the schemes are used according to the problem nature in Chapter 2 and 3. In Chapter 2 we make use of the time-domain BEM with scheme 2. As it is explained in detailed form, this way provides all the solution values at all time steps simultaneously, without the need of an iterative process. Although a large system of matrix equations is obtained contrary to standard BEM equations, this system is solved once and results are obtained on all boundary nodes and at any time step at once. This is the main advantage of the method and more suitable for the problems defined with a PDE rather than a set of PDEs. Therefore, in Chapter 3 the time-domain BEM solution is given for system of partial differential equations and by using scheme 1 since it already provides the transient solution values at the end of each step which can be used to construct a time stepping between the governing equations. Both schemes allow using large time steps since the fundamental solution itself is time-dependent.

1.2 Time-Domain BEM Solution of Nonlinear Reaction-Diffusion Equations and MHD Flow Equations

The common nonlinearities arising in diffusion problems are [52] due to,

- Nonlinear material (i.e. diffusivity coefficient dependent on the potential or its gradients)

- Nonlinear boundary conditions (e.g. due to heat radiation)

- Nonlinear sources inside the domain

- Moving interface problems (e.g. due to phase change).

The present work in Chapter 3 addresses nonlinearities of the third type. More specifically, we treat the system of nonlinear reaction-diffusion equations by using time-domain BEM. Several numerical procedures can be found in the literature for nonlinear reaction-diffusion equations and systems. Adomian [53] derives a series solution for the ordinary and partial differential equations by using Adomian decomposition method valid with small convergence regions. Later, Wazwaz [54, 55] develops modified forms of the Adomian decomposition method to improve the accuracy and accelerate the convergence of the method in order to solve the reaction-diffusion Brusselator model. Finite difference solutions for the system of nonlinear reaction-diffusion equations are also available in the papers of Twizell et. al. [56] and Liao et. al. [57], which require very small time increments. A DRBEM solution with a finite difference time integration scheme is presented by Ang [58]. Although DRBEM uses a rather simple fundamental solution of the governing equation (e.g. Laplace equation) the resulting system of ordinary differential equations are solved by using proper time integration schemes such as FDM and Runge Kutta method. Meral and Tezer-Sezgin [59] solve the nonlinear reaction-diffusion Brusselator system by using differential quadrature method (DQM). In their study also, they use FDM to discretize the time derivative, and a relaxation procedure to avoid the stability problems.

First the time-domain BEM is presented for solving the nonlinear reaction-diffusion equation by using the corresponding time-dependent fundamental solution of the diffusion equation. Then, it is extended to the nonlinear system of reaction-diffusion equations including Brusselator system as a new application. The Brusselator system is a coupled system of time-dependent nonlinear reaction-diffusion equations, and it arises in the modeling of certain chemical reaction-diffusion processes (involving a pair of variable intermediates with input and output chemicals). The chemical system leading the Brusselator system contains only two dependent variables because of the limit-cycle oscillations [56], thus we are able to use of two-dimensional mathematical systems. In addition, an application is given for the solution of the system of nonlinear reaction-diffusion equations defined in a region with curved boundary, which presents the applicability of the method for more complex problems even in more general geometries.

1.2.1 Magnetohydrodynamics

Actually, the main aim of the thesis is to solve the fluid dynamic problems, particularly magnetohydrodynamics (MHD). The MHD flow problem in channels is concerned in several engineering applications such as the motion of liquid metals of nuclear reactors, MHD generators and conducting plasma in physics. The full MHD equations are governed by Maxwell's equations and incompressible Navier-Stokes equations coupled through Ohm's law [60, 61]. It is quite difficult to get analytical solution of the problem except for some special cases. The complexity mainly arises due to the nonlinearities in the equations and the additional terms with the existence of Lorentz force. The divergence-free conditions for both the velocity and the magnetic field must also be satisfied. Therefore, developing efficient numerical methods and algorithms becomes more significant.

There are some applications for fully developed MHD flow problems in channels or ducts when the equations are restricted to a plane which is perpendicular to the direction of the fluid motion. The external magnetic field is directed along x or $y-$axis of this cross-section plane. It is assumed that the velocity and the induced magnetic field have only one component along the axis of the duct ($z-$direction). All physical quantities (except the pressure) are independent of z, and there is no net flow of current in the $z-$direction. The nondimensional form of the governing equations (of MHD duct flow) represents a coupled system of equations in terms of velocity and induced magnetic field. For the solution of steady MHD duct flow problem Zhang et. al. [62] develop a new element free Galerkin method in order to investigate the effects of the Lorentz force. A stabilized FEM solution of the steady MHD flow problem is given by Neslitürk and Tezer-Sezgin [63] for high values of Hartmann number. Tezer-Sezgin and Aydın [64] propose a boundary element method (BEM) for the solution of the steady MHD flow equations which are transformed to inhomogeneous convection-diffusion type equations. An important contribution for the solution of laminar, steady and fully developed MHD flow equations is introduced by Bozkaya [65]. The fundamental solution for this coupled MHD flow equations is derived which allows the direct implementation of the existing BEM methods.

The numerical solutions of time-dependent MHD flow equations have been given by

Singh and Lal [66] in two dimensions and by Salah et. al.[67] in three dimensions using finite element method. The time derivative was evaluated by a finite difference-like expression. Seungsoo and Dulikravich [68] proposed a FDM scheme for three dimensional unsteady MHD flow together with temperature field. They have used explicit Runge-Kutta method for step-by-step computations in time. Sheu and Lin [69] presented convection-diffusion-reaction model for solving unsteady MHD flow applying a FDM on non-staggered grids with a transport scheme in each ADI (alternating direction implicit) predictor-corrector spatial sweep. The solution algorithm in each of these unsteady MHD flow studies is based on explicit time-stepping schemes starting with the given initial conditions. Thus, the time increment must be taken very small to deal with the stability problems, and therefore they are computationally expensive. A numerical scheme which is a combination of the dual reciprocity boundary element method in space and the differential quadrature method (DQM) in time has been proposed by Bozkaya and Tezer-Sezgin [70] for solving unsteady MHD flow problem in a rectangular duct with insulating walls. The solution procedure can be used with large time increments for obtaining the solution directly at the required time level. Computations have been carried out for moderate values of Hartmann number.

The two-dimensional transient MHD flows in channels (ducts) are governed by coupled convection-diffusion type equations for the velocity and the induced magnetic field. When the magnetic field is zero on the walls (insulated walls) the equations and the boundary conditions can be decoupled but for the arbitrary wall conductivity case the decoupling of the equations makes the boundary conditions coupled. Thus, it is quite difficult to treat the equations with BEM for arbitrary wall conductivity. However, a time-domain BEM procedure is developed for the first time in order to solve these unsteady MHD equations as a whole with coupled boundary conditions. This is one of the main contributions presented in this thesis. The details of the numerical implementation of the technique is discussed in the last section of Chapter 3.

1.3 DRBEM Coupled with an Implicit Backward Time Integration Scheme

In spite of its success and its high (second order) accuracy, the BEM is not without its drawbacks. It always requires the corresponding fundamental solution of the governing equations. Usually the initial conditions are taken into account through a domain integration and nonlinear terms can not be inserted to fundamental solutions, which removes the boundary-only character of the technique. To overcome this a time-stepping algorithm should be introduced, where previous solutions are advanced in time through the boundary integrals. When dealing with BEM for the general transport equation, structured by weighting with the fundamental solution of Laplace equation, domain integrals appear at least from the transient, convective and source terms. The use of time-dependent fundamental solutions also generates domain integrals in integral formulations due to the initial conditions and body force. Thus, the dual reciprocity boundary element method (DRBEM) is introduced by Partridge et. al. [24] as an alternative to the BEM procedures in order to eliminate domain integrals. DRBEM represents one of the possibilities for transforming the resulting domain integrals into finite series of boundary integrals. The key point here lies in making use of some approximating functions for both sides of the equations, and thus by using Green's identities all the domain integrals can be transformed into boundary integrals. This technique was first applied to linear diffusion problems by Wrobel et. al. [71]. Nowadays, the application of the DRBEM to various transient problems has been a subject of growing interest. The boundary integral equations for the DRBEM are dependent only on geometrical data and free of interior cells. The resulting DRBEM formulation of initial and boundary value problems (IBVP) is therefore expressed in the standard form of ordinary differential equations of initial value problems which can easily be solved by the usual time integrators [31].

In this thesis, as a further application of the MHD flow in a duct described in Chapter 3, we solve full MHD equations iteratively by using DRBEM. The full MHD equations describe the motion of velocity and induced magnetic field in the direction of the axis of duct but with variations in both x- and y-axis. The current density which is the curl of induced magnetic field has only one component in the direction of the axis of the duct. Various numerical models are developed to solve the incompressible MHD equations in both two- and three-dimensions. Three-dimensional numerical calculations on liquid-metal MHD flow through a rectangular channel in the inlet region, have been performed by Kumamaru et. al. [72] using the finite difference method (FDM). Salah et. al. [67] develope a finite element method for the solution of three-dimensional MHD equations. They give an efficient solution algorithm, valid for both high and low magnetic Reynolds numbers, with various types of formulations such as the Helmholtz, the vector potential and the conservative formulation. Kang and Keyes [73] give a FEM solution for the two-dimensional incompressible MHD flow using a hybrid stream function approach and they prefer an implicit time difference scheme with Newton's method in order to solve the resulting nonlinear equations. Navarro et. al. [74] deal with a stream function-vorticity formulation and present an extension of the generalized Peaceman and Rachford alternating-direction implicit scheme (ADI) in comparison with ADI scheme for the solution of the MHD flow equations at low magnetic Reynolds numbers. The magnetic Reynolds number Re_m is the ratio of the induced magnetic field to the applied magnetic field. Thus, for small values of Re_m, the applied magnetic field dominates the induced magnetic field. Lee and Choi [75] use a direct simulation technique by neglecting the induced magnetic field i.e. at low magnetic Reynolds number in order to examine the effects of Lorentz force for turbulent flows. Sekhar et. al. [76] examine the effect of magnetic Reynolds number on the two-dimensional steady MHD flow around a cylinder by solving the MHD equations using FDM. Kumar and Rajathy [77] solve the steady MHD flow equations for an incompressible fluid past a circular cylinder with and aligned magnetic field for small magnetic Reynolds number and Reynolds number up to 100. They use multigrid method with defect correction technique and the effect of applied magnetic field is discussed. The stability and long-term dissipative properties of a general class of time-stepping algorithms for the transient incompressible MHD equations are analyzed by Armero and Simo [78]. The applications are for the plane Hartmann flow and MHD flow past a circular cylinder.

In the last chapter of this thesis, two applications of fluid dynamics are taken into consideration. Mainly, the full MHD equations which are originated by Navier-Stokes equations and Maxwell equations are solved. A stream function-vorticity-magnetic induction-current density formulation is considered for full MHD equations in two dimensions. As a preliminary work we first deal with the solution of Navier-Stokes equations in stream function-vorticity form. The solution procedure is based on the DRBEM in spatial domain and an unconditionally stable implicit backward difference scheme in time domain. The main idea behind the DRBEM is to establish a boundary integral only formulation of the given problem by using the fundamental solution of the Laplace equation. Then, all the unknowns either on the boundary or inside the domain are able to be computed simultaneously. DRBEM has many advantages for the solution of the aforementioned coupled equations involving poisson and convection diffusion type equations. The main advantage here arises in the derivation of the boundary conditions for the vorticity and current density which are not available in the problem definition. This is because the derivative expressions can be approximated by the radial basis functions. The stream function and magnetic induction equations are of poisson type so that we take the advantage of the usage of DRBEM which is very suitable and accurate on Laplace and Poisson type equations. Besides, although the assembly procedure of DRBEM produces a larger system of matrix equations to be solved, the solution can be obtained at all the boundary and internal nodes at once.

Since DRBEM produces a system of ordinary differential equations for transient problems, a time discretization method is required. Thus, we make use of an implicit backward difference scheme known as Gear scheme [79] or upwind scheme for the time discretization. Gear scheme is unconditionally stable and has second order accuracy. Thus, it still allows to use large time increments when compared with usual finite differences. The DRBEM solution of full MHD equations iteratively constitutes another original part of the thesis.

1.4 Scope of the Thesis

The main aim of the thesis is to solve fluid dynamic problems and particularly magnetohydrodynamic problems by using boundary element method. First, the time-domain boundary element method is presented with applications to the basic equations: diffusion, convection-diffusion and scalar wave equations. The reason of giving the applications on these very well known transient problems is to prove the validity of the method, and thus to give the applications to the system of reaction-diffusion and MHD flow equations later on. As an advantage of the method, the equations can be treated as a whole including the time derivative terms. Thus, the stability problems are eliminated and large time increments can be used. Additionally, the boundary solution can be obtained at all the transient levels and at steady-state at one stroke. Thus, the time-domain BEM is successfully applied to the system of nonlinear reaction-diffusion equations and MHD duct flow equations as new applications. Then, the scope is enlarged to the solution of full magnetohydrodynamic flow equations by making use of the dual reciprocity boundary element method. The basic idea of this approach is to use the fundamental solution of Laplace equation, which is rather simple, and treat all the nonlinear convection terms, the time derivatives as nonhomogeneity. Generally, a stream function-vorticity-magnetic induction-current density form is taken to govern the full MHD equations. The nonlinear convective terms appearing in the vorticity and current density equations, and also the missing boundary conditions for vorticity and current density make problem difficult to solve with usual boundary element techniques. These unknown boundary conditions for vorticity and current density can also be computed by making use of the coordinate matrix of DRBEM which can be counted as one of the main advantages of the technique. Thus, a DRBEM approach which results with integrals defined only on the boundary, coupled with an implicit time integration scheme is presented to solve these full MHD equations as an original contribution in this thesis.

1.5 Plan of the Thesis

Chapter 2 presents an introduction to the boundary element method. The application of the technique is first explained for the steady potential problems governed by the Laplace equation with Dirichlet or Neumann type boundary conditions. The equation is directly treated by using the fundamental solution of the Laplace equation and the boundary is discretized by using constant boundary elements which is simple and practical for computational purpose. Mainly, it is concentrated on the BEM solutions of basic transient boundary value problems governed by some important partial differential equations of diffusion, scalar wave and convection-diffusion types arising in many engineering applications. Unlike the standard BEM, the corresponding time-dependent fundamental solutions are utilized as weighting functions which enable one to treat the unsteady equations as a whole. Thus, introducing the corresponding time-dependent fundamental solutions, we give the details of the time-domain BEM formulations for each problem above. Then, the validity of the technique is shown on some test problems in comparison with the existing analytical solutions. The boundary integral equations presented for the transient PDEs above hold for any physical field such as Navier-Stokes equations and Magnetohydrodynamics which are governed by the same type of partial differential equations. Thus, Chapter 2 constitutes a basis for Chapter 3.

Chapter 3 emphasizes on the solution of magnetohydrodynamic flow equations. We first introduce the solution of nonlinear reaction-diffusion equations. In this type of equations, the nonlinearity locates at the source term as nonhomogeneity. A time-domain BEM is applied to the governing equations and the nonlinearity is overcome by constructing a time-stepping scheme between the equations and then using the obtained solutions as initials for the next time step. Thus, the nonlinearities appear as constant known vectors in matrix equations in the iterative procedure. Numerical examples verify the accuracy and adaptability of the method to the system of equations even governed by nonlinear partial differential equations, and also with more general boundary conditions. In the second part of Chapter 3, mainly the time-domain BEM solution of unsteady magnetohydrodynamic duct flow equations is dealt. The difficulty arises when the fluid flows in a duct with arbitrary wall conductivities. Because of the mixed type boundary conditions of magnetic field, the equations are decoupled but the boundary conditions stay coupled. This is undesirable since BEM requires different boundary conditions defined on different parts of boundary. Therefore, a new approach based on time-domain BEM is derived for the solution of this type of unsteady duct flow problem. This new approach produces a larger system of matrix equations of which unknown vector includes all the required boundary values of unknown solution and its normal derivative values.

In Chapter 4, the Navier-Stokes equations in stream-function vorticity form and the full MHD equations in terms of stream function-vorticity-magnetic induction-current density are solved by using DRBEM due to the nonlinear convection terms. Especially, in the second part of this chapter the solution of full MHD flow is a new application. First, the implementation of DRBEM is introduced for poisson type equations which is the simplest case. Then, the derivation of the matrix-vector equations for the unsteady vorticity transport equation is given in detailed form. The time marching scheme is also introduced on this equation which is of convection-diffusion type. Then, the missing boundary conditions are derived by using coordinate matrix of DRBEM. Similar procedure is followed in the solution of full MHD equations including poisson and convection-diffusion type equations. The validity of the method is emphasized on the benchmark lid-driven cavity problem. Then, a further and a new application is given for the backward facing step flow problem governed by incompressible, laminar, viscous magnetohydrodynamic flow equations.

CHAPTER 2

BOUNDARY ELEMENT METHOD

In this chapter we first deal with the basic concepts of the boundary element method, [14] and give, in general, the boundary element formulation of the Laplace equation as a model problem. We present the derivation of the boundary only integral equation equivalent to the given differential equation. The boundary element formulation assumes that, the boundary of the region under consideration is divided into elements (constant, linear, quadratic or cubic), and the differential equation defined in the region is transformed to an integral equation defined over the boundary of the domain by using the fundamental solution as a weight function together with application of the Divergence theorem [80]. Finally, imposing the available boundary conditions results in an algebraic system of equations. The approximate solution can be expressed in terms of functions defined over the individual elements on the boundary, and any information required inside the region can be extracted from the solution obtained on the boundary. When the problem is in transient nature a time integration scheme has to be enrolled either at the beginning of the solution procedure or to the resulting system of ordinary differential equations in time. Thus, a time-dependent fundamental solution of the differential equation in consideration will be a better choice for the application of boundary element method. In Section 2.3, we introduce time-dependent fundamental solutions of the diffusion, convection-diffusion and scalar wave equations. In Sections 2.4-2.6, the BEM treatments are given in detailed forms for each type of equations, and it will be noted as a main advantage of the method that the use of time-dependent fundamental solution eliminates the need of another time integration scheme and it enables using large time increments.

2.1 Boundary Element Method Formulation of Laplace Equation

The basic idea of BEM is transforming a differential equation defined in a region Ω to an integral equation defined on the surface Γ of the region Ω (Figure 2.1). In order to concentrate on the basic features of the boundary element formulation, we first deal with a simple potential problem defined with Laplace equation in two-dimensions. The steady-state heat conduction in an isotropic medium without heat sources is governed by the Laplace equation

$$\nabla^2 u = 0 \quad \text{in } \Omega \tag{2.1}$$

subject to the boundary conditions

$$\begin{aligned} &Essential \quad \text{conditions} \quad u = \bar{u} \quad \text{on} \quad \Gamma_1 \\ &Natural \quad \text{conditions} \quad q = \frac{\partial u}{\partial n} = \bar{q} \quad \text{on} \quad \Gamma_2 \end{aligned} \tag{2.2}$$

where $\boldsymbol{n}$ is the outward normal to the external boundary $\Gamma = \Gamma_1 + \Gamma_2$ of the domain Ω. u denotes the temperature and q denotes the temperature flux. $\bar{u}$ and $\bar{q}$ are the prescribed values on the boundary for u and its normal derivative q, respectively.

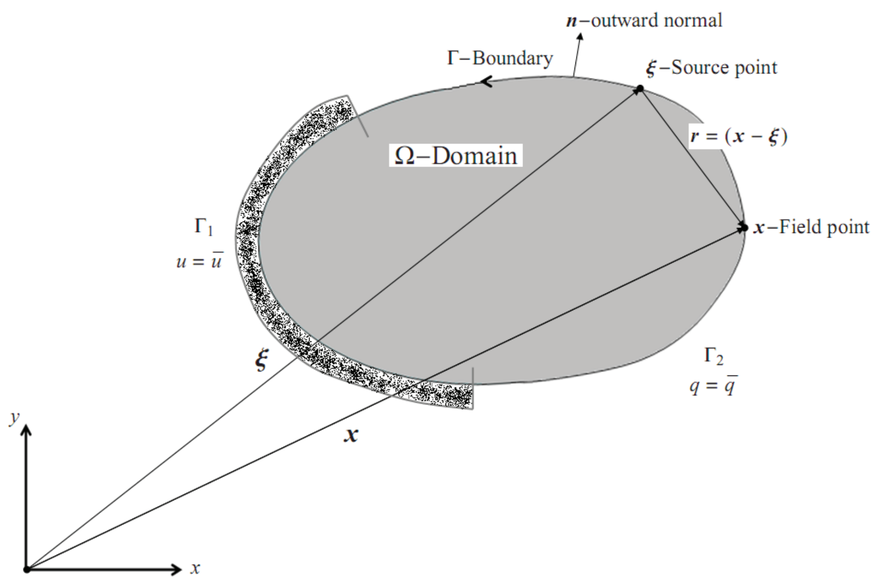

Figure 2.1: A general view of domain and boundary.

Let approximate the solution u by a set of functions $\phi_k(\boldsymbol{x})$ as [24]

$$u \approx \hat{u} = \sum_{k=1}^{n} \alpha_k \phi_k(\boldsymbol{x}), \quad \boldsymbol{x} \in \Omega \tag{2.3}$$

where α_k are undetermined coefficients and ϕ_k are linearly independent functions chosen from a basis for the space. Then, the substitution of the approximation (2.3) into the equations (2.1) and (2.2) produces the error functions (residuals) $\mathcal{R}$, $\mathcal{R}_1$ and $\mathcal{R}_2$

$$\begin{aligned} \nabla^2 \hat{u} \quad &= \mathcal{R} \quad \neq 0 \qquad \text{in} \quad \Omega \\ \hat{u} - \bar{u} \quad &= \mathcal{R}_1 \quad \neq 0 \qquad \text{on} \quad \Gamma_1 \\ \frac{\partial \hat{u}}{\partial n} - \bar{q} \quad &= \mathcal{R}_2 \quad \neq 0 \qquad \text{on} \quad \Gamma_2 \ . \end{aligned} \tag{2.4}$$

In order to minimize the errors in (2.4), one can orthogonalize them with test functions ω, ω_1 and ω_2 as in the weighted residual method [14], and the following integral equation is obtained

$$\int_{\Omega} \mathcal{R}\, \omega \, d\Omega + \int_{\Gamma_1} \mathcal{R}_1\, \omega_1 \, d\Gamma + \int_{\Gamma_2} \mathcal{R}_2\, \omega_2 \, d\Gamma = 0. \tag{2.5}$$

Substituting the residuals from (2.4), we get

$$\int_{\Omega} (\nabla^2 \hat{u})\, \omega \, d\Omega + \int_{\Gamma_1} (\hat{u} - \bar{u})\, \omega_1 \, d\Gamma + \int_{\Gamma_2} (\frac{\partial \hat{u}}{\partial n} - \bar{q})\, \omega_2 \, d\Gamma = 0. \tag{2.6}$$

Now, application of the Green's second identity to the domain integral in (2.6) leads

$$\int_{\Omega} (\nabla^2 \omega)\, \hat{u}\, d\Omega + \int_{\Gamma} (\omega \frac{\partial \hat{u}}{\partial n} - \hat{u} \frac{\partial \omega}{\partial n}) d\Gamma + \int_{\Gamma_1} (\hat{u} - \bar{u})\, \omega_1 \, d\Gamma + \int_{\Gamma_2} (\frac{\partial \hat{u}}{\partial n} - \bar{q})\, \omega_2 \, d\Gamma = 0 \,. \tag{2.7}$$

These weight functions are related to each other to obtain integrals of $\hat{u}$ and $\dfrac{\partial \hat{u}}{\partial n} = \hat{q}$ which are unknowns on Γ_2 and Γ_1, respectively. Then, choosing the weight functions as $\omega_2 = -\omega$ and $\omega_1 = \dfrac{\partial \omega}{\partial n}$ and making the necessary cancellations along both Γ_1 and Γ_2, one can rewrite the integral equation (2.7) in terms of one weight function ω as

$$\int_{\Omega}(\nabla^2\omega)\,\hat{u}\,d\Omega - \int_{\Gamma_2}\hat{u}\,\frac{\partial\omega}{\partial n}\,d\Gamma - \int_{\Gamma_1}\bar{u}\,\frac{\partial\omega}{\partial n}\,d\Gamma + \int_{\Gamma_1}\frac{\partial\hat{u}}{\partial n}\,\omega\,d\Gamma + \int_{\Gamma_2}\bar{q}\,\omega\,d\Gamma \;= 0. \quad (2.8)$$

In order to eliminate the domain integral the weighting function ω can be introduced such that it has continuous first derivatives within Ω and is required to satisfy the equation [81],

$$\nabla^2\omega = -\Delta(\boldsymbol{x} - \boldsymbol{\xi}) \tag{2.9}$$

where $\Delta(\boldsymbol{x}-\boldsymbol{\xi})$ is the Dirac delta function, $\boldsymbol{x}$ and $\boldsymbol{\xi}$ are the field and the source points, respectively. The Dirac delta function is defined as

$$\Delta(\boldsymbol{x} - \boldsymbol{\xi}) = \begin{cases} 0 & if \quad \boldsymbol{x} \neq \boldsymbol{\xi} \\ \infty & if \quad \boldsymbol{x} = \boldsymbol{\xi} \end{cases} \tag{2.10}$$

which leads

$$\int_{\Omega}\hat{u}(\boldsymbol{x})\,\nabla^2\omega(\boldsymbol{x})\,d\Omega(\boldsymbol{x}) = \int_{\Omega}\hat{u}(\boldsymbol{x})\,(-\Delta(\boldsymbol{x} - \boldsymbol{\xi}))\,d\Omega(\boldsymbol{x}) = -\hat{u}(\boldsymbol{\xi}) \tag{2.11}$$

where $\hat{u}(\boldsymbol{\xi})$ represents the value of the unknown function $\hat{u}$ at the point under consideration. By taking the point $\boldsymbol{\xi}$ on the boundary and accounting the jump (Brebbia et al. [13], pp. 63) of the left hand side integral in equation (2.11), the equation (2.8) becomes,

$$c(\boldsymbol{\xi})\hat{u}(\boldsymbol{\xi}) + \int_{\Gamma_1+\Gamma_2}\tilde{u}\,\frac{\partial\omega}{\partial n}\,d\Gamma = \int_{\Gamma_1+\Gamma_2}\tilde{q}\,\omega\,d\Gamma \tag{2.12}$$

where $c(\boldsymbol{\xi})$ is a constant depending on the geometry of the boundary at the point $\boldsymbol{\xi}$ defined as [13, 20],

$$c(\boldsymbol{\xi}) = \begin{cases} \dfrac{\theta_{\xi}}{2\pi} & \text{if} \quad \boldsymbol{\xi} \in \quad \Gamma \\ 1 & \text{if} \quad \boldsymbol{\xi} \in \quad \Omega - \Gamma \end{cases} \tag{2.13}$$

θ_ξ being the internal angle that the boundary Γ makes at the point $\boldsymbol{\xi}$.

In boundary integral (2.12) the functions $\tilde{u}$ and $\tilde{q}$ are given as

$$\tilde{u} = \begin{cases} \bar{u} & if \quad \boldsymbol{\xi} \in \Gamma_1 \\ \hat{u} & if \quad \boldsymbol{\xi} \in \Gamma_2 \end{cases}$$

$$\tilde{q} = \begin{cases} \bar{q} & if \quad \boldsymbol{\xi} \in \Gamma_2 \\ \hat{u} & if \quad \boldsymbol{\xi} \in \Gamma_1 \,. \end{cases}$$

The function ω satisfying equation (2.9) is called a fundamental solution. In general, a fundamental solution u^* is an analytical solution of the adjoint governing equation in Dirac delta function sense. Thus, the weighting function ω in (2.8) can be taken as the fundamental solution u^* of Laplace equation. The two- and three-dimensional fundamental solutions of the Laplace equation are given as

$$\begin{aligned} u^* &= \frac{1}{2\pi}\ln(\frac{1}{r}) \quad \text{in} \quad 2-\text{dimension} \\ u^* &= \frac{1}{4\pi r} \quad \text{in} \quad 3-\text{dimension} \end{aligned} \tag{2.14}$$

where $r = |\boldsymbol{x} - \boldsymbol{\xi}|$ is the distance from the point of application (source point, $\boldsymbol{\xi}$) to the point under consideration (field point, $\boldsymbol{x}$). Then equation (2.12) takes the form

$$c(\boldsymbol{\xi})\hat{u}(\boldsymbol{\xi}) + \int_\Gamma \tilde{u}\, q^*\, d\Gamma = \int_\Gamma \tilde{q}\, u^*\, d\Gamma \tag{2.15}$$

where $q^* = \dfrac{\partial u^*}{\partial n}$.

Defining $\tilde{u}$ and $\tilde{q}$ as u and q in the rest of the formulation, equation (2.15) can be rewritten in terms of u and q as

$$c(\boldsymbol{\xi})u(\boldsymbol{\xi}) + \int_\Gamma u\, q^*\, d\Gamma = \int_\Gamma q\, u^*\, d\Gamma \ . \tag{2.16}$$

For a straight line boundary the angle $\theta_\xi = \pi$ and thus $c(\boldsymbol{\xi}) = \dfrac{1}{2}$ on the boundary. Now, the equation (2.16) is going to be solved on the boundary first and then by taking $c(\boldsymbol{\xi}) = 1$ the solution u can be obtained at any interior point.

2.2 Discretization of the Boundary with Constant Boundary Elements

Now, we proceed with the discretization of the boundary of the domain so that the final integral equation can be converted into a system of equations. The size of the final system is going to be determined by the number of unknowns on the boundary. The BEM is based on a boundary only discretization obtained by dividing the boundary into a series of portions. These portions are called as *boundary elements* [14]. There are several types of boundary elements which are particularly called according to the number of points they accommodate. The points where the solution is required on the boundary are called as *nodes*. When the node is placed at the centre of each boundary element, the elements are named as *constant boundary elements*. The elements with two nodes placed at the ends are *linear elements*. The number of the nodes are increased for higher order elements (e.g. for quadratic elements three nodes are taken, one at the centre and other two at the ends of the elements, Figure 2.2). In this thesis, we will only consider the constant element case, for simplicity.

Let divide the boundary Γ into N straight line segments (elements). Then, assume that u and its normal derivative q have constant variations along each boundary element. Note that with this assumption the unknown u and q values become equal to the values at the centre of each element. While solving u and q on the boundary, the coefficient $c(\boldsymbol{\xi})$ is taken as $\dfrac{1}{2}$ for each source node $\boldsymbol{\xi}$. This is because all the boundary elements are straight lines i.e. they are smooth and the angle θ_ξ becomes π on the boundary. Now, the boundary integrals in equation (2.16) for constant variations of u and q can be written as

$$\frac{1}{2}u_i + \sum_{n=1}^{N} \int_{\Gamma_n} u\, q^*\, d\Gamma_n = \sum_{n=1}^{N} \int_{\Gamma_n} q\, u^*\, d\Gamma_n \qquad (2.17)$$

at the $i-th$ source node $\boldsymbol{\xi}_i$ for N constant boundary elements. Here, the notation u_i

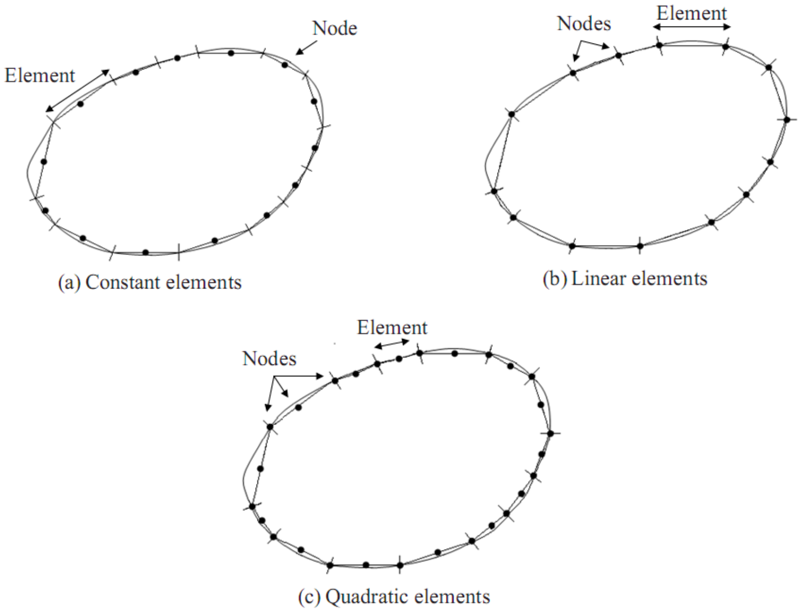

Figure 2.2: Boundary elements.

stands for $u(\boldsymbol{\xi}_i)$ and Γ_n represents the $n-th$ boundary element. Since, u and q are assumed to be constant along each element, one can write the approximations below

$$\left.\begin{aligned} u &\approx u_n \\ q &\approx q_n \end{aligned}\right\} \text{ on } n-th \text{ boundary element } \Gamma_n \tag{2.18}$$

where $i, n = 1, \ldots, N$. Thus, nodal values u_n and q_n can be taken out of integrals and the boundary integral equation becomes

$$\frac{1}{2}u_i + \sum_{n=1}^{N} u_n \int_{\Gamma_n} q^* \, d\Gamma_n = \sum_{n=1}^{N} q_n \int_{\Gamma_n} u^* \, d\Gamma_n \tag{2.19}$$

and for $i = 1, \ldots, N$ we have

$$\frac{1}{2}u_i + \sum_{n=1}^{N} \hat{H}_{in} u_n = \sum_{n=1}^{N} G_{in} \, q_n \tag{2.20}$$

where

$$\hat{H}_{in} = \int_{\Gamma_n} q^* \, d\Gamma_n \quad \text{and} \quad G_{in} = \int_{\Gamma_n} u^* \, d\Gamma_n \tag{2.21}$$

giving the linear system of equations

$$\boldsymbol{H}\,\boldsymbol{u} = \boldsymbol{G}\,\boldsymbol{q}. \tag{2.22}$$

Note that there are N unknowns on the boundary Γ since the discretization is made with N elements and on one part of the boundary Γ_1, q is unknown and on the other part Γ_2, u is unknown. Thus, the system in (2.22) is an $N \times N$ system. Now, taking into consideration the fundamental solution u^* given in (2.14) of the Laplace equation in two-dimensions, the entries of the $N \times N$ matrices $\boldsymbol{H}$ and $\boldsymbol{G}$ are given as

$$
\begin{aligned}
H_{in} &= \frac{1}{2\pi}\int_{\Gamma_n} \frac{(\boldsymbol{x}-\boldsymbol{\xi}_i).\boldsymbol{n}}{\left|\boldsymbol{x}-\boldsymbol{\xi}_i\right|^2}\, d\Gamma_n + \frac{1}{2}\delta_{in} \qquad i,n = 1,\ldots,N \\
G_{in} &= \frac{1}{2\pi}\int_{\Gamma_n} \ln\frac{1}{\left|\boldsymbol{x}-\boldsymbol{\xi}_i\right|}\, d\Gamma_n \qquad i,n = 1,\ldots,N
\end{aligned}
\tag{2.23}
$$

where δ is the Kronecker delta function defined as

$$
\delta_{in} = \begin{cases} 1, & \text{if} \quad i = n \\ 0, & \text{if} \quad i \neq n. \end{cases} \tag{2.24}
$$

When the source point coincides with the field point, which is the case $i = n$, the diagonal entries of $\boldsymbol{G}$ and $\boldsymbol{H}$ can be calculated analytically as

$$
\begin{aligned}
G_{ii} &= \int_{\Gamma_i} u^*\, d\Gamma = \frac{1}{2\pi}\,|r|\,(\ln\frac{1}{|r|} + 1\,) \\
H_{ii} &= \frac{1}{2} + \hat{H}_{ii} = \frac{1}{2}\,.
\end{aligned}
\tag{2.25}
$$

On the boundary $\hat{H}_{ii}$ is zero due to the orthogonality of r and $\boldsymbol{n}$. The insertion of boundary conditions (u is known on Γ_1 and q is known on Γ_2) into the system (2.22) needs the switching of known and unknown values in order to give the final linear system of equations

$$
\boldsymbol{A}\boldsymbol{X} = \boldsymbol{Y}. \tag{2.26}
$$

Here, the matrix $\boldsymbol{A}$ is formed with the columns of the global system matrices $\boldsymbol{H}$ and $\boldsymbol{G}$ corresponding to the known entries of the vectors $\boldsymbol{u}$ and $\boldsymbol{q}$ in the global system (2.22). The vector $\boldsymbol{X}$ contains the unknown nodal values of u on Γ_2 and q on Γ_1. This system of linear equations can be solved by using direct or iterative methods. The coefficient matrix is a full matrix, showing no special form but it contains lots of zero entries scattered arbitrarily. In this thesis, all the resulting systems of this form are solved by using a solver from FORTRAN that makes Gauss elimination with LU factorization based on partial pivoting. In the next section, we introduce the available time-dependent fundamental solutions of the aforementioned transient equations as a preliminary for the applications of the time-domain BEM.

2.3 Time-Dependent Fundamental Solutions

Laplace equation, Poisson equation and the convection-diffusion type equations describe the steady-state or time independent spatial distribution of a physical variable such as temperature, concentration or fluid momentum. If the field changes with time, then the unknown function u depends on the spatial coordinates (x, y) and as well time t.

In one class of problems, physical conservation laws provide us with evolution equations involving the rate of change of the solution expressed by the first time derivative $\dfrac{\partial u}{\partial t}$. Diffusion or heat equation is a good example for this class. In another class of problems, Newton's second law of motion provides us with the evolution equations involving particle acceleration expressed by the second time derivative $\dfrac{\partial^2 u}{\partial t^2}$. For instance, wave equation can be counted in this class. There are three general techniques based on BEM to treat transient problems,

1. Developing an integral equation with the fundamental solution of the unsteady equation representing field due to an impulsive source,
2. Eliminating the time dependence using Laplace transform,
3. Approximating the time derivatives with finite differences and thus obtaining a system of ordinary differential equations.

In this chapter, we build the boundary element method formulations using time-dependent fundamental solutions, since the solution behaviour is both in the space and time domain, physically. This way eliminates the use of another numerical scheme for the time discretization and there is no need to change problem nature as in Laplace transform which first removes the time-dependence. Thus, stability problems do not occur and large time increments are allowed.

2.3.1 Time-dependent fundamental solution for diffusion equation

Generally, the time-dependent fundamental solution for the heat equation can be derived by using Fourier transform and inverse Fourier transform within the Green's functions. Now, we require a solution $u(\boldsymbol{x}, t)$ for the $n-$dimensional heat equation

$$\frac{\partial u(\boldsymbol{x}, t)}{\partial t} - \kappa\, \nabla^2 u(\boldsymbol{x}, t) = 0 \quad \text{for } \boldsymbol{x} \in \mathbb{R}^n,\ t \geq t_0 \tag{2.27}$$

with the initial condition

$$u(\boldsymbol{x}, t) = u_0(\boldsymbol{x}) = h(\boldsymbol{x}) \qquad \text{for } \boldsymbol{x} \in \mathbb{R}^n,\ t = t_0 \tag{2.28}$$

where $\boldsymbol{x} = (x_1, x_2, \ldots, x_n)$ and $|\boldsymbol{x}| = \sqrt{x_1^2 + x_2^2 + \ldots + x_n^2}$ is the norm of it. κ is the diffusion coefficient, and ∇^2 is the Laplace operator

$$\nabla^2 u(\boldsymbol{x}, t) = \frac{\partial^2 u(\boldsymbol{x}, t)}{\partial x_1^2} + \frac{\partial^2 u(\boldsymbol{x}, t)}{\partial x_2^2} + \ldots + \frac{\partial^2 u(\boldsymbol{x}, t)}{\partial x_n^2}. \tag{2.29}$$

A formal solution for the initial value problem above can be obtained by taking the Fourier transformation of the equations (2.27) and (2.28), [80, 82]. The Fourier transformation $\hat{g}$ of a function g is given by

$$\begin{aligned} &\Im[\, g(\boldsymbol{x})\,] = \hat{g}(\boldsymbol{w})\,, \\ &\hat{g}(\boldsymbol{w}) = \int_{\mathbb{R}^n} g(\boldsymbol{x})\, e^{-i\, \boldsymbol{w}\, .\, \boldsymbol{x}}\, d\boldsymbol{x} \end{aligned} \tag{2.30}$$

with the inverse Fourier transform

$$g(\boldsymbol{x}) = \frac{1}{(2\pi)^n} \int_{\mathbb{R}^n} \hat{g}(\boldsymbol{w})\, e^{i\, \boldsymbol{x}\, .\, \boldsymbol{w}}\, d\boldsymbol{w} \tag{2.31}$$

where $\boldsymbol{w} = (w_1, w_2, \ldots, w_n) \in \mathbb{R}^n$ and $\boldsymbol{x} \,.\, \boldsymbol{w} = x_1 w_1 + x_2 w_2 + \ldots + x_n w_n$. In equations (2.30) and (2.31), the integrals over $\mathbb{R}^n$ represent the $n-$tuple improper integrals, i.e.,

$$\int_{\mathbb{R}^n} dA = \int_{-\infty}^{\infty} \cdots \int_{-\infty}^{\infty} dA$$

where dA refers to $d\boldsymbol{x} = dx_1 dx_2 \ldots dx_n$ or $d\boldsymbol{w} = dw_1 dw_2 \ldots dw_n$.

Particularly, we have the Fourier transformations

$$\Im\left[e^{-a\, x_i^2} \right] = \sqrt{\frac{\pi}{a}}\, e^{-w_i^2/4a}\,, \tag{2.32}$$

$$\Im\left[\frac{\partial^2 g(\boldsymbol{x})}{\partial x_i^2} \right] = -w_i^2\, \hat{g}(\boldsymbol{w})\,, \qquad\qquad i = 1, \ldots, n\,. \tag{2.33}$$

Now, let $\hat{u}$ be the Fourier transform of u. Then, by multiplying the equations (2.27) and (2.28) with $e^{-i\,\boldsymbol{w}\,.\,\boldsymbol{x}}$ and integrating over $\mathbb{R}^n$ with respect to $\boldsymbol{x}$, one can obtain the conventions below

$$\int_{\mathbb{R}^n} \left(\frac{\partial u(\boldsymbol{x}, t)}{\partial t} - \kappa \nabla^2 u(\boldsymbol{x}, t) \right) e^{-i\,\boldsymbol{w}\,.\,\boldsymbol{x}}\, d\boldsymbol{x} = 0\,, \tag{2.34}$$

$$\int_{\mathbb{R}^n} u_0(\boldsymbol{x}) e^{-i\,\boldsymbol{w}\,.\,\boldsymbol{x}}\, d\boldsymbol{x} = \int_{\mathbb{R}^n} h(\boldsymbol{x})\, e^{-i\,\boldsymbol{w}\,.\,\boldsymbol{x}}\, d\boldsymbol{x}\,. \tag{2.35}$$

Thus, in view of the Fourier transformation formulas in (2.30), (2.31) and (2.33), equations (2.34) and (2.35) give the initial value problem

$$\begin{aligned} &\frac{\partial \hat{u}(\boldsymbol{w}, t)}{\partial t} + \kappa\, |\boldsymbol{w}|^2\, \hat{u}(\boldsymbol{w}, t) = 0 && \text{for } \ \boldsymbol{w} \in \mathbb{R}^n,\ t > t_0 \\ &\hat{u}_0(\boldsymbol{w}) = \hat{h}(\boldsymbol{w}) && \text{for } \ \boldsymbol{w} \in \mathbb{R}^n,\ t = t_0 \end{aligned} \tag{2.36}$$

where $|\boldsymbol{w}|^2 = w_1^2 + w_2^2 + \ldots + w_n^2$. The solution of the initial value problem (2.36) can be easily found as

$$\hat{u}(\boldsymbol{w}, t) = \hat{h}(\boldsymbol{w})\, e^{-\kappa\,(t\,-\,t_0)\;|\boldsymbol{w}|^2}\,. \tag{2.37}$$

Therefore, inverse Fourier transform of equation (2.37) gives the solution u of (2.27)

$$u(\boldsymbol{x}, t) = \Im^{-1}\,[\,\hat{u}(\boldsymbol{w}, t)\,] = \frac{1}{(2\pi)^n} \int_{\mathbb{R}^n} \hat{u}(\boldsymbol{w}, t)\, e^{i\,\boldsymbol{x}\,.\,\boldsymbol{w}}\, d\boldsymbol{w}. \tag{2.38}$$

When $\hat{u}$ in (2.37) is substituted into (2.38) we obtain

$$u(\boldsymbol{x}, t) = \frac{1}{(2\pi)^n} \int_{\mathbb{R}^n} \hat{h}(\boldsymbol{w})\, e^{-\kappa\,(t\,-\,t_0)\;|\boldsymbol{w}|^2}\, e^{i\,\boldsymbol{x}\,.\,\boldsymbol{w}}\, d\boldsymbol{w}. \tag{2.39}$$

The inverse Fourier transformation $\hat{h}$ of the initial condition h is

$$\hat{h}(\boldsymbol{w}) = \int_{\mathbb{R}^n} h(\boldsymbol{\xi})\, e^{-i\,\boldsymbol{w}\,.\,\boldsymbol{\xi}}\, d\boldsymbol{\xi} \tag{2.40}$$

where $\boldsymbol{\xi} \in \mathbb{R}^n$. Therefore, (2.39) can be rewritten as

$$u(\boldsymbol{x}, t) = \int_{\mathbb{R}^n} h(\boldsymbol{\xi}) \left(\frac{1}{(2\pi)^n} \int_{\mathbb{R}^n} e^{-\kappa\,(t\,-\,t_0)\;|\boldsymbol{w}|^2}\, e^{i\,(\boldsymbol{x}\,-\,\boldsymbol{\xi})\,.\,\boldsymbol{w}}\, d\boldsymbol{w} \right) d\boldsymbol{\xi}. \tag{2.41}$$

Now, denote the inner integral as the heat kernel $K(\boldsymbol{x} - \boldsymbol{\xi}, t)$,

$$\begin{aligned} K(\boldsymbol{x} - \boldsymbol{\xi}, t) \;&= \frac{1}{(2\pi)^n} \int_{\mathbb{R}^n} e^{-\kappa\,(t\,-\,t_0)\;|\boldsymbol{w}|^2}\, e^{i\,(\boldsymbol{x}\,-\,\boldsymbol{\xi})\,.\,\boldsymbol{w}}\, d\boldsymbol{w} \\ &= \frac{1}{(2\pi)^n} \int_{-\infty}^{\infty} e^{-\kappa\,(t\,-\,t_0)\,w_1^2}\, e^{i\,(x_1\,-\,\xi_1)w_1}\, dw_1 \\ &\quad \ldots \int_{-\infty}^{\infty} e^{-\kappa\,(t\,-\,t_0)\,w_n^2}\, e^{i\,(x_n\,-\,\xi_n)w_n}\, dw_n. \end{aligned} \tag{2.42}$$

Concentrating on the inverse Fourier transform definition in (2.30) one can realize that each integral in (2.42) represents a fourier transform of type given in (2.32). Therefore, we have

$$K(\boldsymbol{x}-\boldsymbol{\xi},t)=\frac{1}{(2\pi)^n}\,\Im\left[e^{-\kappa\,(t-t_0)\,w_1^2}\right]\ldots\Im\left[e^{-\kappa\,(t-t_0)\,w_n^2}\right]. \tag{2.43}$$

Thus, making use of (2.32) the heat kernel becomes

$$\begin{aligned}
K(\boldsymbol{x}-\boldsymbol{\xi},t) &= \frac{1}{(2\pi)^n}\underbrace{\sqrt{\frac{\pi}{\kappa(t-t_0)}}\,e^{\left(\frac{-(x_1-\xi_1)^2}{4\kappa(t-t_0)}\right)}\cdots\sqrt{\frac{\pi}{\kappa(t-t_0)}}\,e^{\left(\frac{-(x_n-\xi_n)^2}{4\kappa(t-t_0)}\right)}}_{n\ \text{terms}}\\
&= \frac{1}{(2\pi)^n}\left(\frac{\pi}{\kappa(t-t_0)}\right)^{n/2} e^{\left(-\frac{(x_1-\xi_1)^2+\ \ldots\ +(x_n-\xi_n)^2}{4\,\kappa\,(t-t_0)}\right)}\\
&= \frac{1}{(4\,\pi\,\kappa\,(t-t_0))^{n/2}}\ e^{\left(-\frac{|\,\boldsymbol{x}-\boldsymbol{\xi}\,|^2}{4\,\kappa\,(t-t_0)}\right)}
\end{aligned} \tag{2.44}$$

for $t > t_0$. Thus, including the case $t \le t_0$, the kernel can be defined as

$$K(\boldsymbol{x}-\boldsymbol{\xi},t)=\frac{H[\,t-t_0\,]}{(4\,\pi\,\kappa\,(t-t_0))^{n/2}}\ \exp\left(-\frac{|\,\boldsymbol{x}-\boldsymbol{\xi}\,|^2}{4\,\kappa\,(t-t_0)}\right) \tag{2.45}$$

where H is the Heaviside function which is zero for $t \le t_0$ and is equal to 1 for $t > t_0$. Now, the kernel in (2.45) is the time-dependent fundamental solution u^*, [35, 83] of the heat equation (2.27).

2.3.2 Time-dependent fundamental solution for scalar wave equation

Following a similar procedure as in Section 2.3.1 and the method of descent, the time-dependent fundamental solutions in one, two- and three-dimensions for the scalar wave equation

$$\nabla^2 u-\frac{1}{c^2}\frac{\partial^2 u}{\partial t^2}=0 \tag{2.46}$$

can be obtained as, [22]

(a) in one-dimension

$$u^*(\boldsymbol{\xi}, \tau; \boldsymbol{x}, t) = \frac{H[\ c(\tau - t) - r\ ]}{2\,c} \tag{2.47}$$

(b) in two-dimensions

$$u^*(\boldsymbol{\xi}, \tau; \boldsymbol{x}, t) = \frac{c}{2\pi\ \ (c^2(\tau - t)^2 - r^2)^{1/2}}\ H[\ c(\tau - t) - r\ ] \tag{2.48}$$

(c) in three-dimensions

$$u^*(\boldsymbol{\xi}, \tau; \boldsymbol{x}, t) = \frac{1}{4\,\pi\,c^2\,r}\,\Delta(\frac{r}{c} - (\tau - t)) \tag{2.49}$$

where $r = |\boldsymbol{x} - \boldsymbol{\xi}|$ is the distance between a source point $\boldsymbol{\xi}$ and a field point $\boldsymbol{x}$, c is the wave velocity. τ and t represent the maximum time level and the time variation, respectively. The equation (2.49) describes a spherical shell expanding away from the origin with radial velocity c.

2.3.3 Time-dependent fundamental solution for convection-diffusion equation

Consider the two-dimensional convection-diffusion equation

$$\frac{\partial u}{\partial t} + \mathbf{v}.\nabla u - \kappa \nabla^2 u = 0 \tag{2.50}$$

where u is the temperature, t is time, $\mathbf{v} = (\mathrm{v}_1, \mathrm{v}_2)$ the velocity field in two-dimensions and $\kappa = \dfrac{1}{Pe}$ is the diffusivity constant, Pe being the Péclet number. The two-dimensional time-dependent fundamental solution for this equation is given by Carslaw [35], as

$$u^*(\boldsymbol{\xi}, \tau; \boldsymbol{x}, t) = \frac{H[\tau - t]}{4\kappa\,\pi(\tau - t)} \exp\left(-\frac{|(\boldsymbol{x} - \boldsymbol{\xi}) + \mathbf{v}(\tau - t)|^2}{4\kappa(\tau - t)}\right) \tag{2.51}$$

where τ and t are maximum time level and time variation, respectively.

2.4 BEM Application to the Diffusion Equation with Time-Dependent Fundamental Solution

For transient physical problems the time-domain BEM is especially suitable for catching time evolution of the solution. Also, the solution is obtained at one stroke for a required time level as well as at intermediate time levels by solving only one system.

We consider the nonhomogeneous diffusion equation in two-dimensional domain Ω

$$\frac{\partial u(\boldsymbol{x},t)}{\partial t} - \kappa \nabla^2 u(\boldsymbol{x},t) = f \qquad \boldsymbol{x} \in \Omega\,, \quad t \geq 0 \tag{2.52}$$

with the Dirichlet and Neumann type boundary conditions

$$\begin{aligned} u(\boldsymbol{x},t) &= \bar{u}(\boldsymbol{x},t) && \boldsymbol{x} \in \Gamma_1, \quad t \geq 0 \\ q(\boldsymbol{x},t) &= \frac{\partial u(\boldsymbol{x},t)}{\partial n(\boldsymbol{x})} = \bar{q}(\boldsymbol{x},t) && \boldsymbol{x} \in \Gamma_2, \quad t \geq 0 \end{aligned} \tag{2.53}$$

and the initial condition

$$u(\boldsymbol{x},t) = u_0(\boldsymbol{x}) \qquad \boldsymbol{x} \in \Omega\,. \tag{2.54}$$

f is the source function which is known. The two-dimensional time-dependent fundamental solution of the diffusion equation is from (2.45)

$$u^*(\boldsymbol{\xi},\tau;\boldsymbol{x},t) = \frac{H[\tau - t]}{4\pi\kappa(\tau - t)} \exp\Big(- \frac{|\boldsymbol{x} - \boldsymbol{\xi}|^2}{4\kappa(\tau - t)} \Big) \tag{2.55}$$

where $\boldsymbol{\xi}$ and $\boldsymbol{x}$ are the source and field points in Ω, τ and t are the maximum time and time variation, κ is the diffusivity constant and H is the Heaviside function defined as,

$$H[\tau - t] = \begin{cases} 0, & t \geq \tau \\ 1, & t < \tau\,. \end{cases} \tag{2.56}$$

Thus, $u^* = 0$ for $t = \tau$. Now, we apply the method of weighted residuals [13], using u^* as a weight function which has the advantage of treating the equation as a whole. Thus, we get the weighted residual statement below with the time-dependent fundamental solution u^* in (2.55),

$$\underbrace{\int_0^\tau \int_\Omega \Big(\nabla^2 u - \frac{1}{\kappa}\frac{\partial u}{\partial t}\Big) u^* d\Omega\, dt}_{I} + \frac{1}{\kappa}\int_0^\tau \int_\Omega f\, u^*\, d\Omega\, dt$$
$$+ \int_0^\tau \int_{\Gamma_1} (u - \bar{u}\,)\, q^*\, d\Gamma dt - \int_0^\tau \int_{\Gamma_2} (q - \bar{q}\,)\, u^*\, d\Gamma dt = 0. \tag{2.57}$$

The idea is to obtain a boundary integral equation equivalent to the diffusion problem. Therefore, we make use of the Green's second identity for the part including Laplace term and integration by parts for the part with time derivative to reduce the domain integral I into boundary integrals. We divide I into two parts,

$$I = \int_0^\tau \int_\Omega \Big(\nabla^2 u - \frac{1}{\kappa}\frac{\partial u}{\partial t}\Big) u^* d\Omega\, dt$$
$$= \underbrace{\int_0^\tau \int_\Omega (\,\nabla^2 u)\, u^* d\Omega\, dt}_{I_1} - \underbrace{\int_0^\tau \int_\Omega \frac{1}{\kappa}\frac{\partial u}{\partial t}\, u^* d\Omega\, dt}_{I_2} \tag{2.58}$$

then by using Green's second identity we get

$$I_1 = \int_0^\tau \int_\Omega (\,\nabla^2 u^*)\, u\, d\Omega\, dt + \int_0^\tau \int_\Gamma \Big(u^* \frac{\partial u}{\partial n} - u\frac{\partial u^*}{\partial n}\Big) d\Gamma dt. \tag{2.59}$$

For the integral I_2, we use integration by parts with respect to t to obtain

$$I_2 \;\; = \frac{1}{\kappa}\int_\Omega \Big(u^*(\boldsymbol{\xi}, \tau; \boldsymbol{x}, \tau) u(\boldsymbol{x}, \tau) - u^*(\boldsymbol{\xi}, \tau; \boldsymbol{x}, 0) u_0(\boldsymbol{x})\Big) d\Omega$$
$$-\frac{1}{\kappa}\int_\Omega \int_0^\tau \frac{\partial u^*}{\partial t}\, u\, dt\, d\Omega. \tag{2.60}$$

Here, $u^*(\boldsymbol{\xi}, \tau; \boldsymbol{x}, \tau) = 0$ by the property of the Heaviside function. Therefore, the simplified form of I_2 becomes

$$I_2 = -\frac{1}{\kappa}\int_\Omega u^*(\boldsymbol{\xi},\tau;\boldsymbol{x},0)\,u_0(\boldsymbol{x})\,d\Omega - \frac{1}{\kappa}\int_\Omega\int_0^\tau \frac{\partial u^*}{\partial t}\,u\,dt\,d\Omega. \tag{2.61}$$

Thus, substitution of $I = I_1 - I_2$ into the equation (2.57) gives

$$\begin{aligned}
&\frac{1}{\kappa}\int_0^\tau\int_\Omega\left(\kappa\nabla^2u^* + \frac{\partial u^*}{\partial t}\right)u\,d\Omega\,dt + \int_0^\tau\int_\Gamma\left(u^*\frac{\partial u}{\partial n} - u\frac{\partial u^*}{\partial n}\right)d\Gamma dt\\
&+\frac{1}{\kappa}\int_\Omega u^*(\boldsymbol{\xi},\tau;\boldsymbol{x},0)\,u_0(\boldsymbol{x})\,d\Omega + \frac{1}{\kappa}\int_0^\tau\int_\Omega fu^*d\Omega\,dt \qquad (2.62)\\
&-\int_0^\tau\int_{\Gamma_2}\left(q-\bar{q}\right)u^*d\Gamma dt + \int_0^\tau\int_{\Gamma_1}\left(u-\bar{u}\right)q^*d\Gamma dt = 0.
\end{aligned}$$

The fundamental solution is a function which satisfies the differential equation with right hand side zero at every point except the source point at which it jumps to infinity. Thus, the definition coincides with the definition of the Green's function of the corresponding differential equation. Therefore, the time-dependent fundamental solution u^* satisfies the adjoint of the diffusion equation in Dirac delta function sense,

$$\frac{\partial u^*}{\partial t} + \kappa\nabla^2u^* = -\Delta(\boldsymbol{\xi}-\boldsymbol{x})\Delta(\tau-t). \tag{2.63}$$

This is because the adjoint operator is involved in the Green's theorem and as it is proved by Morse and Feshbach ([83], chp. 7) the Green's function is the same for self-adjoint equations. Now, substituting (2.63) into (2.62) and simplifying the similar terms side by side we get

$$\begin{aligned}
&\underbrace{-\frac{1}{\kappa}\int_0^\tau\int_\Omega \Delta(\boldsymbol{\xi}-\boldsymbol{x})\Delta(\tau-t)\,u(\boldsymbol{x},t)\,d\Omega\,dt}_{c(\boldsymbol{\xi})u(\boldsymbol{\xi},\tau)}\\
&+\int_0^\tau\int_{\Gamma=\Gamma_1+\Gamma_2} q\,u^*\,d\Gamma\,dt - \int_0^\tau\int_{\Gamma=\Gamma_1+\Gamma_2} u\,q^*\,d\Gamma\,dt \qquad (2.64)\\
&+\frac{1}{\kappa}\int_\Omega u^*(\boldsymbol{\xi},\tau;\boldsymbol{x},0)\,u_0(\boldsymbol{x})\,d\Omega + \frac{1}{\kappa}\int_0^\tau\int_\Omega f\,u^*d\Omega\,dt = 0
\end{aligned}$$

where $u = \bar{u}$ on Γ_1 and $q = \bar{q}$ on Γ_2 are known values. Finally, multiplying by '$-\kappa$', equation (2.64) can be rewritten as,

$$
\begin{aligned}
c(\boldsymbol{\xi})u(\boldsymbol{\xi},\tau) \quad &+ \kappa \int_0^\tau \int_\Gamma u(\boldsymbol{x},t) q^*(\boldsymbol{\xi},\tau;\boldsymbol{x},t)\, d\Gamma dt \\
&= \kappa \int_0^\tau \int_\Gamma q(\boldsymbol{x},t)\, u^*(\boldsymbol{\xi},\tau;\boldsymbol{x},t)\, d\Gamma dt \qquad (2.65) \\
&+ \int_\Omega u^*(\boldsymbol{\xi},\tau;\boldsymbol{x},0)\, u_0(\boldsymbol{x})\, d\Omega + \int_0^\tau \int_\Omega f\, u^*(\boldsymbol{\xi},\tau;\boldsymbol{x},t)\, d\Omega\, dt
\end{aligned}
$$

where the constant $c(\boldsymbol{\xi})$ is as defined in (2.13).

Now, we will discretize both the boundary and the time interval. The boundary Γ is divided into N constant boundary elements while the time interval $[0,\tau]$ is divided into M subintervals. Then, assuming that the functions u and q are constants both on the boundary elements $\Gamma_n(\, n = 1, \ldots, N)$, and on each time interval $[t_{m-1}, t_m](\, m = 1, \ldots, M)$, the integral equation (2.65) results in

$$
\begin{aligned}
c_i\, u_i^j \quad &+ \kappa \sum_{m=1}^{M} \sum_{n=1}^{N} u_n^m \int_{t_{m-1}}^{t_m} \int_{\Gamma_n} (q^*)_i^j\, d\Gamma_n\, dt \\
&= \kappa \sum_{m=1}^{M} \sum_{n=1}^{N} q_n^m \int_{t_{m-1}}^{t_m} \int_{\Gamma_n} (u^*)_i^j\, d\Gamma_n\, dt \qquad (2.66) \\
&+ \int_\Omega u(\boldsymbol{x},0) u^*(\boldsymbol{\xi}_i,\tau_j;\boldsymbol{x},0)\, d\Omega + \int_0^\tau \int_\Omega f\, u^*(\boldsymbol{\xi}_i,\tau_j;\boldsymbol{x},t)\, d\Omega\, dt.
\end{aligned}
$$

Here, i and j indicate the mid-points of the $i-th$ boundary element and the $j-th$ time interval, respectively where $i = 1, \ldots, N$ and $j = 1, \ldots, M$. $c_i = c(\boldsymbol{\xi})$ since $\boldsymbol{\xi}$ is one of the boundary nodes and $c_i = 1/2$ for constant elements. u_n^m and q_n^m are approximations to the unknowns $u(\boldsymbol{x},t)$ and $q(\boldsymbol{x},t)$, respectively at the $n-th$ boundary node and $m-th$ time interval, i.e.

$$\begin{aligned} u_n^m &= u(\boldsymbol{\xi}_n, \tau_m) \approx u(\boldsymbol{x}, t) \\ q_n^m &= q(\boldsymbol{\xi}_n, \tau_m) \approx q(\boldsymbol{x}, t) \end{aligned} \tag{2.67}$$

where $\boldsymbol{\xi}_n$ represents the centre spatial coordinate of the $n-th$ boundary element and τ_m is located at the centre of the $m-th$ time interval $[t_{m-1}, t_m]$. When the discretized equation (2.66) is repeated N times (for N source points) for each time interval $[t_{m-1}, t_m]$, we get NM equations, so does an $NM \times NM$ linear system of equations. The resulting system with the following matrix-vector notation is given as

$$\boldsymbol{H}\boldsymbol{u} - \boldsymbol{G}\boldsymbol{q} = \boldsymbol{f_1} + \boldsymbol{f_2}. \tag{2.68}$$

The time process always restarts from initial time $t_0 = 0$ (Figure 2.3), despite the increase in the size of system (2.68), the solution is obtained at one stroke at all transient time levels as well as the required maximum time level without an iteration. The bold capital letters represent matrices of size $NM \times NM$ while small bold letters represent the vectors of size $NM \times 1$. The entries of the matrices $\boldsymbol{H}$ and $\boldsymbol{G}$ and the vectors $\boldsymbol{f_1}$ and $\boldsymbol{f_2}$ are formed by indices for $i, n = 1, \ldots, N$ and $j, m = 1, \ldots, M$. Here, the indices i and n are for the spatial domain where i ranges over the source nodes and n ranges over the boundary nodes. Similarly, j and m are for the time variation and they represent that we are studying with the centre levels of the $j-th$ and $m-th$ time intervals, respectively. Now, the entries of $\boldsymbol{H}$ and $\boldsymbol{G}$ matrices, and $\boldsymbol{f_1}$ and $\boldsymbol{f_2}$ vectors are defined as follows

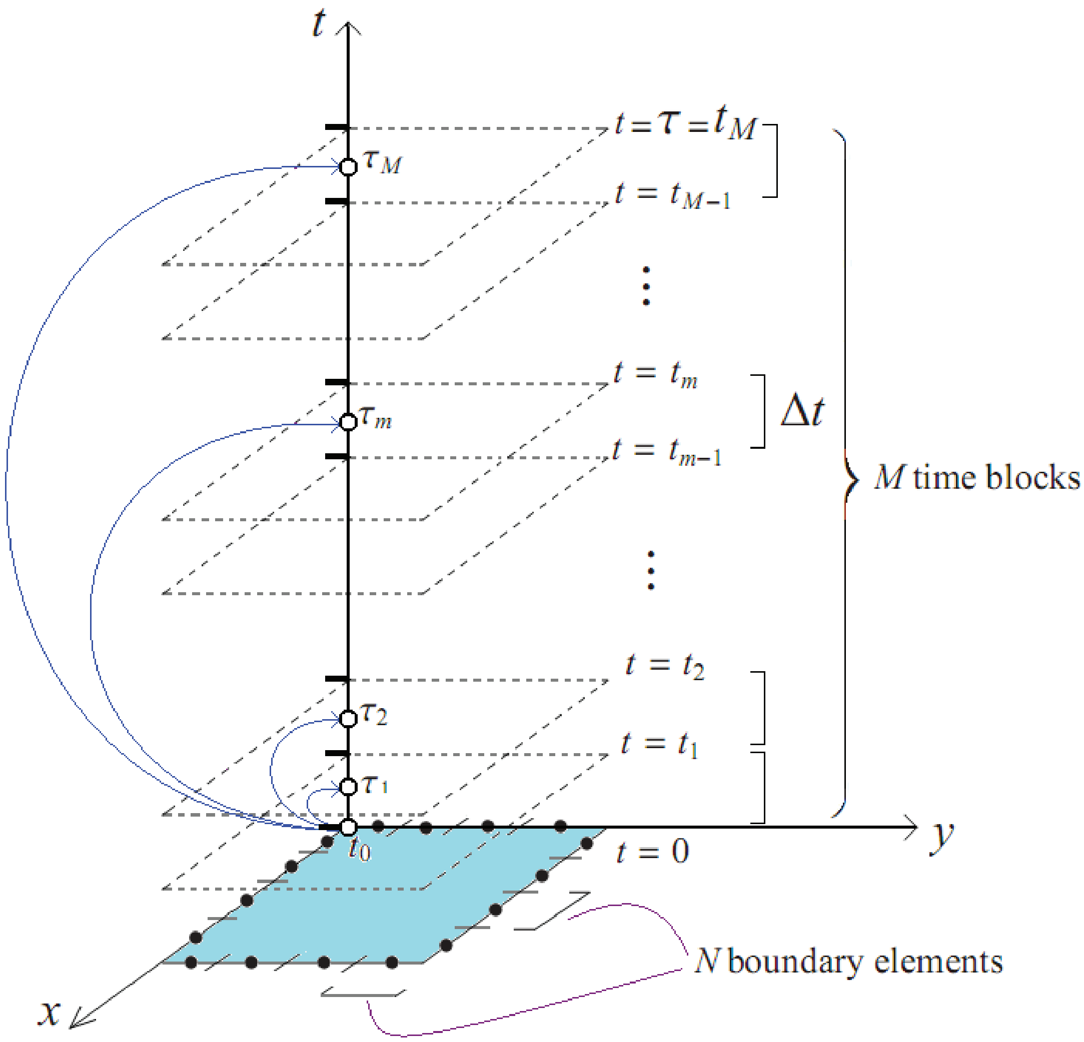

Figure 2.3: Time progress giving $NM \times NM$ system.

$$
\begin{aligned}
H_{in}^{jm} &= \kappa \int_{t_{m-1}}^{t_m} \int_{\Gamma_n} (q^*)_i^j \, d\Gamma_n \, dt + \frac{1}{2}\delta_{in} \\
G_{in}^{jm} &= \kappa \int_{t_{m-1}}^{t_m} \int_{\Gamma_n} (u^*)_i^j \, d\Gamma_n \, dt \\
(f_1)_i^j &= \int_{\Omega} u_0(\boldsymbol{x}) \, u^*(\boldsymbol{\xi}_i, \tau_j; \boldsymbol{x}, 0) \, d\Omega \\
(f_2)_i^j &= \int_0^{\tau} \int_{\Omega} f \, u^*(\boldsymbol{\xi}_i, \tau_j; \boldsymbol{x}, t) \, d\Omega \, dt.
\end{aligned}
\tag{2.69}
$$

One can notice that the entries of the vector $\boldsymbol{f}_1$ is computed always at $t = 0$ but takes the nodal values $(f_1)_i^j$ for each source node $\boldsymbol{\xi}_i$ at each time level τ_j.

By differentiating the fundamental solution u^* with respect to the outward normal vector $\boldsymbol{n}(\boldsymbol{x})$ we get

$$q^* = \frac{\partial u^*}{\partial n} = \frac{-H[\tau - t]}{8\pi\kappa^2(\tau - t)^2} \exp\left(-\frac{r^2}{4\kappa(\tau - t)}\right) ((\boldsymbol{x} - \boldsymbol{\xi}).\boldsymbol{n}) \tag{2.70}$$

where $r = |\boldsymbol{x} - \boldsymbol{\xi}|$ is the distance from a source node $\boldsymbol{\xi}$ to a field (extreme) point $\boldsymbol{x}$. The term δ in H_{in}^{jm} denotes the Kronecker delta function defined in (2.24).

In Table 2.1, we present how the entries H_{in}^{jm} and u_i^j are located in the global system matrix $\boldsymbol{H}_{NM\times NM}$ and the vector $\boldsymbol{u}_{NM\times 1}$. Therefore, the entry H_{in}^{jm} is located to the $k-th$ row and $l-th$ column of the global system matrix $\boldsymbol{H}$ where i, j, m, n are related to k and l with the following relations

$$k = (j-1)N + i \qquad \text{and} \qquad l = (m-1)N + n \tag{2.71}$$

within

$$H(k,l) = H((j-1)N + i, (m-1)N + n) \tag{2.72}$$

where $k, l = 1, \ldots, NM$. Similarly, $k - th$ entry of $\boldsymbol{u}$ is addressed with u_i^j where $k = (j-1)N + i$.

The boundary and time integrals are computed by using Gauss Legendre integration. To approximate the domain and time-domain integrals, we apply the Gauss Legendre integration in domain and as well in time interval.

Now, we substitute the boundary conditions (2.53) into the system (2.68). The resulting system of equations can be arranged in order to accommodate all the unknowns only on one side of the equation. This arrangement can be done by switching the columns (matching with the known entries of the vectors $\boldsymbol{u}$ and $\boldsymbol{q}$) of the global system matrices $\boldsymbol{H}$ and $\boldsymbol{G}$. Thus, one can obtain a final system

$$
\boldsymbol{H} = \left[\begin{array}{ccccc|c|ccccc|c|ccccc}
H^{1,1}_{1,1} & \cdots & H^{1,1}_{1,n} & \cdots & H^{1,1}_{1,N} & & H^{1,m}_{1,1} & \cdots & H^{1,m}_{1,n} & \cdots & H^{1,m}_{1,N} & & H^{1,M}_{1,1} & \cdots & H^{1,M}_{1,n} & \cdots & H^{1,M}_{1,N} \\
\vdots & \ddots & \vdots & \ddots & \vdots & & \vdots & \ddots & \vdots & \ddots & \vdots & & \vdots & \ddots & \vdots & \ddots & \vdots \\
H^{1,1}_{i,1} & \cdots & H^{1,1}_{i,n} & \cdots & H^{1,1}_{i,N} & \cdots & H^{1,m}_{i,1} & \cdots & H^{1,m}_{i,n} & \cdots & H^{1,m}_{i,N} & \cdots & H^{1,M}_{i,1} & \cdots & H^{1,M}_{i,n} & \cdots & H^{1,M}_{i,N} \\
\vdots & \ddots & \vdots & \ddots & \vdots & & \vdots & \ddots & \vdots & \ddots & \vdots & & \vdots & \ddots & \vdots & \ddots & \vdots \\
H^{1,1}_{N,1} & \cdots & H^{1,1}_{N,n} & \cdots & H^{1,1}_{N,N} & & H^{1,m}_{N,1} & \cdots & H^{1,m}_{N,n} & \cdots & H^{1,m}_{N,N} & & H^{1,M}_{N,1} & \cdots & H^{1,M}_{N,n} & \cdots & H^{1,M}_{N,N} \\
\hline
 & & \vdots & & & \ddots & & & \vdots & & & \ddots & & & \vdots & & \\
\hline
H^{j,1}_{1,1} & \cdots & H^{j,1}_{1,n} & \cdots & H^{j,1}_{1,N} & & H^{j,m}_{1,1} & \cdots & H^{j,m}_{1,n} & \cdots & H^{j,m}_{1,N} & & H^{j,M}_{1,1} & \cdots & H^{j,M}_{1,n} & \cdots & H^{j,M}_{1,N} \\
\vdots & \ddots & \vdots & \ddots & \vdots & & \vdots & \ddots & \vdots & \ddots & \vdots & & \vdots & \ddots & \vdots & \ddots & \vdots \\
H^{j,1}_{i,1} & \cdots & H^{j,1}_{i,n} & \cdots & H^{j,1}_{i,N} & \cdots & H^{j,m}_{i,1} & \cdots & H^{j,m}_{i,n} & \cdots & H^{j,m}_{i,N} & \cdots & H^{j,M}_{i,1} & \cdots & H^{j,M}_{i,n} & \cdots & H^{j,M}_{i,N} \\
\vdots & \ddots & \vdots & \ddots & \vdots & & \vdots & \ddots & \vdots & \ddots & \vdots & & \vdots & \ddots & \vdots & \ddots & \vdots \\
H^{j,1}_{N,1} & \cdots & H^{j,1}_{N,n} & \cdots & H^{j,1}_{N,N} & & H^{j,m}_{N,1} & \cdots & H^{j,m}_{N,n} & \cdots & H^{j,m}_{N,N} & & H^{j,M}_{N,1} & \cdots & H^{j,M}_{N,n} & \cdots & H^{j,M}_{N,N} \\
\hline
 & & \vdots & & & \ddots & & & \vdots & & & \ddots & & & \vdots & & \\
\hline
H^{M,1}_{1,1} & \cdots & H^{M,1}_{1,n} & \cdots & H^{M,1}_{1,N} & & H^{M,m}_{1,1} & \cdots & H^{M,m}_{1,n} & \cdots & H^{M,m}_{1,N} & & H^{M,M}_{1,1} & \cdots & H^{M,M}_{1,n} & \cdots & H^{M,M}_{1,N} \\
\vdots & \ddots & \vdots & \ddots & \vdots & & \vdots & \ddots & \vdots & \ddots & \vdots & & \vdots & \ddots & \vdots & \ddots & \vdots \\
H^{M,1}_{i,1} & \cdots & H^{M,1}_{i,n} & \cdots & H^{M,1}_{i,N} & \cdots & H^{M,m}_{i,1} & \cdots & H^{M,m}_{i,n} & \cdots & H^{M,m}_{i,N} & \cdots & H^{M,M}_{i,1} & \cdots & H^{M,M}_{i,n} & \cdots & H^{M,M}_{i,N} \\
\vdots & \ddots & \vdots & \ddots & \vdots & & \vdots & \ddots & \vdots & \ddots & \vdots & & \vdots & \ddots & \vdots & \ddots & \vdots \\
H^{M,1}_{N,1} & \cdots & H^{M,1}_{N,n} & \cdots & H^{M,1}_{N,N} & & H^{M,m}_{N,1} & \cdots & H^{M,m}_{N,n} & \cdots & H^{M,m}_{N,N} & & H^{M,M}_{N,1} & \cdots & H^{M,M}_{N,n} & \cdots & H^{M,M}_{N,N}
\end{array}\right]
\qquad
\boldsymbol{u} = \left[\begin{array}{c}
u^1_1 \\ \vdots \\ u^1_i \\ \vdots \\ u^1_N \\ \hline \vdots \\ \hline u^j_1 \\ \vdots \\ u^j_i \\ \vdots \\ u^j_N \\ \hline \vdots \\ \hline u^M_1 \\ \vdots \\ u^M_i \\ \vdots \\ u^M_N
\end{array}\right]
$$

Table 2.1: Location of the entries of the coefficient matrix $\boldsymbol{H}$ and the vector $\boldsymbol{u}$.

$$\boldsymbol{A}\boldsymbol{X} = \boldsymbol{Y} \tag{2.73}$$

where $\boldsymbol{X}$ contains unknown values of u on Γ_2 and q on Γ_1. The right hand side vector $\boldsymbol{Y}$ contains the given boundary information and the contribution from the domain and time-domain integrals. This system can be solved by using direct or iterative methods. For the interior u values, the equation (2.66) is made use of with the constant $c_i = 1$.

In conclusion, we have the advantage of handling the governing equation as a whole with the help of the time-dependent fundamental solution. Also, note that we have $NM \times NM$ system to be solved for the $NM \times 1$ unknown vector $\boldsymbol{X}$. This is one other goal of the method that the solution is obtained for all boundary nodes at each time level at one stroke, so that we do not need to make iterations between the time steps. Now, the time-domain BEM application to the scalar wave equation is going to be given in Section 2.5 in detailed form.

2.5 BEM Application to the Scalar Wave Equation with Time-Dependent Fundamental Solution

Consider the scalar wave problem in two-dimensional space

$$\nabla^2 u(\boldsymbol{x}, t) - \frac{1}{c^2} \frac{\partial^2 u(\boldsymbol{x}, t)}{\partial t^2} = 0, \qquad \boldsymbol{x} \in \Omega, \ \ t \geq 0 \tag{2.74}$$

with boundary conditions of the types

$$\begin{aligned} u(\boldsymbol{x}, t) &= \ \bar{u}(\boldsymbol{x}, t), && \boldsymbol{x} \ \in \Gamma_1, \ \ t \geq 0 \\ q(\boldsymbol{x}, t) &= \ \frac{\partial u(\boldsymbol{x}, t)}{\partial n(\boldsymbol{x})} = \bar{q}(\boldsymbol{x}, t), && \boldsymbol{x} \ \in \Gamma_2, \ \ t \geq 0 \end{aligned} \tag{2.75}$$

and the initial conditions at $t = 0$

$$
\begin{aligned}
u(\boldsymbol{x},t) &= u_0(\boldsymbol{x}), && \boldsymbol{x} \in \Omega \\
\frac{\partial u(\boldsymbol{x},t)}{\partial t} &= \left[\frac{\partial u(\boldsymbol{x},t)}{\partial t}\right]_{t=0}, && \boldsymbol{x} \in \Omega.
\end{aligned}
\tag{2.76}
$$

As in the case of diffusion equation in Section 2.4, the problem represented by the equation (2.74) subject to the boundary and initial conditions (2.75)-(2.76), can also be transformed into an integral equation for the unknown function u and its normal derivative q, (Brebbia,Telles and Wrobel [13]).

Concentrating on the corresponding time-dependent fundamental solution u^* in equation (2.48),

$$
u^*(\boldsymbol{\xi},\tau;\boldsymbol{x},t) = \frac{c\,H\left[c(\tau-t)-|\boldsymbol{x}-\boldsymbol{\xi}|\right]}{2\pi\,\left(c^2(\tau-t)^2-|\boldsymbol{x}-\boldsymbol{\xi}|^2\right)^{1/2}}
\tag{2.77}
$$

the method of weighted residuals [14], for the scalar wave equation (2.74) reads

$$
\begin{aligned}
&\int_0^\tau \int_\Omega \left(\nabla^2 u - \frac{1}{c^2}\frac{\partial^2 u}{\partial t^2}\right) u^*\, d\Omega\, dt \\
&+ \int_0^\tau \int_{\Gamma_1} (u-\bar{u})\, q^*\, d\Gamma dt - \int_0^\tau \int_{\Gamma_2} (q-\bar{q})\, u^*\, d\Gamma dt = 0.
\end{aligned}
\tag{2.78}
$$

Here, q^* is the normal derivative of u^* and it is defined as

$$
q^* = \frac{\partial u^*}{\partial n} = \frac{c\,r\,H[\,c(\tau-t)-r\,]}{2\pi\,(\,c^2(t-\tau)^2-r^2\,)^{3/2}}\,\frac{\partial r}{\partial n}
\tag{2.79}
$$

where

$$
r = |\boldsymbol{x}-\boldsymbol{\xi}| \quad \text{and} \quad \frac{\partial r}{\partial n} = \frac{(\boldsymbol{x}-\boldsymbol{\xi}).\boldsymbol{n}}{r}\,.
$$

Now, the first term in equation (2.78) is treated in two parts. We apply integration by parts twice to the integral containing the second order time derivative term, and use

Green's second identity to reduce the dimension of the domain integral having the Laplace term as an integrand. Thus, one can arrive at the integral representation

$$\begin{aligned}
&\int_0^\tau \int_\Omega \left(\nabla^2 u^* - \frac{1}{c^2}\frac{\partial^2 u^*}{\partial t^2}\right) u \, d\Omega \, dt + \int_0^\tau \int_{\Gamma=\Gamma_1+\Gamma_2} (u^* \, q - u \, q^*) \, d\Gamma dt \\
&+\frac{1}{c^2} \int_\Omega \left[u^*(\boldsymbol{\xi}, \tau; \boldsymbol{x}, t) \frac{\partial u(\boldsymbol{x}, t)}{\partial t} - u(\boldsymbol{x}, t) \frac{\partial u^*(\boldsymbol{\xi}, \tau; \boldsymbol{x}, t)}{\partial t} \right]_{t=0}^{t=\tau} d\Omega \\
&+ \int_0^\tau \int_{\Gamma_1} (u - \bar{u}) q^* \, d\Gamma dt - \int_0^\tau \int_{\Gamma_2} (q - \bar{q}) u^* \, d\Gamma dt = 0.
\end{aligned} \tag{2.80}$$

In equation (2.80), the boundary integral terms can be simplified by canceling the similar terms on the portions Γ_1 and Γ_2 of the boundary. In addition to this, the domain integral becomes zero for $t = \tau$ due to the Heaviside function appearing in u^* and $\dfrac{\partial u^*}{\partial t}$, where the time derivative of the fundamental solution is

$$\frac{\partial u^*(\boldsymbol{\xi}, \tau; \boldsymbol{x}, t)}{\partial t} = \frac{c^3(\tau - t) H[c(\tau - t) - r]}{2\pi \, (c^2(\tau - t)^2 - r^2)^{3/2}} \; . \tag{2.81}$$

Then, equation (2.80) can be rewritten as

$$\begin{aligned}
&\int_0^\tau \int_\Omega \left(\nabla^2 u^* - \frac{1}{c^2}\frac{\partial^2 u^*}{\partial t^2}\right) u \, d\Omega \, dt + \int_0^\tau \int_\Gamma (u^* \, q - u \, q^*) \, d\Gamma dt \\
&+\frac{1}{c^2} \int_\Omega \left(u^*(\boldsymbol{\xi}, \tau; \boldsymbol{x}, 0) \left.\frac{\partial u(\boldsymbol{x}, t)}{\partial t}\right|_{t=0} - u(\boldsymbol{x}, 0) \left.\frac{\partial u^*(\boldsymbol{\xi}, \tau; \boldsymbol{x}, t)}{\partial t}\right|_{t=0} \right) d\Omega = 0.
\end{aligned} \tag{2.82}$$

The fundamental solution u^* is satisfying the scalar wave equation (2.74) in the Dirac delta function sense that

$$\nabla^2 u^*(\boldsymbol{\xi}, \tau; \boldsymbol{x}, t) - \frac{1}{c^2} \frac{\partial^2 u^*(\boldsymbol{\xi}, \tau; \boldsymbol{x}, t)}{\partial t^2} = -\Delta(\boldsymbol{\xi} - \boldsymbol{x}) \Delta(\tau - t). \tag{2.83}$$

For scalar wave equation there is a symmetry with respect to time 't' in the sense that $u^*(\boldsymbol{\xi}, \tau; \boldsymbol{x}, t) = u^*(\boldsymbol{\xi}, \tau; \boldsymbol{x}, -t)$ due to the second order time derivative, [83]. Thus, the fundamental solution u^* satisfies the scalar wave equation itself, in contrast with the diffusion and convection-diffusion equations involving first order time derivatives. Then, the time-domain boundary integral formulation of the scalar wave equation is obtained as

$$
\begin{aligned}
c(\boldsymbol{\xi})u(\boldsymbol{\xi},\tau) \quad &+ \int_0^\tau \int_\Gamma u(\boldsymbol{x},t)q^*(\boldsymbol{\xi},\tau;\boldsymbol{x},t)\,d\Gamma\,dt \\
&= \int_0^\tau \int_\Gamma q(\boldsymbol{x},t)u^*(\boldsymbol{\xi},\tau;\boldsymbol{x},t)\,d\Gamma\,dt \\
&+\frac{1}{c^2}\int_\Omega \left(u^*(\boldsymbol{\xi},\tau;\boldsymbol{x},0)\frac{\partial u(\boldsymbol{x},t)}{\partial t}\bigg|_{t=0} - u_0(\boldsymbol{x})\frac{\partial u^*(\boldsymbol{\xi},\tau;\boldsymbol{x},t)}{\partial t}\bigg|_{t=0}\right) d\Omega.
\end{aligned} \tag{2.84}
$$

Discretization of (2.84) using N constant boundary elements and M subintervals in time direction gives

$$
\begin{aligned}
c_i u_i^j \quad &+ \sum_{m=1}^{M}\sum_{n=1}^{N} u_n^m \int_{t_{m-1}}^{t_m} \int_{\Gamma_n} (q^*)_i^j\,d\Gamma_n\,dt \\
&= \sum_{m=1}^{M}\sum_{n=1}^{N} q_n^m \int_{t_{m-1}}^{t_m} \int_{\Gamma_n} (u^*)_i^j\,d\Gamma_n\,dt \\
&+\frac{1}{c^2}\int_\Omega \left(u^*(\boldsymbol{\xi}_i,\tau_j;\boldsymbol{x},0)\frac{\partial u(\boldsymbol{x},t)}{\partial t}\bigg|_{t=0} - u_0(\boldsymbol{x})\frac{\partial u^*(\boldsymbol{\xi}_i,\tau_j;\boldsymbol{x},t)}{\partial t}\bigg|_{t=0}\right) d\Omega
\end{aligned} \tag{2.85}
$$

where $i,n = 1,\ldots,N$ and $j,m = 1,\ldots,M$, and the following approximations are held

$$u_n^m = u(\boldsymbol{\xi}_n,\tau_m) \approx u(\boldsymbol{x},t) \qquad \text{and} \qquad q_n^m = q(\boldsymbol{\xi}_n,\tau_m) \approx q(\boldsymbol{x},t)$$

where $\boldsymbol{\xi}_n$ and τ_m denote the mid-point coordinates of the $n-th$ boundary element and $m-th$ time interval, respectively. $c_i = 1/2$ again for boundary nodes on constant elements. Writing equation (2.85) for all $i,n = 1,\ldots,N$ and $j,m = 1,\ldots,M$, one can obtain the resulting $NM \times NM$ linear system of equations

$$\boldsymbol{H}\,\boldsymbol{u} - \boldsymbol{G}\,\boldsymbol{q} = \boldsymbol{f} \tag{2.86}$$

and make use of initial values at $t = 0$ for obtaining solution at all transient levels, simultaneously. Now, we describe the entries of the global system matrices with the help of the indexed terms (superscripts; j, m and subscripts; i, n)

$$\begin{aligned}
H_{in}^{jm} &= \int_{t_{m-1}}^{t_m} \int_{\Gamma_n} (q^*)_i^j \, d\Gamma_n \, dt + \frac{1}{2}\delta_{in} \\
G_{in}^{jm} &= \int_{t_{m-1}}^{t_m} \int_{\Gamma_n} (u^*)_i^j \, d\Gamma_n \, dt \\
f_i^j &= \frac{1}{c^2} \int_{\Omega} \left(\left. \frac{\partial u(\boldsymbol{x}, t)}{\partial t} \right|_{t=0} u^*(\boldsymbol{\xi}_i, \tau_j; \boldsymbol{x}, 0) - u_0(\boldsymbol{x}) \left. \frac{\partial u^*(\boldsymbol{\xi}_i, \tau_j; \boldsymbol{x}, t)}{\partial t} \right|_{t=0} \right) d\Omega
\end{aligned} \tag{2.87}$$

and they are all located in the global system matrices $\boldsymbol{H}$, $\boldsymbol{G}$ and the vector $\boldsymbol{f}$ as in Table 2.1.

Finally, inserting boundary conditions to the equation (2.86) leads a linear system of algebraic equations of the form

$$\boldsymbol{A}\boldsymbol{X} = \boldsymbol{Y}. \tag{2.88}$$

The vector $\boldsymbol{X}$ contains unknown displacement u and the traction $\frac{\partial u}{\partial n}$ values on the parts Γ_2 and Γ_1 of the boundary, respectively. For the computation of interior u values the equation (2.85) is made use of by taking the constant $c_i = 1$, and the matrix-vector multiplications are carried out within obtained boundary values of u and q.

In the next section, we proceed with the time-domain BEM solution of the convection-diffusion type equations. Actually, this is going to provide a basis for the application of the method to some other significant problems in physics and chemistry which are particularly, governed by the system of equations including Laplace, diffusion and convection-diffusion type equations. Thus, the time-domain BEM procedure is going to be adapted to the system of equations for the first time, and supported with remarkable numerical examples.

2.6 BEM Application to the Convection-Diffusion Type Equations with Time-Dependent Fundamental Solution

In this section, we give the time-domain boundary element method treatment of the convection-diffusion type equations. The transient convection-diffusion equation is defined as

$$\frac{\partial u(\boldsymbol{x},t)}{\partial t} + \mathbf{v}.\nabla u(\boldsymbol{x},t) = \kappa \nabla^2 u(\boldsymbol{x},t) + f \tag{2.89}$$

where u is the temperature, t is time, $\boldsymbol{x}$ is the two-dimensional spatial variable, $\mathbf{v}$ is the velocity field, and $\kappa = \dfrac{1}{Pe}$ is the diffusivity constant where Pe is the Péclet number. f is a given force function. A well-posed boundary and initial value problem can be defined with the Dirichlet and Neumann type boundary conditions

$$\begin{aligned} u(\boldsymbol{x},t) &= \bar{u} && \text{on} \quad \Gamma_1 \\ \frac{\partial u(\boldsymbol{x},t)}{\partial n} &= q(\boldsymbol{x},t) = \bar{q} && \text{on} \quad \Gamma_2 \end{aligned} \tag{2.90}$$

and the initial condition

$$u(\boldsymbol{x},0) = u_0(\boldsymbol{x}). \tag{2.91}$$

We will establish the time-domain BEM formulation of this problem by making use of integration by parts and Green's identities. Substituting approximations for u and q in the equations above we get the following weighted residual statement

$$\begin{aligned} &\int_0^\tau \int_\Omega \left(\nabla^2 u - \frac{1}{\kappa}\frac{\partial u}{\partial t} - \frac{1}{\kappa}\mathbf{v}.\nabla u \right) u^* d\Omega\, dt + \int_0^\tau \int_\Omega \frac{1}{\kappa} f u^* d\Omega\, dt \\ &= \int_0^\tau \int_{\Gamma_2} \left(\frac{\partial u}{\partial n} - \bar{q} \right) u^* d\Gamma dt - \int_0^\tau \int_{\Gamma_1} \left(u - \bar{u} \right) q^* d\Gamma dt. \end{aligned} \tag{2.92}$$

Here, we use the time-dependent fundamental solution u^*, [35], (available for the convection-diffusion type equations with $f = 0$ given in Section 2.3.3), as a weight function,

$$u^*(\boldsymbol{\xi}, \tau; \boldsymbol{x}, t) = \frac{H[\tau - t]}{(4\kappa\pi(\tau - t))} \exp\Big(-\frac{\left|(\boldsymbol{x} - \boldsymbol{\xi}) + \mathbf{v}(\tau - t)\right|^2}{4\kappa(\tau - t)}\Big). \tag{2.93}$$

Now, we will develop a boundary integral equation equivalent to the problem defined by equations (2.89)-(2.91). Referring to the equation (2.92), let

$$\begin{aligned}
I &= \int_0^\tau \int_\Omega \Big(\nabla^2 u - \frac{1}{\kappa}\frac{\partial u}{\partial t} - \frac{1}{\kappa}(\mathbf{v}.\nabla u)\Big) u^* d\Omega\, dt \quad \text{and} \\
I_1 &= -\int_0^\tau \int_\Omega \frac{1}{\kappa}\frac{\partial u}{\partial t} u^* d\Omega\, dt \\
I_2 &= -\int_0^\tau \int_\Omega \frac{1}{\kappa}(\mathbf{v}.\nabla u)\, u^* d\Omega\, dt \\
I_3 &= \int_0^\tau \int_\Omega (\nabla^2 u)\, u^* d\Omega\, dt.
\end{aligned} \tag{2.94}$$

Applying integration by parts with respect to t and making use of the Heaviside function's property (i.e. $H[\tau - t] = 0$ for $t \geq \tau$), I_1 can be rewritten as

$$I_1 = \frac{1}{\kappa}\int_\Omega u^*(\boldsymbol{\xi}, \tau; \boldsymbol{x}, 0)\, u(\boldsymbol{x}, 0)\, d\Omega + \frac{1}{\kappa}\int_0^\tau \int_\Omega u(\boldsymbol{x}, t)\frac{\partial u^*}{\partial t}(\boldsymbol{\xi}, \tau; \boldsymbol{x}, t)\, d\Omega\, dt. \tag{2.95}$$

Green's identity aplication with respect to spatial variable for I_2, gives

$$I_2 = -\frac{1}{\kappa}\int_0^\tau \int_\Gamma u^* u\, \mathbf{v}_n\, d\Gamma\, dt + \frac{1}{\kappa}\int_0^\tau \int_\Omega (\mathbf{v}.\nabla u^*) u\, d\Omega\, dt \tag{2.96}$$

where $\mathbf{v}_n = \mathbf{v}.\boldsymbol{n}$ and $\boldsymbol{n}$ is the outward normal. Then, making use of the Green's second identity, I_3 results in

$$I_3 = \int_0^\tau \int_\Omega (\nabla^2 u^*)\, u\, d\Omega\, dt + \int_0^\tau \int_\Gamma \Big(u^*\frac{\partial u}{\partial n} - u\frac{\partial u^*}{\partial n}\Big) d\Gamma\, dt\,. \tag{2.97}$$

Therefore, the simplified form of $I = I_1 + I_2 + I_3$ reads

$$\begin{aligned} I \;&= \int_0^\tau \int_\Omega \Big(\nabla^2 u^* + \frac{1}{\kappa}\frac{\partial u^*}{\partial t} + \frac{1}{\kappa}\mathbf{v}.\nabla u^*\Big) u(\boldsymbol{x}, t)\, d\Omega\, dt \\ &+ \int_\Omega \frac{1}{\kappa} u^*(\boldsymbol{\xi}, \tau; \boldsymbol{x}, 0)\, u_0(\boldsymbol{x}) d\Omega \\ &- \int_0^\tau \int_\Gamma \frac{1}{\kappa}\, u^* u \mathbf{v}_n\, d\Gamma\, dt + \int_0^\tau \int_\Gamma \Big(u^* \frac{\partial u}{\partial n} - u\frac{\partial u^*}{\partial n}\Big) d\Gamma\, dt. \end{aligned} \tag{2.98}$$

Then, substituting equation (2.98) into the equation (2.92) one can obtain

$$\begin{aligned} &\int_0^\tau \int_\Omega \Big(\nabla^2 u^* + \frac{1}{\kappa}\frac{\partial u^*}{\partial t} + \frac{1}{\kappa}\mathbf{v}.\nabla u^*\Big) u(\boldsymbol{x}, t) d\Omega dt + \int_\Omega \frac{1}{\kappa} u^*(\boldsymbol{\xi}, \tau; \boldsymbol{x}, 0)\, u_0(\boldsymbol{x}) d\Omega \\ &- \int_0^\tau \int_\Gamma \frac{1}{\kappa} u^* u\, \mathbf{v}_n\, d\Gamma\, dt + \int_0^\tau \int_\Gamma \Big(u^* \frac{\partial u}{\partial n} - u\frac{\partial u^*}{\partial n}\Big) d\Gamma\, dt + \int_0^\tau \int_\Omega \frac{1}{\kappa} f u^*\, d\Omega\, dt \\ &= \int_0^\tau \int_{\Gamma_2} \Big(\frac{\partial u}{\partial n} - \bar{q}\Big) u^* d\Gamma dt - \int_0^\tau \int_{\Gamma_1} \Big(u - \bar{u}\Big) q^*\, d\Gamma\, dt. \end{aligned} \tag{2.99}$$

When we cancel similar boundary integrals appearing on both sides of (2.99), and use the fundamental solution u^* possessing the following properties (fundamental solution satisfies the adjoint of convection-diffusion equation in Dirac delta function sense)

$$\begin{aligned} &\kappa \nabla^2 u^* + \frac{\partial u^*}{\partial t} + \mathbf{v}.\nabla u^* = -\Delta(\boldsymbol{\xi} - \boldsymbol{x})\Delta(\tau - t) \\ &\lim_{t \to \tau} u^*(\boldsymbol{\xi}, \tau; \boldsymbol{x}, t) = 0 \end{aligned} \tag{2.100}$$

we finally get

$$\begin{aligned} c(\boldsymbol{\xi}) u(\xi, \tau) \;&+ \int_0^\tau \int_\Gamma (\kappa\, q^* + \mathbf{v}_n\, u^*)\, u\, d\Gamma\, dt - \int_0^\tau \int_\Gamma \kappa\, q\, u^* d\Gamma\, dt \\ &= \int_\Omega u^*(\boldsymbol{\xi}, \tau; \boldsymbol{x}, 0)\, u_0(\boldsymbol{x})\, d\Omega + \int_0^\tau \int_\Omega f u^*(\boldsymbol{\xi}, \tau; \boldsymbol{x}, t)\, d\Omega\, dt. \end{aligned} \tag{2.101}$$

Similar to the discretization of boundary integral in the diffusion equation (2.65), we divide the boundary into N portions and the time interval into M intervals (blocks). Then, assuming constant variations along each boundary element and time interval, one can derive the discretized equation for (2.101).

$$
\begin{aligned}
c_i u_i^j \quad &+ \sum_{m=1}^{M} \sum_{n=1}^{N} u_n^m \int_{t_{m-1}}^{t_m} \int_{\Gamma_n} \left(\kappa \, (q^*)_i^j + \mathbf{v}_n \, (u^*)_i^j \right) d\Gamma_n \, dt \\
&= \sum_{m=1}^{M} \sum_{n=1}^{N} q_n^m \int_{t_{m-1}}^{t_m} \int_{\Gamma_n} \kappa \, (u^*)_i^j \, d\Gamma_n \, dt \\
&+ \int_{\Omega} u_0(\boldsymbol{x}) u^*(\boldsymbol{\xi}_i, \tau_j; \boldsymbol{x}, 0) \, d\Omega + \int_0^{\tau} \int_{\Omega} f \, u^*(\boldsymbol{\xi}_i, \tau_j; \boldsymbol{x}, t) \, d\Omega \, dt
\end{aligned}
\tag{2.102}
$$

where

$$
\begin{aligned}
u_n^m &= u(\boldsymbol{\xi}_n, \tau_m) \approx u(\boldsymbol{x}, t) \\
q_n^m &= q(\boldsymbol{\xi}_n, \tau_m) \approx q(\boldsymbol{x}, t)
\end{aligned}
\tag{2.103}
$$

in which $\boldsymbol{\xi}_n$ represents the mid-point coordinate of the $n-th$ boundary element and τ_m represents the central value of the time interval $[t_{m-1}, t_m]$. $c_i = \frac{1}{2}$ for constant boundary element use. Thus, the solution is going to be found at the constant nodes spatially, and at the mid-point of each time interval simultaneously. Now, ranging $i, n = 1, \ldots, N$ and $j, m = 1, \ldots, M$ we obtain the $NM \times NM$ linear system of equations

$$
\boldsymbol{H}\,\boldsymbol{u} - \boldsymbol{G}\,\boldsymbol{q} = \boldsymbol{f_1} + \boldsymbol{f_2}. \tag{2.104}
$$

Concentrating on the entries of the global system matrices ($\boldsymbol{H}$ and $\boldsymbol{G}$) and vectors ($\boldsymbol{f_1}$ and $\boldsymbol{f_2}$), we describe the related terms below which are addressed with the indices i, n in spatial domain, and j, m in time domain

$$
\begin{aligned}
H_{in}^{jm} &= \int_{t_{m-1}}^{t_m} \int_{\Gamma_n} (\kappa (q^*)_i^j + \mathbf{v}_n (u^*)_i^j)\, d\Gamma_n\, dt + \frac{1}{2}\delta_{in} \\
G_{in}^{jm} &= \int_{t_{m-1}}^{t_m} \int_{\Gamma_n} \kappa (u^*)_i^j \, d\Gamma_n\, dt \\
(f_1)_i^j &= \int_{\Omega} u_0(\boldsymbol{x}) u^*(\boldsymbol{\xi}_i, \tau_j; \boldsymbol{x}, 0)\, d\Omega \\
(f_2)_i^j &= \int_0^{\tau} \int_{\Omega} f\, u^*(\boldsymbol{\xi}_i, \tau_j; \boldsymbol{x}, t)\, d\Omega\, dt.
\end{aligned}
\tag{2.105}
$$

The time-domain BEM matrix $\boldsymbol{H}$ differs from the $\boldsymbol{H}$ matrix obtained for the diffusion equation (equation (2.69)) as containing the contribution coming from convection terms. Nevertheless, the location of the so-called entries H_{in}^{jm}, G_{in}^{jm}, $(f_1)_i^j$ and $(f_2)_i^j$ are the same as shown in Table 2.1.

The normal derivative of the fundamental solution is simply derived as

$$
q^* = \frac{\partial u^*}{\partial n} = -\frac{(\boldsymbol{x} - \boldsymbol{\xi}) + \mathbf{v}(\tau - t)}{2\kappa(\tau - t)} u^*. \tag{2.106}
$$

All the integrals are computed numerically by using Gauss Legendre integration. Finally, making use of the given boundary conditions and doing necessary arrangements on the columns of the global system matrices, we get the system

$$
\boldsymbol{AX} = \boldsymbol{Y}. \tag{2.107}
$$

$\boldsymbol{A}$ can always be obtained as a diagonally dominant matrix (for smooth boundaries especially), thus we use the standard Gauss elimination to solve the final system for $\boldsymbol{X}$. Again, when $c_i = 1$ in equation (2.102), the resulting discretized equation provides us the interior solution u, i.e. we have

$$
u_i^j = -\sum_{m=1}^{M} \sum_{n=1}^{N} H_{in}^{jm} u_n^m + \sum_{m=1}^{M} \sum_{n=1}^{N} G_{in}^{jm} q_n^m + (f_1)_i^j + (f_2)_i^j. \tag{2.108}
$$

Now, the index i represents the $i-th$ interior node, thus, all the contributions in the terms H^{ij}_{nm} and G^{ij}_{nm} are from an interior node $\boldsymbol{\xi}_i$ to a boundary element Γ_n. Therefore, we only make matrix vector multiplications and then reach the interior solution wherever it is required.

In the next section, we discuss the efficiency of the method numerically on all the three types of equations we mentioned above. In comparison with the other numerical methods for these very well known problems, we have the advantage of treating the equations as a whole so that we do not require another numerical scheme for the time derivative. Also, the method is based on the BEM on spatial domain, thus, it provides an easy discretization that we only deal with the division of the boundary not the whole domain. Although the time discretization leads a linear system of large size, once it is solved the solution is obtained at each time level without the need of an iteration. In other words, we solve a larger system but only once since the concurrent discretization of the spatial and time domains does not require iteration to obtain the solution at the other time levels.

2.7 Numerical Results and Discussions

In this section we present numerical applications of the time-domain boundary element method. In this sense, we write a computer algorithm in FORTRAN language and customize the algorithm to test problems of these three types in order to reach the solutions.

2.7.1 Diffusion problem

The test problem is defined on a unit square $[0, 1] \times [0, 1]$ with initial temperature

$$u_0(\boldsymbol{x}) = u(x, y, 0) = sin(\pi x) + sin(\pi y)$$

where $\boldsymbol{x} = (x, y)$ is the spatial variable in two-dimensions, and $0 \leq x, y \leq 1$. The two-dimensional linear diffusion equation

$$\frac{\partial u}{\partial t} - \kappa\nabla^2 u = 0 \tag{2.109}$$

is defined with the thermal diffusivity $\kappa = 0.1$, and subject to the boundary conditions taken from the exact solution of the problem

$$u(\boldsymbol{x}, t) = (sin(\pi x) + sin(\pi y))e^{-\kappa\pi^2 t} \quad \text{for } t \geq 0. \tag{2.110}$$

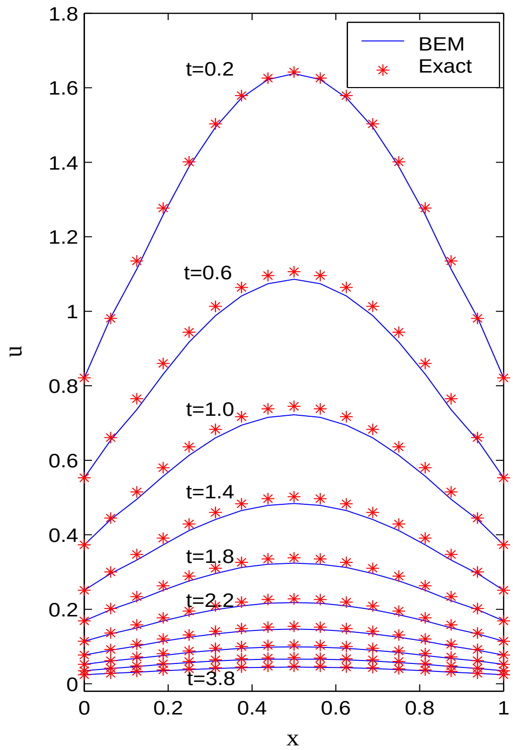

Figure 2.4: Solution of diffusion problem at $y = 0.5$ with $\Delta t = 0.4$ on $[0, 4]$.

Numerical solutions presented in Figures 2.4 and 2.5 are obtained at $y = 0.5$ by using $N = 12$ boundary elements and $M = 10$ time intervals in $[0, 4]$. So, the maximum time level is $\tau = 4$, and the time step is $\Delta t = \tau/M = 0.4$. Due to the time discretization process used in the time-domain BEM, we obtain the solution at the centre level of each time interval. In Figure 2.4, the solution is visualised at the time levels $\tau_1 = 0.2$, $\tau_2 = 0.6$, $\ldots$, $\tau_{10} = 3.8$ where it reaches steady-state. It is obviously seen in Figure 2.5 that the numerical and exact solutions agree very well at the centre point

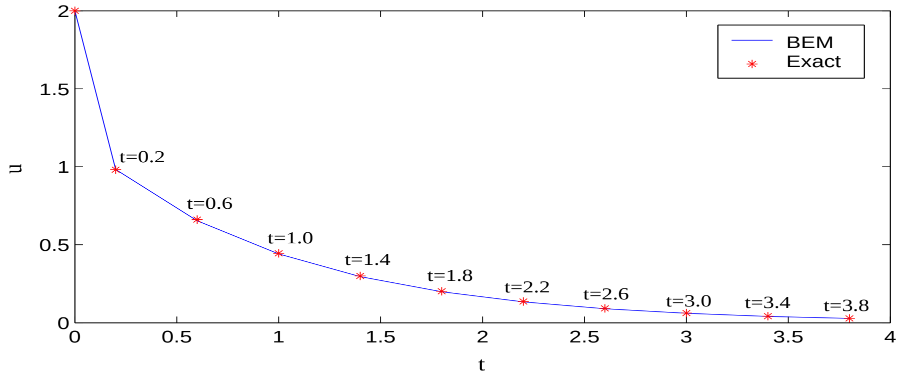

Figure 2.5: Solution of diffusion problem at $(x, y) = (0.5, 0.5)$ with $\Delta t = 0.4$ on $[0, 4]$.

$(x, y) = (0.5, 0.5)$ for increasing values of time.

Figure 2.6 shows the behaviour of the solution at $y = 0.5$ along $x-$direction on $[0, 10]$. Another comparison, between exact and numerical solutions, is given in Figure 2.7 at $(x, y) = (0.5, 0.5)$ with respect to time scale. The number of boundary elements is $N = 12$ and the time interval is divided into $M = 10$ intervals in order to get the solution at higher time levels with larger time step $\Delta t = 1.0$. The numerical solution is in good agreement with the exact solution despite the large time increment, that is, we do not encounter stability problems.

Figure 2.8 depicts the conformity of the numerical and exact solutions of the problem along $x-$direction at $y = 0.5$, by using $N = 12$ and $M = 20$. The behaviour of the solution at $(x, y) = (0.5, 0.5)$ is visualised in Figure 2.9 with respect to time. Now, the time interval is $[0, 30]$, and we are able to reach steady-state with quite large time increment $\Delta t = 1.5$.

One can see that, as the gradient between the end points decreases, the solution approaches a steady-state value which is zero for this problem. We conclude that the solution is in a good agreement with the exact solution even by using remarkably large time increments.

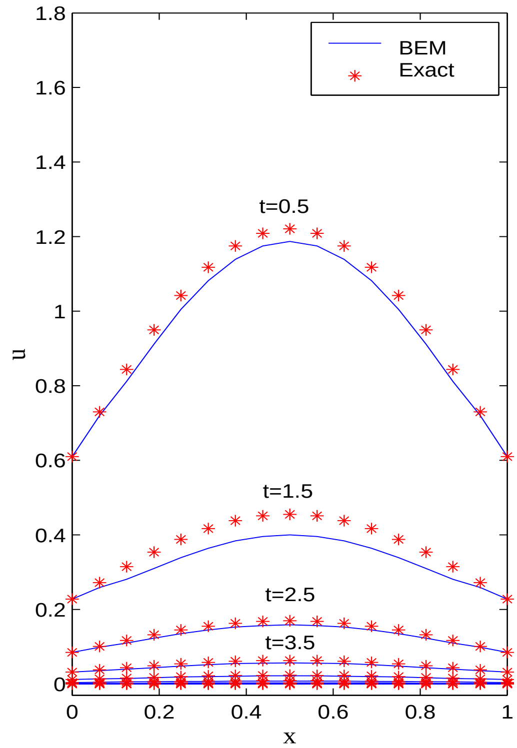

Figure 2.6: Solution of diffusion problem at $y = 0.5$ with $\Delta t = 1.0$ on $[0, 10]$.

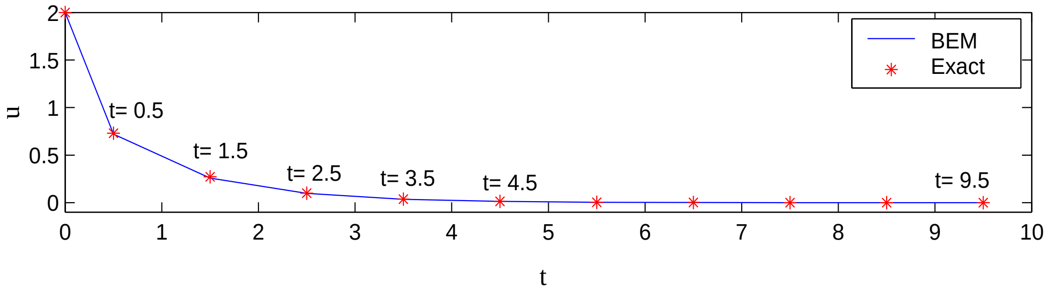

Figure 2.7: Solution of diffusion problem at $(x, y) = (0.5, 0.5)$ with $\Delta t = 1.0$ on $[0, 10]$.

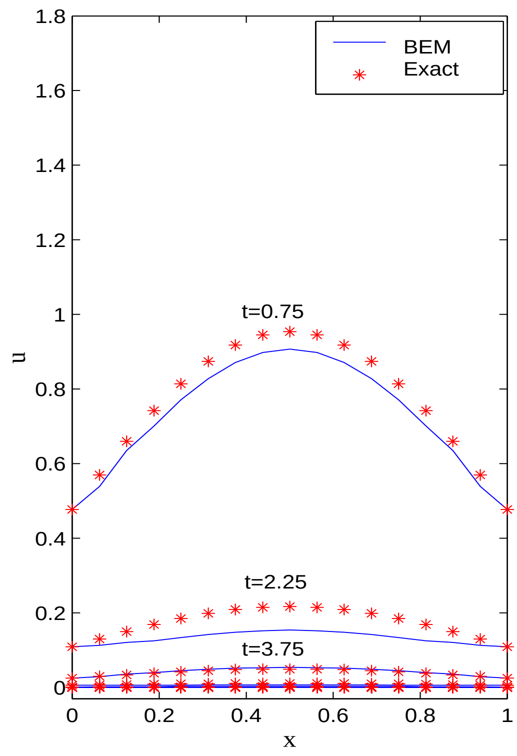

Figure 2.8: Solution of diffusion problem at $y = 0.5$ with $\Delta t = 1.5$ on $[0, 30]$.

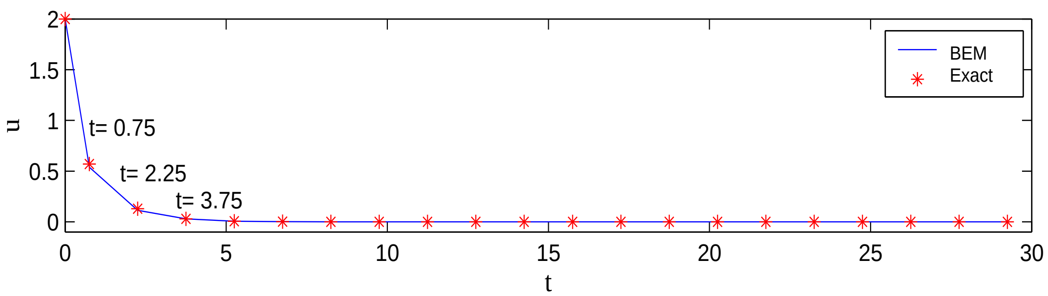

Figure 2.9: Solution of diffusion problem at $(x, y) = (0.5, 0.5)$ with $\Delta t = 1.5$ on $[0, 30]$.

2.7.2 Wave problem

The scalar wave equation (2.74) with velocity $c = 0.1$ in a square region $[0, 1] \times [0, 1]$ is solved with the initial conditions

$$\begin{aligned} &u(x, y, 0) = (x - x^2)(y - y^2), \qquad 0 \le x, y \le 1 \\ &\frac{\partial u}{\partial t}(x, y, 0) = 0, \qquad 0 \le x, y \le 1 \end{aligned} \tag{2.111}$$

and homogeneous Dirichlet boundary conditions, [31]. An infinite series solution is given by Sneddon [84],

$$u(x, y, t) = \sum_{l=1}^{\infty} \sum_{k=1}^{\infty} \frac{16}{\pi^6} \frac{1 - (-1)^l}{l^3} \frac{1 - (-1)^k}{k^3} \sin(l\pi x) \sin(k\pi y) \cos(\pi \sqrt{l^2 + k^2}\, ct). \tag{2.112}$$

In order to give a comparison between the series solution and the numerical solution, we compute the sum in (2.112) up to 100. The computations are carried out with $N = 20$ boundary elements. Figures 2.10 and 2.11 present the comparative solutions at a fixed point for increasing values of time with $\Delta t = 1.5$ on the time interval $[0, 30]$. The problem is symmetric with respect to the mid-plane $x = 0.5$ thus, we get the same results for the pairs $(x, y) = (0.25, 0.5)$, $(x, y) = (0.75, 0.5)$ and $(x, y) = (0.1, 0.5)$, $(x, y) = (0.9, 0.5)$. The agreement of the exact and BEM solutions is observed despite to the oscillations in both solutions.

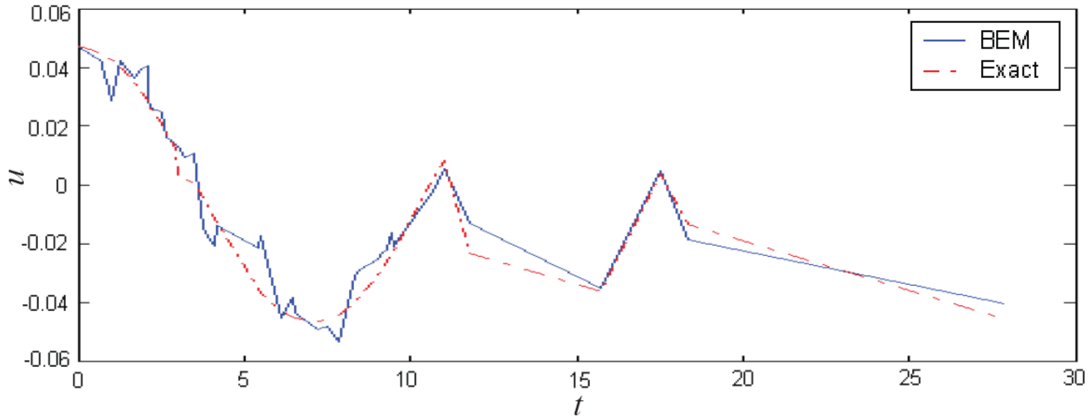

Figure 2.10: Solution of scalar wave equation at $(x, y) = (0.25, 0.5)$.

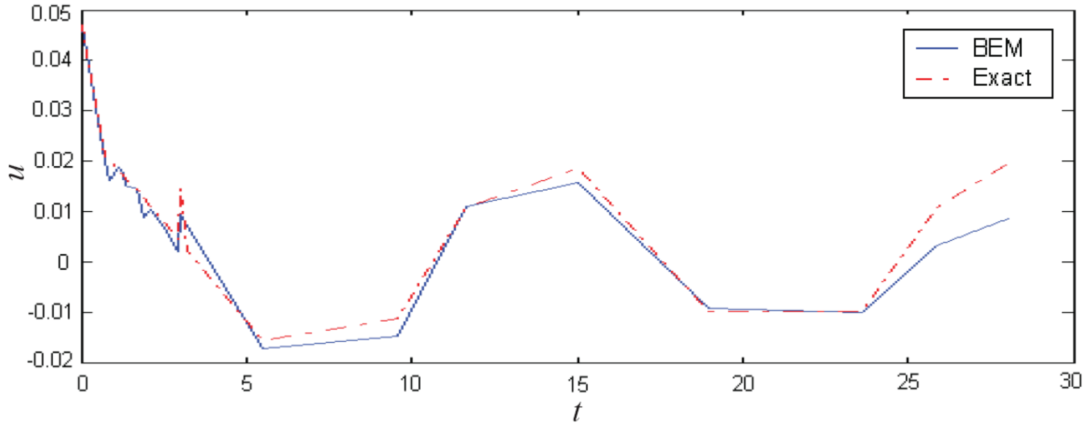

Figure 2.11: Solution of scalar wave equation at $(x, y) = (0.1, 0.5)$.

2.7.3 Convection-diffusion problem

We consider the problem defined with the convection-diffusion equation

$$\frac{\partial u}{\partial t} + \frac{1}{2}\frac{\partial u}{\partial x} + \frac{1}{2}\frac{\partial u}{\partial y} = \frac{1}{2}\nabla^2 u, \qquad (x, y) \in [0, 1] \times [0, 1], \quad t \geq 0 \tag{2.113}$$

subject to the initial and boundary conditions taken from the existing analytical solution (Chawla and Al-Zanaidi, [85])

$$u(x, y, t) = \frac{1}{\sqrt{s}} \exp(-50(x + y - t)^2/s) \tag{2.114}$$

where $\boldsymbol{x} = (x, y)$ and $s = 1 + 200\,t$.

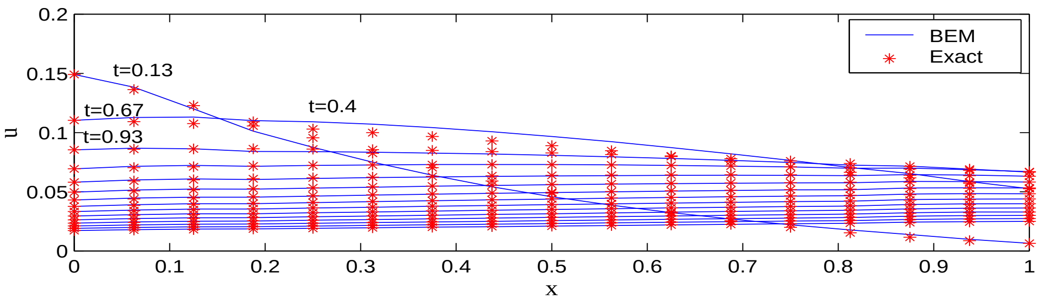

Figure 2.12: Solution of convection problem at $y = 0.5$ with $\Delta t = 0.27$ on $[0, 4]$.

Figures 2.12, 2.14 and 2.16 show the behaviour of the solution in comparison with the exact solution on the time intervals $[0, 4]$, $[0, 20]$ and $[0, 30]$, respectively. We divide the time intervals into $M = 15$ portions, so that we study with time increments $\Delta t = 0.27$, $\Delta t = 1.33$ and $\Delta t = 2.0$, in order. The boundary of the square region $[0, 1] \times [0, 1]$ is discretized by using $N = 12$ uniform and constant boundary elements. All the computations are carried out for $y = 0.5$ along $x-$direction. The behaviour of the solution at the centre point $(x, y) = (0.5, 0.5)$ is visualized in Figures 2.13, 2.15 and 2.17 for increasing time values on the time intervals $[0, 4]$, $[0, 20]$ and $[0, 30]$, respectively.

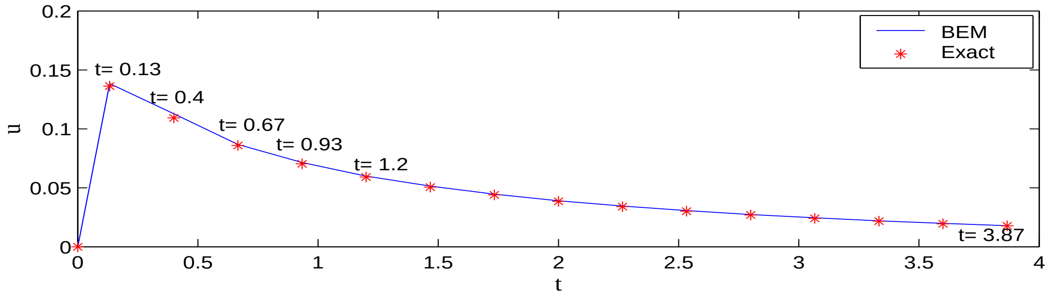

Figure 2.13: Solution of convection problem at $(x, y) = (0.5, 0.5)$ with $\Delta t = 0.27$ on $[0, 4]$.

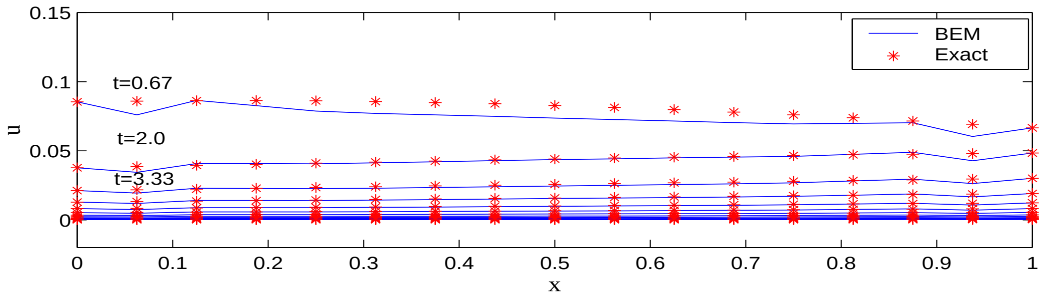

Figure 2.14: Solution of convection problem at $y = 0.5$ with $\Delta t = 1.33$ on $[0, 20]$.

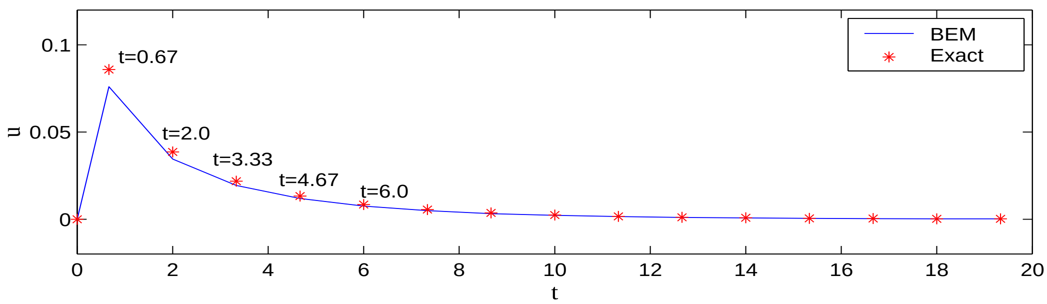

Figure 2.15: Solution of convection problem at $(x, y) = (0.5, 0.5)$ with $\Delta t = 1.33$ on $[0, 20]$.

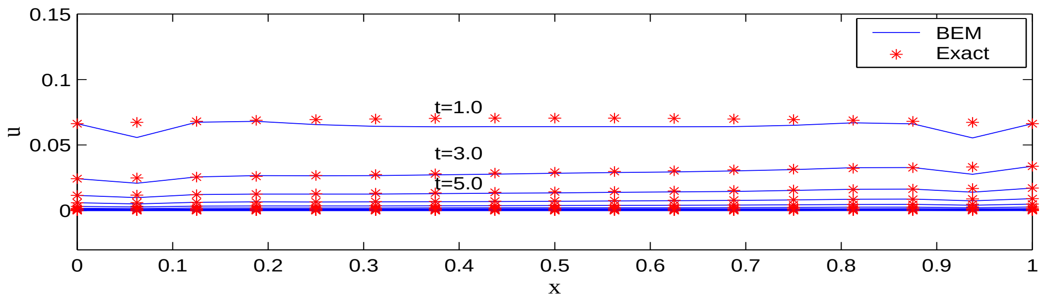

Figure 2.16: Solution of convection problem at $y = 0.5$ with $\Delta t = 2.0$ on $[0, 30]$.

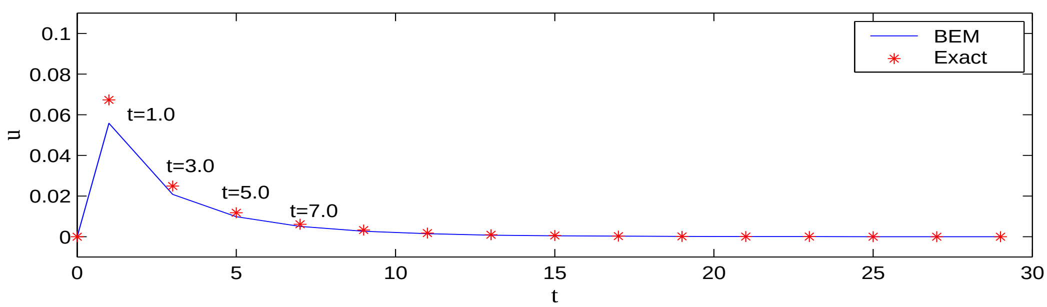

Figure 2.17: Solution of convection problem at $(x, y) = (0.5, 0.5)$ with $\Delta t = 2.0$ on $[0, 30]$.

The numerical results prove that the time-domain BEM is very capable to capture the behaviour of the solution at transient levels. One can note that very small number of boundary elements (e.g. $N = 12$) and quite large time increments (e.g. $\Delta t = 1.0, 2.0$) are used to reach such considerably accurate results.

The application of the time-domain BEM to the test problems shows that the algorithm suits very well for diffusion and convection-diffusion problems in the sense of good accuracy in comparison with the exact solutions. For scalar wave problem the accuracy is not as good as in the diffusion and convection-diffusion problems. This may be due to the second order time derivative which is also discretized by constant or linear variations in time direction. due to this weak accuracy in time-domain BEM solution of scalar wave problem, the procedure is not going to be continued with the elastodynamic problems which contain second order time derivatives. Instead, the applications are concentrated to nonlinear reaction-diffusion and MHD flow problems which are diffusion and convection-diffusion type equations.Thus, in Chapter 3, time-domain BEM is extended to nonlinear reaction-diffusion system of equations, MHD flow equations in rectangular ducts which are important applications from the physical point of view in engineering problems.

CHAPTER 3

TIME-DOMAIN BOUNDARY ELEMENT METHOD SOLUTIONS FOR THE SYSTEM OF NONLINEAR REACTION-DIFFUSION EQUATIONS AND MAGNETOHYDRODYNAMIC FLOW EQUATIONS

In this chapter, we employ the time-domain boundary element method to the system of nonlinear reaction-difusion equations, and magnetohydrodynamic (MHD) flow equations. The system of nonlinear reaction-diffusion equations are coupled time-dependent diffusion equations involving nonlinear reaction terms. In the time-domain BEM application, an iterative process is constructed between the governing equations of the system. The iteration is based on time and then the time-domain boundary integral equations are repeated for each time interval. Thus, this makes the difference from the time-domain BEM procedure presented in Chapter 2. Since the time variation of solution and its normal derivative is not known a priori, a time-stepping technique (not to be confused with usual finite difference one) has to be introduced for the numerical discretization of resulting boundary integral equation. The governing equations are still treated as a whole by using the time-dependent fundamental solution of diffusion equation, but the resulting system of boundary integral equations are solved for each time interval, iteratively. The iteration uses the previously obtained solutions to reach the next time level and consequently to steady-state. Therefore, the process is first tested on a single nonlinear reaction-diffusion equation to emphasize the validity of the method, and also to show the treatment of the nonlinear term, in detail. Then, the application is extended to the system of nonlinear reaction-diffusion equations in a circular region, and the Brusselator system as a new application.

In Section 3.3, the main application is given for the solution of the MHD flow problem in a duct with arbitrary wall conductivity. The two-dimensional MHD flow in channels are governed by coupled convection-diffusion type equations for the velocity and induced magnetic field. By making proper transformations, the equations can be decoupled into two homogeneous convection-diffusion type equations. When the walls of the duct are insulated, the boundary conditions can also be decoupled and therefore, two separate (convection-diffusion type) initial and boundary value problems (IBVP) are obtained, one for velocity field and the other for induced magnetic field only. Thus, the time-domain BEM based on a time iteration (as in Section 3.1) is applied to both of the problems separately. The unknown velocity and magnetic field values are obtained at each time level by assuming the previously obtained values as initial values for the next time interval. Thus, the application of time-domain BEM with time iteration process is first given on a convection-diffusion equation. This is different from the time-domain BEM application given in Chapter 2, which gives the solution in the whole time-domain at once. Then, it is extended to decoupled MHD equations for insulated wall case, since these equations are of the same type.

When the walls have arbitrary conductivity (i.e. the mixed type boundary conditions are imposed), the necessary transformations used for decoupling the equations, bring out coupled boundary conditions. Thus, it becomes quite difficult to treat the equations with standard BEM since the boundary conditions are not of the usual type required in BEM applications. However, a time-domain BEM procedure is developed for the first time in order to solve these unsteady MHD equations as a whole with coupled boundary conditions. This is one of the main contributions presented in this thesis. Due to the coupled boundary conditions, the total number of unknowns on the boundary is doubled, considering both function (solution) and its normal derivative as unknowns on the boundary. Thus, the resulting BEM systems (one for velocity and one for magnetic field) with coupled boundary conditions are arranged in such a way that we obtain a $2N \times 2N$ system of equations for one variable and its normal derivative, only. Then, the other variable and its normal derivative, which are coupled to the first ones with boundary conditions, are obtained on the boundary through the relation between them.

In both Sections 3.1 and 3.3 the main applications are supported by test problems having analytical solutions. The numerical results verify that the very well known characteristics of Brusselator system and MHD flow equations are caught. Particularly, Section 3.3 for unsteady MHD duct flow with arbitrary wall conductivity forms one of the original parts of this thesis.

3.1 Nonlinear Reaction-Diffusion Equations

In this section, a time-domain BEM solution, based on an iterative process in time, is presented for the nonlinear reaction-diffusion equation. We first give the solution procedure on a single nonlinear reaction-diffusion equation to emphasize the efficiency of the method. Then, it is extended to the nonlinear system of reaction-diffusion equations including Brusselator system. The nonlinear reaction terms are treated as nonhomogeneities, and computed by using previous time level solution, iteratively. We still take the advantage of using time-dependent fundamental solutions in the application of BEM. The time-domain BEM does not require another time integration scheme since the use of time-dependent fundamental solution allows one to apply BEM directly to the governing equations. Also, in contrast with finite difference schemes, the iterations can be carried with remarkably large time increments.

3.1.1 The nonlinear reaction-diffusion equation

We first consider solving nonlinear reaction-diffusion equation together with the initial and boundary conditions given below

$$
\begin{aligned}
&\frac{\partial u}{\partial t}(\boldsymbol{x},t) = \kappa\nabla^2 u(\boldsymbol{x},t) + f(u,\boldsymbol{x},t) && \boldsymbol{x}\in\Omega,\ t\geq 0, && \text{(3.1a)}\\
&u(\boldsymbol{x},0) = u_0(\boldsymbol{x}) && \boldsymbol{x}\in\Omega, && \text{(3.1b)}\\
&u(\boldsymbol{x},t) = \bar{u} && \boldsymbol{x}\in\Gamma_1,\ t\geq 0, && \text{(3.1c)}\\
&q(\boldsymbol{x},t) = \bar{q} && \boldsymbol{x}\in\Gamma_2,\ t\geq 0 && \text{(3.1d)}
\end{aligned}
$$

where $\Gamma = \Gamma_1+\Gamma_2$ is the boundary of the domain Ω, $q = \partial u/\partial n$ is the normal derivative of the potential u, and $\bar{u}$ and $\bar{q}$ are known values on the boundary for potential and flux values, respectively. f is the nonlinear function of u, $\boldsymbol{x}$ and t, and κ is the diffusivity constant.

The two-dimensional time-dependent fundamental solution of the homogeneous diffusion equation is given by

$$
u^*(\boldsymbol{\xi},\tau;\boldsymbol{x},t) = \frac{H[\tau-t]}{4\pi\kappa(\tau-t)}\exp\left(-\frac{|\boldsymbol{x}-\boldsymbol{\xi}|^2}{4\kappa(\tau-t)}\right) \tag{3.2}
$$

which is derived by taking the Fourier and inverse Fourier transforms of the linear diffusion equation (Section 2.3.1, equation (2.45)). Here, $\boldsymbol{\xi}$ and $\boldsymbol{x}$ are source and field points in $\Omega \subset \mathbb{R}^2$, and t and τ are time variation and maximum time level, respectively. And, H is the Heaviside function described as in Chapter 2, equation (2.56).

When the method of weighted residuals [13] is applied to problem (3.1) using u^* in (3.2) as a weight function, one can obtain the weighted residual statement below

$$
\begin{aligned}
&\underbrace{\int_0^\tau\int_\Omega\left(\nabla^2 u - \frac{1}{\kappa}\frac{\partial u}{\partial t}\right)u^*\,d\Omega\,dt}_{I} + \frac{1}{\kappa}\int_0^\tau\int_\Omega f(u,\boldsymbol{x},t)u^*\,d\Omega dt = \\
&\int_0^\tau\int_{\Gamma_2}\left(\frac{\partial u}{\partial n}-\bar{q}\right)u^*\,d\Gamma dt - \int_0^\tau\int_{\Gamma_1}\left(u-\bar{u}\right)q^*\,d\Gamma dt
\end{aligned} \tag{3.3}
$$

where $\boldsymbol{x} \in \Omega$ and $t \geq 0$ and $q^* = \partial u^*/\partial n$ which can be derived from (3.2) in the direction of the normal $\boldsymbol{n}$ of the boundary Γ as

$$q^* = \frac{\partial u^*}{\partial n} = \frac{-H[\tau - t]}{8\pi\kappa^2(\tau - t)^2} \exp\left(-\frac{|\boldsymbol{x} - \boldsymbol{\xi}|^2}{4\kappa(\tau - t)}\right) ((\boldsymbol{x} - \boldsymbol{\xi}).\boldsymbol{n}). \tag{3.4}$$

Now, we make use of Green's second identity for the part including Laplace term, and integration by parts for the time derivative to reduce the domain integral I into boundary integrals. Finally, as in Chapter 2, Section 2.4 the boundary integral equation equivalent to (3.3) can be obtained as,

$$\begin{aligned} c(\boldsymbol{\xi})u(\boldsymbol{\xi}, \tau) + \kappa \int_0^\tau \int_\Gamma u\, q^* d\Gamma\, dt &= \kappa \int_0^\tau \int_\Gamma q\, u^* d\Gamma\, dt \\ + \int_\Omega u^*(\boldsymbol{\xi}, \tau; \boldsymbol{x}, 0) u(\boldsymbol{x}, 0) d\Omega &+ \int_0^\tau \int_\Omega f(u, \boldsymbol{x}, t) u^* d\Omega\, dt. \end{aligned} \tag{3.5}$$

The nonlinearity lies now in the last time-domain integral in equation (3.5) due to the nonlinear function f of u. The domain and time-domain integrals containing the initial condition and the nonlinearity can not be transformed into boundary integrals. However, they are still able to be computed easily by using numerical integration. The nonlinear term $f(u, \boldsymbol{x}, t)$ is linearized by using the approximation of u which is obtained at the previous time level. Now, the boundary Γ is discretized into a series of constant boundary elements (N elements), and the time interval $[0, \tau]$ is partitioned into the subintervals, $[t_{m-1}, t_m]$ where $m = 1, \ldots, M$. Then, unlike the idea used for time direction in Chapter 2, each time block is considered as a new problem having the left end point 't_{m-1}' as the initial time and right end point 't_m' as the maximum time level (Figure 3.1). Then the integral equation (3.5) can be rewritten for each time interval as

$$\begin{aligned} c_i u_i^m + \kappa \sum_{n=1}^{N} \int_{\Gamma_n} \int_{t_{m-1}}^{t_m} u q_i^* dt d\Gamma &= \kappa \sum_{n=1}^{N} \int_{\Gamma_n} \int_{t_{m-1}}^{t_m} q u_i^* dt d\Gamma \\ + \underbrace{\int_\Omega u^*(\boldsymbol{\xi}_i, t_m; \boldsymbol{x}, t_{m-1}) u(\boldsymbol{x}, t_{m-1}) d\Omega}_{F_{1i}} &+ \underbrace{\int_\Omega \int_{t_{m-1}}^{t_m} f(u, \boldsymbol{x}, t) u^*(\boldsymbol{\xi}_i, t_m; \boldsymbol{x}, t) dt d\Omega}_{F_{2i}} \end{aligned} \tag{3.6}$$

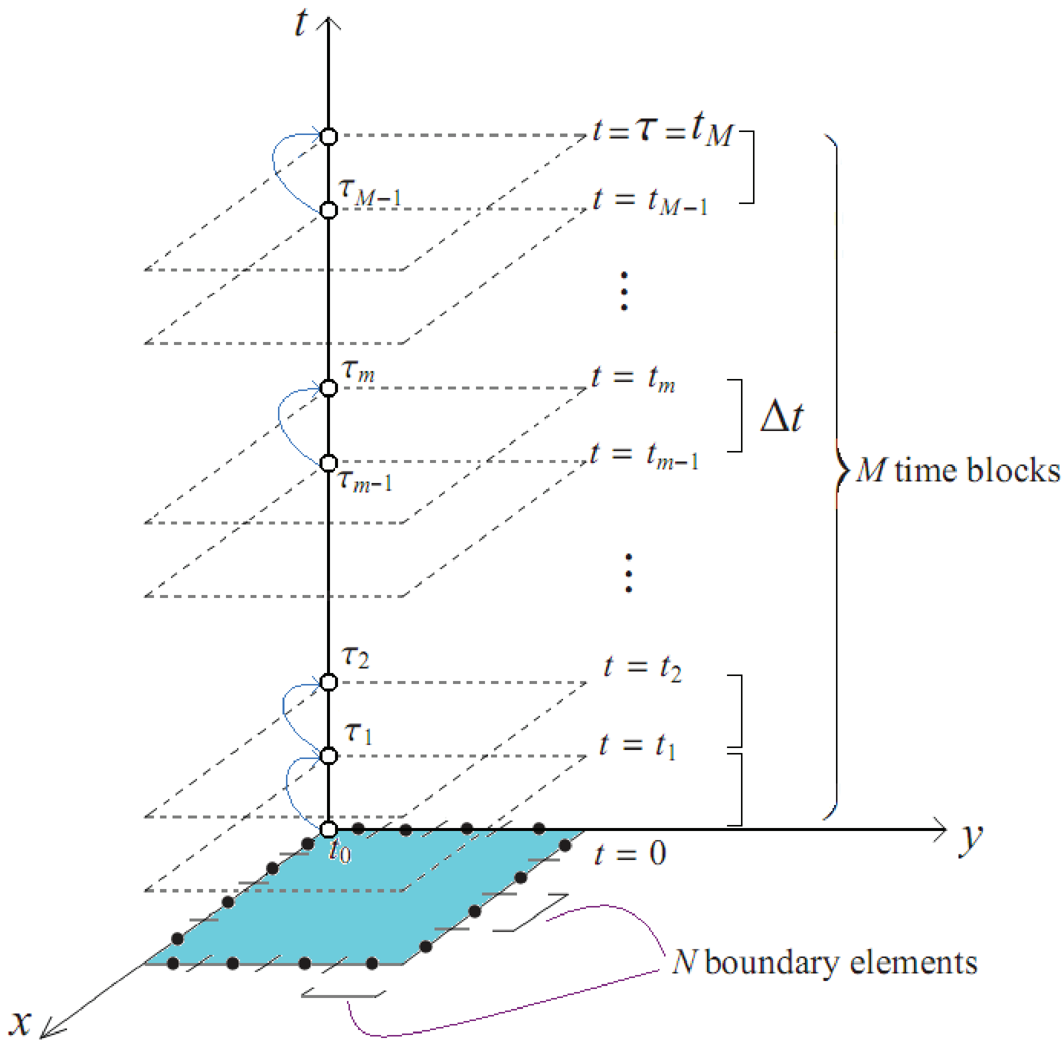

Figure 3.1: Time iteration giving $N \times N$ system for each time block.

for $i, n = 1, \ldots, N$. Note that $u(\boldsymbol{x}, t_{m-1})$ is taken to be the initial condition in each time interval $[t_{m-1}, t_m]$. For simplicity, we assume constant variations of both the solution u and its normal derivative q over boundary elements and time intervals. Thus, the approximations for the potential and its normal derivative are brought out as

$$u_n^m = u(\boldsymbol{\xi}_n, t_m) \approx u(\boldsymbol{x}, t)$$
$$q_n^m = q(\boldsymbol{\xi}_n, t_m) \approx q(\boldsymbol{x}, t) \tag{3.7}$$

where $\boldsymbol{\xi}_n$ represents the centre spatial coordinate of the $n - th$ boundary element and t_m is the upper end point of the time interval $[t_{m-1}, t_m]$, with the initial time t_{m-1}.

Then, with the approximations in (3.7) the final form of the integral equation can be rewritten as

$$c_i u_i^m + \kappa \sum_{n=1}^{N} u_n^m \int_{\Gamma_n} \left(\int_{t_{m-1}}^{t_m} q_i^* dt \right) d\Gamma = \kappa \sum_{n=1}^{N} q_n^m \int_{\Gamma_n} \left(\int_{t_{m-1}}^{t_m} u_i^* dt \right) d\Gamma + F_{1i} + F_{2i}. \tag{3.8}$$

In the case of constant boundary elements, the boundary is always smooth at the boundary nodes since each node accommodates at the centre of the corresponding boundary element. Hence, c_i is always $1/2$ on the boundary. Figure 3.2 presents configuration of the discretization for regular and irregular regions using $N = 16$ and $N = 12$ constant boundary elements.

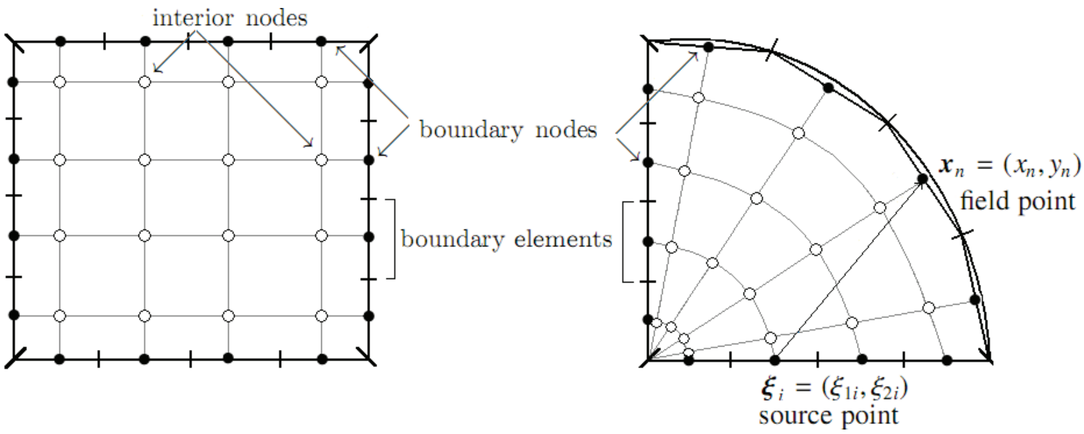

Figure 3.2: (a) Mesh in a square with $N = 16$ (b) Mesh in a quarter disk with $N = 12$.

Further, for each time block one can write an $N \times N$ linear system of algebraic equations by ranging $i, n = 1, \ldots, N$. This is different than the procedure presented in Chapter 2 which gives solution for the whole time domain at once. Thus, equation (3.8) leads to the matrix-vector form for vectors $\boldsymbol{u}$ and $\boldsymbol{q}$ containing unknown nodal values on the boundary Γ

$$\boldsymbol{Hu} - \boldsymbol{Gq} = \boldsymbol{R} \tag{3.9}$$

where the entries of the matrices $\boldsymbol{H}$ and $\boldsymbol{G}$, and the vector $\boldsymbol{R}$ are defined as

$$H_{in}^m = \kappa \int_{\Gamma_n} \int_{t_{m-1}}^{t_m} q_i^* dt d\Gamma_n + \frac{1}{2}\delta_{in}$$

$$G_{in}^m = \kappa \int_{\Gamma_n} \int_{t_{m-1}}^{t_m} u_i^* dt d\Gamma_n \tag{3.10}$$

$$R_i^m = F_{1i} + F_{2i}$$

with

$$F_{1i} = \int_{\Omega} u^*(\boldsymbol{\xi}_i, t_m; \boldsymbol{x}, t_{m-1}) u(\boldsymbol{x}, t_{m-1})\, d\Omega$$

$$F_{2i} = \int_{\Omega} \int_{t_{m-1}}^{t_m} f(u, \boldsymbol{x}, t) u^*(\boldsymbol{\xi}_i, t_m; \boldsymbol{x}, t)\, dt d\Omega. \tag{3.11}$$

The system (3.9) is going to be solved at each time interval $[t_{m-1}, t_m]$ using the newly obtained solution as initial value for the next time interval. The use of boundary conditions rearranges all the unknowns to be just on one side of the equation to obtain a system $\boldsymbol{AX} = \boldsymbol{Y}$, and we solve it for $\boldsymbol{X}$ by using Gauss elimination. The vector $\boldsymbol{X}$ contains either unknown u or its normal derivative nodal values on the boundary. Then, we use the computed boundary values to solve the problem inside the domain just by taking the coefficient $c_i = 1$, and leaving alone the term u_i^m on one side of the equation (3.8) i.e.

$$\boldsymbol{u_I} = \begin{bmatrix} u_1^m \\ u_2^m \\ \vdots \\ u_{IP}^m \end{bmatrix} = -\bar{\boldsymbol{H}}\boldsymbol{u_B} + \boldsymbol{G}\boldsymbol{q_B} + \boldsymbol{R} \tag{3.12}$$

$\boldsymbol{u_I}$ is the vector of internal nodal values with the entries, u_i^m, $i = 1, \ldots, IP$ where IP is the number of internal nodes. Similarly, $\boldsymbol{u_B}$ and $\boldsymbol{q_B}$ represent the vectors containing the boundary values of u and q as entries from 1 to N. Now, the contributions in the entries of $\bar{\boldsymbol{H}}$ and $\boldsymbol{G}$ matrices are from an interior node to a boundary element, i.e. the index i represents the interior nodes as the source point in the entries of the global system matrices which are described as

$$\bar{H}_{in}^{m} = \kappa \int_{\Gamma_n} \int_{t_{m-1}}^{t_m} q_i^* dt d\Gamma_n$$
$$G_{in}^{m} = \kappa \int_{\Gamma_n} \int_{t_{m-1}}^{t_m} u_i^* dt d\Gamma_n \tag{3.13}$$

where $i = 1, \ldots, IP$, and $n = 1 \ldots, N$. The nonlinearity in F_2 is overcome by approximating $f(u, \boldsymbol{x}, t)$ with the previously obtained value u^{m-1}, for the time step t_m at the point $\boldsymbol{x}$. Thus, nonlinear term is corrected during the time iteration process. In time-domain BEM, the domain integrals F_{1i} and F_{2i} can be evaluated numerically, either by using Gauss integrations or Monte Carlo method [24].

In the above described numerical procedure only the boundary of the domain is discretized and the solution is obtained at some required interior points. Thus, the resulting linear system of BEM equations is considerably small in size, compared to other domain discretization methods as FDM and Finite element method (FEM).

3.1.2 The time-domain BEM formulation of Brusselator system

Now, the proposed time-domain BEM procedure can be extended to the system of nonlinear reaction-diffusion equations. The numerical approach is given for the Brusselator system which is modeled mathematically as, [86]

$$\frac{\partial u}{\partial t} = B + u^2 v - (A+1)u + \alpha(\frac{\partial^2 u}{\partial x^2} + \frac{\partial^2 u}{\partial y^2}), \quad 0 < x, y < L, \quad t > 0$$
$$\frac{\partial v}{\partial t} = Au - u^2 v + \alpha(\frac{\partial^2 v}{\partial x^2} + \frac{\partial^2 v}{\partial y^2}), \quad 0 < x, y < L, \quad t > 0 \tag{3.14}$$

subject to the initial conditions

$$
\begin{aligned}
u(x,y,0) &= u_0(x,y), \qquad (x,y) \in \Omega \\
\upsilon(x,y,0) &= \upsilon_0(x,y), \qquad (x,y) \in \Omega
\end{aligned}
\tag{3.15}
$$

and the boundary conditions

$$
\begin{aligned}
&\frac{\partial u}{\partial x} = \frac{\partial \upsilon}{\partial x} = 0 \qquad \text{on the lines} \quad x = 0 \quad \text{and} \quad x = L \\
&\frac{\partial u}{\partial y} = \frac{\partial \upsilon}{\partial y} = 0 \qquad \text{on the lines} \quad y = 0 \quad \text{and} \quad y = L.
\end{aligned}
\tag{3.16}
$$

Here, $u = u(x,y,t)$ and $\upsilon = \upsilon(x,y,t)$ represent the concentrations of two, two-dimensional reaction products at time t. A and B are constant concentrations of two reagents, α is the diffusivity constant and L is the reactor length. Similar to the equation (3.8) the discretized boundary integral equations for the concentrations u and υ are derived as

$$
c_i u_i^m + \alpha \sum_{n=1}^{N} u_n^m \int_{\Gamma_n} \int_{t_{m-1}}^{t_m} \left(\frac{\partial u^*}{\partial n}\right)_i dt d\Gamma = \alpha \sum_{n=1}^{N} \left(\frac{\partial u}{\partial n}\right)_n^m \int_{\Gamma_n} \int_{t_{m-1}}^{t_m} u_i^* dt d\Gamma + F_{1i}^u + F_{2i}^u \tag{3.17}
$$

$$
c_i \upsilon_i^m + \alpha \sum_{n=1}^{N} \upsilon_n^m \int_{\Gamma_n} \int_{t_{m-1}}^{t_m} \left(\frac{\partial \upsilon^*}{\partial n}\right)_i dt d\Gamma = \alpha \sum_{n=1}^{N} \left(\frac{\partial \upsilon}{\partial n}\right)_n^m \int_{\Gamma_n} \int_{t_{m-1}}^{t_m} \upsilon_i^* dt d\Gamma + F_{1i}^\upsilon + F_{2i}^\upsilon \tag{3.18}
$$

where F_{li}^u and F_{li}^υ, $l = 1,2$ and $i = 1,\ldots,N$, represent the domain and time-domain integrals as in equation (3.6) for u and υ, respectively. The corresponding entries are described as

$$F^u_{1i} = \int_\Omega u^*(\boldsymbol{\xi}_i, t_m; \boldsymbol{x}, t_{m-1}) u(\boldsymbol{x}, t_{m-1}) d\Omega, \tag{3.19a}$$

$$F^u_{2i} = \int_\Omega \int_{t_{m-1}}^{t_m} f(u, \upsilon, \boldsymbol{x}, t)\, u^*(\boldsymbol{\xi}_i, t_m; \boldsymbol{x}, t) dt d\Omega, \tag{3.19b}$$

$$F^\upsilon_{1i} = \int_\Omega \upsilon^*(\boldsymbol{\xi}_i, t_m; \boldsymbol{x}, t_{m-1}) \upsilon(\boldsymbol{x}, t_{m-1}) d\Omega, \tag{3.19c}$$

$$F^\upsilon_{2i} = \int_\Omega \int_{t_{m-1}}^{t_m} g(u, \upsilon, \boldsymbol{x}, t)\, \upsilon^*(\boldsymbol{\xi}_i, t_m; \boldsymbol{x}, t) dt d\Omega. \tag{3.19d}$$

The fundamental solutions u^*, υ^* and their normal derivatives are actually the same, taken from equations (3.2) and (3.4), respectively. For the integral equation of u, $f(u, \upsilon, \boldsymbol{x}, t)$ corresponds to $B+u^2\upsilon-(A+1)u$ and for the integral equation υ, $g(u, \upsilon, \boldsymbol{x}, t)$ represents the nonlinearity $Au - u^2\upsilon$. Since the initial conditions for u and υ are provided, the final systems of algebraic equations for u and υ (similar to equation (3.9)) resulting from the integral Equations (3.17) and (3.18) are solved iteratively for reaching a required time level or steady-state. In the iterative process, the nonlinearities are computed by using previously obtained solution values. All the boundary integrals are computed numerically, by making use of Gauss quadrature. The domain (F_1) and time-domain (F_2) integrals appearing on the right side are also computed using numerical integration of Gauss type. For irregular boundaries we are still allowed to use numerical integration with a proper transformation to a regular region. Alternatively, Monte Carlo [24] technique can be adapted easily just by using all the discretization points (interior and boundary) as random integration points.

3.2 Numerical Results

3.2.1 Problem 1

First, we solve the two-dimensional nonlinear reaction-diffusion equation

$$\frac{\partial u}{\partial t} = \frac{1}{2}\left(\frac{\partial^2 u}{\partial x^2} + \frac{\partial^2 u}{\partial y^2}\right) + u^2(1-u), \qquad 0 < x, y < 1,\ t > 0 \tag{3.20}$$

subject to the initial and boundary conditions taken from the exact solution given by Chawla et al.[85],

$$u(x,y,t) = \frac{1}{1+e^{p(x+y-pt)}} \qquad \text{where} \quad p = \frac{1}{\sqrt{2}}. \tag{3.21}$$

Equation (3.20) is a diffusion type equation with the nonlinear term $f(u) = u^2(1-u)$. The time-domain BEM formulation along each time interval $[t_{m-1}, t_m]$ is given as

$$\begin{aligned} c_i u_i^m + \kappa \sum_{n=1}^{N} u_n^m \int_{\Gamma_n} \int_{t_{m-1}}^{t_m} q_i^* dt\, d\Gamma &= \kappa \sum_{n=1}^{N} q_n^m \int_{\Gamma_n} \int_{t_{m-1}}^{t_m} u_i^* dt\, d\Gamma \\ &+ \int_{\Omega} u^*(\boldsymbol{\xi}_i, t_m; \boldsymbol{x}, t_{m-1}) u(\boldsymbol{x}, t_{m-1}) d\Omega + \int_{\Omega} \int_{t_{m-1}}^{t_m} f(u) u_i^* dt d\Omega \end{aligned} \tag{3.22}$$

for $i = 1, \ldots, N$ where $\kappa = 1/2$, and q and q^* are the normal derivatives of u and u^*, respectively.

The domain and time-domain integrals contain known terms $u(\boldsymbol{x}, t_{m-1})$ and $f(u)$ from the previous time level t_{m-1}. Thus, the last two terms of (3.22) can be approximated by

$$\int_{\Omega} u^*(\boldsymbol{\xi}_i, t_m; \boldsymbol{x}, t_{m-1}) u(\boldsymbol{x}, t_{m-1}) d\Omega \approx u_i^{m-1} \int_{\Omega} u^*(\boldsymbol{\xi}_i, t_m; \boldsymbol{x}, t_{m-1}) d\Omega \tag{3.23}$$

$$\int_{\Omega} \int_{t_{m-1}}^{t_m} f(u) u_i^* dt d\Omega \approx f(u_i^{m-1}) \int_{\Omega} \int_{t_{m-1}}^{t_m} u^*(\boldsymbol{\xi}_i, t_m; \boldsymbol{x}, t) dt d\Omega \tag{3.24}$$

$i = 1, \ldots, N$, and can be computed by using Gauss quadrature,

$$\int_{\Omega} u^*(\boldsymbol{\xi}_i, t_m; \boldsymbol{x}, t_{m-1}) d\Omega = \sum_{l=1}^{LG} \sum_{k=1}^{KG} \frac{1}{4}\, \omega_l \omega_k\, u^*(\boldsymbol{\xi}_i, t_m; (\boldsymbol{x_G})_{lk}, t_{m-1}) \tag{3.25}$$

$$\int_{\Omega} \int_{t_{m-1}}^{t_m} u^*(\boldsymbol{\xi}_i, t_m; \boldsymbol{x}, t) dt d\Omega = \sum_{n=1}^{NG} \sum_{l=1}^{LG} \sum_{k=1}^{KG} \frac{(t_m - t_{m-1})}{8} \omega_l \omega_k \omega_n\, u^*(\boldsymbol{\xi}_i, t_m; (\boldsymbol{x_G})_{lk}, (t_G)_n) \tag{3.26}$$

where LG, KG and NG are the numbers of Gauss Legendre points used in x, y and t directions, respectively. And, the new variables $\boldsymbol{x_G}$ and t_G are described as

$$(\boldsymbol{x_G})_{lk} = ((x_G)_l, (y_G)_k) = \left(\frac{1}{2}G_l + \frac{1}{2}, \frac{1}{2}G_k + \frac{1}{2}\right) \tag{3.27}$$

$$(t_G)_n = \frac{t_m - t_{m-1}}{2}G_n + \frac{t_m + t_{m-1}}{2} \tag{3.28}$$

where G_l, G_k and G_n are the Gauss Legendre points with the weights ω_l, ω_k and ω_n, respectively. The domain integral in equation (3.23) is computed once during the whole iteration process, however the time-domain integral has to be computed for each iteration due to the time integrals. This is not very expensive and time consuming since only 8 Gauss Legendre points are used in order to approximate the domain integral quite accurately. For time integration we need more Gauss Legendre points as N increases.

We present the numerical solution in comparison with the existing analytical solution to show the accuracy and the reliability of the current time-domain BEM. The results are obtained by using considerably small number of constant boundary elements ($N = 12, \ldots, 60$), and the time increment $\Delta t = 1.0$ or $\Delta t = 2.0$ until reaching steady-state solution with a tolerance 10^{-5}. Table 3.1 and 3.2 show absolute errors for several boundary element numbers at transient levels as well as at steady-state by using $\Delta t = 1.0$ and 2.0, respectively. One can notice the decrease of errors as N increases especially close to the steady-state.

Figures 3.3 and 3.4 show the good agreement with the exact solution at the centre point $(x, y) = (0.5, 0.5)$ for increasing values of time, from $t = 0$ to $t = 16$ with $\Delta t = 1.0$ and $\Delta t = 2.0$, respectively. In Figures 3.5 and 3.6, the numerical and exact solutions are visualized at the centre line $y = 0.5$ for $x \in [0, 1]$ by using $\Delta t = 1.0$ and 2.0, respectively. The curves, from bottom to top, represent the solutions up to time level $t = 16$. The time increments $\Delta t = 1.0$ and $\Delta t = 2.0$ are remarkably large compared to the other time integration schemes like FDM. Figures 3.7 and 3.8 give absolute error behaviour at steady-state for increasing values of N, again for $\Delta t = 1.0$

and 2.0, respectively. Although, there is a slight increase in the error when $\Delta t = 2.0$, is used the steady-state is reached with a number of iterations which is almost the half of the iterations used in the case $\Delta t = 1.0$. Thus, the corresponding computational cost is naturally decreased with larger Δt.

Table 3.1: Absolute errors at varying time levels for $\Delta t = 1.0$.

	N=12	N=20	N=28	N=36	N=44	N=60
t=1	0.0016	0.0033	0.0040	0.0045	0.0049	0.0056
t=2	0.0012	0.0040	0.0053	0.0063	0.0070	0.0081
t=4	0.0010	0.0049	0.0066	0.0079	0.0089	0.0103
t=7	0.0017	0.0009	0.0017	0.0022	0.0027	0.0034
t=10	0.0026	0.0006	0.0004	0.0002	0.0000	0.0003
t=14	0.0027	0.0010	0.0008	0.0008	0.0007	0.0005
t=16	0.0027	0.0010	0.0009	0.0008	0.0007	0.0006
CPU*	0.359375	2.4375	8.90625	23.1875	50.78125	180.6406

Table 3.2: Absolute errors at varying time levels for $\Delta t = 2.0$.

	N=12	N=20	N=28	N=36	N=44	N=60
t=2	0.0007	0.0002	0.0016	0.0024	0.0028	0.0034
t=4	0.0062	0.0053	0.0076	0.0089	0.0097	0.0108
t=6	0.0064	0.0057	0.0079	0.0091	0.0098	0.0108
t=8	0.0004	0.0002	0.0017	0.0025	0.0029	0.0034
t=10	0.0013	0.0020	0.0003	0.0004	0.0007	0.0011
t=12	0.0019	0.0026	0.0010	0.0004	0.0001	0.0002
t=14	0.0021	0.0028	0.0012	0.0006	0.0003	0.0001
t=16	0.0022	0.0029	0.0013	0.0007	0.0004	0.0002
CPU*	0.328125	1.9375	6.84375	18.75	41.54688	151.2188

*CPU shows the computer usage time in seconds.

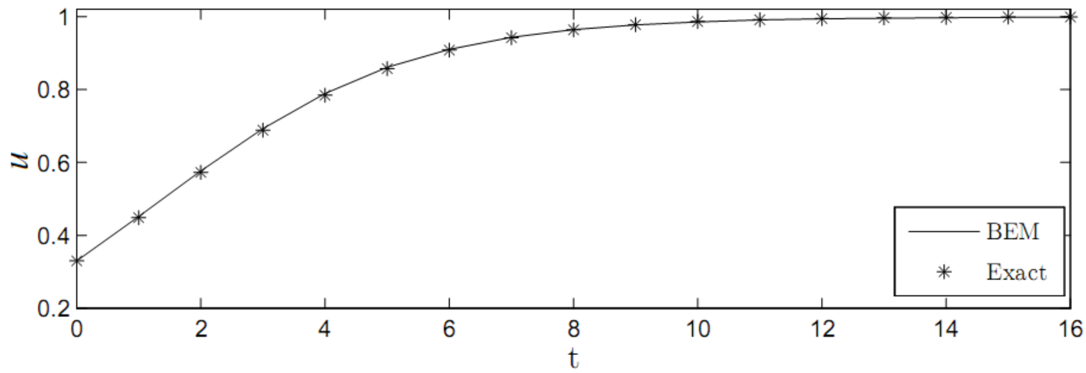

Figure 3.3: The solution u versus time at $(x, y) = (0.5, 0.5)$ with $\Delta t = 1.0$ and $N = 20$.

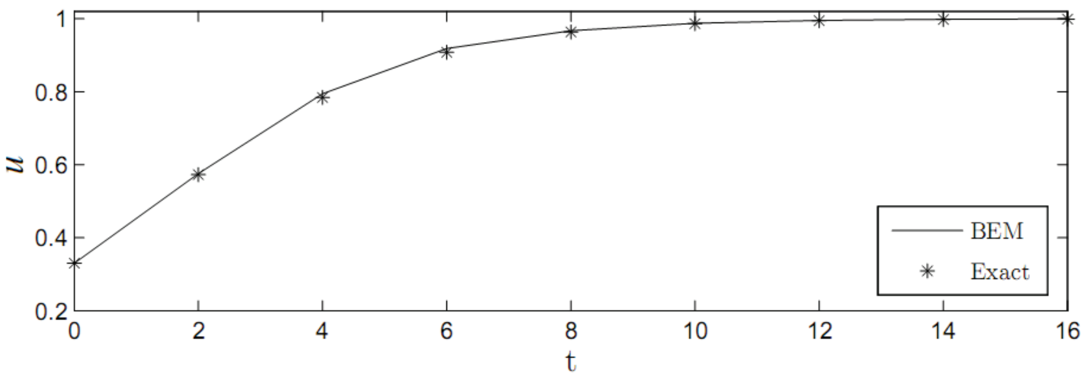

Figure 3.4: The solution u versus time at $(x, y) = (0.5, 0.5)$ with $\Delta t = 2.0$ and $N = 20$.

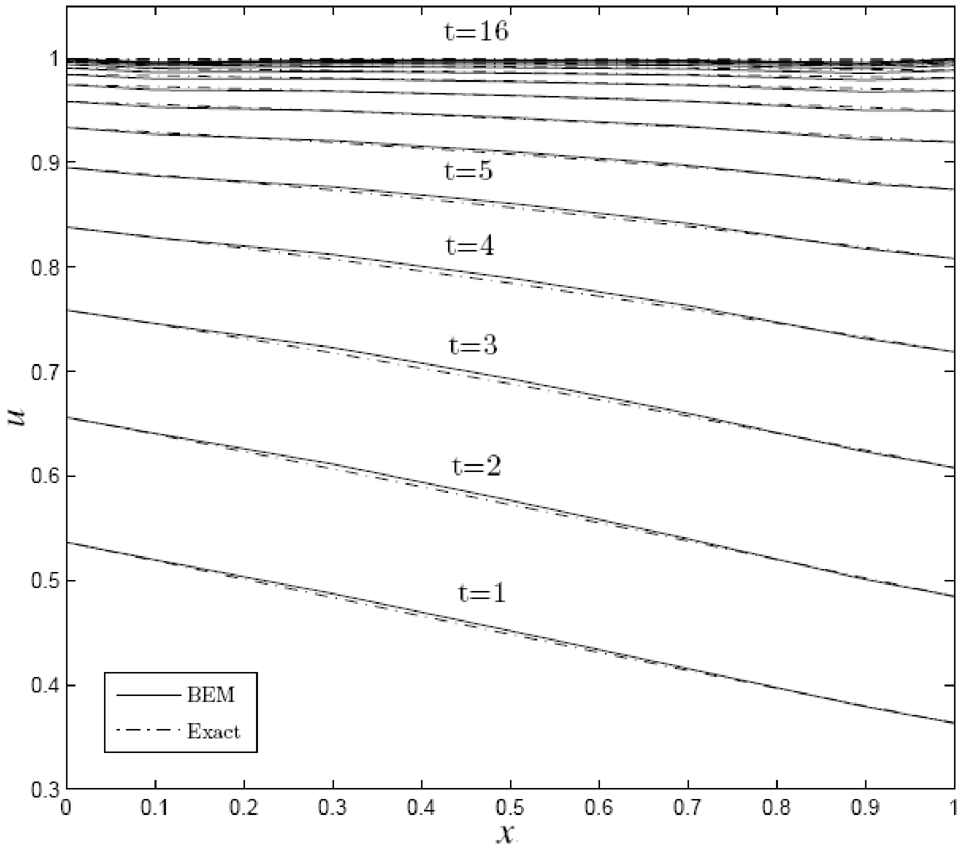

Figure 3.5: The solution u at $y = 0.5$ for increasing time levels with $\Delta t = 1.0$ and $N = 20$.

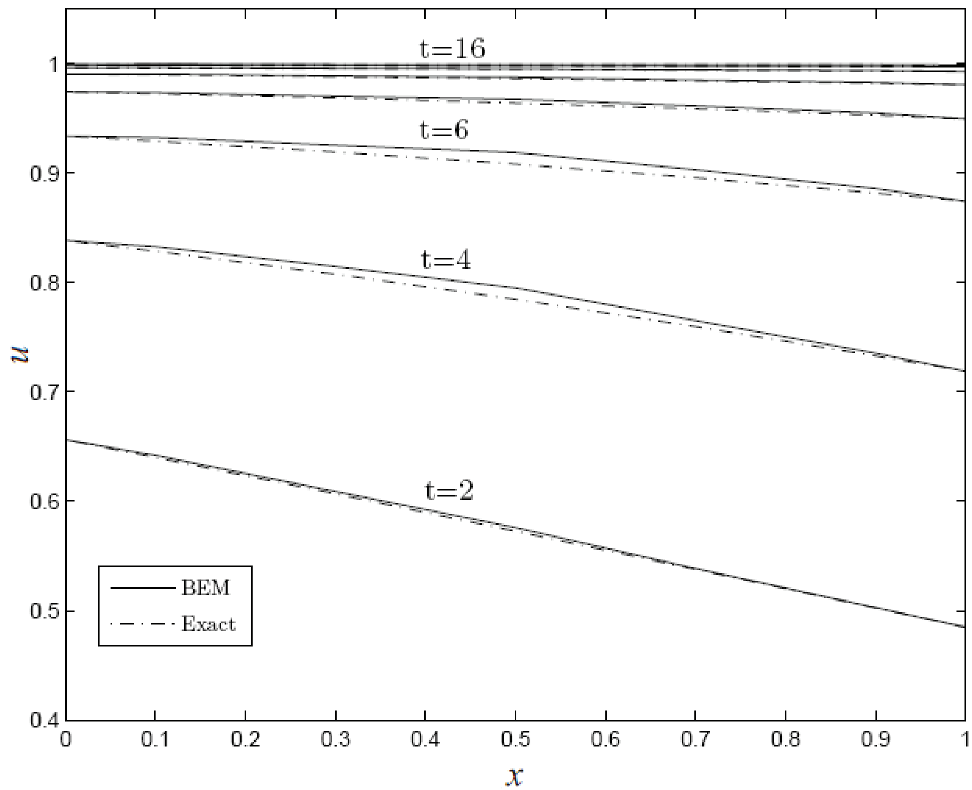

Figure 3.6: The solution u at $y = 0.5$ for increasing time levels with $\Delta t = 2.0$ and $N = 20$.

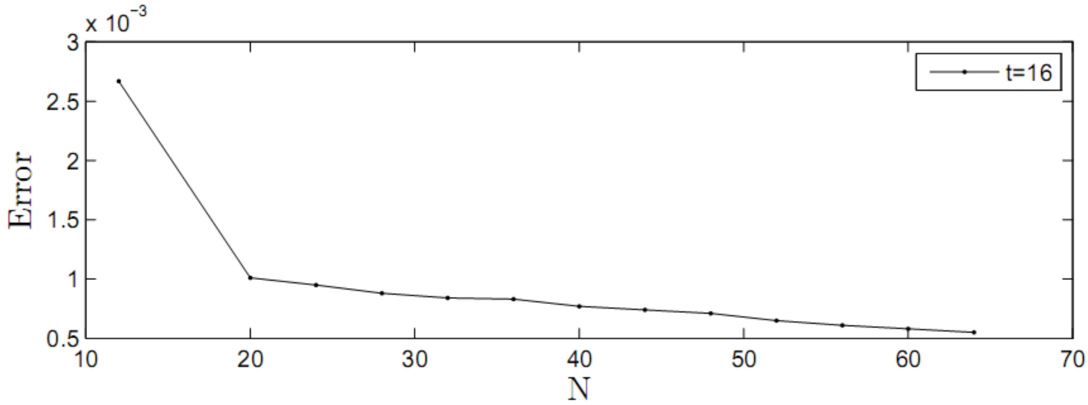

Figure 3.7: Absolute error versus N at steady-state $t = 16$ with $\Delta t = 1$.

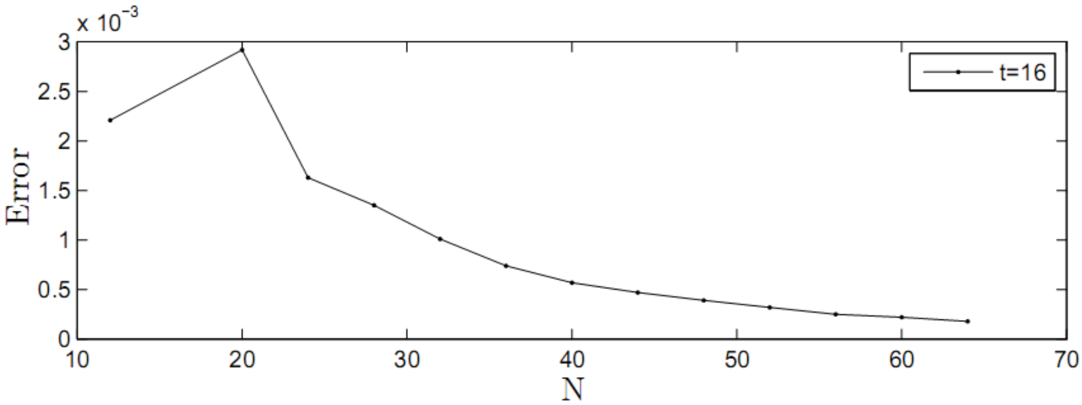

Figure 3.8: Absolute error versus N at steady-state $t = 16$ with $\Delta t = 2$.

3.2.2 Problem 2: Circular region

Consider the system of nonlinear reaction-diffusion equations

$$\begin{aligned} \frac{\partial u}{\partial t} &= u^2\,\upsilon - 2\,u + \frac{1}{4}\nabla^2 u \\ \frac{\partial \upsilon}{\partial t} &= u - u^2\,\upsilon + \frac{1}{4}\nabla^2 \upsilon \end{aligned} \tag{3.29}$$

defined in the quarter disk $\Omega = \{(x, y) \mid x^2 + y^2 \leq 1,\ x \geq 0,\ y \geq 0\}$. The initial and boundary conditions are selected to satisfy the exact solution of the profiles (u, υ), [58],

$$(u,\ \upsilon) = (\exp(-t/2 - x - y),\ \exp(t/2 + x + y)) \qquad \text{for} \quad t \geq 0. \tag{3.30}$$

When the time-domain BEM is applied to the system, the corresponding boundary integral discretizations of u and υ profiles are obtained as

$$\begin{aligned} c_i u_i^m \; &+ \frac{1}{4}\sum_{n=1}^{N} u_n^m \int_{\Gamma_n}\int_{t_{m-1}}^{t_m}\left(\frac{\partial u^*}{\partial n}\right)_i dt d\Gamma = \frac{1}{4}\sum_{n=1}^{N}\left(\frac{\partial u}{\partial n}\right)_n^m \int_{\Gamma_n}\int_{t_{m-1}}^{t_m} u_i^* dt d\Gamma \\ &+ \underbrace{\int_{\Omega} u^*(\boldsymbol{\xi}_i, t_m; \boldsymbol{x}, t_{m-1}) u(\boldsymbol{x}, t_{m-1}) d\Omega}_{F_{1i}^u} + \underbrace{\int_{\Omega}\int_{t_{m-1}}^{t_m} f(u, \upsilon) u^*(\boldsymbol{\xi}_i, t_m; \boldsymbol{x}, t) dt d\Omega,}_{F_{2i}^u} \end{aligned} \tag{3.31}$$

$$\begin{aligned} c_i \upsilon_i^m \; &+ \frac{1}{4}\sum_{n=1}^{N} \upsilon_n^m \int_{\Gamma_n}\int_{t_{m-1}}^{t_m}\left(\frac{\partial \upsilon^*}{\partial n}\right)_i dt d\Gamma = \frac{1}{4}\sum_{n=1}^{N}\left(\frac{\partial \upsilon}{\partial n}\right)_n^m \int_{\Gamma_n}\int_{t_{m-1}}^{t_m} \upsilon_i^* dt d\Gamma \\ &+ \underbrace{\int_{\Omega} \upsilon^*(\boldsymbol{\xi}_i, t_m; \boldsymbol{x}, t_{m-1}) \upsilon(\boldsymbol{x}, t_{m-1}) d\Omega}_{F_{1i}^\upsilon} + \underbrace{\int_{\Omega}\int_{t_{m-1}}^{t_m} g(u, \upsilon) \upsilon^*(\boldsymbol{\xi}_i, t_m; \boldsymbol{x}, t) dt d\Omega..}_{F_{2i}^\upsilon} \end{aligned} \tag{3.32}$$

The nonlinear terms are denoted by $f(u,\upsilon)$ and $g(u,\upsilon)$ for u and υ, respectively where

$$f(u,\upsilon) = u^2\upsilon - 2u, \tag{3.33}$$

$$g(u,\upsilon) = u - u^2\upsilon. \tag{3.34}$$

Since, the solution is based on the iteration in time between the two equations, the domain and time-domain integrals are approximated with the help of the previously obtained solutions for u and υ profiles. Thus, the domain and time-domain integrals are computed on each time interval $[t_{m-1}, t_m]$ as

$$F^u_{1i} \approx u_i^{m-1} \int_\Omega u^*(\boldsymbol{\xi}_i, t_m; \boldsymbol{x}, t_{m-1}) d\Omega, \tag{3.35}$$

$$F^\upsilon_{1i} \approx \upsilon_i^{m-1} \int_\Omega \upsilon^*(\boldsymbol{\xi}_i, t_m; \boldsymbol{x}, t_{m-1}) d\Omega, \tag{3.36}$$

$$F^u_{2i} \approx \left[(u_i^{m-1})^2 \upsilon_i^{m-1} - 2u_i^{m-1}\right] \int_\Omega \int_{t_{m-1}}^{t_m} u_i^* dt d\Omega, \tag{3.37}$$

$$F^\upsilon_{2i} \approx \left[u_i^m - (u_i^m)^2 \upsilon_i^{m-1}\right] \int_\Omega \int_{t_{m-1}}^{t_m} \upsilon_i^* dt d\Omega. \tag{3.38}$$

The definitions of the fundamental solutions u^* and υ^* are the same as given in equation (3.2). Thus, the domain and time-domain integrals appearing in Equations (3.35)-(3.38) are computed once for each iteration which decrease the computational cost.

As an alternative to the Gauss Legendre integration, the domain integrals are evaluated with Monte Carlo method, [24], which is more suitable for regions of more general geometries. By using the discretization nodes (taken either on the boundary or in the region) as randomly chosen numerical integration points, the corresponding integral approximations are obtained as,

$$\int_\Omega u^*(\boldsymbol{\xi}_i, t_m; \boldsymbol{x}, t_{m-1}) d\Omega \approx \frac{A(\Omega)}{N + IP} \sum_{l=1}^{N+IP} u^*(\boldsymbol{\xi}_i, t_m; \boldsymbol{x}_l, t_{m-1}), \tag{3.39}$$

$$\int_{\Omega}\int_{t_{m-1}}^{t_m} u^*(\boldsymbol{\xi}_i, t_m; \boldsymbol{x}, t)dtd\Omega \approx \frac{A(\Omega)}{N+IP}\sum_{l=1}^{N+IP}\sum_{n=1}^{NG}\frac{t_m - t_{m-1}}{2}\omega_n u^*(\boldsymbol{\xi}_i, t_m; \boldsymbol{x}_l, (t_G)_n). \tag{3.40}$$

where $N + IP$ is the total number of the boundary and interior nodes and NG is the number of Gauss Legendre points used in the discretization of the time integral. $(t_G)_n$ is the transformed value of t into $[-1, 1]$, due to Gauss Legendre integration, i.e.,

$$(t_G)_n = \frac{t_m - t_{m-1}}{2}G_n + \frac{t_m + t_{m-1}}{2} \tag{3.41}$$

and $\boldsymbol{x}_l = (x_l, y_l)$, $l = 1, \ldots, N + IP$, are the boundary and interior nodes chosen to discretize the domain as in Figure 3.2(b). And, $A(\Omega)$ represents the area of the given domain.

Figures 3.9 and 3.10 are obtained by using Monte Carlo technique for domain integrals. We also present Figure 3.11 and 3.12 which are obtained by using Gauss Legendre for the computation of the domain integrals. They all present the behaviour of the solutions of u and v profiles versus time t at $(x, y) = (0.5, 0.5)$, respectively. The computations are carried out by using $N = 24$ boundary elements and the time step is taken to be $\Delta t = 1.0$. It is seen from the figures that the numerical solution coincides with the existing analytical solution of the problem. It is found that the domain integral treatment with Monte Carlo technique gives more accurate results than Gauss Legendre for more general geometries.

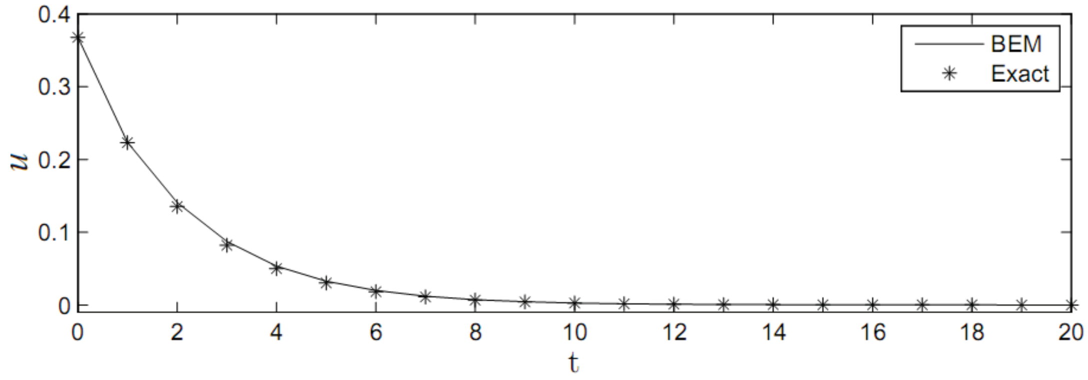

Figure 3.9: u profile versus t with $\Delta t = 1$, $N = 24$ at $(x, y) = (0.5, 0.5)$ for Problem 2, using Monte Carlo technique for domain integrals.

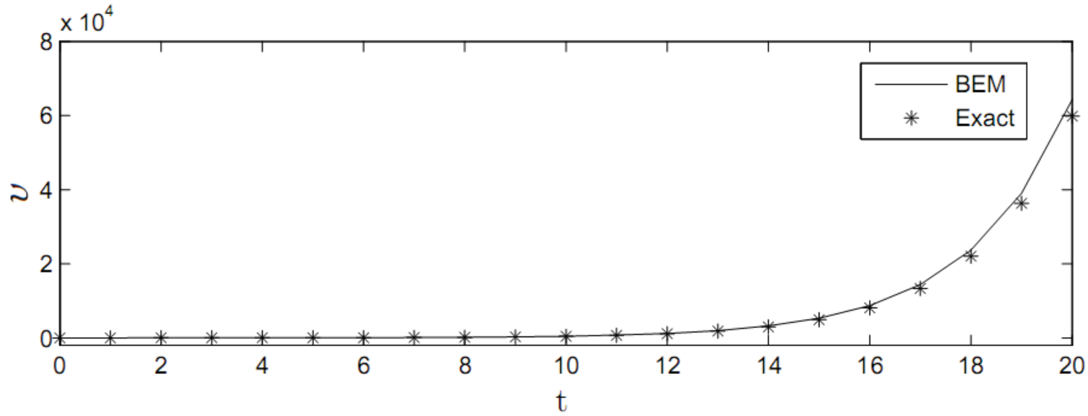

Figure 3.10: υ profile versus t with $\Delta t = 1$, $N = 24$ at $(x, y) = (0.5, 0.5)$ for Problem 2, using Monte Carlo technique for domain integrals.

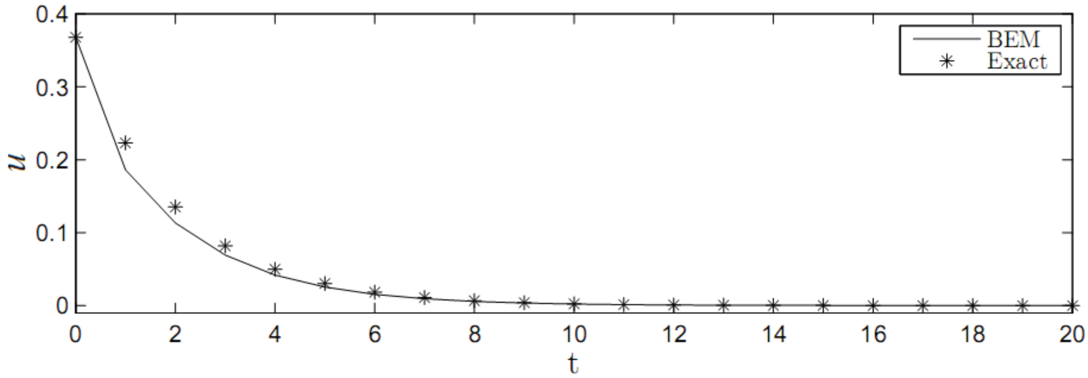

Figure 3.11: u profile versus t with $\Delta t = 1.0$, $N = 24$ at $(x, y) = (0.5, 0.5)$ for Problem 2.

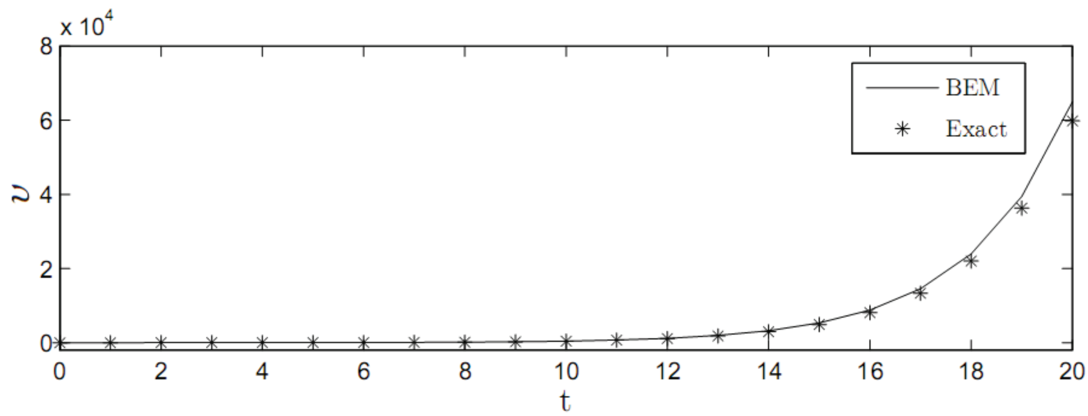

Figure 3.12: υ profile versus t with $\Delta t = 1.0$, $N = 24$ at $(x, y) = (0.5, 0.5)$ for Problem 2.

3.2.3 Problem 3: Brusselator System

The numerical results for the Brusselator system are obtained in a square region $[0, 1] \times [0, 1]$ with the parameters

$$L = 1, \quad A = 1/2, \quad B = 1, \quad \alpha = \frac{1}{500}$$

i.e., we have the governing equations

$$\frac{\partial u}{\partial t} = 1 + u^2 \upsilon - \frac{3}{2}u + \frac{1}{500}(\frac{\partial^2 u}{\partial x^2} + \frac{\partial^2 u}{\partial y^2}), \quad 0 < x, y < 1, \;\; t > 0 \tag{3.42}$$

$$\frac{\partial \upsilon}{\partial t} = \frac{1}{2}u - u^2 \upsilon + \frac{1}{500}(\frac{\partial^2 \upsilon}{\partial x^2} + \frac{\partial^2 \upsilon}{\partial y^2}), \quad 0 < x, y < 1, \;\; t > 0 \tag{3.43}$$

subject to the initial conditions

$$u(x, y, 0) = \frac{1}{2}x^2 - \frac{1}{3}x^3 \quad \text{and} \qquad \upsilon(x, y, 0) = \frac{1}{2}y^2 - \frac{1}{3}y^3$$

and the Neumann type boundary conditions

$$\frac{\partial u}{\partial x} = 0 \quad \text{and} \quad \frac{\partial \upsilon}{\partial x} = 0 \quad \text{on} \quad x = 0, \; x = 1,$$

$$\frac{\partial u}{\partial y} = 0 \quad \text{and} \quad \frac{\partial \upsilon}{\partial y} = 0 \quad \text{on} \quad y = 0, \; y = 1.$$

The discrete forms of the concentrations are obtained as

$$\begin{aligned} c_i u_i^m \quad &+ \frac{1}{500}\sum_{n=1}^{N} u_n^m \int_{\Gamma_n} \int_{t_{m-1}}^{t_m} \left(\frac{\partial u^*}{\partial n}\right)_i dt d\Gamma = \frac{1}{500}\sum_{n=1}^{N} \left(\frac{\partial u}{\partial n}\right)_n^m \int_{\Gamma_n} \int_{t_{m-1}}^{t_m} u_i^* dt d\Gamma \\ &+ \underbrace{\int_{\Omega} u^*(\boldsymbol{\xi}_i, t_m; \boldsymbol{x}, t_{m-1}) u(\boldsymbol{x}, t_{m-1}) d\Omega}_{F_{1i}^u} + \underbrace{\int_{\Omega} \int_{t_{m-1}}^{t_m} f(u, \upsilon) u^*(\boldsymbol{\xi}_i, t_m; \boldsymbol{x}, t) dt d\Omega,}_{F_{2i}^u} \end{aligned} \tag{3.44}$$

$$c_i\upsilon_i^m \quad + \frac{1}{500}\sum_{n=1}^{N}\upsilon_n^m\int_{\Gamma_n}\int_{t_{m-1}}^{t_m}\left(\frac{\partial\upsilon^*}{\partial n}\right)_i dtd\Gamma = \frac{1}{500}\sum_{n=1}^{N}\left(\frac{\partial\upsilon}{\partial n}\right)_n^m\int_{\Gamma_n}\int_{t_{m-1}}^{t_m}\upsilon_i^* dtd\Gamma$$

$$+ \underbrace{\int_{\Omega}\upsilon^*(\boldsymbol{\xi}_i, t_m; \boldsymbol{x}, t_{m-1})\upsilon(\boldsymbol{x}, t_{m-1})d\Omega}_{F_{1i}^{\upsilon}} + \underbrace{\int_{\Omega}\int_{t_{m-1}}^{t_m} g(u,\upsilon)\upsilon^*(\boldsymbol{\xi}_i, t_m; \boldsymbol{x}, t)dtd\Omega.}_{F_{2i}^{\upsilon}} \tag{3.45}$$

Here, the nonlinearities for u and υ are caused by the reaction terms

$$f(u,\upsilon) = 1 + u^2\upsilon - \frac{3}{2}u, \tag{3.46}$$

$$g(u,\upsilon) = \frac{1}{2}u - u^2\upsilon, \tag{3.47}$$

respectively. Therefore, the computations at the time level $t = t_m$ are carried out with the previously obtained values of the concentrations u^{m-1} and υ^{m-1}. Thus, the approximations of the domain (F_{1i}^u and F_{1i}^υ) and time-domain (F_{2i}^u and F_{2i}^υ) integrals can be represented as

$$F_{1i}^u \approx u_i^{m-1}\int_{\Omega}u^*(\boldsymbol{\xi}_i, t_m; \boldsymbol{x}, t_{m-1})d\Omega, \tag{3.48}$$

$$F_{1i}^\upsilon \approx \upsilon_i^{m-1}\int_{\Omega}\upsilon^*(\boldsymbol{\xi}_i, t_m; \boldsymbol{x}, t_{m-1})d\Omega, \tag{3.49}$$

$$F_{2i}^u \approx \left[1 + (u_i^{m-1})^2\upsilon_i^{m-1} - \frac{3}{2}u_i^{m-1}\right]\int_{\Omega}\int_{t_{m-1}}^{t_m} u_i^* dtd\Omega, \tag{3.50}$$

$$F_{2i}^\upsilon \approx \left[\frac{1}{2}u_i^m - (u_i^m)^2\upsilon_i^{m-1}\right]\int_{\Omega}\int_{t_{m-1}}^{t_m}\upsilon_i^* dtd\Omega. \tag{3.51}$$

As it is seen in equation (3.51), while solving equation (3.45) for υ, we use the newly obtained u values in the approximation of the nonlinear reaction term $g(u,\upsilon)$ in (3.47). Then, we solve the final linear system of equations (obtained by imposing the initial and boundary conditions to (3.44) and (3.45)), iteratively. The numerical solution of the problem is obtained for $N = 20$ boundary elements with $\Delta t = 0.8$. Thus, as in the case of previous problems, we are able to use such large time increment $\Delta t = 0.8$ as a result of the use of time-domain BEM. In Figures 3.13 and 3.14, we present the

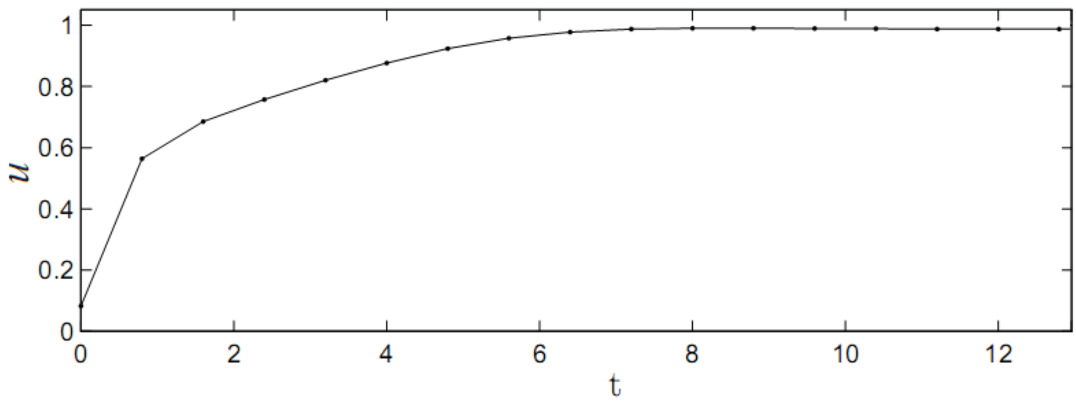

Figure 3.13: u profile versus time with $\Delta t = 0.8$, $N = 20$ at $(x, y) = (0.5, 0.5)$ for Problem 3.

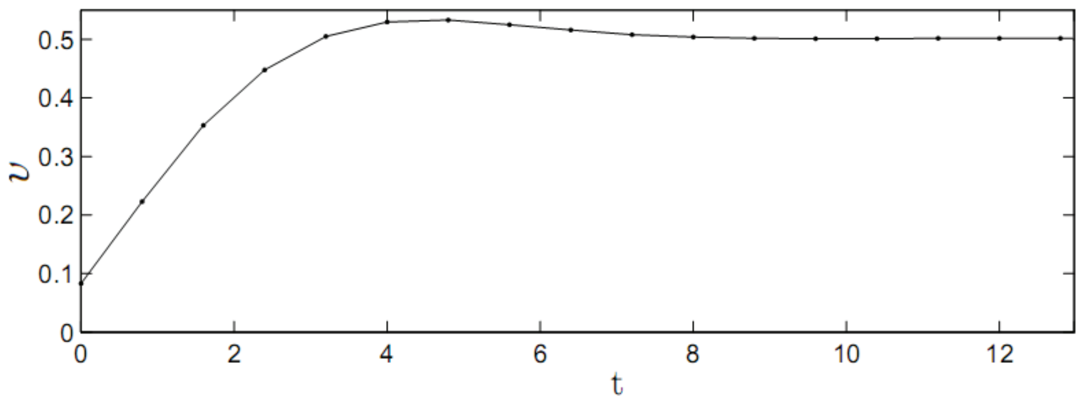

Figure 3.14: υ profile versus time with $\Delta t = 0.8$, $N = 20$ at $(x, y) = (0.5, 0.5)$ for Problem 3.

solution profiles u and υ at the centre point $(x, y) = (0.5, 0.5)$ for increasing values of time, and we see that the solutions reach steady-state around $t = 8$ with 10^{-5} accuracy. It is obvious that u and υ converge to B and A/B, respectively. This is a well known characteristic of this chemical system which can be compared with the solutions given by Twizell et al. [56], i.e. $(u, \upsilon) \to (B, A/B) = (1, 1/2)$ as is also mentioned by Ang [58].

3.3 Magnetohydrodynamic Flow in a Duct

In this section, the time-domain BEM is used to solve the two-dimensional convection-diffusion type equations. The emphasis is given on the solution of magnetohydrodynamic (MHD) duct flow problems, which are also governed by convection-diffusion type equations, with arbitrary wall conductivity. First, the time-domain BEM solution procedure is tested on some convection-diffusion problems and on the MHD duct flow problem with insulated walls, since the progress in time direction is different given in Chapter 2. The numerical results for these sample problems verify the efficiency of the method since they compare very well with the existing analytical solutions. Then, a time-domain BEM formulation of MHD duct flow problem with arbitrary wall conductivity is obtained for the first time in such a way that the equations are solved as a whole with the coupled boundary conditions. This approach is particularly well suited for transient analysis of unsteady MHD flow problems. The use of time-dependent fundamental solution enables one to obtain numerical solutions to this problem for Hartmann number values up to 300, and for several values of conductivity parameter.

3.3.1 Convection-Diffusion Equation

We first consider the time-dependent convection-diffusion problem governed by

$$\frac{\partial u(\boldsymbol{x},t)}{\partial t} + \mathbf{v}\cdot\nabla u(\boldsymbol{x},t) = \kappa\nabla^2 u(\boldsymbol{x},t)\,, \qquad \boldsymbol{x}\in\Omega\,,\ t>0 \tag{3.52}$$

subject to the initial condition

$$u(\boldsymbol{x},0) = u_0(\boldsymbol{x}) \qquad \text{at} \qquad t=0 \qquad \text{for} \qquad \boldsymbol{x}\in\Omega \tag{3.53}$$

and the given Dirichlet and Neumann type boundary conditions

$$
\begin{aligned}
u(\boldsymbol{x}, t) &= \bar{u}(\boldsymbol{x}, t) \qquad \text{on} \qquad \boldsymbol{x} \in \Gamma_1 \\
\frac{\partial u}{\partial n}(\boldsymbol{x}, t) &= \bar{q}(\boldsymbol{x}, t) \qquad \text{on} \qquad \boldsymbol{x} \in \Gamma_2.
\end{aligned}
\tag{3.54}
$$

Here, $\boldsymbol{x} = (x, y)$ are the the spatial coordinates, $\mathbf{v} = (\mathrm{v}_1, \mathrm{v}_2)$ are the velocity components of the flow and $\kappa = \dfrac{1}{Pe}$ is the diffusivity constant, Pe being the Péclet number. $\Gamma = \Gamma_1 + \Gamma_2$ is the boundary of the domain $\Omega \subset \mathbb{R}^2$ and $\boldsymbol{n} = (n_1, n_2)$ is the outward normal. $u_0(\boldsymbol{x})$, $\bar{u}(\boldsymbol{x}, t)$ and $\bar{q}(\boldsymbol{x}, t)$ are given functions.

As it is explained in Chapter 2, Section 2.6, one can derive the corresponding time-domain boundary integral equation (similar to equation (2.101) in Chapter 2) of the problem by making use of weighted residual method within integration by parts and Green's identities. Thus, the time-domain BEM formulation (in absence of external force) can be obtained as

$$
\begin{aligned}
c(\boldsymbol{\xi})u(\boldsymbol{\xi}, \tau) &+ \int_0^\tau \int_\Gamma \Big\{ \mathbf{v}_n\, u^*(\boldsymbol{\xi}, \tau; \boldsymbol{x}, t) + \kappa \frac{\partial u^*}{\partial n}(\boldsymbol{\xi}, \tau; \boldsymbol{x}, t) \Big\} u(\boldsymbol{x}, t) d\Gamma dt \\
&= \int_0^\tau \int_\Gamma \kappa\, u^*(\boldsymbol{\xi}, \tau; \boldsymbol{x}, t) \frac{\partial u}{\partial n}(\boldsymbol{x}, t) d\Gamma dt \\
&+ \int_\Omega u(\boldsymbol{x}, 0) u^*(\boldsymbol{\xi}, \tau; \boldsymbol{x}, 0) d\Omega
\end{aligned}
\tag{3.55}
$$

by using the two-dimensional time-dependent fundamental solution of convection-diffusion equation [35],

$$
u^*(\boldsymbol{\xi}, \tau; \boldsymbol{x}, t) = \frac{H[\tau - t]}{4\kappa\pi(\tau - t)} \exp\Big(- \frac{|\, \boldsymbol{x} - \boldsymbol{\xi} + \mathbf{v}\,(\tau - t)\,|^2}{4\kappa(\tau - t)} \Big) \tag{3.56}
$$

where $\boldsymbol{\xi} = (\xi_1, \xi_2)$ and $\boldsymbol{x} = (x, y)$ are the source (fixed) and field (variable) points in Ω, τ and t are the maximum time and time variation, respectively. H denotes the Heaviside function.

Now, we construct an iteration based on time by dividing the time interval $[0, \tau]$ into M subintervals and rewrite the equation (3.55) for each time interval $[t_{m-1}, t_m]$, $m =$

$1, \ldots, M$, so that we can adapt the method to the system of convection-diffusion type equations. The boundary Γ is discretized by using N constant boundary elements. Then, we assume constant variations for u and its normal derivative on each time step $[t_{m-1}, t_m]$ and along each boundary element Γ_n, $n = 1, \ldots, N$, such that

$$\begin{aligned} u_n^m &= u(\boldsymbol{\xi}_n, t_m) \approx u(\boldsymbol{x}, t) \\ \left(\frac{\partial u}{\partial n}\right)_n^m &= \frac{\partial u}{\partial n}(\boldsymbol{\xi}_n, t_m) \approx \frac{\partial u}{\partial n}(\boldsymbol{x}, t) \end{aligned} \tag{3.57}$$

where $\boldsymbol{\xi}_n$ denotes the center of the *n-th* boundary element. Then the integral equation (3.55) yields

$$\begin{aligned} c_i u_i^m + \sum_{n=1}^{N} u_n^m \int_{t_{m-1}}^{t_m} \int_{\Gamma_n} \left(\mathbf{v}_n \, u^*(\boldsymbol{\xi}_i, t_m; \boldsymbol{x}, t) + \kappa \frac{\partial u^*}{\partial n}(\boldsymbol{\xi}_i, t_m; \boldsymbol{x}, t) \right) d\Gamma_n dt \\ = \sum_{n=1}^{N} \left(\frac{\partial u}{\partial n}\right)_n^m \int_{t_{m-1}}^{t_m} \int_{\Gamma_n} \kappa \, u^*(\boldsymbol{\xi}_i, t_m; \boldsymbol{x}, t) \, d\Gamma_n dt \\ + \int_{\Omega} u(\boldsymbol{x}, t_{m-1}) u^*(\boldsymbol{\xi}_i, t_m; \boldsymbol{x}, t_{m-1}) d\Omega \end{aligned} \tag{3.58}$$

for one boundary node $\boldsymbol{\xi}_i$ and thus $c_i = \dfrac{1}{2}$. Now ranging i and n from 1 to N (for each fixed choice of source point $\boldsymbol{\xi}_i = (\xi_{1i}, \xi_{2i})$ from 1 to N and ranging the field point $\boldsymbol{x}_n = (x_n, y_n)$ also from 1 to N) we obtain an $N \times N$ linear system of algebraic equations

$$\boldsymbol{H}\,\boldsymbol{u} - \boldsymbol{G}\,\boldsymbol{q} = \boldsymbol{F} \tag{3.59}$$

with the vectors $\boldsymbol{u}$ and $\boldsymbol{q}$ formed with the nodal values u_i and q_i , $i = 1, \ldots, N$. This is the main difference from the time progress used in Chapter 2. We solve the smaller system (3.59) for each time block and use the previously obtained values at the time level t_{m-1} for the next iteration as starting values. The entries of the matrices $\boldsymbol{H}, \boldsymbol{G}$ and the vector $\boldsymbol{F}$ are given as

$$H_{in}^m = \int_{t_{m-1}}^{t_m} \int_{\Gamma_n} \left(\mathbf{v}_n \, u_i^* + \kappa \left(\frac{\partial u^*}{\partial n} \right)_i \right) d\Gamma_n dt + \frac{1}{2} \delta_{in}$$

$$G_{in}^m = \int_{t_{m-1}}^{t_m} \int_{\Gamma_n} \kappa \, u^*(\boldsymbol{\xi}_i, t_m; \boldsymbol{x}, t) \, d\Gamma_n dt \tag{3.60}$$

$$F_i = \int_{\Omega} u(\boldsymbol{x}, t_{m-1}) \, u^*(\boldsymbol{\xi}_i, t_m; \boldsymbol{x}, t_{m-1}) \, d\Omega$$

where

$$u_i^* = u^*(\boldsymbol{\xi}_i, t_m; \boldsymbol{x}, t)$$

and

$$\left(\frac{\partial u^*}{\partial n} \right)_i = \frac{\partial u}{\partial n}(\boldsymbol{\xi}_i, t_m; \boldsymbol{x}, t)$$

in two-dimensional space. δ is the Kronecker delta function described as in Chapter 2, Section 2.2, equation (2.24). The substitution of the given boundary conditions (3.54) into the equation (3.59) results in a linear system of equations

$$\boldsymbol{A}\boldsymbol{X} = \boldsymbol{Y} \tag{3.61}$$

which can be solved by Gauss elimination for the unknown vector $\boldsymbol{X}$. Here $\boldsymbol{X}$ contains the unknown u and $q = \dfrac{\partial u}{\partial n}$ values on the boundary. Then, these boundary values are used in the equation (3.58) by taking $c_i = 1$, to compute u values at each interior point, i.e.

$$u_i^m = - \sum_{n=1}^{N} \bar{H}_{in} \, u_n^m + \sum_{n=1}^{N} G_{in} \, q_n^m + F_i \tag{3.62}$$

where

$$\bar{H}_{in} = \int_{t_{m-1}}^{t_m} \int_{\Gamma_n} \left(\mathbf{v}_n \, u_i^* + \kappa \left(\frac{\partial u^*}{\partial n} \right)_i \right) d\Gamma_n dt.$$

Equation (3.62) generates the matrix-vector equation

$$\boldsymbol{u_I} = -\boldsymbol{H} \, \boldsymbol{u_B} + \boldsymbol{G} \, \boldsymbol{q_B} + \boldsymbol{F} \tag{3.63}$$

where $\boldsymbol{u_I}$ is the vector containing the interior nodal values u_i, $i = 1, \ldots, IP$ and $\boldsymbol{u_B}$, $\boldsymbol{q_B}$ contain the boundary values of u and q, respectively. This time the contributions in the entries (the distance $|\boldsymbol{x}_n - \boldsymbol{\xi}_i|$) will be from an interior node $\boldsymbol{\xi}_i = (\xi_{1i}, \xi_{2i})$ to the *n-th* boundary element. Therefore $\bar{\boldsymbol{H}}$, $\boldsymbol{G}$ are of size $IP \times N$ and $\boldsymbol{F}$ is of size $IP \times 1$. Thus, the required interior values are produced just by making simple matrix-vector calculations on the right hand side of equation (3.63).

Next section mainly emphasizes the solution of unsteady MHD flow problem in a rectangular duct with arbitrary wall conductivity. In addition to the applications of a single convection-diffusion equation (Section 3.3.1), also the unsteady MHD duct flow problem with insulated walls is included to establish the validity of the approach comparing the results with the existing analytical solution. For the MHD flow in a duct with arbitrary wall conductivity, the BEM formulation with time-dependent fundamental solution is presented for the two equations as a whole with coupled boundary conditions which is a new application, and forms one of the main points of this thesis. This approach is particularly well suited for transient analysis of unsteady MHD flow problems. And it is shown in numerical results that the well known characteristics of the behaviour of MHD flow together with wall conductivity effect can be visualized in terms of velocity and induced magnetic field graphs.

3.3.2 Governing Equations of MHD Duct Flow Problem

We consider the unsteady, laminar flow of an incompressible, viscous and electrically conducting fluid driven by a constant applied pressure gradient in a rectangular duct. The axis of the duct is chosen as the $z-$axis. A uniform magnetic field of strength (intensity, inductance) B_0 is imposed along the $x-$axis. The fluid motion is fully developed (i.e. the duct is assumed to be of infinite length and end-effects are neglected). It is assumed that the sides of the duct are electrically insulated or have variable conductivity.

The basic equations governing the MHD duct flow have been obtained from Maxwell' s equations of the electromagnetic field, Ohm' s law, equation of continuity and the Navier-Stokes equations [60]. There is only one component $V_z(x, y, t)$ of the velocity field and one component $B_z(x, y, t)$ of the induced magnetic field in the $z-$direction. All physical quantities except pressure are independent of z, the magnetic field vector takes the form $B = (B_0,\ 0,\ B_z(x, y, t))$. We also assume that displacement currents are negligible. Thus, the $z-$components of the governing equations become

$$\begin{aligned} \nabla^2 B_z + \sigma\mu_e B_0 \frac{\partial V_z}{\partial x} &= 0 \\ \mu\nabla^2 V_z + \frac{B_0}{\mu_e}\frac{\partial B_z}{\partial x} &= \frac{\partial p}{\partial z} \end{aligned} \tag{3.64}$$

where σ, μ are the electrical conductivity and the coefficients of viscosity of the fluid, respectively. μ_e is the magnetic permeability and p is the pressure. So, the partial differential equations (in nondimensional form) in terms of velocity $V(x, y, t)$ and induced magnetic field $B(x, y, t)$ are

$$\begin{aligned} \nabla^2 V + Ha\frac{\partial B}{\partial x} &= -1 + \frac{\partial V}{\partial t} \\ \nabla^2 B + Ha\frac{\partial V}{\partial x} &= \frac{\partial B}{\partial t} \end{aligned} \tag{3.65}$$

where nondimensionalization was performed with a characteristic length L_0 and a characteristic velocity V_0 (mean axis velocity). The dimensionless variables are

$$V = \frac{V_z}{V_0}, \quad B = \frac{\sigma\mu^{-1/2}\, B_z}{V_0\mu_e}, \quad V_0 = \frac{-L_0^2\frac{\partial p}{\partial z}}{\mu}$$

and Ha is the Hartmann number given by

$$Ha = \frac{B_0 L_0\sqrt{\sigma}}{\sqrt{\mu}}.$$

Now, the time-domain BEM approach is used to solve the unsteady MHD flow problem in a square duct with either insulating walls or with variable conductivity on the walls. First, we present the BEM application to the unsteady MHD flow problem in a square duct with insulated walls which has an exact solution.

3.3.3 MHD flow in a rectangular duct with insulated walls

The nondimensional equations of the unsteady, laminar, viscous flow of an incompressible and electrically conducting fluid, in terms of the velocity V and the induced magnetic field B are

$$\begin{aligned} \nabla^2 V + Ha\frac{\partial B}{\partial x} &= -1 + \frac{\partial V}{\partial t} \\ \nabla^2 B + Ha\frac{\partial V}{\partial x} &= \frac{\partial B}{\partial t} \end{aligned} \tag{3.66}$$

in the rectangular section Ω of a duct with the boundary and initial conditions

$$\begin{aligned} &V(x,y,t) = 0, \qquad B(x,y,t) = 0 \qquad (x,y) \in \partial\Omega\,,\ t \geq 0 \\ &V(x,y,0) = 0, \qquad B(x,y,0) = 0 \qquad (x,y) \in \Omega\,. \end{aligned} \tag{3.67}$$

If we make the change of variables

$$U_1 = V + B, \qquad U_2 = V - B \tag{3.68}$$

the MHD equations in (3.66) can be decoupled as

$$\begin{aligned} \nabla^2 U_1 + (Ha)\frac{\partial U_1}{\partial x} &= -1 + \frac{\partial U_1}{\partial t} \\ \nabla^2 U_2 - (Ha)\frac{\partial U_2}{\partial x} &= -1 + \frac{\partial U_2}{\partial t} \end{aligned} \qquad (x,y,t) \in \Omega \times [0,\infty) \tag{3.69}$$

with the corresponding boundary and initial conditions

$$\begin{aligned} &U_1(x,y,t) = 0 \qquad U_2(x,y,t) = 0 \qquad (x,y) \in \partial\Omega \\ &U_1(x,y,0) = 0 \qquad U_2(x,y,0) = 0 \qquad (x,y) \in \Omega. \end{aligned} \tag{3.70}$$

A further simplification by the transformations

$$(Ha)U_1 = (Ha)W_1 - x, \qquad (Ha)U_2 = (Ha)W_2 + x \tag{3.71}$$

results in two separate initial and boundary value problems

$$\begin{cases} \dfrac{\partial W_1}{\partial t} - Ha\dfrac{\partial W_1}{\partial x} = \nabla^2 W_1 \quad \text{in } \Omega \\ \\ W_1(x,y,t) = \dfrac{x}{Ha} \quad \text{on } \partial\Omega \\ \\ W_1(x,y,0) = \dfrac{x}{Ha} \quad \text{in } \Omega \end{cases} \qquad \begin{cases} \dfrac{\partial W_2}{\partial t} + Ha\dfrac{\partial W_2}{\partial x} = \nabla^2 W_2 \quad \text{in } \Omega \\ \\ W_2(x,y,t) = -\dfrac{x}{Ha} \quad \text{on } \partial\Omega \\ \\ W_2(x,y,0) = -\dfrac{x}{Ha} \quad \text{in } \Omega. \end{cases} \tag{3.72}$$

Now, the BEM approach in Section 3.3.1 can be applied to these convection-diffusion type problems. The decoupled equations in (3.72) can be weighted as

$$\begin{aligned} &\int_0^\tau \int_\Omega \Big(\frac{\partial W_1}{\partial t} - Ha\frac{\partial W_1}{\partial x} - \nabla^2 W_1 \Big) W_1{}^* d\Omega dt = 0 \\ &\int_0^\tau \int_\Omega \Big(\frac{\partial W_2}{\partial t} + Ha\frac{\partial W_2}{\partial x} - \nabla^2 W_2 \Big) W_2{}^* d\Omega dt = 0 \end{aligned} \tag{3.73}$$

where $W_1{}^*$ and $W_2{}^*$ are the corresponding time-dependent fundamental solutions as in (3.56), i.e.

$$\begin{aligned} W_1{}^*(\boldsymbol{\xi}, \tau; \boldsymbol{x}, t) &= \frac{H[\tau - t]}{4\pi(\tau - t)} \exp\Big(- \frac{|\,\boldsymbol{x} - \boldsymbol{\xi} + \mathbf{v}\,(\tau - t)\,|^2}{4(\tau - t)} \Big) \\ W_2{}^*(\boldsymbol{\xi}, \tau; \boldsymbol{x}, t) &= \frac{H[\tau - t]}{4\pi(\tau - t)} \exp\Big(- \frac{|\,\boldsymbol{x} - \boldsymbol{\xi} + \widetilde{\mathbf{v}}\,(\tau - t)\,|^2}{4(\tau - t)} \Big) \end{aligned} \tag{3.74}$$

which are only differing in the velocity components $\mathbf{v} = (-Ha, 0)$ and $\widetilde{\mathbf{v}} = (Ha, 0)$ respectively. $\boldsymbol{\xi} = (\xi_1, \xi_2)$ and $\boldsymbol{x} = (x, y)$ are the source and field points in Ω. The source and field points vary from boundary nodes to boundary elements for the computations on the boundary however for the interior computations, the source point is chosen from the interior of the domain Ω.

Applying integration by parts and Green's second identity to the equations in (3.73) one can obtain the boundary integral equations

$$
\begin{aligned}
c(\boldsymbol{\xi})W_1(\boldsymbol{\xi},\tau) + \int_0^\tau \int_\Gamma \Big(\mathbf{v}_n W_1^* + \frac{\partial W_1^*}{\partial n}\Big) W_1(\boldsymbol{x},t) d\Gamma dt \\
= \int_0^\tau \int_\Gamma W_1^* \frac{\partial W_1}{\partial n}(\boldsymbol{x},t) d\Gamma dt \\
+ \int_\Omega W_1(\boldsymbol{x},0) W_1^*(\boldsymbol{\xi},\tau;\boldsymbol{x},0) d\Omega
\end{aligned}
\tag{3.75}
$$

$$
\begin{aligned}
c(\boldsymbol{\xi})W_2(\boldsymbol{\xi},\tau) + \int_0^\tau \int_\Gamma \Big(\widetilde{\mathbf{v}}_n W_2^* + \frac{\partial W_2^*}{\partial n}\Big) W_2(\boldsymbol{x},t) d\Gamma dt \\
= \int_0^\tau \int_\Gamma W_2^* \frac{\partial W_2}{\partial n}(\boldsymbol{x},t)\, d\Gamma dt \\
+ \int_\Omega W_2(\boldsymbol{x},0) W_2^*(\boldsymbol{\xi},\tau;\boldsymbol{x},0)\, d\Omega
\end{aligned}
\tag{3.76}
$$

where $\mathbf{v}_n = \mathbf{v}\cdot\boldsymbol{n} = -(Ha)\,n_1$ and $\widetilde{\mathbf{v}}_n = \widetilde{\mathbf{v}}\cdot\boldsymbol{n} = (Ha)\,n_1$ since the outward normal has the components $\boldsymbol{n} = (n_1, n_2)$.

Then, the discretization of the boundary with N constant boundary elements with the assumption of constant variations for W_1 and W_2 and their normal derivatives along each time interval $[t_{m-1}, t_m]$, gives the following discretized equations

$$
\begin{aligned}
c_i(W_1)_i^m + \sum_{n=1}^N (W_1)_n^m \int_{t_{m-1}}^{t_m} \int_{\Gamma_n} \Big(\mathbf{v}_n (W_1)_i^* + (\frac{\partial W_1^*}{\partial n})_i\Big) d\Gamma_n dt \\
= \sum_{n=1}^N \Big(\frac{\partial W_1}{\partial n}\Big)_n^m \int_{t_{m-1}}^{t_m} \int_{\Gamma_n} (W_1)_i^*\, d\Gamma_n dt \\
+ \int_\Omega W_1(\boldsymbol{x},t_{m-1}) W_1^*(\boldsymbol{\xi}_i, t_m; \boldsymbol{x}, t_{m-1})\, d\Omega
\end{aligned}
\tag{3.77}
$$

$$c_i(W_2)_i^m + \sum_{n=1}^{N}(W_2)_n^m \int_{t_{m-1}}^{t_m}\int_{\Gamma_n}\Big(\widetilde{\mathbf{v}}_n\,(W_2)_i^* + (\frac{\partial W_2^*}{\partial n})_i\Big)\,d\Gamma_n dt$$

$$= \sum_{n=1}^{N}\Big(\frac{\partial W_2}{\partial n}\Big)_i^m \int_{t_{m-1}}^{t_m}\int_{\Gamma_n}(W_2)_i^*\,d\Gamma_n dt \qquad (3.78)$$

$$+ \int_{\Omega} W_2(\boldsymbol{x}, t_{m-1})W_2^*(\boldsymbol{\xi}_i, t_m; \boldsymbol{x}, t_{m-1})\,d\Omega.$$

Thus, we obtain the $N \times N$ linear system of equations

$$\boldsymbol{H}\{W_1\} - \boldsymbol{G}\left\{\frac{\partial W_1}{\partial n}\right\} = \boldsymbol{F} \qquad (3.79)$$

$$\widetilde{\boldsymbol{H}}\{W_2\} - \widetilde{\boldsymbol{G}}\left\{\frac{\partial W_2}{\partial n}\right\} = \widetilde{\boldsymbol{F}} \qquad (3.80)$$

where the entries of the coefficient matrices $\boldsymbol{H}, \boldsymbol{G}, \widetilde{\boldsymbol{H}}, \widetilde{\boldsymbol{G}}$ and right hand side vectors $\boldsymbol{F}, \widetilde{\boldsymbol{F}}$ are similarly defined as in (3.60). $\{W_1\}, \{W_2\}, \left\{\frac{\partial W_1}{\partial n}\right\}, \left\{\frac{\partial W_2}{\partial n}\right\}$ are the vectors containing the nodal boundary values of $W_1, W_2, \frac{\partial W_1}{\partial n}, \frac{\partial W_2}{\partial n}$, respectively. The insulated boundary conditions $W_1 = \frac{x}{Ha}$ and $W_2 = \frac{-x}{Ha}$ are inserted to the systems (3.79) and (3.80) by rearranging the equations to include the known values to the right hand sides of the equations. This yields the linear system of algebraic equations

$$\boldsymbol{A}\boldsymbol{X} = \boldsymbol{Y} \qquad (3.81)$$

$$\widetilde{\boldsymbol{A}}\widetilde{\boldsymbol{X}} = \widetilde{\boldsymbol{Y}} \qquad (3.82)$$

equation (3.81) for W_1 and equation (3.82) for W_2. Therefore, $\boldsymbol{X}$ contains the unknown $\frac{\partial W_1}{\partial n}$ values and $\widetilde{\boldsymbol{X}}$ contains the unknown $\frac{\partial W_2}{\partial n}$ values on the boundary since W_1 and W_2 are already known on the boundary. All the known boundary information are combined with the vectors $\boldsymbol{F}$ and $\widetilde{\boldsymbol{F}}$, thus forming the right hand sides $\boldsymbol{Y}$ and $\widetilde{\boldsymbol{Y}}$. Hence, the solution of the final systems give the required unknowns $\frac{\partial W_1}{\partial n}$ and $\frac{\partial W_2}{\partial n}$ on the boundary. We take $c_i = 1$ in the discretized equations (3.77) and (3.78) in order to compute W_1 and W_2 at the interior points. Then one can obtain the original unknowns V and B by backward substitution through the transformations (3.71) and (3.68).

3.3.4 MHD Flow in a Rectangular Duct Having Variable Wall Conductivity

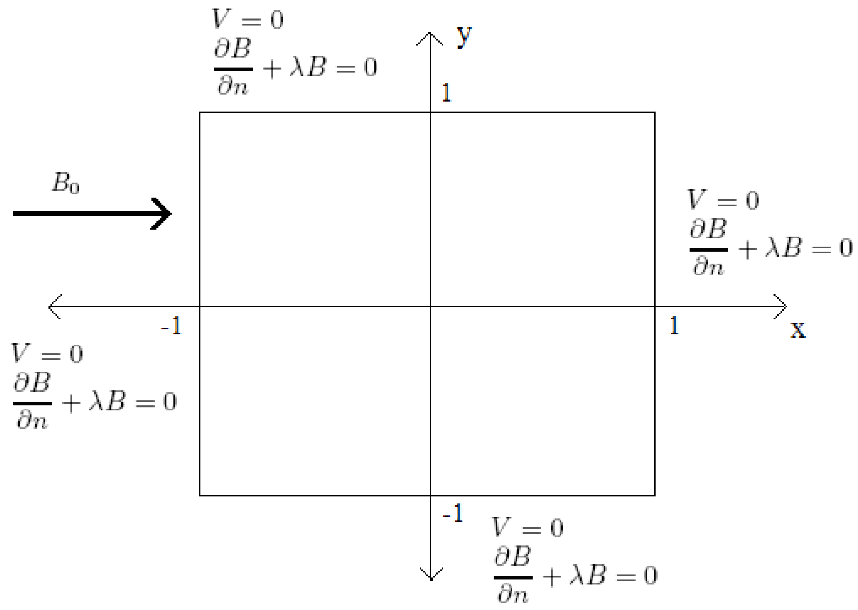

Figure 3.15: Square section of the duct with variable wall conductivity.

Having variable electrical conductivity on the walls of the duct means we have mixed type boundary conditions for the magnetic field, i.e.

$$\frac{\partial B}{\partial n} + \lambda B = 0 \tag{3.83}$$

on the boundary of the flow region shown in Figure 3.15. When $\lambda = 0$ the walls are perfectly conducting, when $\lambda \to \infty$ the walls are insulated. For the other values of $\lambda > 0$ the walls are having variable electrical conductivity. Therefore, this unsteady MHD duct flow problem is also defined by the nondimensional equations (3.66)

$$\begin{aligned} \nabla^2 V + Ha\frac{\partial B}{\partial x} &= -1 + \frac{\partial V}{\partial t} \\ \nabla^2 B + Ha\frac{\partial V}{\partial x} &= \frac{\partial B}{\partial t} \end{aligned} \tag{3.84}$$

with the zero initial conditions

$$V(x, y, 0) = 0, \qquad B(x, y, 0) = 0 \qquad\qquad (x, y) \in \Omega \tag{3.85}$$

and the zero boundary condition for velocity, and the mixed type boundary condition for the induced magnetic field

$$V(x, y, t) = 0, \qquad \frac{\partial B}{\partial n}(x, y, t) + \lambda B(x, y, t) = 0 \qquad\qquad (x, y) \in \partial\Omega,\ t \geq 0\,. \tag{3.86}$$

Now, using the transformations in (3.68) and (3.71) one can again obtain the decoupled form of the equations in (3.84) in terms of W_1 and W_2

$$\begin{aligned} \frac{\partial W_1}{\partial t} - Ha\frac{\partial W_1}{\partial x} - \nabla^2 W_1 &= 0 \\ \frac{\partial W_2}{\partial t} + Ha\frac{\partial W_2}{\partial x} - \nabla^2 W_2 &= 0 \end{aligned} \tag{3.87}$$

with the decoupled initial conditions

$$W_1(x, y, 0) = \frac{x}{Ha}, \qquad W_2(x, y, 0) = \frac{-x}{Ha} \qquad\qquad (x, y) \in \Omega. \tag{3.88}$$

But this time we have coupled boundary conditions such that

$$\left.\begin{aligned} &W_1 + W_2 = 0 \\ &\frac{\partial W_2}{\partial n} - \frac{\partial W_1}{\partial n} = \lambda(W_1 - W_2) - \frac{2}{Ha}\frac{\partial x}{\partial n} - 2\lambda\frac{x}{Ha} \end{aligned}\right\} \quad \text{on} \quad \partial\Omega \tag{3.89}$$

because of the mixed type boundary condition for the induced magnetic field.

However, we can still apply the BEM using the time-dependent fundamental solution to the resulting equations in (3.87) which are defining two convection-diffusion type equations. Thus, the BEM applications result in the same linear system of equations as (3.79) and (3.80),

$$\boldsymbol{H}\,\{W_1\} - \boldsymbol{G}\left\{\frac{\partial W_1}{\partial n}\right\} = \boldsymbol{F} \tag{3.90}$$

$$\widetilde{\boldsymbol{H}}\,\{W_2\} - \widetilde{\boldsymbol{G}}\left\{\frac{\partial W_2}{\partial n}\right\} = \widetilde{\boldsymbol{F}}. \tag{3.91}$$

Since the boundary conditions are coupled we do not know directly neither W_1 and W_2 nor their normal derivatives on the boundary. Therefore, the number of unknown values are doubled when compared with usual discretized BEM equations. Thus, the $N \times N$ systems in (3.90) and (3.91) can not be converted into $\boldsymbol{AX} = \boldsymbol{Y}$ and $\widetilde{\boldsymbol{A}}\widetilde{\boldsymbol{X}} = \widetilde{\boldsymbol{Y}}$ forms separately as in the insulated wall case explained in Section 3.3.3. Then, we observe that the final systems should have to be solved together by using the coupled boundary conditions and we present a new solution procedure in this sense.

Now, concentrating on the coupled boundary conditions in (3.89), W_2 can be written in terms of W_1, and $\dfrac{\partial W_2}{\partial n}$ can be written in terms of W_1 and $\dfrac{\partial W_1}{\partial n}$, i.e.

$$\left.\begin{aligned} W_2 &= -W_1 \\ \frac{\partial W_2}{\partial n} &= \frac{\partial W_1}{\partial n} + 2\lambda W_1 - \frac{2}{Ha}\frac{\partial x}{\partial n} - 2\lambda\frac{x}{Ha} \end{aligned}\right\} \quad \text{on} \quad \partial\Omega. \tag{3.92}$$

Thus, the substitution of the equations in (3.92) into (3.91) results in

$$-\widetilde{\boldsymbol{H}}\,\{W_1\} - \widetilde{\boldsymbol{G}}\left\{\frac{\partial W_1}{\partial n}\right\} - 2\lambda\widetilde{\boldsymbol{G}}\,\{W_1\} + \frac{2}{Ha}\widetilde{\boldsymbol{G}}\left\{\frac{\partial x}{\partial n} + \lambda x\right\} = \widetilde{\boldsymbol{F}} \tag{3.93}$$

and it can be rewritten as

$$(-\widetilde{\boldsymbol{H}} - 2\lambda\widetilde{\boldsymbol{G}})\,\{W_1\} - \widetilde{\boldsymbol{G}}\left\{\frac{\partial W_1}{\partial n}\right\} = \widetilde{\boldsymbol{F}} - \frac{2}{Ha}\widetilde{\boldsymbol{G}}\left\{\frac{\partial x}{\partial n} + \lambda x\right\}. \tag{3.94}$$

In this system, $\left\{\dfrac{\partial x}{\partial n} + \lambda x\right\}$ is an $N{\times}1$ vector of which entries are functions of x and can be computed easily at the boundary nodes. Thus, the right hand side of the equation (3.94) is known but on the left hand side of the equation we have two unknown vectors

$\{W_1\}$ and $\left\{\dfrac{\partial W_1}{\partial n}\right\}$ as in the equation (3.90). Now, the system in (3.90) together with the system in (3.94) generate $2N$ equations for $2N$ unknowns covering W_1 and $\dfrac{\partial W_1}{\partial n}$ on the boundary. Therefore, we combine them in such a way that

$$\begin{bmatrix} H & -G \\ -\widetilde{H} - 2\lambda\widetilde{G} & -\widetilde{G} \end{bmatrix}_{2N\times 2N} \begin{bmatrix} W_1 \\ \dfrac{\partial W_1}{\partial n} \end{bmatrix}_{2N\times 1} = \begin{bmatrix} F \\ \widetilde{F} - \dfrac{2}{Ha}\widetilde{G}\left\{\dfrac{\partial x}{\partial n} + \lambda x\right\} \end{bmatrix}_{2N\times 1} \qquad (3.95)$$

in order to produce a $2N \times 2N$ linear system of algebraic equations of the form $\boldsymbol{AX} = \boldsymbol{Y}$ at the end. Finally, this system is solved for W_1 and its normal derivative on the boundary by using a solver which uses LU factorization of the coefficient matrix based on Gauss elimination with partial pivoting. Afterwards, by making use of the relationships in (3.92), the nodal values of W_2 and its normal derivative are computed on the boundary. Similar to the procedure in Section 3.3.1 through the equations (3.62)-(3.63), the interior solutions for W_1 and W_2 are obtained by the help of the discretized equations (3.77) and (3.78), respectively. Hence, the original unknowns V, B are computed by using the transformations (3.71) and (3.68) in order.

3.4 Numerical Results and Discussions

Convection-diffusion type problems

We first consider two convection-diffusion problems for testing the accuracy of our solution procedure. The domain of the first problem is a unit square in the $(x, y)-$plane with the Dirichlet type boundary conditions. The second problem is defined in a rectangular region $0 \leq x \leq 1$ and $0 \leq y \leq 0.7$, and it is solved with Dirichlet and Neumann type boundary conditions. All integrations appearing in the entries of the BEM matrices are computed numerically by using Gauss Legendre integration with

16 to 64 points. The solutions are obtained at steady-state and they are compared with the available steady-state exact solutions. The computations are carried out by using only 20 constant boundary elements and interior values are obtained at uniformly spaced interior nodes with a dense $(N/4)^2$. Comparing to other time integration methods we are able to use quite large time increments (length of time blocks such that $\Delta t = 1.0, 2.0$) in this procedure since the time-dependent fundamental solution is used.

3.4.1 Problem 1

We solve the convection-diffusion equation [38],

$$\frac{\partial u}{\partial t} + \frac{\partial u}{\partial x} + \frac{1}{2}\frac{\partial u}{\partial y} = \nabla^2 u \,, \qquad 0 \leq x \leq 1 \,, \; 0 \leq y \leq 1 \,, \; t > 0$$

with the nonzero initial condition

$$u(x, y, 0) = \exp(-((x + 1/4)^2 + y^2)/4)$$

and the time-dependent Dirichlet type boundary conditions taken from the exact solution

$$u(x, y, t) = \frac{1}{1+t} \exp\left[-((x - t + 1/4)^2 + (y - t/2)^2)/(4(1 + t))\right].$$

The boundary of the square region $[0, 1] \times [0, 1]$ is discretized with $N = 20$ constant boundary elements and $IP = \left(\frac{N}{4}\right)^2 = 25$ equally spaced interior points. Figure 3.16 shows the behaviour of the solution at $y = 0.5$ along x-direction at several time levels. After 27 time steps with the time increment $\Delta t = 1.0$ the solution approaches the steady-state, which is zero, in a good agreement with the exact solution.

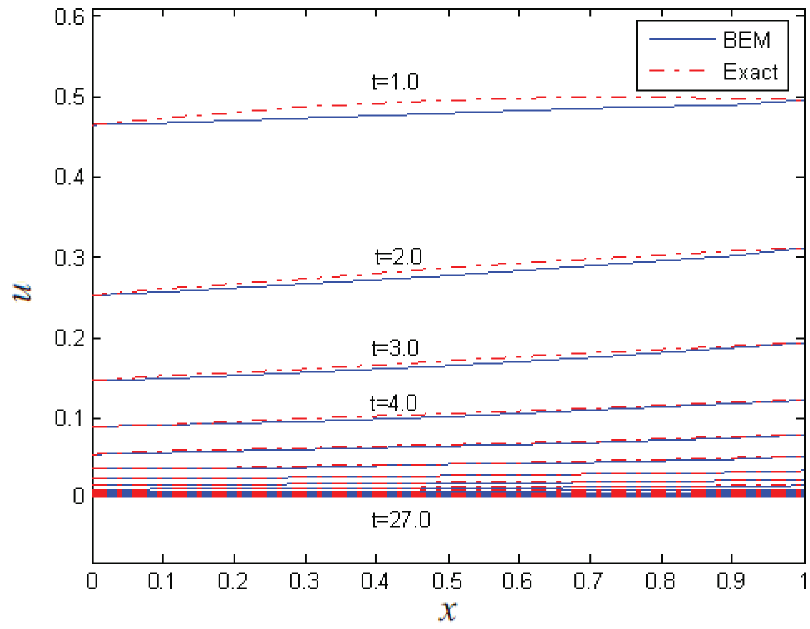

Figure 3.16: Solution of the convection-diffusion problem 1 at $y = 0.5$ with $\Delta t = 1.0$.

3.4.2 Problem 2

The aim of considering this problem is the similarity with the MHD duct flow equations which will be considered in Section 3.4.3. The problem is governed by the convection-diffusion equation [24],

$$\nabla^2 u - \log\left(\frac{10}{300}\right)\frac{\partial u}{\partial x} = \frac{\partial u}{\partial t}, \qquad 0 \leq x \leq 1\,,\ 0 \leq y \leq 0.7\,,\ t > 0$$

in a rectangular region $[0, 1]\times[0, 0.7]$, with the Dirichlet and Neumann type boundary conditions

$$
\left.\begin{aligned}
u(0,y,t) &= 300 \\
u(1,y,t) &= 10
\end{aligned}\right\} \quad 0 \le y \le 0.7\,,\ t > 0
$$

$$
\left.\begin{aligned}
\frac{\partial u}{\partial n}(x,0,t) &= 0 \\
\frac{\partial u}{\partial n}(x,0.7,t) &= 0
\end{aligned}\right\} \quad 0 \le x \le 1\,,\ t > 0
$$

and the zero initial condition

$$u(x,y,0) = 0.$$

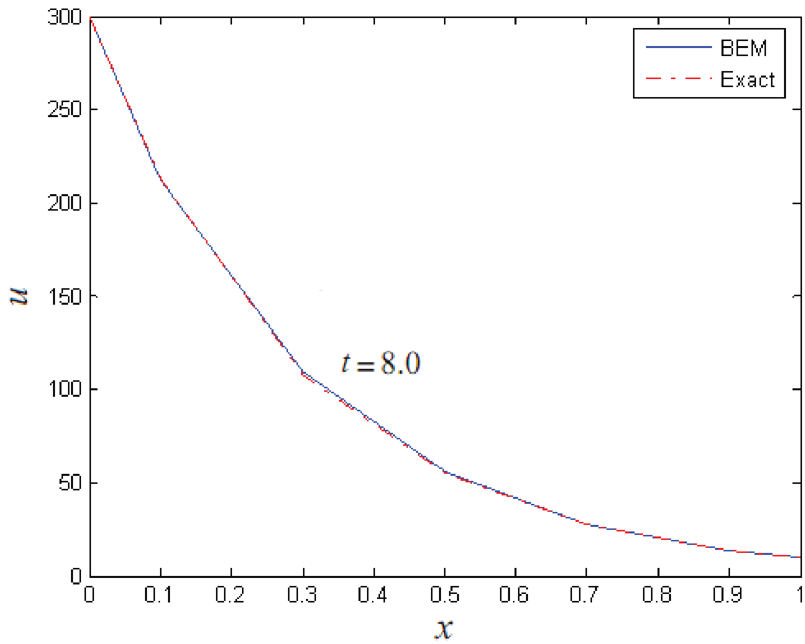

Figure 3.17: Solution of the convection-diffusion problem 2 at $y = 0.35$ with $\Delta t = 2.0$.

The computations are again carried out for $N = 20$ constant boundary elements. The results are obtained at the steady-state $t = 8.0$ after 4 time steps with the time increment $\Delta t = 2.0$. As it is observed in Figure 3.17 that the numerical solution, obtained at the centre point of the interval $0 \le y \le 0.7$ along $x-$direction, agrees very well with the existing analytical solution [87] at steady-state. It is clear that for small values of Δt one needs more iteration to reach the steady-state solution.

3.4.3 The unsteady MHD duct flow

The unsteady MHD equations defining laminar, viscous flow of an incompressible and electrically conducting fluid in a square duct with variable wall conductivity are solved. The resulting BEM matrix equations are arranged in such a way that we are allowed to solve the equations with the coupled boundary conditions caused by the variable conductivity on the walls.

To establish the validity of the numerical results we first solve the unsteady MHD flow of an incompressible fluid in a square duct with insulated walls having a cross section $-1 \leq x, y \leq 1$. The numerical results are obtained until reaching the steady-state solution as $\tau \rightarrow \infty$ for the time domain $(0, \tau)$ with an accuracy 10^{-5}. In the discretization of the boundary of the duct we use constant boundary elements ranging from 80 to 100. About 400-625 interior points are used for drawing graphics. In the time domain $(0, \tau)$ we assume again constant variation over each time step. We have obtained the solution of this problem for Hartmann number values up to 300.

In Figures 3.18 and 3.19, the velocity and the induced magnetic field contours are presented at the steady-state respectively for Hartmann numbers $Ha = 30, 200$. We observe that as Ha increases we need smaller Δt values to increase the accuracy. However, either with small Ha (e.g. 30) or larger Ha (e.g. 200) the number of steps of computations for reaching steady-state (rate of convergence) is always around 3 and 5 with an accuracy 10^{-5}. We can see from the Figures 3.18 and 3.19 that our steady-state solutions for the velocity and the induced magnetic field agree very well with the exact solution given by Sherliff [61]. One can also notice from the Figures 3.18-(a) and 3.19-(a) that as Ha increases velocity becomes uniform at the center of the duct and contour values are decreased when getting closer to the insulated walls, i.e. V has its maximum value through the center of the duct and forms boundary layer close to the walls which are the well known behaviours of the MHD flow.

Now we consider the unsteady MHD flow in a duct with arbitrary conductivity on the walls of the duct. Similar to the insulated wall case the BEM is employed to the governing equations using $N = 80, 100$ constant boundary elements with $IP = 400, 625$ interior nodes, respectively. Again constant variation is assumed for each time step and the problem is solved on the time domain $(0, \tau)$ as $\tau \to \infty$ up to Hartmann number values 300. Figures 3.20 and 3.21 present a comparison between the behaviour of the numerical results for variable conductivity case ($\lambda = 0, 30$ respectively) and the exact solution for the insulated wall case at the steady-state for $Ha = 5$.

One can see that when $\lambda = 0$ which is the pure conducting wall case the induced magnetic field contours are perpendicular to the walls. As λ increases ($\lambda \to \infty$ means the walls are almost insulated) the induced magnetic field contours show the behaviour of solution of MHD flow with insulated walls. On the figures the notations VC and IW denote variable wall conductivity and insulated wall in the MHD duct flow contours, respectively.

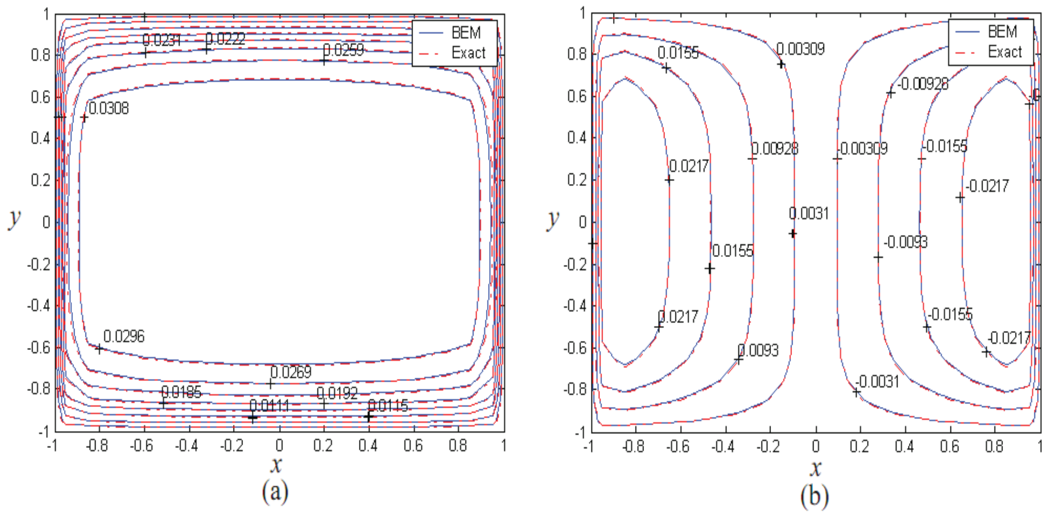

Figure 3.18: (a)Velocity for $Ha = 30$, $\tau = 1.2$, (b) Magnetic field for $Ha = 30$, $\tau = 1.2$.

To see the effect of increase in Ha we present Figures 3.22, 3.24 for showing equal velocity and induced magnetic field lines respectively for $Ha = 20, 300$, and for conductivity parameter $\lambda = 0$. In the velocity curves we notice that the flow is separated symmetrically in the $y-$direction. This is the effect of applied magnetic field in the direction of $x-$axis and the pure conductivity of the wall ($\lambda = 0$). As Ha increases the seperation is more pronounced, the fluid is stagnant at the center region whereas close to the boundaries at $y = \pm 1$ boundary layers are formed.

In Figures 3.25-3.27 similar behaviour for increasing Ha is observed for velocity and

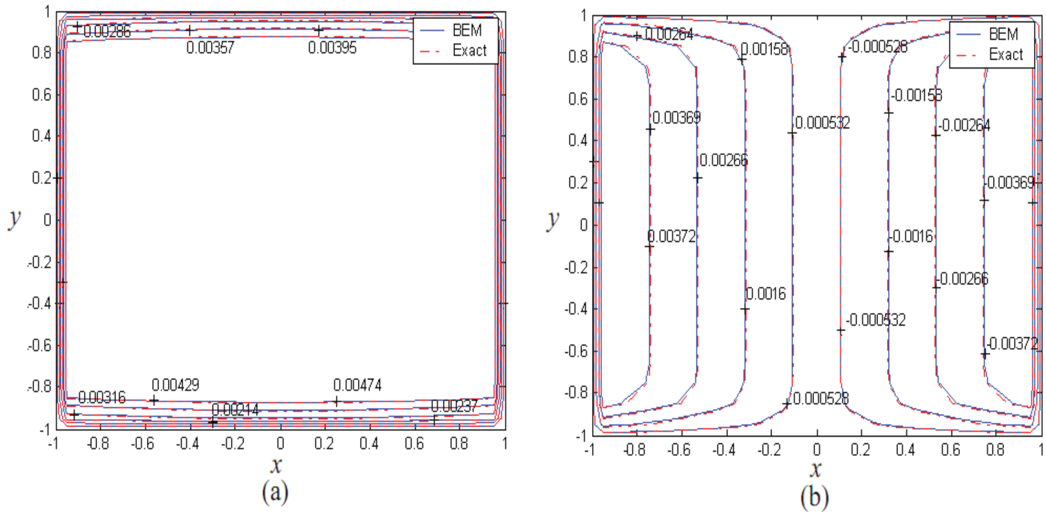

Figure 3.19: (a)Velocity for Ha = 200, τ = 0.15, (b) Magnetic field for Ha = 200, τ = 0.15.

induced magnetic field for $\lambda = 5$. One can notice from figures 3.25-(a) and 3.27-(a) that, the higher the conductivity of the walls is the more stagnant region at the center region of the duct for the fluid.

In conclusion, the two-dimensional MHD duct flow equations which are convection-diffusion type, are solved by using BEM with the time-dependent fundamental solution. The BEM formulation of MHD flow equations in a duct with arbitrary wall conductivity is given in such a way that the resulting equations are solved as a whole with coupled boundary conditions. The effects of values of Hartmann number and wall conductivity parameter are visualized in terms of graphics showing the characteristics of MHD flow.

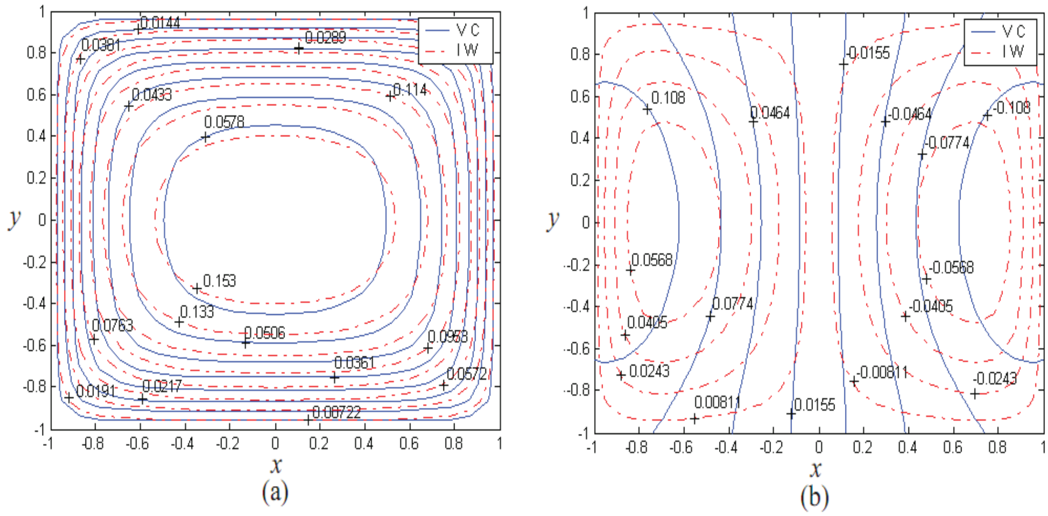

Figure 3.20: (a)Velocity for $Ha = 5$, $\lambda = 0$, $\Delta t = 0.5$, $\tau = 3.0$, (b) Magnetic field for $Ha = 5$, $\lambda = 0$, $\Delta t = 0.5$, $\tau = 3.0$.

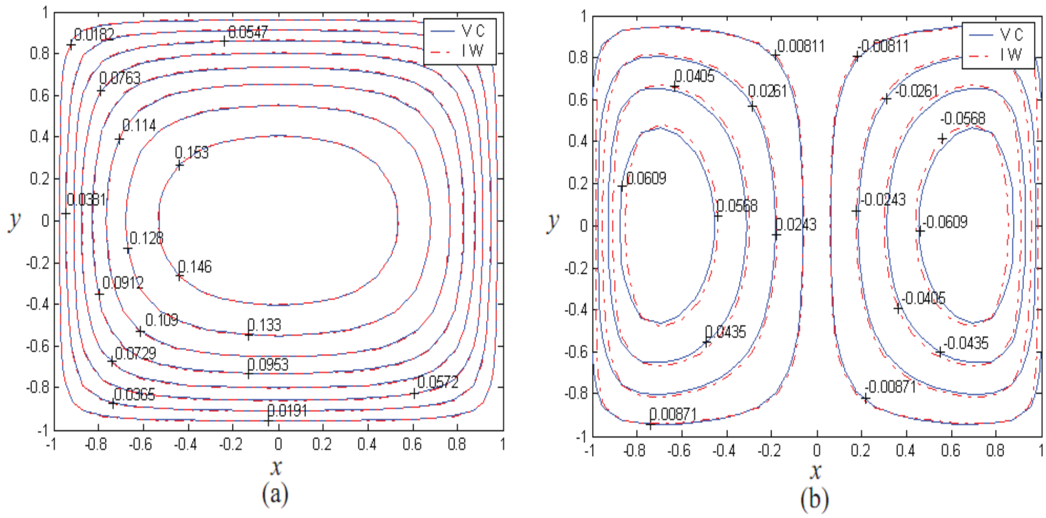

Figure 3.21: (a)Velocity for $Ha = 5$, $\lambda = 30$, $\Delta t = 0.5$, $\tau = 2.5$, (b) Magnetic field for $Ha = 5$, $\lambda = 30$, $\Delta t = 0.5$, $\tau = 2.5$.

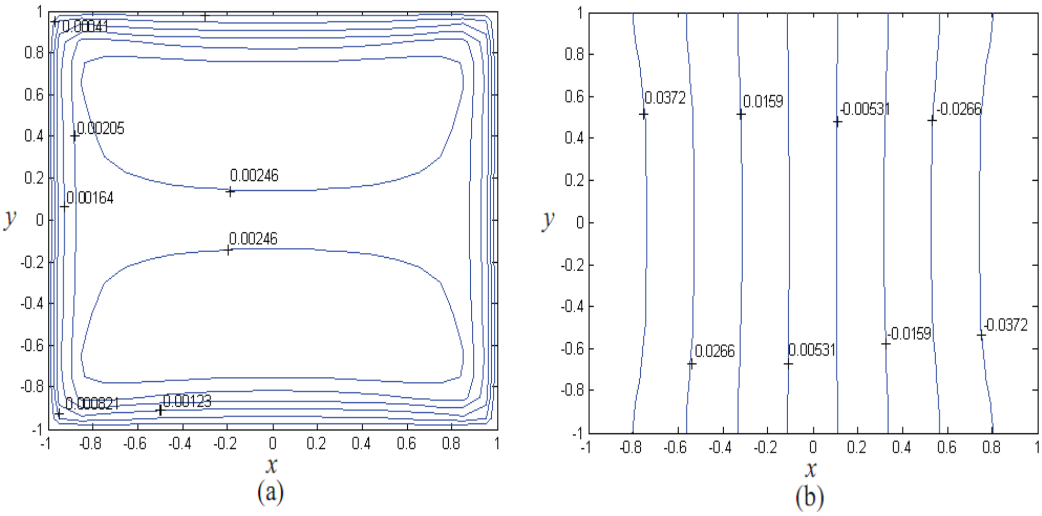

Figure 3.22: (a)Velocity for $Ha = 20$, $\lambda = 0$, $\Delta t = 0.5$, $\tau = 2.0$, (b) Magnetic field for $Ha = 20$, $\lambda = 0$, $\Delta t = 0.5$, $\tau = 2.0$.

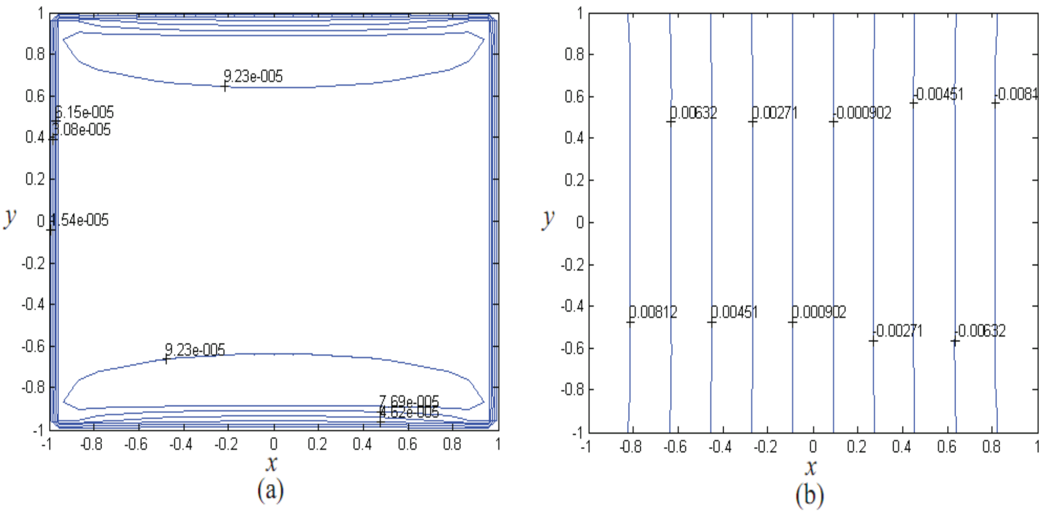

Figure 3.23: (a)Velocity for $Ha = 100$, $\lambda = 0$, $\Delta t = 0.2$, $\tau = 0.6$, (b) Magnetic field for $Ha = 100$, $\lambda = 0$, $\Delta t = 0.2$, $\tau = 0.6$.

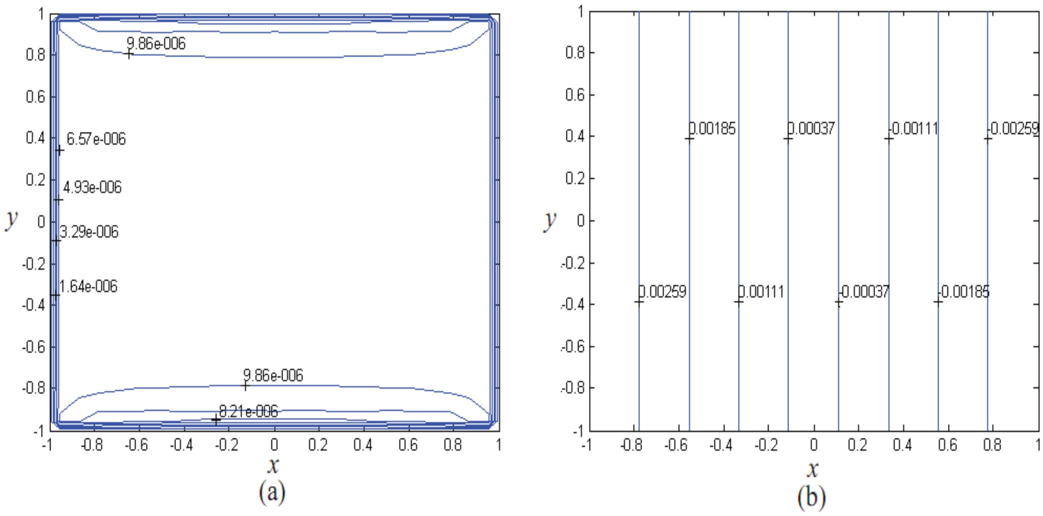

Figure 3.24: (a)Velocity for $Ha = 300$, $\lambda = 0$, $\Delta t = 0.03$, $\tau = 0.09$, (b) Magnetic field for $Ha = 300$, $\lambda = 0$, $\Delta t = 0.03$, $\tau = 0.09$.

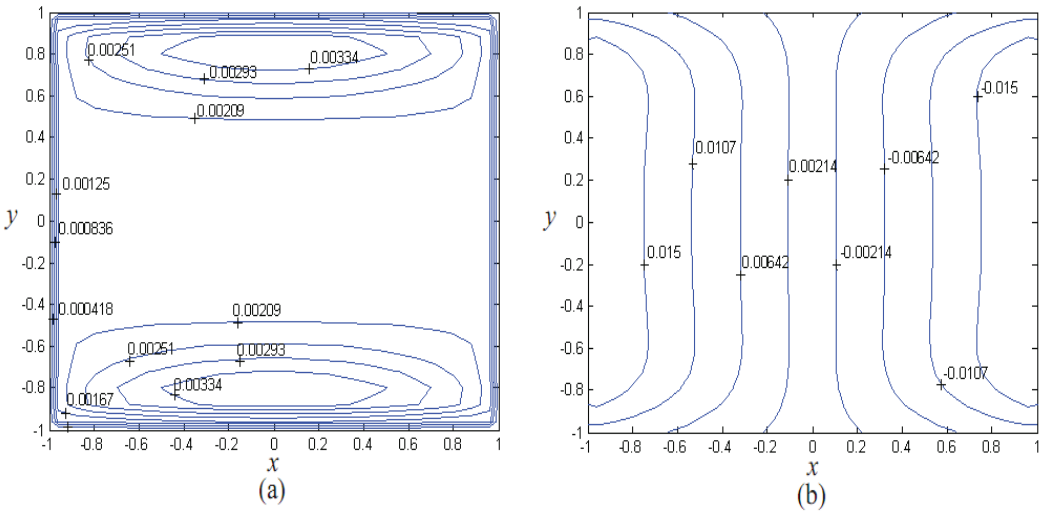

Figure 3.25: (a)Velocity for $Ha = 50$, $\lambda = 5$, $\Delta t = 0.5$, $\tau = 1.5$, (b) Magnetic field for $Ha = 50$, $\lambda = 5$, $\Delta t = 0.5$, $\tau = 1.5$.

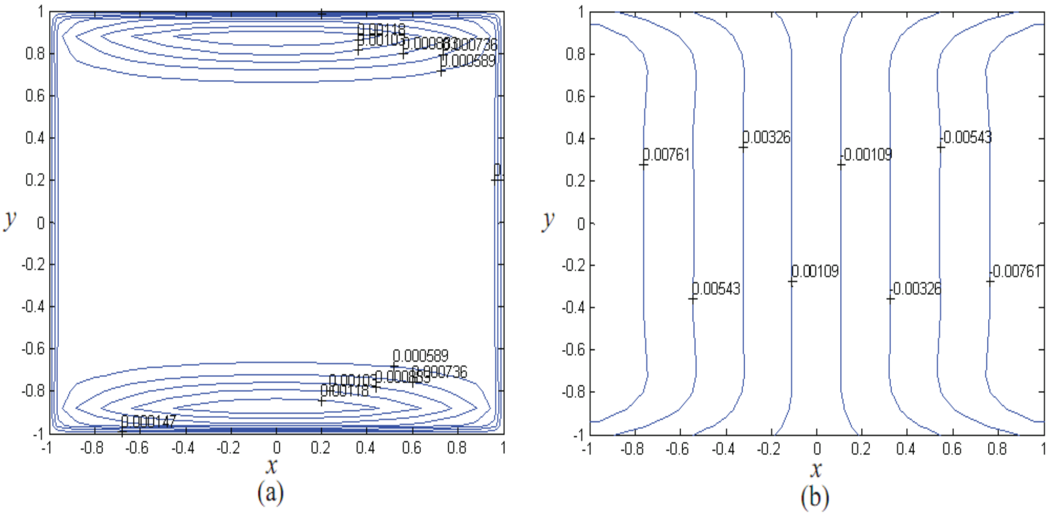

Figure 3.26: (a)Velocity for $Ha = 100$, $\lambda = 5$, $\Delta t = 0.2$, $\tau = 0.6$, (b) Magnetic field for $Ha = 100$, $\lambda = 5$, $\Delta t = 0.2$, $\tau = 0.6$.

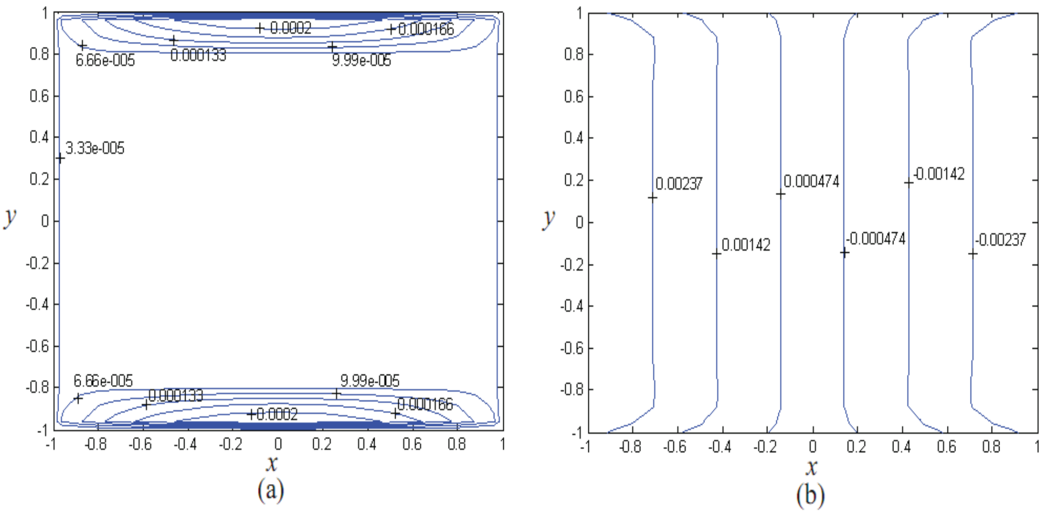

Figure 3.27: (a)Velocity for $Ha = 300$, $\lambda = 5$, $\Delta t = 0.03$, $\tau = 0.09$, (b) Magnetic field for $Ha = 300$, $\lambda = 5$, $\Delta t = 0.03$, $\tau = 0.09$.

CHAPTER 4

THE DUAL RECIPROCITY BOUNDARY ELEMENT METHOD SOLUTION OF NAVIER-STOKES EQUATIONS AND FULL MAGNETOHYDRODYNAMIC FLOW EQUATIONS

Fluid dynamics analyzes motion of the fluids. The two states of matter, liquids and gases, are called as fluids. The essential difference between a liquid and a gas lies in the rate of change of their density. The rate of change of density of a gas is faster than a liquid. However, they can be treated in the same way if the variation of density ρ of the fluid is negligible. In this case fluid is called *incompressible*. One other basic property of a fluid is viscosity. The moving fluid which encounters an internal frictional force in the direction of motion is called *viscous fluid*. If the frictional force, which is also known as shearing stress, is negligibly small than the fluid is considered inviscid and is called *perfect* or *ideal* fluid. However, in many situations viscosity can not be neglected near boundaries since boundary layers may occur due to the no-slip boundary conditions. Thus, even a small amount of viscosity generates vorticity. In dimensionless analysis for most types of fluids, a nondimensional number, *Re*, called as Reynolds number, arises. Reynolds number is used to characterize different flow regimes, such as laminar or *turbulent* flow. When *Re* increases, the flow fluctuates widely and for larger *Re* values the flow becomes turbulent. As *Re* decreases the flow becomes gentle and called as *laminar* at low Reynolds numbers ($Re \leq 2000$).

In this chapter, we mainly deal with laminar, unsteady flow of viscous, incompressible fluids in two-dimensions. There are two sets of viscous flow equations, the equation of continuity and the equations of motion. The continuity equation is derived from the law of conservation of mass and the equations of motion or the Navier-Stokes equations are derived from the law of conservation of momentum [88]. Newton's second law with continuity equation

$$\nabla \cdot \boldsymbol{V} = 0 \tag{4.1}$$

leads the following form of the momentum equations for viscous flow of an incompressible fluid

$$\frac{\partial \boldsymbol{V}}{\partial t'} + \boldsymbol{V} \cdot \nabla \boldsymbol{V} = -\frac{1}{\rho}\nabla p' + \nu \nabla^2 \boldsymbol{V} + \boldsymbol{f_{ext}} \tag{4.2}$$

where the vectors $\boldsymbol{V} = (u', \upsilon')$ and $\boldsymbol{f_{ext}}$ represent the velocity field and the external force, respectively. ν is the kinematic viscosity, ρ is the density, p' is the pressure. The continuity equation and Navier-Stokes equations can be rewritten in cartesian coordinates as

$$\frac{\partial u'}{\partial x'} + \frac{\partial \upsilon'}{\partial y'} = 0 \tag{4.3}$$

$$\begin{aligned} \frac{\partial u'}{\partial t'} + u'\frac{\partial u'}{\partial x'} + \upsilon'\frac{\partial u'}{\partial y'} &= -\frac{1}{\rho}\frac{\partial p'}{\partial x'} + \nu\nabla^2 u' \\ \frac{\partial \upsilon'}{\partial t'} + u'\frac{\partial \upsilon'}{\partial x'} + \upsilon'\frac{\partial \upsilon'}{\partial y'} &= -\frac{1}{\rho}\frac{\partial p'}{\partial y'} + \nu\nabla^2 \upsilon' \end{aligned} \tag{4.4}$$

with the absence of external forces. When a nondimensional process, in terms of a characteristic velocity U' and a characteristic length L', is introduced to the equations (4.3) and (4.4), one obtains the nondimensional equations

$$\frac{\partial u}{\partial x} + \frac{\partial \upsilon}{\partial y} = 0 \tag{4.5}$$

$$\frac{\partial u}{\partial t} + u\frac{\partial u}{\partial x} + \upsilon\frac{\partial u}{\partial y} = -\frac{\partial p}{\partial x} + \frac{1}{Re}\nabla^2 u \tag{4.6}$$

$$\frac{\partial \upsilon}{\partial t} + u\frac{\partial \upsilon}{\partial x} + \upsilon\frac{\partial \upsilon}{\partial y} = -\frac{\partial p}{\partial y} + \frac{1}{Re}\nabla^2 \upsilon \tag{4.7}$$

with the dimensionless quantities

$$u = \frac{u'}{U'}, \quad \upsilon = \frac{\upsilon'}{U'}, \quad x = \frac{x'}{L'}, \quad y = \frac{y'}{L'}, \quad t = \frac{t'}{L'/U'}, \quad p = \frac{p'}{(U')^2\rho}. \tag{4.8}$$

where Reynolds number, Re is defined by

$$Re = \frac{U'\,L'}{\nu}. \tag{4.9}$$

In equations (4.6) and (4.7) when the time derivative terms vanish, the flow becomes steady. The terms other than time derivative are convection terms on the left hand sides. Pressure gradients provide driving force to the fluid motion. The second terms on the right-hand sides of (4.6) and (4.7) are viscous terms. Now, equations (4.5)-(4.7) need to be solved for the nondimensional velocity $\mathbf{v} = (u, \upsilon)$ and the pressure p. The difficulty arises from the absence of pressure equation and the satisfaction of continuity equation. To deal with this problem, the continuity equation (4.5) and Navier-Stokes equations (4.6)-(4.7) which are in primitive variables (u, υ, p) can be transformed to stream function-vorticity equations in two-dimensions. Since the velocity vector $\mathbf{v} = (u, \upsilon)$ has the same direction with the tangent vector at every point on a streamline, one has

$$u\,dy - \upsilon\,dx = 0. \tag{4.10}$$

A planar curve can be expressed by means of a function in two variables, say $\psi(x, y)$. When $\psi(x, y)$ is a smooth function, the total derivative along a streamline must be equal to zero

$$d\psi = \frac{\partial \psi}{\partial x}dx + \frac{\partial \psi}{\partial y}dy = 0 \tag{4.11}$$

where ψ is called a stream function and therefore equations (4.10) and (4.11) result in

$$u = \frac{\partial \psi}{\partial y}\ , \qquad \upsilon = -\frac{\partial \psi}{\partial x}\,. \tag{4.12}$$

Now, curl of the velocity field $\mathbf{v} = (u, \upsilon)$ gives the vorticity vector $\boldsymbol{\omega} = (0, 0, \omega)$ in two-dimensions as,

$$\boldsymbol{\omega} = \nabla \times \mathbf{v} \tag{4.13}$$

producing

$$\omega = \frac{\partial \upsilon}{\partial x} - \frac{\partial u}{\partial y}\,. \tag{4.14}$$

The continuity equation (4.5) with the definitions in (4.12) is satisfied automatically whereas vorticity definition (4.14) results in stream function equation

$$\nabla^2 \psi = -\omega. \tag{4.15}$$

When x derivative of $y-$component is subtracted from the y derivative of $x-$component of Navier-Stokes equations (equations (4.6) and (4.7)), one can easily eliminate the pressure terms and then obtain the vorticity transport equation

$$\frac{\partial \omega}{\partial t} + \frac{\partial \psi}{\partial y}\frac{\partial \omega}{\partial x} - \frac{\partial \psi}{\partial x}\frac{\partial \omega}{\partial y} = \frac{1}{Re}\nabla^2 \omega\,. \tag{4.16}$$

Thus, the stream function-vorticity form of unsteady Navier-Stokes equations for an incompressible, viscous fluid in two-dimensions is introduced as

$$
\begin{aligned}
&\nabla^2\psi = -\omega \\
&\frac{\partial\omega}{\partial t} + \frac{\partial\psi}{\partial y}\frac{\partial\omega}{\partial x} - \frac{\partial\psi}{\partial x}\frac{\partial\omega}{\partial y} = \frac{1}{Re}\nabla^2\omega \, .
\end{aligned}
\tag{4.17}
$$

Although the number of equations is reduced to two in this form and the pressure is eliminated, one is faced with the difficulty of obtaining vorticity boundary conditions now. These fluid flow equations now are going to be solved by using boundary element method which is a numerical scheme discretizing only the boundary of the problem domain. The BEM provides an efficient alternative to the to the finite difference and finite element methods. Mainly, the advantage lies in its unique ability that it produces the solution on the boundary by solving considerably small sized discretized systems. Then, the solution can be obtained at any interior point. However, it always requires a fundamental solution to the original differential equation in order to obtain an equivalent boundary integral equation. Also, the nonhomogeneous and nonlinear terms can cause domain integrals in the integral formulation, and then the method loses the attraction of its boundary-only character. Many different approaches have been developed to overcome these problems. One of the techniques which is quite efficient is the dual reciprocity boundary element method. The basic idea of this approach is to treat the dual part of the governing equation by using a fundamental solution corresponding to a simpler equation, like Laplace equation, through a procedure which involves a series expansion including approximating functions. In Section 4.1, a general DRBEM procedure is presented for the solution of poisson-type equations including nonhomogeneous terms depending on function values or space and time derivatives. Thus, by using DRBEM a boundary only integral formulation is obtained for the equations even with too complex nonhomogeneous terms.

In this chapter, we consider the stream function- vorticity form of Navier-Stokes equations which often suits the numerical computation for two-dimensional laminar flow of viscous, incompressible fluid. A DRBEM approach is presented for the solution of the governing equations in which stream function equation is of poisson and vorticity equation is of convection-diffusion type. The solution procedure for this coupled partial differential equations is based on the iteration in time direction. Unlike the time-domain BEM approach performed in Chapters 2 and 3, the equations here can not be treated as a whole since the fundamental solution of Laplace equation, which is time independent, is used in DRBEM formulation. For the vorticity transport equation the dual reciprocity idea produces a system of ordinary differential equations in time. Thus, we make use of an unconditionally stable backward difference scheme in time direction for solving this system. Section 4.1.1 gives the implementation of this time integration scheme.

Then, we introduce the DRBEM solution of Magnetohydrodynamics (MHD) flow equations for the case of induced magnetic field inside the fluid can not be neglected. The full MHD flow equations govern the dynamics of electrically conducting fluids. Plasmas, liquid metals and salt water are examples of such fluids. The set of equations are a combination of Navier-Stokes equations of fluid dynamics and Maxwell equations of electromagnetism. The electric current density which is related to the curl of induced magnetic field, is also considered as an unknown in the equations. Thus, Section 4.1.1 forms a preliminary to the DRBEM application of Magnetohydrodynamics. As is done for Navier-Stokes equations standard nondimensional form of full MHD equations are transformed to stream function-vorticity and magnetic field-current density form. The details of full MHD equations in original variables and the transformation to above mentioned form are given in Section 4.2. The equations are solved iteratively by using the previously obtained solution values as initials where they are required for the next time iteration.

The dual reciprocity boundary element method with a finite difference (FD) type time integration scheme for solving either Navier-Stokes equations or full MHD equations has many advantages. These are the discretization of only the boundary, the simplicity of obtaining boundary integrals due to the fundamental solution of Laplace equation used in DRBEM, and obtaining the solution iteratively at transient time levels and at steady-state. The FD type time discretizations are also simple and do not present stability problems especially when they are implicit in nature. Thus, an internal discretization is eliminated in contrast to the finite element method (FEM) and other domain discretization schemes. However, for obtaining the solution on the boundary and at some selected interior points a larger system is obtained including the interior required unknowns in the final system simultaneously. Navier-Stokes equations are solved in lid-driven cavity and two applications are given for the full MHD equations, one defined in a square cavity and another in a channel with a backward facing step.

4.1 The Dual Reciprocity Boundary Element Method

The dual reciprocity boundary element method is performed for Poisson's equation for simplicity. Then, the extensions to Navier-Stokes and full MHD equations are going to be provided considering the DRBEM application for convection-diffusion type equations [24]. Consider Poisson's equation

$$\nabla^2 u = d \tag{4.18}$$

in a region $\Omega \subset \mathbb{R}^2$ bounded by Γ. The dual reciprocity formulation of this equation is based on developing an equivalent integral equation on the boundary Γ by using the fundamental solution of Laplace equation. The nonhomogeneous given function d which may be a function of x, y, u, u_x, u_y and u_t is expanded with approximating functions, i.e.,

$$d \approx \sum_{k=1}^{N+IP} \alpha_k \, \phi_k(x, y) \tag{4.19}$$

where α_k are unknown coefficients which may depend on time t, and ϕ_k are approximating distance (coordinate) functions formed between N boundary and IP interior nodes. ϕ_k's are linked with a series of particular solutions, $\hat{u}_k$'s, of equation (4.18) through

$$\nabla^2 \hat{u}_k = \phi_k. \tag{4.20}$$

Substitution of the equations (4.19) and (4.20) into (4.18) introduces the approximation

$$\nabla^2 u \approx \sum_{k=1}^{N+IP} \alpha_k \nabla^2 \hat{u}_k. \tag{4.21}$$

Now, equation (4.21) is weighted over the domain Ω with the fundamental solution

$$u^* = \frac{1}{2\pi} \ln(\frac{1}{r}) \tag{4.22}$$

of Laplace equation in two-dimensions where $r = |\boldsymbol{x} - \boldsymbol{\xi}|$ is the distance from a source point $\boldsymbol{\xi}$ to a field point $\boldsymbol{x}$. It is the solution of the inhomogeneous equation

$$\nabla^2 u^* = -\Delta(\boldsymbol{x} - \boldsymbol{\xi}) \tag{4.23}$$

where Δ is the Dirac delta function defined in Chapter 2, equation (2.10). Thus, the method of weighted residuals for (4.21) gives

$$\int_\Omega \left(\nabla^2 u\right) u^* \, d\Omega = \sum_{k=1}^{N+IP} \alpha_k \int_\Omega \left(\nabla^2 \hat{u}_k\right) u^* d\Omega. \tag{4.24}$$

Applying Green's second identity to the domain integrals as shown in Chapter 2, one can arrive at the boundary only integral equation for each source node $\boldsymbol{\xi}_i$ as,

$$c_i u_i + \int_\Gamma q^* u \, d\Gamma - \int_\Gamma u^* q \, d\Gamma = \sum_{k=1}^{N+IP} \alpha_k \Big(c_i \hat{u}_{ik} + \int_\Gamma q^* \hat{u}_k \, d\Gamma - \int_\Gamma u^* \hat{q}_k \, d\Gamma \Big) \tag{4.25}$$

where $q = \dfrac{\partial u}{\partial n}$, $q^* = \dfrac{\partial u^*}{\partial n}$ and $\hat{q} = \dfrac{\partial \hat{u}}{\partial n}$, $i = 1, \ldots, N$, and $c_i = c(\boldsymbol{\xi}_i)$ is the constant given in Chapter 2, equation (2.13).

Similar to the previous discretizations, the boundary is divided into N partitions of constant boundary elements. Therefore, equation (4.25) yields

$$c_i u_i + \sum_{n=1}^{N} \int_{\Gamma_n} q^* \, u \, d\Gamma - \sum_{n=1}^{N} \int_{\Gamma_n} u^* \, q \, d\Gamma \;\; = \sum_{k=1}^{N+IP} \alpha_k \Big(c_i \hat{u}_{ik} + \sum_{n=1}^{N} \int_{\Gamma_n} q^* \, \hat{u}_k \, d\Gamma - \sum_{n=1}^{N} \int_{\Gamma_n} u^* \, \hat{q}_k \, d\Gamma \Big) \tag{4.26}$$

where $i,\ n = 1, \ldots, N$.

Once the approximating functions ϕ_k's are given, $\hat{u}_k$ can be derived in terms of the distance function $r = |\boldsymbol{x} - \boldsymbol{\xi}|$ from the relationship in equation (4.20). Then the normal derivative of $\hat{u}$

$$\frac{\partial \hat{u}}{\partial n} = \frac{\partial \hat{u}}{\partial r}\frac{\partial r}{\partial n} = \hat{q}$$

gives $\hat{q}$ in terms of r as well. Therefore, taking into consideration the nodal values of $\hat{u}$ and $\hat{q}$ and approximating the variations of u and q values within each constant boundary element Γ_n, equation (4.26) can be written as

$$c_i u_i + \sum_{n=1}^{N} u_n \int_{\Gamma_n} q^* \, d\Gamma \;\; - \sum_{n=1}^{N} q_n \int_{\Gamma_n} u^* \, d\Gamma = \sum_{k=1}^{N+IP} \alpha_k \Big(c_i \, \hat{u}_{ik} + \sum_{n=1}^{N} \hat{u}_{nk} \int_{\Gamma_n} q^* \, d\Gamma - \sum_{n=1}^{N} \hat{q}_{nk} \int_{\Gamma_n} u^* \, d\Gamma \Big). \tag{4.27}$$

Thus, ranging i and n from 1 to N, equation (4.27) can be expressed in matrix vector form as

$$\boldsymbol{H}\,\boldsymbol{u} - \boldsymbol{G}\,\boldsymbol{q} = \sum_{k=1}^{N+IP} \alpha_k \, (\boldsymbol{H}\,\hat{\boldsymbol{u}}_{\boldsymbol{k}} - \boldsymbol{G}\hat{\boldsymbol{q}}_{\boldsymbol{k}})\,. \tag{4.28}$$

The vectors $\hat{\boldsymbol{u}}_{\boldsymbol{k}}$ and $\hat{\boldsymbol{q}}_{\boldsymbol{k}}$ are defining the $k-th$ column of the matrices $\hat{\boldsymbol{U}}$ and $\hat{\boldsymbol{Q}}$, respectively. Therefore, equation (4.28) results in

$$\boldsymbol{H}\,\boldsymbol{u} - \boldsymbol{G}\,\boldsymbol{q} = (\boldsymbol{H}\,\hat{\boldsymbol{U}} - \boldsymbol{G}\hat{\boldsymbol{Q}})\boldsymbol{\alpha} \tag{4.29}$$

where the vector $\boldsymbol{\alpha}$ is formed by α_k's.

The transition from equation (4.27) to (4.29) is provided with the incorporation of the coefficients c_i's onto the main diagonal of the matrix $\boldsymbol{H}$ and the solution of equation (4.29) gives the unknown boundary values where i ranging from 1 to N. Thus, by taking $c_i = 1$, the BEM matrices $\boldsymbol{H}_{IP\times N}$ and $\boldsymbol{G}_{IP\times N}$ are computed due to the contributions coming from the interior points and equation (4.29) turns into

$$\begin{aligned}\boldsymbol{I}_{IP\times IP}\,\boldsymbol{u}_{IP\times 1} &= \boldsymbol{G}_{IP\times N}\,\boldsymbol{q}_{N\times 1} - \boldsymbol{H}_{IP\times N}\,\boldsymbol{u}_{N\times 1} + \Big[\,\boldsymbol{I}_{IP\times IP}\,\hat{\boldsymbol{U}}_{IP\times(N+IP)} \\ &\quad + \boldsymbol{H}_{IP\times N}\,\hat{\boldsymbol{U}}_{N\times IP} - \boldsymbol{G}_{IP\times N}\hat{\boldsymbol{Q}}_{N\times(N+IP)}\Big]\boldsymbol{\alpha}_{N+IP}\end{aligned} \tag{4.30}$$

in order to produce the interior unknown values of u. Associating (4.28) and (4.30), a global scheme can now be obtained which is valid for both internal and boundary nodes, as follows

$$\left[\begin{array}{c|c}\boldsymbol{H}^{BS}_{N\times N} & \boldsymbol{0} \\ \hline \boldsymbol{H}^{IS}_{IP\times N} & \boldsymbol{I}\end{array}\right]\left[\begin{array}{c}\boldsymbol{u}^{BS}_{N\times 1} \\ \hline \boldsymbol{u}^{IS}_{IP\times 1}\end{array}\right] - \left[\begin{array}{c|c}\boldsymbol{G}^{BS}_{N\times N} & \boldsymbol{0} \\ \hline \boldsymbol{G}^{IS}_{IP\times N} & \boldsymbol{0}\end{array}\right]\left[\begin{array}{c}\boldsymbol{q}^{BS}_{N\times 1} \\ \hline \boldsymbol{0}\end{array}\right]$$

$$= \left(\left[\begin{array}{c|c}\boldsymbol{H}^{BS}_{N\times N} & \boldsymbol{0} \\ \hline \boldsymbol{H}^{IS}_{IP\times N} & \boldsymbol{I}\end{array}\right]\left[\begin{array}{c}\hat{\boldsymbol{U}}^{BS}_{N\times(N+IP)} \\ \hline \hat{\boldsymbol{U}}^{IS}_{IP\times(N+IP)}\end{array}\right] - \left[\begin{array}{c|c}\boldsymbol{G}^{BS}_{N\times N} & \boldsymbol{0} \\ \hline \boldsymbol{G}^{IS}_{IP\times N} & \boldsymbol{0}\end{array}\right]\left[\begin{array}{c}\hat{\boldsymbol{Q}}^{BS}_{N\times(N+IP)} \\ \hline \boldsymbol{0}\end{array}\right]\right)\left[\begin{array}{c}\boldsymbol{\alpha}^{BS}_{N\times 1} \\ \hline \boldsymbol{\alpha}^{IS}_{IP\times 1}\end{array}\right] \tag{4.31}$$

In equation (4.31) IS and BS denote the internal and boundary solutions, respectively. And the sizes of the matrices and vectors are as they are expressed. Empty blocks are represented by $\boldsymbol{0}$, and $\boldsymbol{I}$ stands for the identity matrix.

Then, the system (4.31) can be rewritten in a compact form

$$\boldsymbol{H}\,\boldsymbol{u} - \boldsymbol{G}\,\boldsymbol{q} = (\boldsymbol{H}\,\hat{\boldsymbol{U}} - \boldsymbol{G}\hat{\boldsymbol{Q}})\boldsymbol{\alpha} \tag{4.32}$$

where all the matrices are of size $(N+IP)\times(N+IP)$ and vectors $\boldsymbol{u}$, $\boldsymbol{q}$ and $\boldsymbol{\alpha}$ are of sizes $(N+IP)\times 1$. The same notations as in (4.29) are used for the extended matrices and vectors in (4.31) for simplicity. The coordinate function ϕ_k at each $k-th$ point builds the entries of the matrix $\boldsymbol{F}$ of size $(N+IP)\times(N+IP)$. Thus, equation (4.19) gives a system for α vector

$$\boldsymbol{d} = \boldsymbol{F}\,\boldsymbol{\alpha} \tag{4.33}$$

which is in turn

$$\boldsymbol{\alpha} = \boldsymbol{F}^{-1}\boldsymbol{d} \tag{4.34}$$

where the approximating function ϕ should be defined so that $\boldsymbol{F}$ is nonsingular. To this end we define the approximating function ϕ , [89], as a linear function of the distance $r = |\boldsymbol{x} - \boldsymbol{\xi}|$ between a source point $(\boldsymbol{\xi})$ and a field point $(\boldsymbol{x})$, i.e.,

$$\phi = 1 + r. \tag{4.35}$$

The presence of the constant in the definition of ϕ generates nonzero leading diagonal entries for $\boldsymbol{F}$ so that $\boldsymbol{F}$ is invertible. Then, the entries of the matrices $\hat{\boldsymbol{U}}$ and $\hat{\boldsymbol{Q}}$ are described as follows

$$\hat{\boldsymbol{U}}_{ik} = \frac{r_{ik}^2}{4} + \frac{r_{ik}^3}{9} \tag{4.36}$$

$$\hat{\boldsymbol{Q}}_{ik} = \left(r_x\frac{\partial x}{n} + r_y\frac{\partial y}{n}\right)\left(\frac{1}{2} + \frac{r_{ik}}{3}\right) \tag{4.37}$$

for $i = 1,\ldots,N+IP$ and $k = 1,...,N+IP$.

Thus, equation (4.32) within equation (4.34) results in

$$\boldsymbol{H}\,\boldsymbol{u} - \boldsymbol{G}\,\boldsymbol{q} = (\boldsymbol{H}\,\hat{\boldsymbol{U}} - \boldsymbol{G}\hat{\boldsymbol{Q}})\boldsymbol{F}^{-1}\boldsymbol{d}. \tag{4.38}$$

Now, the right hand side of the above equation is a known vector and it produces $N + IP$ equations including $N + IP$ unknowns. There are N unknown values of either u or q on the boundary and IP unknown values of u at interior nodes. Therefore, when the boundary conditions are applied the usual linear system of algebraic equations

$$\boldsymbol{A}\,\boldsymbol{X} = \boldsymbol{Y} \tag{4.39}$$

is obtained which is an $(N + IP) \times (N + IP)$ system. $\boldsymbol{X}$ contains N boundary values of u or q and IP interior u values. Thus, when equation (4.39) is solved for $\boldsymbol{X}$, the unknown values of u both at the boundary and interior nodes are provided simultaneously.

The solution u can also be approximated by the same coordinate functions $\phi_k(x, y)$ as

$$u \approx \sum_{k=1}^{N+IP} \beta_k\, \phi_k(x, y) \tag{4.40}$$

which results in a similar system to (4.33)

$$\boldsymbol{u} = \boldsymbol{F}\,\boldsymbol{\beta} \tag{4.41}$$

where $\beta_k \neq \alpha_k$, and entries of $\boldsymbol{\beta}$ can be computed from

$$\boldsymbol{\beta} = \boldsymbol{F}^{-1}\boldsymbol{u}. \tag{4.42}$$

Now, this representation is used for obtaining spatial derivatives of $\boldsymbol{u}$ in (4.41) as approximations

$$\frac{\partial \boldsymbol{u}}{\partial x} = \frac{\partial \boldsymbol{F}}{\partial x}\boldsymbol{F}^{-1}\boldsymbol{u}, \tag{4.43}$$

$$\frac{\partial \boldsymbol{u}}{\partial y} = \frac{\partial \boldsymbol{F}}{\partial y}\boldsymbol{F}^{-1}\boldsymbol{u}. \tag{4.44}$$

In the next section the DRBEM formulation of stream function and vorticity equations are going to be given for the purpose of solving Navier-Stokes equations.

4.1.1 DRBEM formulation of Navier-Stokes equations

The DRBEM formulation of the stream function equation (4.15)

$$\nabla^2\psi = -\omega \tag{4.45}$$

defined in a region Ω bounded by Γ is based on developing an equivalent integral equation on Γ by using the fundamental solution of the Laplace equation [24]. The nonhomogeneous term here is the negative of vorticity function. Thus, the Poisson's equation (4.45), as equation (4.18), is transformed to a boundary integral equation by taking the function d as $-\omega$, and following the procedure in the previous section, one can arrive at the DRBEM matrix equation

$$\boldsymbol{H\psi} - \boldsymbol{G}\,\boldsymbol{q_\psi} = \left[\boldsymbol{H\hat{U}} - \boldsymbol{G\hat{Q}}\right]\boldsymbol{F}^{-1}(-\boldsymbol{\omega}) \tag{4.46}$$

by replacing $d = -\omega$ in (4.38) for stream function $\boldsymbol{\psi}$ and its normal derivative $\boldsymbol{q_\psi}$. Here, $\boldsymbol{q_\psi}$ is the vector of which entries are formed by the nodal values of the normal derivative of ψ. The matrices $\boldsymbol{\hat{U}}$ and $\boldsymbol{\hat{Q}}$ are formed coloumwise by computing the particular solutions and their normal derivatives at $N + IP$ points, and the radial basis functions $\phi = 1 + r$ form the entries of the matrix $\boldsymbol{F}$. The entries of the matrices $\boldsymbol{H}$ and $\boldsymbol{G}$ are given by

$$\begin{aligned} H_{in} &= c_i\delta_{in} + \frac{1}{2\pi}\int_{\Gamma_n}\frac{\partial}{\partial n}\left(\ln\left(\frac{1}{r}\right)\right)d\Gamma \\ G_{in} &= \frac{1}{2\pi}\int_{\Gamma_n}\ln\left(\frac{1}{r}\right)d\Gamma \end{aligned} \tag{4.47}$$

where δ_{in} is the Kronecker delta function for $i, n = 1, \ldots, N$ and r is the distance from the $i-th$ node to the $n-th$ element. The implementation of the boundary conditions for ψ and its normal derivative gives a linear system of algebraic equations $\boldsymbol{A}\boldsymbol{X} = \boldsymbol{Y}$ which can be solved for the unknown vector $\boldsymbol{X}$. Here $\boldsymbol{X}$ contains the unknown values of stream function ψ and its normal derivative $\partial\psi/\partial n$. Then, the velocity components can be computed by using the coordinate matrix $\boldsymbol{F}$ as in (4.43) and (4.44)

$$\boldsymbol{u} = \frac{\partial \boldsymbol{\psi}}{\partial y} = \frac{\partial \boldsymbol{F}}{\partial y}\boldsymbol{F}^{-1}\boldsymbol{\psi}, \quad \boldsymbol{v} = -\frac{\partial \boldsymbol{\psi}}{\partial x} = -\frac{\partial \boldsymbol{F}}{\partial x}\boldsymbol{F}^{-1}\boldsymbol{\psi} \tag{4.48}$$

Now, we consider the vorticity transport equation with Laplace term left alone on one side of the equation (4.16)

$$\nabla^2\omega = Re\left(\frac{\partial\omega}{\partial t} + u\frac{\partial\omega}{\partial x} + v\frac{\partial\omega}{\partial y}\right). \tag{4.49}$$

The right hand side is treated as nonhomogeneous function d similar to the stream function equation (4.45). Thus, a similar procedure through the equations (4.18)-(4.38), leads the following DRBEM matrix system for the vorticity transport equation

$$\boldsymbol{H}\,\boldsymbol{\omega} - \boldsymbol{G}\,\boldsymbol{q}_\omega = Re(\boldsymbol{H}\hat{\boldsymbol{U}} - \boldsymbol{G}\hat{\boldsymbol{Q}})\boldsymbol{F}^{-1}\left(\frac{\partial\boldsymbol{\omega}}{\partial t} + \boldsymbol{u}\frac{\partial\boldsymbol{\omega}}{\partial x} + \boldsymbol{v}\frac{\partial\boldsymbol{\omega}}{\partial y}\right). \tag{4.50}$$

Here, the products of vectors in the convection terms are handled by extending the vectors $\boldsymbol{u}$ and $\boldsymbol{v}$ into $(N+IP)\times(N+IP)$ diagonal matrices of which entries are assumed to be the entries of $\boldsymbol{u}$ and $\boldsymbol{v}$, respectively. The vector multiplying $\boldsymbol{F}^{-1}$ in (4.50) contains the time derivative of vorticity which brings the need of a time integration scheme. Actually, this system can be rearranged in order to form a system of ordinary differential equations for vorticity

$$\frac{\partial\boldsymbol{\omega}}{\partial t} = \boldsymbol{Z}(\boldsymbol{\omega}, t) \tag{4.51}$$

where the vector function $\boldsymbol{Z}$ is described as

$$\boldsymbol{Z}(\boldsymbol{\omega}, t) = \frac{1}{Re}\boldsymbol{F}(\boldsymbol{H}\hat{\boldsymbol{U}} - \boldsymbol{G}\hat{\boldsymbol{Q}})^{-1}\Big(\boldsymbol{H}\boldsymbol{\omega} - \boldsymbol{G}\,\boldsymbol{q}_\omega\Big) - \boldsymbol{u}\frac{\partial\boldsymbol{\omega}}{\partial x} - \boldsymbol{v}\frac{\partial\boldsymbol{\omega}}{\partial y}. \tag{4.52}$$

Thus, for the solution of the first order ordinary differential equations in (4.51), we make use of an implicit time integration scheme which is an unconditionally stable second order backward difference scheme, namely Gear scheme or upwind scheme [79],

$$\frac{3\boldsymbol{\omega}^{m+1} - 4\boldsymbol{\omega}^{m} + \boldsymbol{\omega}^{m-1}}{2\Delta t} = Z(\boldsymbol{\omega}^{m+1}, t_{m+1}) \tag{4.53}$$

for each time interval $[t_{m-1}, t_m]$, $m = 1, \ldots, M$ and M is the number of time intervals determined by the increment Δt. Therefore, the following discretized matrix-vector equation is produced for $\boldsymbol{\omega}$

$$\left(\frac{1}{Re}\widetilde{\boldsymbol{H}} - \frac{3\boldsymbol{I}}{2\Delta t} - \boldsymbol{u}^m\frac{\partial}{\partial x} - \boldsymbol{v}^m\frac{\partial}{\partial y}\right)\boldsymbol{\omega}^{m+1} - \frac{1}{Re}\widetilde{\boldsymbol{G}}\frac{\partial \boldsymbol{\omega}^{m+1}}{\partial n} = -\frac{2\boldsymbol{I}}{\Delta t}\boldsymbol{\omega}^m + \frac{\boldsymbol{I}}{2\Delta t}\boldsymbol{\omega}^{m-1} \tag{4.54}$$

which requires two previous time level values for obtaining the solution at a required time level. In this representation the operators $\partial/\partial x$ and $\partial/\partial y$ are approximated by the coordinate matrix $\boldsymbol{F}$, i.e.

$$\frac{\partial \Theta}{\partial x} \approx \frac{\partial \boldsymbol{F}}{\partial x}\boldsymbol{F}^{-1}\Theta \qquad \text{and} \qquad \frac{\partial \Theta}{\partial y} \approx \frac{\partial \boldsymbol{F}}{\partial y}\boldsymbol{F}^{-1}\Theta \tag{4.55}$$

where Θ denotes the vorticity vector $\boldsymbol{\omega}^{m+1}$ and I denotes the $(N + IP) \times (N + IP)$ identity matrix. $\widetilde{\boldsymbol{H}}$ and $\widetilde{\boldsymbol{G}}$ are stated as

$$\widetilde{\boldsymbol{H}} = \boldsymbol{F}(\boldsymbol{H}\hat{\boldsymbol{U}} - \boldsymbol{G}\hat{\boldsymbol{Q}})^{-1}\boldsymbol{H} \qquad \text{and} \qquad \widetilde{\boldsymbol{G}} = \boldsymbol{F}(\boldsymbol{H}\hat{\boldsymbol{U}} - \boldsymbol{G}\hat{\boldsymbol{Q}})^{-1}\boldsymbol{G}. \tag{4.56}$$

Now, the missing boundary conditions of vorticity are obtained from the definition of vorticity (equation (4.14)) which in turn can easily be computed with the help of coordinate matrix $\boldsymbol{F}$ as

$$\boldsymbol{\omega} = \frac{\partial \boldsymbol{v}}{\partial x} - \frac{\partial \boldsymbol{u}}{\partial y} = \frac{\partial \boldsymbol{F}}{\partial x}\boldsymbol{F}^{-1}\boldsymbol{v} - \frac{\partial \boldsymbol{F}}{\partial y}\boldsymbol{F}^{-1}\boldsymbol{u} \tag{4.57}$$

Once the resulting boundary conditions for vorticity are imposed to the final system (4.54) one can reach a linear system of algebraic equations of the form

$$\widetilde{\boldsymbol{A}}\widetilde{\boldsymbol{X}} = \widetilde{\boldsymbol{Y}} \tag{4.58}$$

of which the solution $\widetilde{\boldsymbol{X}}$ gives the unknown vorticity values at interior nodes and vorticity flux values on the boundary. Shortly, the stream function and vorticity transport equations are solved iteratively by using DRBEM with a backward difference time scheme. The iterative procedure starts by taking vorticity initially zero on the right hand side of the stream function equation. The solution algorithm is tested on the benchmark problem governed by Navier-Stokes equations in a square cavity with a moving top.

4.1.2 Numerical results (Lid-driven cavity problem)

We consider lid-driven cavity flow in two-dimensions defined in a unit square. No-slip boundary condition is imposed on the fixed walls whereas the top lid is moving with a constant velocity to the right (Figure 4.1). The Navier-Stokes equations are considered in stream function-vorticity form. The fluid is assumed to be initially motionless, and the top surface is forced to move horizontally from left to right with a constant velocity, $u = 1$. We use $\Delta t = 1.0$ and the computations are carried out with 10^{-4} tolerance within the difference between the two consecutive iteration values. $N = 100$ constant boundary elements are used, and the solution is obtained for Reynolds number values up to 2000.

As it is seen from the Figures 4.2-4.5, when $Re = 100$ the streamline primary vortex moves towards to the right wall due to the movement of the top lid. At a Reynolds number of around $Re = 400$ and more, the primary vortex tends to move to the cavity centre. As Re gets larger secondary vortices are developed at the bottom corners, and finally around $Re = 2000$ at the upper left corner. As Re increases, the vorticity contours move away from the cavity centre and accumulate on the walls of the cavity forming boundary layers, especially on the moving lid developing strong vorticity gradients. A stagnant region develops at the centre of the cavity where *Re* increases. These are expected behaviours of cavity flow, and are in good agreement with the behaviours observed in [90].

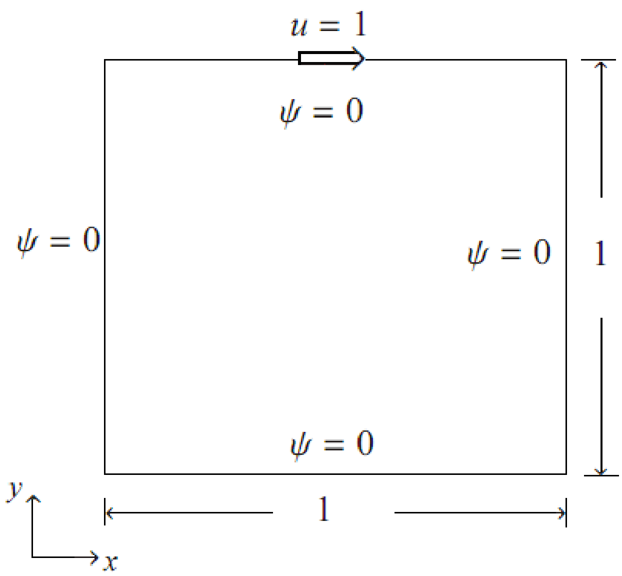

Figure 4.1: Square cavity with moving top at a constant velocity $u = 1$.

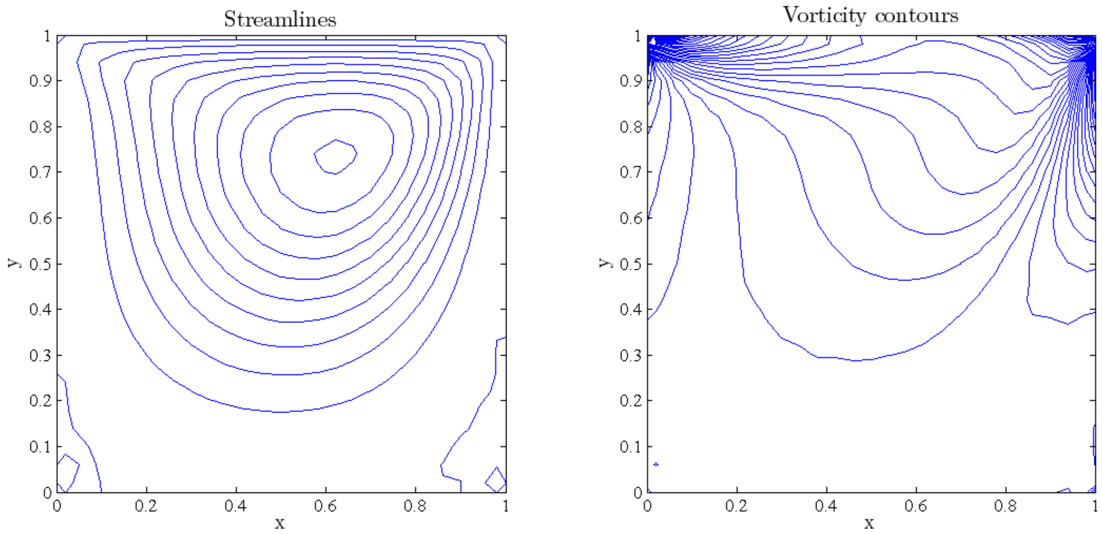

Figure 4.2: Streamlines and vorticity contours for Re = 100.

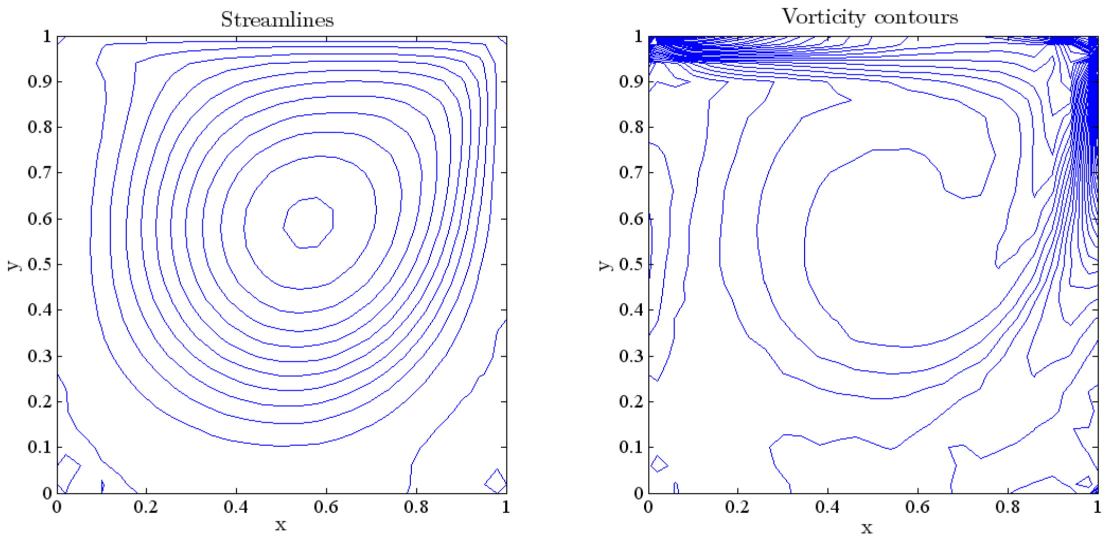

Figure 4.3: Streamlines and vorticity contours for Re = 400.

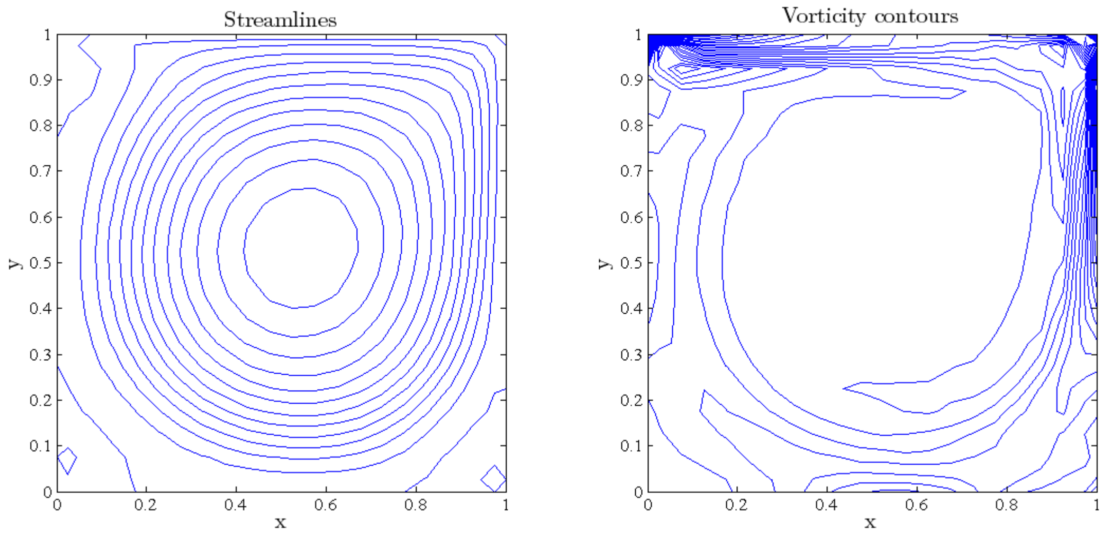

Figure 4.4: Streamlines and vorticity contours for Re = 1000.

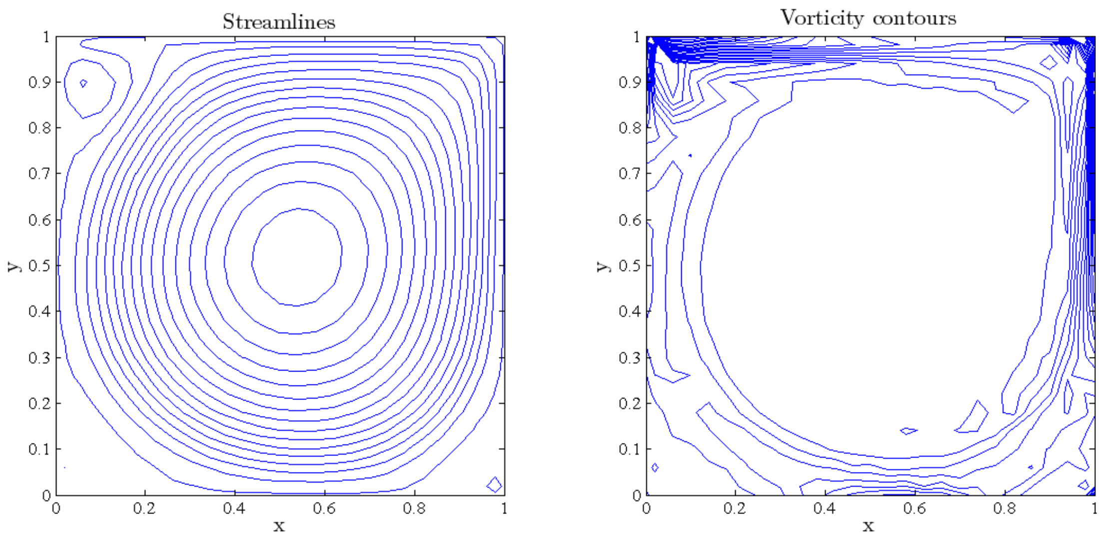

Figure 4.5: Streamlines and vorticity contours for Re = 2000.

4.2 Application to Full Magnetohydrodynamic Flow Equations

This section presents a dual reciprocity boundary element method (DRBEM) formulation coupled with an implicit backward difference time integration scheme for the solution of the incompressible magnetohydrodynamic (MHD) flow equations. The governing equations are the coupled system of Navier-Stokes equations and Maxwell's equations of electromagnetics through Ohm's law. We are concerned with a stream function-vorticity-magnetic induction-current density formulation of the full MHD equations in two-dimensions. The stream function and magnetic induction equations which are poisson type, are solved by using DRBEM with the fundamental solution of Laplace equation. In the DRBEM solution of the time-dependent vorticity and current density equations all the terms apart from the Laplace term are treated as nonhomogeneities. The time derivatives are approximated by an implicit backward difference while the convective terms are approximated by radial basis functions. The applications are given for the full MHD flow, in a square cavity and in a backward-facing step. The numerical results for the square cavity problem in the presence of a magnetic field are visualized for several values of Reynolds, Hartmann and magnetic Reynolds numbers. The effect of each parameter is analyzed with the graphs presented in terms of stream function, vorticity, current density and magnetic induction contours. Then, we provide the solution of the step flow problem in terms of velocity field, vorticity, current density and magnetic field for increasing values of Hartmann number.

4.2.1 Full magnetohydrodynamic flow equations

The MHD flow for an incompressible electrically conducting fluid is governed by a set of equations including Maxwell's equations of electromagnetics and Navier-Stokes equations of fluid dynamics. The standard form of the Maxwell's equations are given by [60, 61]

$$\nabla \times \boldsymbol{E} = -\frac{\partial \boldsymbol{B}}{\partial t}, \tag{4.59}$$

$$\nabla \times \boldsymbol{H_s} = \boldsymbol{J} + \frac{\partial \boldsymbol{D}}{\partial t}, \tag{4.60}$$

$$\nabla \cdot \boldsymbol{D} = \rho_c, \tag{4.61}$$

$$\nabla \cdot \boldsymbol{B} = 0. \tag{4.62}$$

Equation (4.59) is known as Faraday's law where $\boldsymbol{E}$ and $\boldsymbol{B}$ are electric field and magnetic induction, respectively. Equation (4.60) is the Ampère's law describing the source of the magnetic field with the magnetic field strength $\boldsymbol{H_s}$, the current density $\boldsymbol{J}$ and the time rate of electric displacement field $\boldsymbol{D}$. The relationships $\boldsymbol{B} = \mu \boldsymbol{H_s}$ and $\boldsymbol{D} = \epsilon \boldsymbol{E}$ are valid for the free space where μ is the magnetic permeability and ϵ is the electric permittivity. The third equation displays the Gauss's law where ρ_c is the free electric charge density, and equation (4.62) states that the divergence of a magnetic field is zero. The displacement current $\partial \boldsymbol{D}/\partial t$ is assumed to be negligibly small in comparison with other terms.

The Navier-Stokes equations describing the motion of an incompressible viscous fluid are

$$\begin{aligned} &\nabla \cdot \boldsymbol{V} = 0, \\ &\frac{\partial \boldsymbol{V}}{\partial t'} + \boldsymbol{V} \cdot \nabla \boldsymbol{V} = -\frac{1}{\rho} \nabla p' + \nu \nabla^2 \boldsymbol{V} + \boldsymbol{f_{ext}} \end{aligned} \tag{4.63}$$

where $\boldsymbol{V}$ is the velocity field, ν is the kinematic viscosity, ρ is the density, p' is the pressure and $\boldsymbol{f_{ext}}$ is the external force due to the Lorentz force $(\nabla \times \boldsymbol{B}) \times \boldsymbol{B}$ and body force. These equations are combined with the equations (4.59)-(4.62) through Ohm's law

$$\boldsymbol{J} = \sigma(\boldsymbol{E} + \boldsymbol{V} \times \boldsymbol{B}) \tag{4.64}$$

where σ is the electrical conductivity.

Then, a set of nondimensional equations for an incompressible MHD flow can be obtained as [78],

$$\frac{\partial \mathbf{v}}{\partial t} + \mathbf{v}\cdot\nabla\mathbf{v} = -\nabla p + \frac{1}{Re}\nabla^2\mathbf{v} + Al(\nabla\times\boldsymbol{b})\times\boldsymbol{b} + \boldsymbol{g},$$

$$\frac{\partial \boldsymbol{b}}{\partial t} - \nabla\times(\mathbf{v}\times\boldsymbol{b}) = \frac{1}{Re_m}\nabla^2\boldsymbol{b}, \tag{4.65}$$

$$\nabla\cdot\mathbf{v} = 0,$$

$$\nabla\cdot\boldsymbol{b} = 0$$

where $\mathbf{v}$, $\boldsymbol{b}$, p denote the nondimensional velocity field, magnetic field and pressure, respectively with

$$\mathbf{v} = \frac{\boldsymbol{V}}{U'},\quad \boldsymbol{b} = \frac{\boldsymbol{B}}{B'} \text{ and } p = \frac{p'}{\rho(U')^2}.$$

$Re = U'L'/\nu$ is the Reynolds number, $Al = (B')^2/\mu\rho U'^2$ is the Alfvèn number and $Re_m = \sigma\mu U'L'$ is the induced magnetic Reynolds number described in terms of the characteristic velocity U', characteristic length L' and characteristic magnetic induction B' (the intensity of the applied magnetic field), respectively and $\boldsymbol{g}$ is the body force.

In two-dimensional case, equations (4.65) are also expressed in terms of stream functions, vorticity and current density [74]. Thus, we give an alternative formulation in terms of stream function, vorticity, magnetic induction and current density as

$$\nabla^2\psi = -\omega\,, \tag{4.66}$$

$$\nabla^2\omega = Re\Big(\frac{\partial\omega}{\partial t} + u\frac{\partial\omega}{\partial x} + \upsilon\frac{\partial\omega}{\partial y} - g_\omega\Big), \tag{4.67}$$

$$\nabla^2 b_x = -Re_m\frac{\partial j}{\partial y}, \tag{4.68}$$

$$\nabla^2 b_y = Re_m \frac{\partial j}{\partial x}, \tag{4.69}$$

$$\nabla^2 j = Re_m \Big(\frac{\partial j}{\partial t} + u\frac{\partial j}{\partial x} + \upsilon\frac{\partial j}{\partial y} - g_j \Big), \tag{4.70}$$

which define a Dirichlet-type problem with the available boundary conditions for the velocity field $\mathbf{v} = (u, \upsilon, 0)^T$ and magnetic field $\boldsymbol{b} = (b_x, b_y, 0)^T$. Here g_ω and g_j denote

$$g_\omega = S_t \Big(b_x \frac{\partial j}{\partial x} + b_y \frac{\partial j}{\partial y} \Big) \tag{4.71}$$

$$\begin{aligned} g_j = \frac{1}{Re_m} \Big(b_x \frac{\partial \omega}{\partial x} + b_y \frac{\partial \omega}{\partial y} \Big) + \frac{2}{Re_m} \Big(\frac{\partial b_x}{\partial x} \big(\frac{\partial \upsilon}{\partial x} + \frac{\partial u}{\partial y} \big) \\ + \frac{\partial \upsilon}{\partial y} \big(\frac{\partial b_y}{\partial x} + \frac{\partial b_x}{\partial y} \big) \Big) \end{aligned} \tag{4.72}$$

where $S_t = Re_m Al$ is the Stuart number giving the ratio of the electromagnetic force to the inertial force and related to the Hartmann number $Ha = B'L'(\sigma/\nu\rho)^{1/2}$ through the equation $S_t = Ha^2/Re$.

In order to obtain equations (4.66)-(4.70), we take the curl of both sides of the equations $(4.65)_1$ and $(4.65)_2$ within the definitions for vorticity field $\boldsymbol{\omega} = (0, 0, \omega)^T$, stream function $\boldsymbol{\psi} = (0, 0, \psi)^T$

$$\boldsymbol{\omega} = \nabla \times \mathbf{v} \quad , \quad \mathbf{v} = \nabla \times \boldsymbol{\psi}, \tag{4.73}$$

and the nondimensional electric current density $\boldsymbol{j} = (0, 0, j)^T$

$$\boldsymbol{j} = \frac{1}{Re_m} \nabla \times \boldsymbol{b} \tag{4.74}$$

thus,

$$j = \frac{1}{Re_m}\left(\frac{\partial b_y}{\partial x} - \frac{\partial b_x}{\partial y}\right) \tag{4.75}$$

and also we enforce the resulting equations to satisfy the divergence-free conditions.

Now, similar to the DRBEM procedure performed in Section 4.1, the equations (4.66) through (4.70) are solved iteratively for ψ, ω, b_x, b_y and j in order.

4.2.2 DRBEM formulation of full MHD equations

DRBEM application to full MHD equations are carried by treating the right hand sides in equations (4.66)-(4.70) as the nonhomogeneities for stream function, vorticity, magnetic induction and current density unknowns, respectively. Thus, the matrix-vector equations are obtained after the discretization with N constant boundary elements and for IP interior nodes

$$\boldsymbol{H}\,\boldsymbol{\psi} - \boldsymbol{G}\,\boldsymbol{q_\psi} = (\boldsymbol{H}\,\hat{\boldsymbol{U}} - \boldsymbol{G}\hat{\boldsymbol{Q}})\boldsymbol{F}^{-1}\,(-\boldsymbol{\omega}) \tag{4.76}$$

$$\boldsymbol{H}\,\boldsymbol{\omega} - \boldsymbol{G}\,\boldsymbol{q_\omega} = Re(\boldsymbol{H}\,\hat{\boldsymbol{U}} - \boldsymbol{G}\,\hat{\boldsymbol{Q}})\boldsymbol{F}^{-1}\left(\frac{\partial \boldsymbol{\omega}}{\partial t} + \boldsymbol{u}\frac{\partial \boldsymbol{\omega}}{\partial x} + \boldsymbol{v}\frac{\partial \boldsymbol{\omega}}{\partial y} - \boldsymbol{g_\omega}\right), \tag{4.77}$$

$$\boldsymbol{H}\,\boldsymbol{b_x} - \boldsymbol{G}\,\boldsymbol{q_{b_x}} = (\boldsymbol{H}\,\hat{\boldsymbol{U}} - \boldsymbol{G}\,\hat{\boldsymbol{Q}})\boldsymbol{F}^{-1}\left(-Re_m\frac{\partial \boldsymbol{j}}{\partial y}\right), \tag{4.78}$$

$$\boldsymbol{H}\,\boldsymbol{b_y} - \boldsymbol{G}\,\boldsymbol{q_{b_y}} = (\boldsymbol{H}\,\hat{\boldsymbol{U}} - \boldsymbol{G}\,\hat{\boldsymbol{Q}})\boldsymbol{F}^{-1}\left(Re_m\frac{\partial \boldsymbol{j}}{\partial x}\right), \tag{4.79}$$

$$\boldsymbol{H}\,\boldsymbol{j} - \boldsymbol{G}\,\boldsymbol{q_j} = Re_m(\boldsymbol{H}\,\hat{\boldsymbol{U}} - \boldsymbol{G}\,\hat{\boldsymbol{Q}})\boldsymbol{F}^{-1}\left(\frac{\partial \boldsymbol{j}}{\partial t} + \boldsymbol{u}\frac{\partial \boldsymbol{j}}{\partial x} + \boldsymbol{v}\frac{\partial \boldsymbol{j}}{\partial y} - \boldsymbol{g_j}\right) \tag{4.80}$$

respectively for equations (4.66)-(4.70). In these equations bold letters denote $(N + IP) \times (N + IP)$ matrices, and $(N + IP) \times 1$ vectors corresponding to unknowns through the equations (4.66)-(4.70). The vectors $\boldsymbol{g_\omega}$ and $\boldsymbol{g_j}$ are also formed by using equations (4.71)-(4.72) at $N + IP$ points. The matrix-vector equations for $\boldsymbol{b_x}$ and $\boldsymbol{b_y}$ in

(4.78) and (4.79) resemble the matrix-vector form of stream function equation in (4.76). Thus, the required values of $\boldsymbol{b_x}$, $\boldsymbol{b_y}$ and their normal derivatives can be computed easily just by making use of initial approximations to the right hand side terms of (4.78) and (4.79) consisting of $y-$ and $x-$derivatives of current density $\boldsymbol{j}$. However, the matrix-vector forms of vorticity and current density equations contain the time rates which bring the need of a time integration scheme. Moreover, the boundary conditions for both the vorticity and current density are unknown. In this sense, we first employ an implicit backward difference scheme [79, 91] to approximate the time derivatives $\partial\boldsymbol{\omega}/\partial t$ and $\partial\boldsymbol{j}/\partial t$. For these equations, the DRBEM applications coupled with a backward difference scheme are similar to the application which is presented in Section 4.1.1 for vorticity equation. Here, equations (4.67) and (4.70) differ only with the right hand sides from the vorticity transport equation (4.16) of Navier-Stokes equations in Section 4.1.1. Thus, after the solution of the stream function equation, the right hand side of vorticity equation of Magnetohydrodynamics becomes known. Then, the final DRBEM system (4.77) is solved for vorticity as is done with the equations (4.50)-(4.58). Hence, letting these values to be used as initials for the current density equation (4.70), the same procedure is repeated this time to reach the current density values.

Thus, the DRBEM application coupling with the present time integration scheme for vorticity $\boldsymbol{\omega}$ and current density j, results in

$$\left(\frac{1}{Re}\widetilde{\boldsymbol{H}} - \frac{3\boldsymbol{I}}{2\Delta t} - \boldsymbol{u}^m\frac{\partial}{\partial x} - \boldsymbol{v}^m\frac{\partial}{\partial y}\right)\boldsymbol{\omega}^{m+1} - \frac{1}{Re}\widetilde{\boldsymbol{G}}\frac{\partial\boldsymbol{\omega}}{\partial n}^{m+1} = -\frac{2\boldsymbol{I}}{\Delta t}\boldsymbol{\omega}^m + \frac{\boldsymbol{I}}{2\Delta t}\boldsymbol{\omega}^{m-1} - \boldsymbol{g_\omega}^m \tag{4.81}$$

$$\left(\frac{1}{Re_m}\widetilde{\boldsymbol{H}} - \frac{3\boldsymbol{I}}{2\Delta t} - \boldsymbol{u}^m\frac{\partial}{\partial x} - \boldsymbol{v}^m\frac{\partial}{\partial y}\right)\boldsymbol{j}^{m+1} - \frac{1}{Re_m}\widetilde{\boldsymbol{G}}\,\boldsymbol{q_j}^{m+1} = -\frac{2\boldsymbol{I}}{\Delta t}\boldsymbol{j}^m + \frac{\boldsymbol{I}}{2\Delta t}\boldsymbol{j}^{m-1} - \boldsymbol{g_j}^m. \tag{4.82}$$

where

$$\widetilde{\boldsymbol{H}} = \boldsymbol{F}(\boldsymbol{H}\hat{\boldsymbol{U}} - \boldsymbol{G}\hat{\boldsymbol{Q}})^{-1}\boldsymbol{H} \qquad \text{and} \qquad \widetilde{\boldsymbol{G}} = \boldsymbol{F}(\boldsymbol{H}\hat{\boldsymbol{U}} - \boldsymbol{G}\hat{\boldsymbol{Q}})^{-1}\boldsymbol{G}. \tag{4.83}$$

The boundary conditions for vorticity and current density are also derived from their definitions

$$\boldsymbol{\omega} = \frac{\partial \boldsymbol{v}}{\partial x} - \frac{\partial \boldsymbol{u}}{\partial y} = \frac{\partial \boldsymbol{F}}{\partial x}\boldsymbol{F}^{-1}\boldsymbol{v} - \frac{\partial \boldsymbol{F}}{\partial y}\boldsymbol{F}^{-1}\boldsymbol{u} \tag{4.84}$$

$$\boldsymbol{j} = \frac{1}{Re_m}\left(\frac{\partial \boldsymbol{b_y}}{\partial x} - \frac{\partial \boldsymbol{b_x}}{\partial y}\right) = \frac{1}{Re_m}\left(\frac{\partial \boldsymbol{F}}{\partial x}\boldsymbol{F}^{-1}\boldsymbol{b_y} - \frac{\partial \boldsymbol{F}}{\partial y}\boldsymbol{F}^{-1}\boldsymbol{b_x}\right) \tag{4.85}$$

with the relationships (4.55) and by taking Θ as $\boldsymbol{u}$, $\boldsymbol{v}$ and $\boldsymbol{b_y}, \boldsymbol{b_x}$.

Then, the resulting boundary value problems are solved for the internal ω and j, and the vorticity and current density flux values on the boundary. The initial vorticity and current density values are taken as zero in order to start the iterative process. Then, the $x-$ and $y-$ derivatives of vorticity and current density are approximated by (4.55) that

$$\frac{\partial \boldsymbol{\omega}}{\partial x} = \frac{\partial \boldsymbol{F}}{\partial x}\boldsymbol{F}^{-1}\boldsymbol{\omega} \quad \text{and} \quad \frac{\partial \boldsymbol{\omega}}{\partial y} = \frac{\partial \boldsymbol{F}}{\partial y}\boldsymbol{F}^{-1}\boldsymbol{\omega} \tag{4.86}$$

$$\frac{\partial \boldsymbol{j}}{\partial x} = \frac{\partial \boldsymbol{F}}{\partial x}\boldsymbol{F}^{-1}\boldsymbol{j} \quad \text{and} \quad \frac{\partial \boldsymbol{j}}{\partial y} = \frac{\partial \boldsymbol{F}}{\partial y}\boldsymbol{F}^{-1}\boldsymbol{j} \tag{4.87}$$

to be used in the next iteration where they are needed initially.

4.2.3 Method of solution

The governing equations (4.66)-(4.70) form a nonlinearly coupled system of equations in magnetohydrodynamics. The DRBEM discretized matrix equations (4.76)-(4.80) are going to be solved iteratively for obtaining the solution of MHD flow with proper boundary conditions. First the stream function equation (4.76) is solved by taking vorticity as zero initially. Then we compute the velocity field components (4.48) by approximating the $x-$ and $y-$ derivatives of the stream function with the help of the coordinate matrix in terms of radial basis functions. Therefore, the substitution of $\boldsymbol{u}$ and $\boldsymbol{v}$ values into the vorticity equation (4.77) yields a linear convection-diffusion-type equation. The nonhomogeneous term is caused by the Lorentz force including magnetic field components and $x-$ and $y-$ derivatives of current density which are unknown (equation (4.71)). In order to start the iterative process these unknowns are assumed to be zero for the first iteration. For further iterations they are known from the previous time level in which they would be computed from the equations (4.78)- (4.80). Afterwards, we can apply an implicit backward difference scheme in time for the solution of vorticity. Again, the derivatives of vorticity are computed with the help of the coordinate matrix, which are needed in the solution of (4.80). For the other terms $\boldsymbol{b_x}$, $\boldsymbol{b_y}$ and their mixed derivatives appearing on the right hand side of the equation (4.80), the poisson type equations (4.78) and (4.79) are solved for $\boldsymbol{b_x}$ and $\boldsymbol{b_y}$ analogous the procedure followed in the solution of the stream function equation. Then, all the required terms, $x-$ and $y-$ derivatives of the velocity field components and magnetic field components are obtained on the boundary and inside with the help of radial basis function approximations. Finally, the equation (4.80) becomes a linear convection-diffusion type equation, and it is solved for $\boldsymbol{j}$ as in the solution of the vorticity equation. Further, the approximations for the derivatives $\partial \boldsymbol{j}/\partial x$ and $\partial \boldsymbol{j}/\partial y$ are obtained in order to continue the iterative process. Thus, a summary of the iterative process can be given as,

1. Solve the stream function equation (4.76) by taking vorticity initially zero.

2. Compute the nodal values of velocity components $\boldsymbol{u}$ and $\boldsymbol{v}$ and their $x-$ and $y-$derivatives. In order to find derivatives with respect to the spatial variables, x or y, use the coordinate matrix $\boldsymbol{F}$ in terms of radial basis functions such that

$$\boldsymbol{u} = \frac{\partial \boldsymbol{F}}{\partial y}\boldsymbol{F}^{-1}\boldsymbol{\psi}, \qquad \boldsymbol{v} = -\frac{\partial \boldsymbol{F}}{\partial x}\boldsymbol{F}^{-1}\boldsymbol{\psi}.$$

3. Compute the boundary conditions for vorticity by using the definition $\boldsymbol{\omega} = \partial \boldsymbol{v}/\partial x - \partial \boldsymbol{u}/\partial y$ with the DRBEM approach again by using coordinate matrix $\boldsymbol{F}$.

4. Solve the vorticity equation with an implicit backward difference scheme in time (equation (4.81)).

5. Compute derivatives of vorticity with the help of the coordinate matrix (equation (4.86)).

6. Solve equations (4.78) and (4.79) for the induced magnetic field components b_x and b_y analogous to the stream function equation (4.76).

7. Once the magnetic field components are obtained, find the spatial derivatives using (4.55) which are needed in the current density equation.

8. Solve current density equation (4.82) analogous to the vorticity transport equation (4.81).

9. Obtain the $x-$ and $y-$derivatives of the current density from (4.87) in order to use in the next iteration.

10. Describe a stopping criteria to be satisfied with the iterative procedure in order to get results at the steady-state and repeat the steps (1)-(10) reaching steady-state with a given tolerance.

4.2.4 Full MHD flow equations in a Lid-driven cavity

We consider the incompressible MHD equations in a square duct of which cross section is a unit square $\Omega = [0,1] \times [0,1]$. The upper wall of the duct is moving with a constant velocity $\mathbf{v} = (u, \upsilon, 0) = (1, 0, 0)$. On the other walls no-slip boundary conditions are given. The external applied magnetic field is imposed in-plane, transversal to the flow and it is taken as $\boldsymbol{b} = (b_x, b_y, 0) = (0, 1, 0)$ on the boundary. The computations are carried out with a uniform mesh with $N = 80$ constant boundary elements and $IP = 400$ interior nodes. The time step Δt is taken as 0.1 and the tolerance to reach the steady-state is 10^{-3}. The numerical solutions are presented for several values of magnetic Reynolds number, Reynolds number and Hartmann number. In order to see the effect of each parameter the other two are fixed. The computations are carried out untill reaching steady-state solutions.

In Figure 4.6 we present the stream function, vorticity, current density and induced magnetic field contours all together obtained for Reynolds number values $Re = 10, 100, 400, 1000$ with the fixed values of Hartmann number $Ha = 10$ and magnetic Reynolds number $Re_m = 100$. As Re increases, both vorticity and stream function contours start to accumulate close to the upper right corner due to the movement of the upper lid. Besides, the stream function develops new vortices at the lower corners and finally at the upper left corner while the vortex of the fluid is moving to the center of the duct. It is also noticed that vorticity develops circulations, and boundary layers are formed close to the upper lid and the right wall due to the increasing values of Re. A similar behaviour is observed in current density contours as in Figure 4.6-(c). The induced magnetic field lines become straight in the direction of the positive $y-$axis when Reynolds number increases suppressing the effect of magnetic Reynolds number which is $Re_m = 100$ large enough.

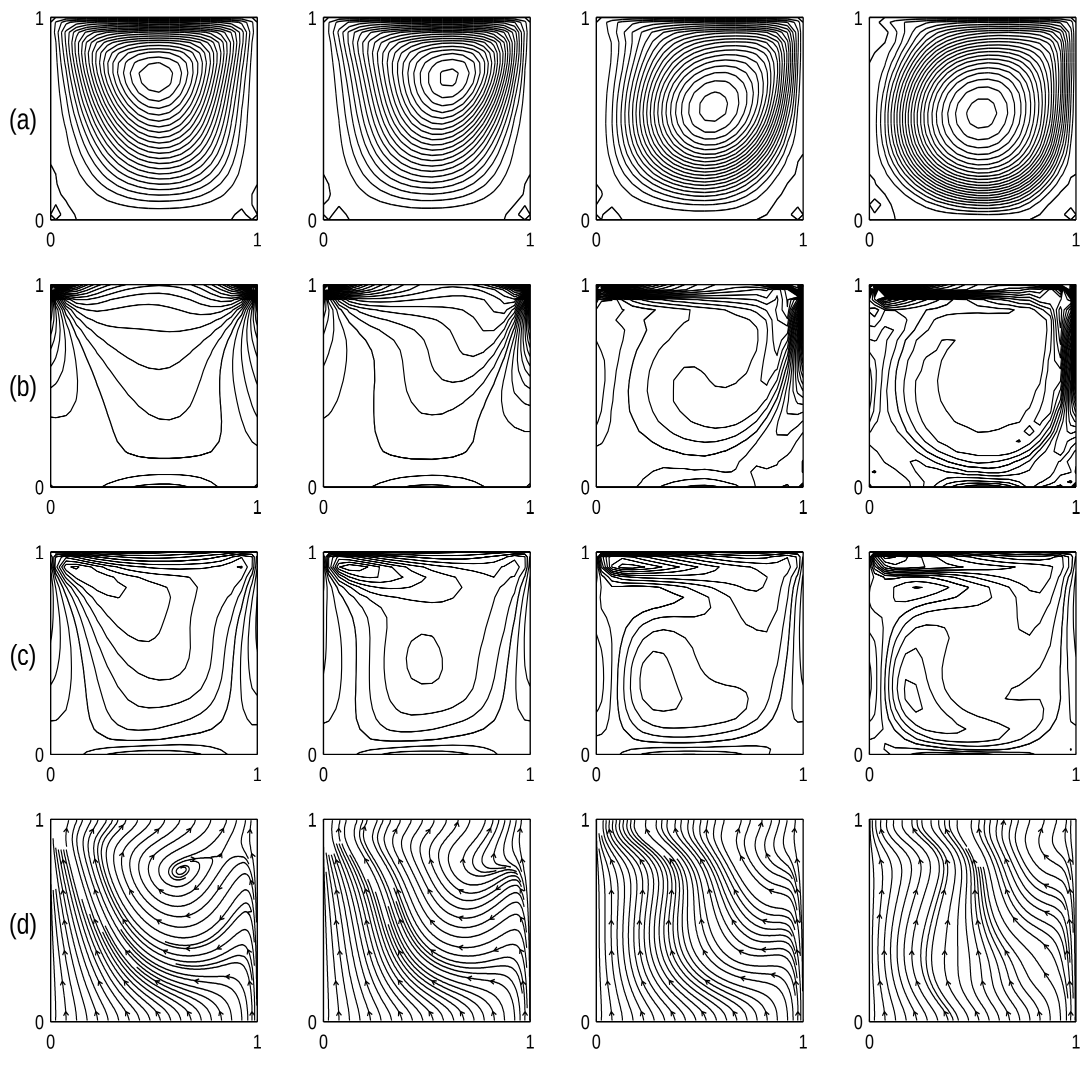

Figure 4.6: (a) Stream function, (b) vorticity, (c) current density and (d) induced magnetic field for $Re = 10, 100, 400, 1000$ where $Re_m = 100, Ha = 10$.

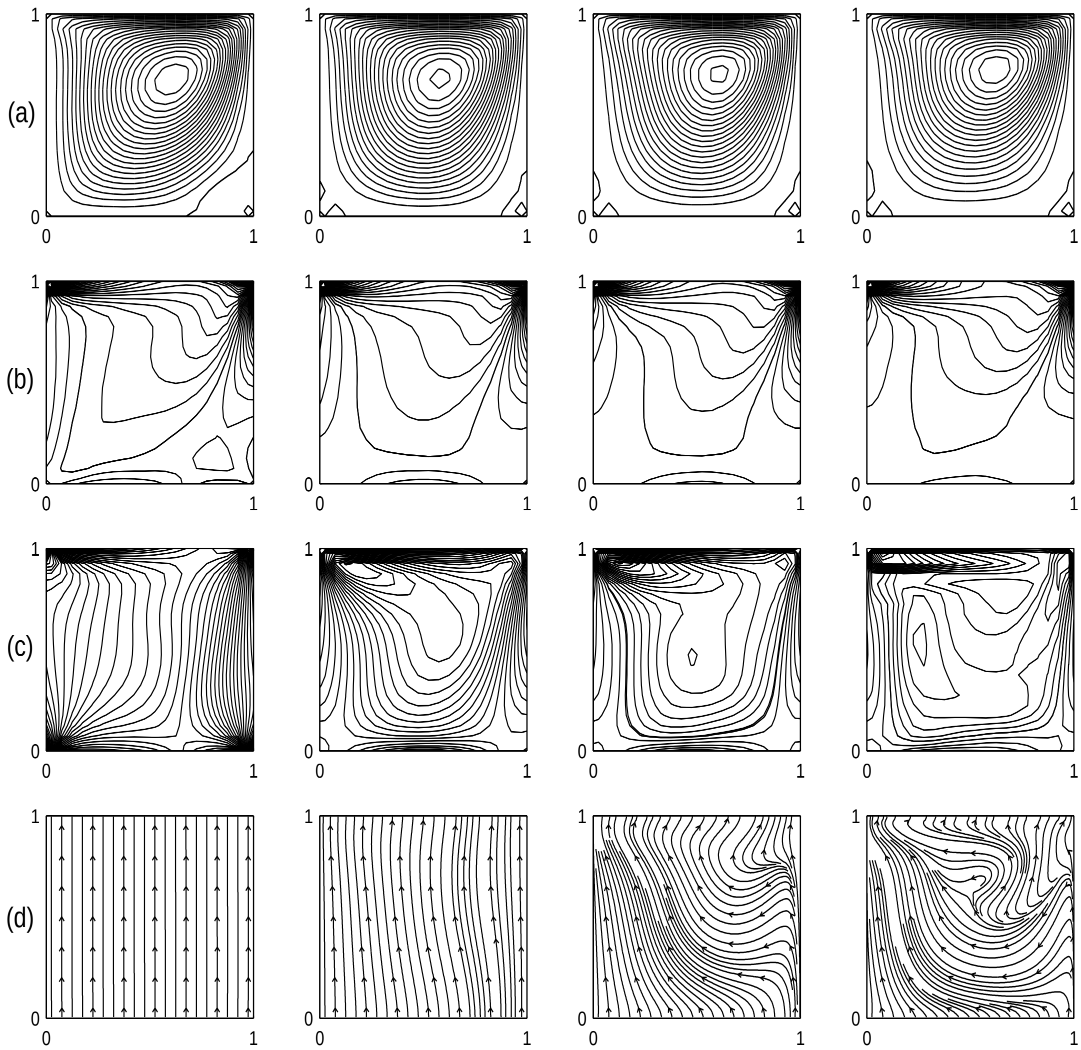

Figure 4.7: (a) Stream function, (b) vorticity, (c) current density and (d) induced magnetic field for $Re_m = 0.1, 10, 100, 500$ where $Re = 100, Ha = 10$.

It is shown in Figure 4.7-(a,b) that stream function and vorticity are not affected much as Re_m increases since the corresponding equations do not include Re_m directly. But, current density develops circulations when Re_m increases due to the strong effect of Lorentz force. At small values of magnetic Reynolds number, the applied magnetic field dominates the induced magnetic field. Thus, when Re_m increases, the magnetic induction lines start to be affected and circulate inside the channel as in figure (4.7)-(d).

Figure (4.8) shows the behaviour of stream function, vorticity, current density and magnetic field for increasing values of Hartmann number as $Ha = 0, 10, 50, 100$

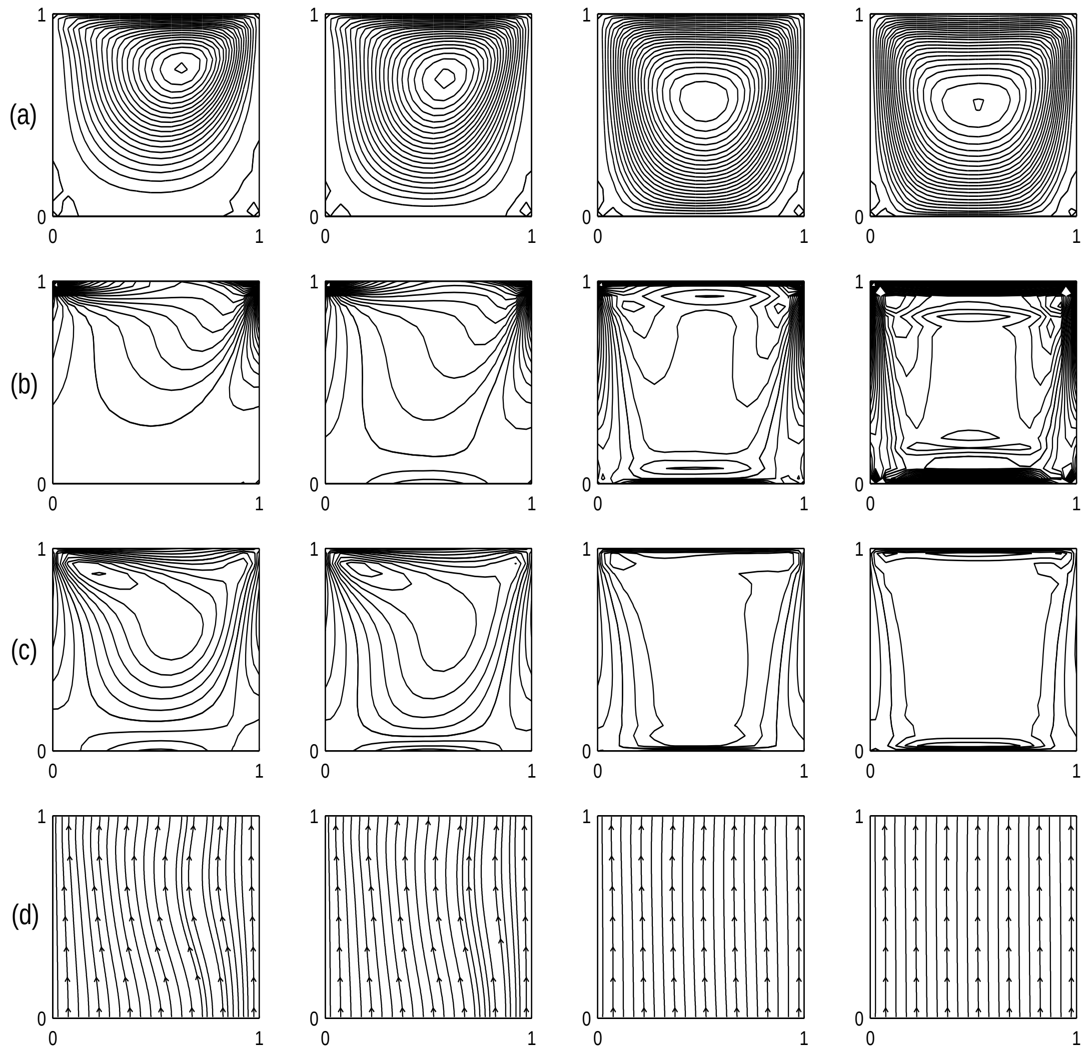

Figure 4.8: (a) Stream function, (b) vorticity, (c) current density and (d) induced magnetic field for $Ha = 0, 10, 50, 100$ where $Re = 100, Re_m = 10$.

with the fixed values $Re = 100$ and $Re_m = 10$. As it is expected, boundary layers are formed close to the walls for both the vorticity and the current density due to the strong applied magnetic field intensity (as Ha increases). The vortex of the fluid moves through the center as it is seen from the stream contours in Figure 4.8-(a). The induced magnetic field lines in Figure 4.8-(d) steer up smoothly indicating the dominance of the high value of Hartmann number.

4.2.5 MHD flow over a backward-facing step

Now, we consider the MHD flow, over a backward-facing step. The fluid motion is described in Figure 4.9. The boundary conditions for the stream function and the velocity field are the same as in the reference study [92]. The flow of the fluid is through $+x$-direction and the applied magnetic field is through $+y$-direction with an intensity B'. The top and bottom boundaries are stationary walls and no-slip boundary conditions are applied for the velocity. The inlet velocity has a parabolic profile defined by $u = 24y(0.5 - y)$ at $0 \leq y \leq 0.5$ with a maximum inflow velocity 1.5 at $y = 0.25$. The step face located at $-0.5 \leq y \leq 0$ is also stationary and the no-slip boundary conditions for velocity components occur. The boundary conditions for the applied magnetic field are taken as

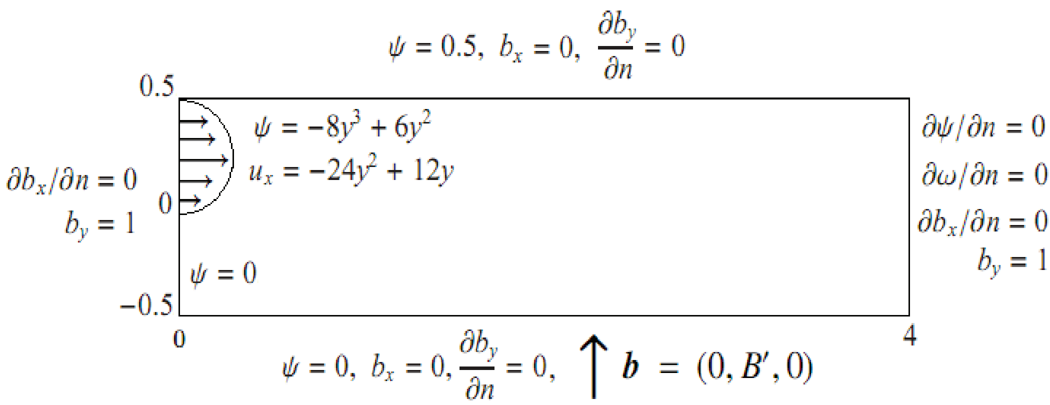

Figure 4.9: MHD flow geometry over a backward-facing step with boundary conditions.

$$
\begin{aligned}
&b_x = 0,\ \frac{\partial b_y}{\partial n} = 0 \quad \text{on} \quad y = -0.5 \ \text{ and } \ y = 0.5 \\
&\frac{\partial b_x}{\partial n} = 0,\ b_y = 1 \quad \text{on} \quad x = 0 \ \text{ and } \ x = 4
\end{aligned}
\tag{4.88}
$$

which fit with the conditions given by Aydın et. al. [93].

In Figures 4.10 and 4.11, the behavior of the stream function and the $x-$ component of the induced magnetic field are visualized. It is obviously seen that increasing number of boundary elements in both directions (by taking three times more elements in $x-$direction than in $y-$direction) leads smoother contour lines. Here, the effect of the number of boundary elements is more visible since the problem is defined in a rectangular region i.e. the channel height is one fourth of the channel length. The results are obtained with $N = 80$ and $N = 128$ constant boundary elements with an accuracy of 10^{-3}, and the time increment is $\Delta t = 0.5$. The parameters are fixed as $Re = 400, Re_m = 1$ and $Ha = 10$. In Figures 4.12-4.16 we present the contour lines of the velocity field, vorticity, current density and the magnetic field for Hartmann number values $Ha = 0, 5, 10, 50, 100$, respectively. Here, the magnetic Reynolds and Reynolds numbers are fixed as $Re_m = 1$ and $Re = 100$. As it is seen in parts (a) of each figure, a recirculation zone occurs after the step face located at $-0.5 < y < 0$, and it decreases as Hartmann number increases. This is an expected behavior analogous to the available numerical results of Aydın et. al. [93]. Similar to the lid-driven cavity problem, the induced magnetic field lines become straight in the positive $y-$direction (the direction of the applied magnetic field) as a result of using large Hartmann numbers which eliminates the effect of the Reynolds number (see part (d) of Figures 4.12-4.16). When we focus on the contour lines of vorticity and current density, we observe boundary layers close to the top and bottom walls as Ha increases. The circulations with two cores adhered the inlet boundary ($x = 0$, $-0.5 < y < 0.5$) for both vorticity and current density intend to get closer to the left wall(the lengths of circulations decrease). The speed of the flow is damped by the step and then the vorticity becomes more stagnant closer to the outlet boundary as Hartmann number increases.

4.3 Discussions

The incompressible full MHD flow equations in terms of stream function, vorticity, magnetic induction and current density are solved numerically. We make use of the DRBEM for the solution of all the corresponding poisson type equations. Thus, we take the advantage of obtaining the results both on the boundary and inside the domain simultaneously. Also, the iterative process is cost-effective, since the matrix-vector form for all equations are in terms of standard DRBEM matrices of which entries are computed once and used in all the iterative process invariably. The resulting initial value problems for the vorticity and current density equations are treated by an implicit backward difference scheme which is unconditionally stable. Therefore, the need of small time increments is eliminated. The unknown boundary conditions for vorticity and current density are figured out with the approximations done by radial basis function theory of DRBEM. The numerical examples demonstrate the well known MHD flow characteristics.

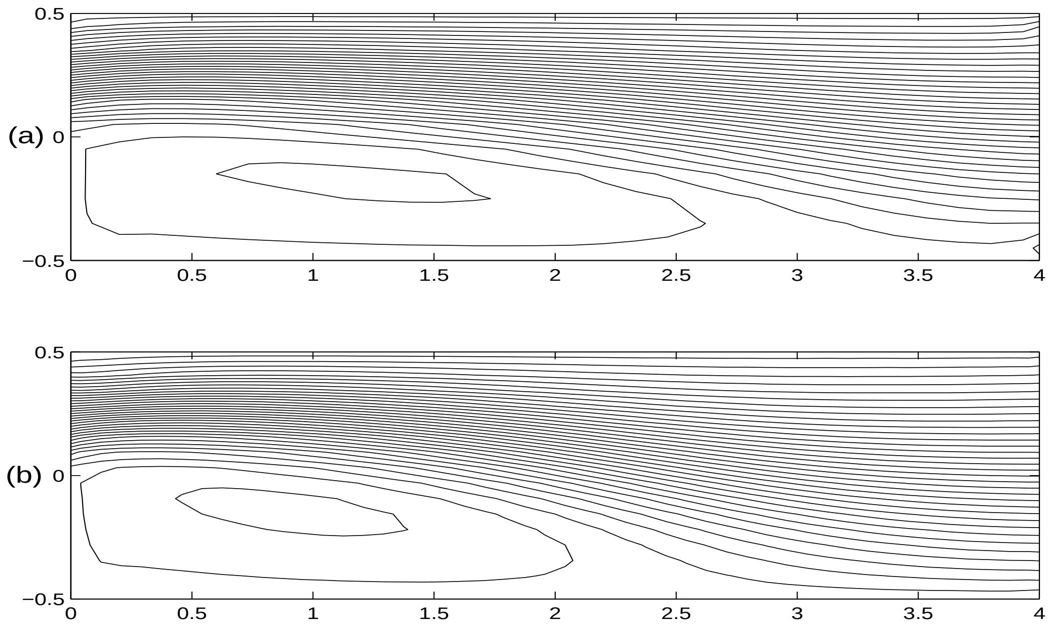

Figure 4.10: (a)Stream lines with $N = 80$, (b)Stream lines with $N = 128$ for $Ha = 10$, $Re = 400, Re_m = 1$.

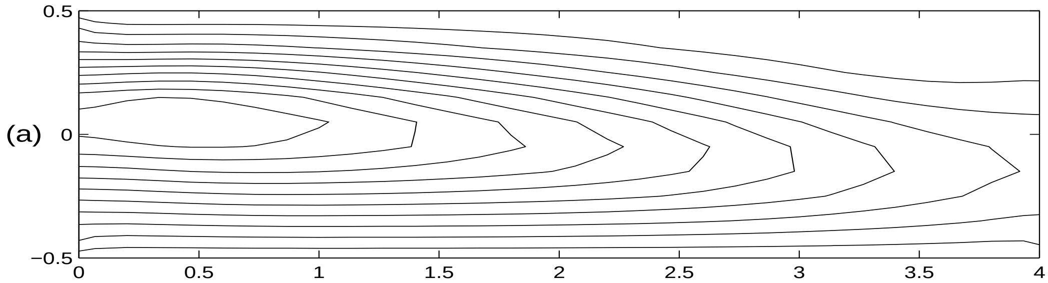

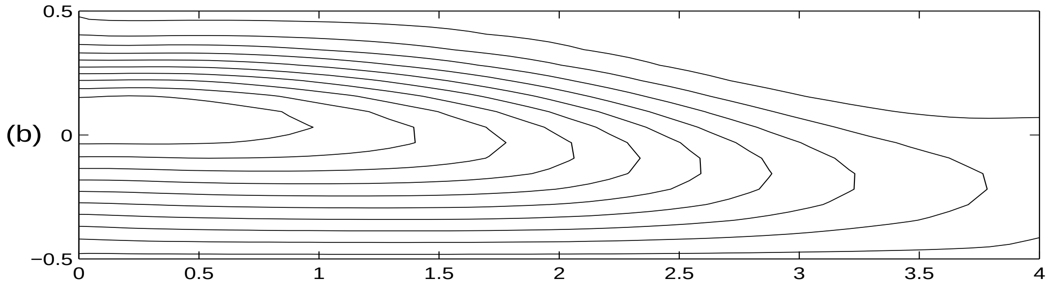

Figure 4.11: (a) b_x contours with N = 80, (b)b_x contours with N = 128 for Ha = 10, Re = 400, Re_m = 1.

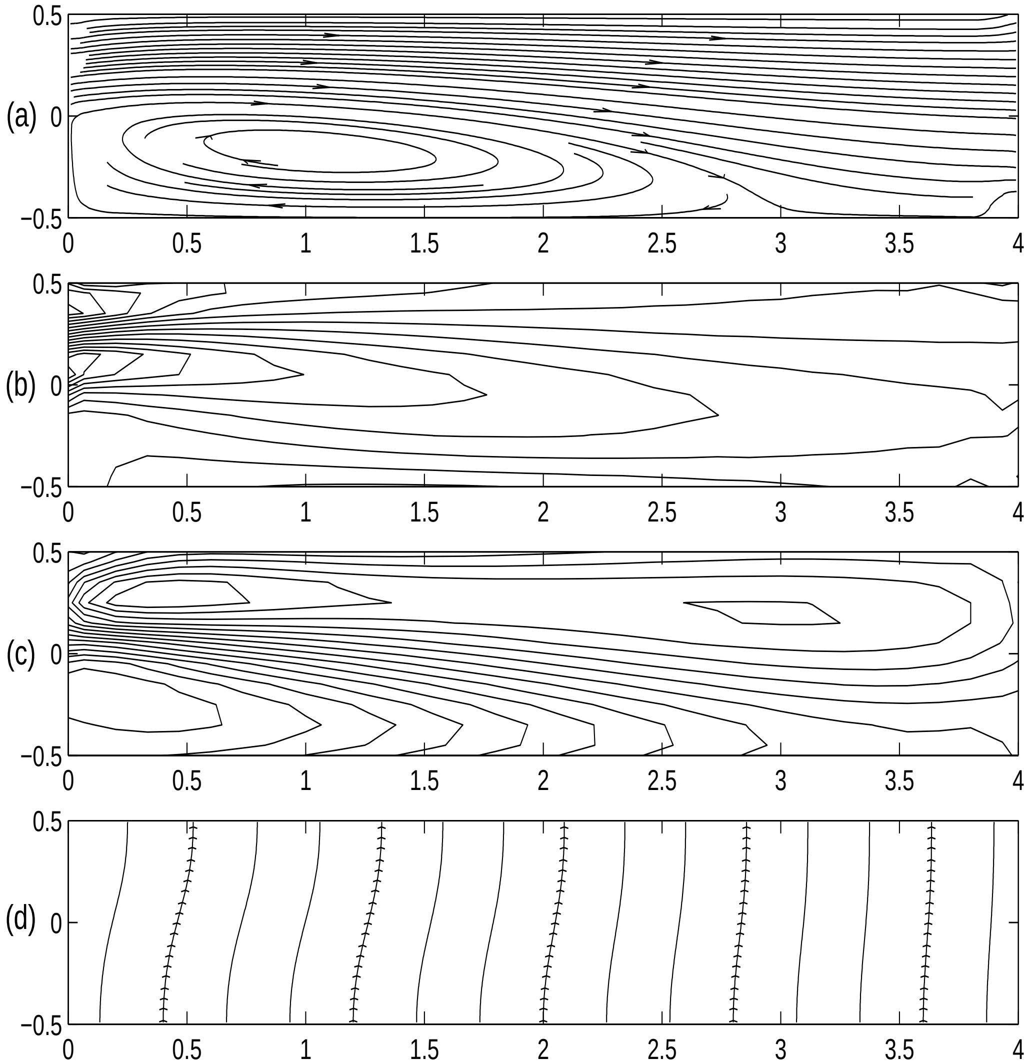

Figure 4.12: (a) Velocity field, (b) vorticity , (c) current density and (d) induced magnetic field for $Ha = 0$ where $Re = 100, Re_m = 1$.

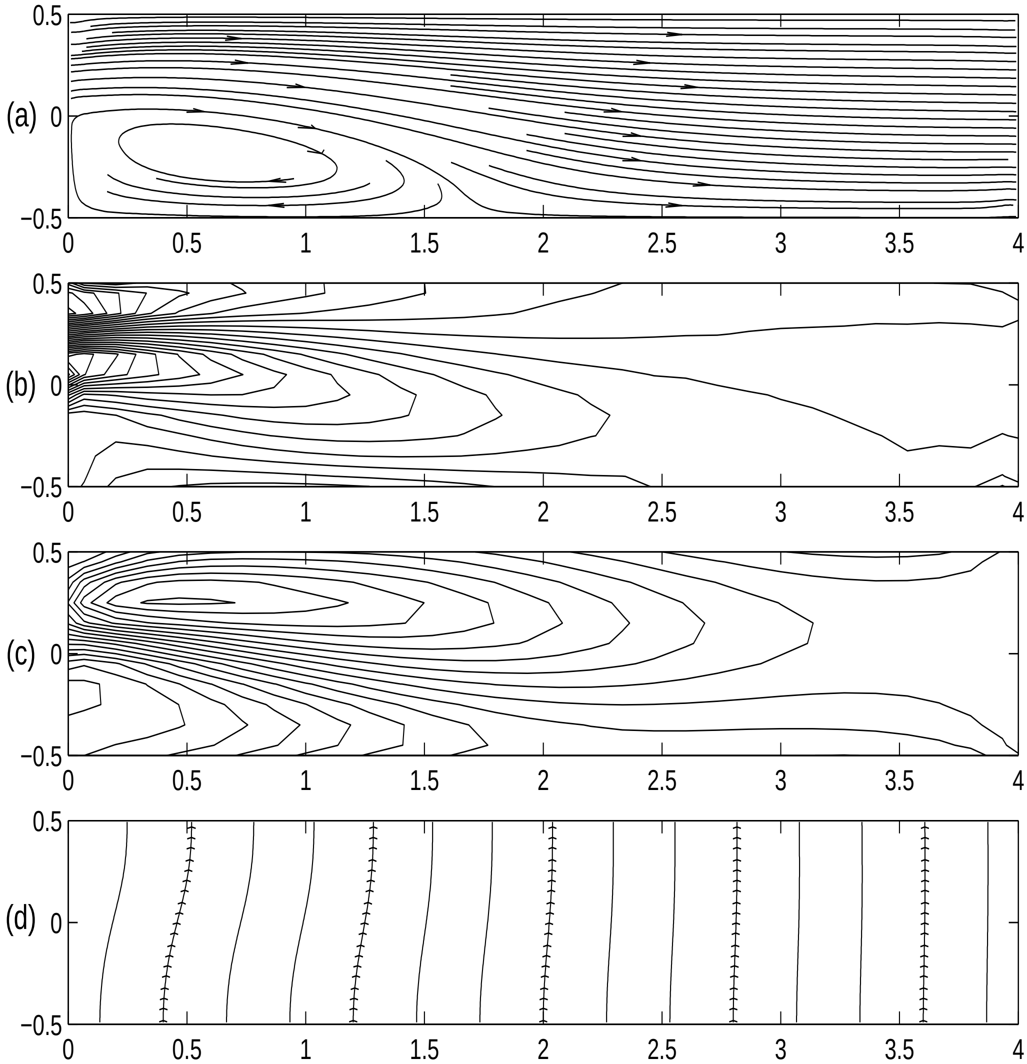

Figure 4.13: (a) Velocity field, (b) vorticity , (c) current density and (d) induced magnetic field for $Ha = 5$ where $Re = 100, Re_m = 1$.

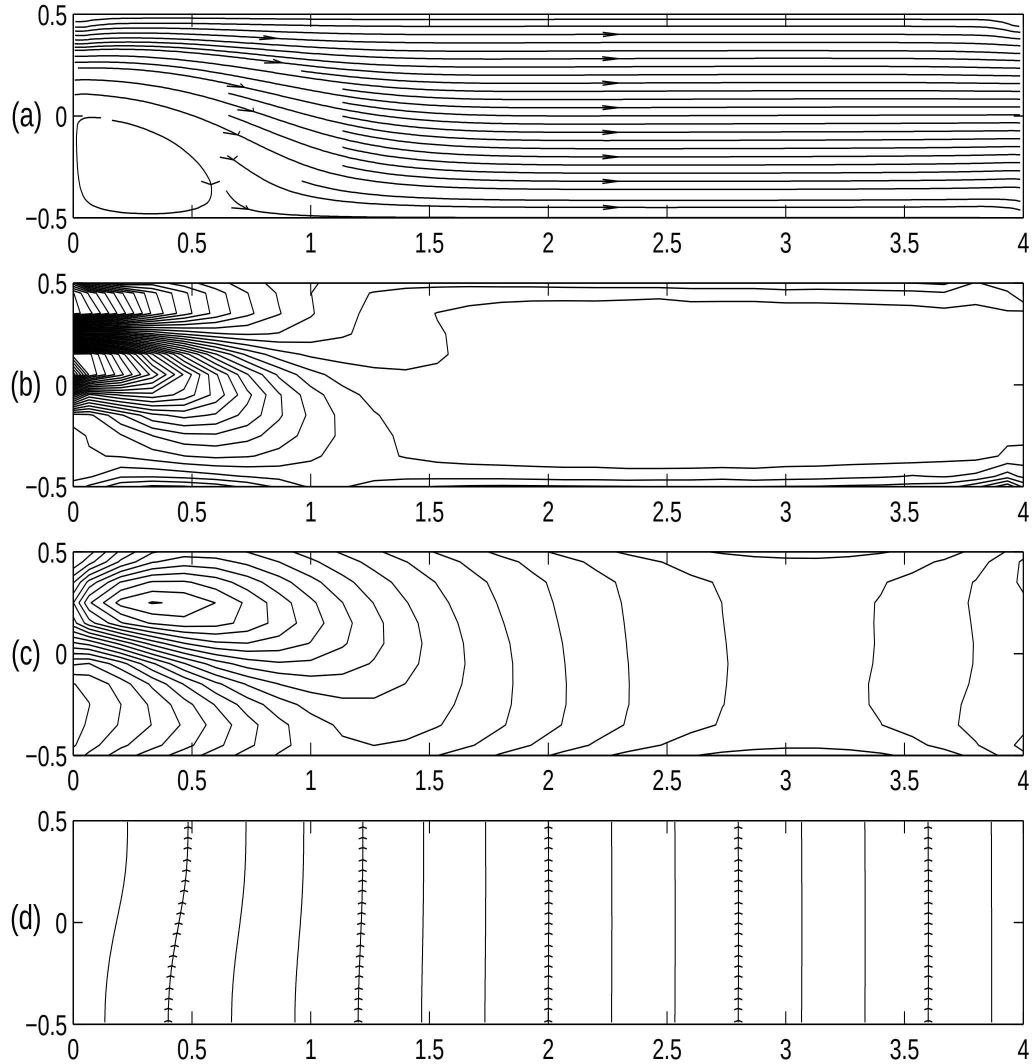

Figure 4.14: (a) Velocity field, (b) vorticity , (c) current density and (d) induced magnetic field for $Ha = 10$ where $Re = 100, Re_m = 1$.

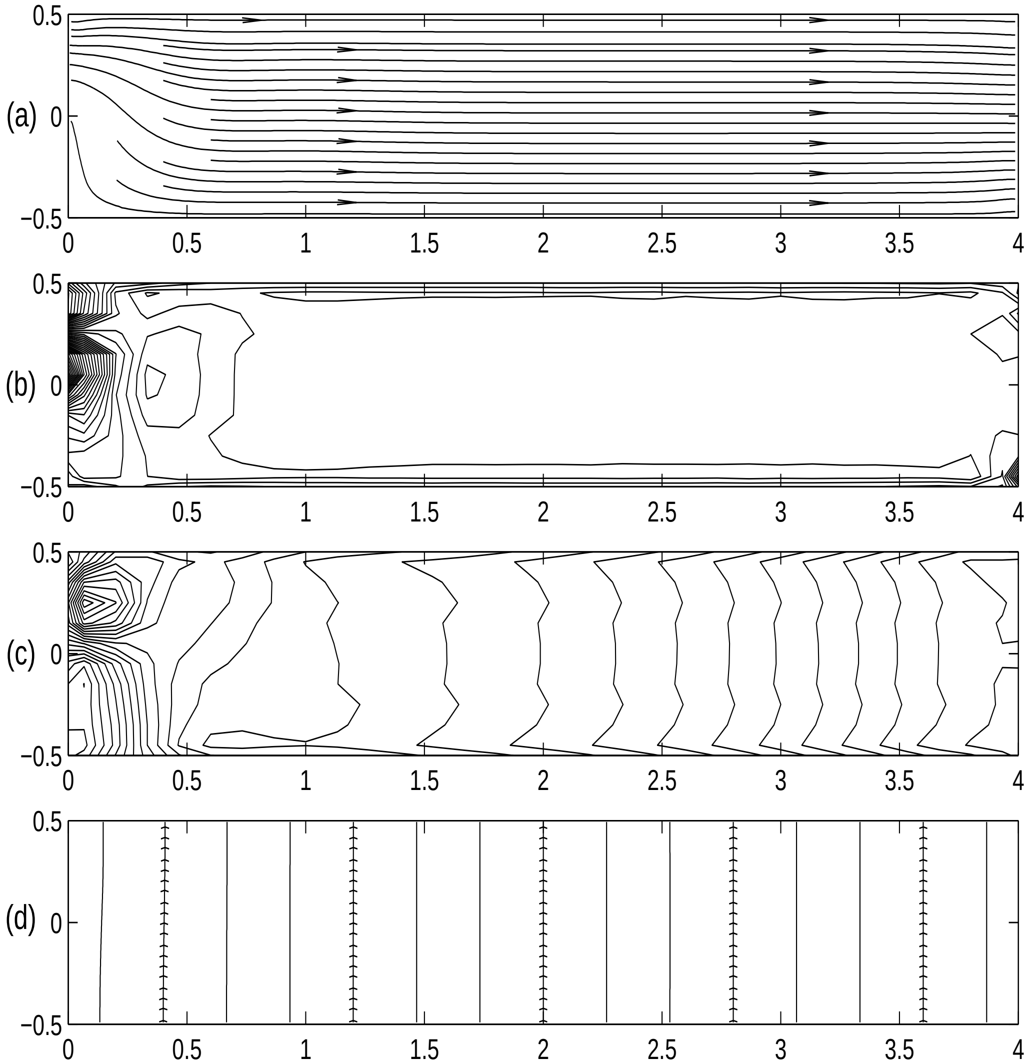

Figure 4.15: (a) Velocity field, (b) vorticity , (c) current density and (d) induced magnetic field for $Ha = 50$ where $Re = 100, Re_m = 1$.

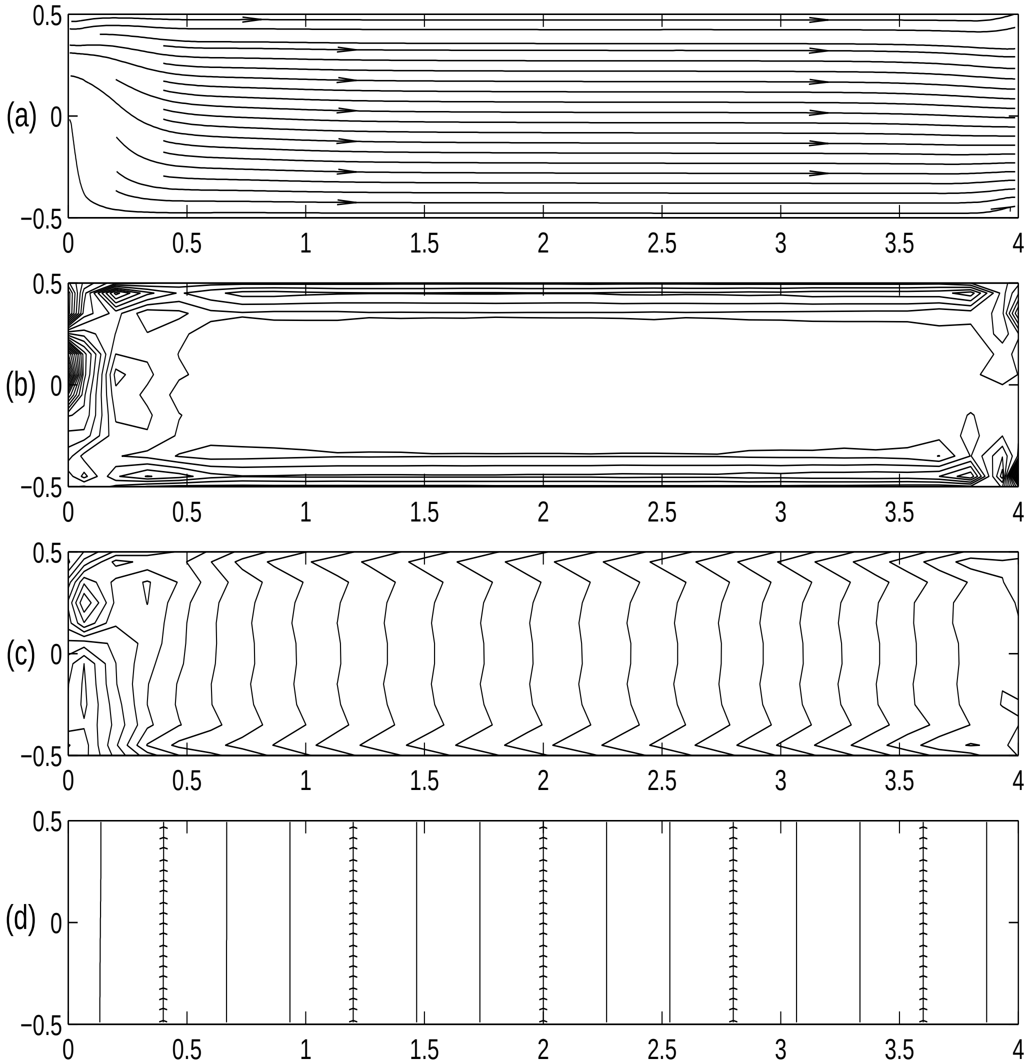

Figure 4.16: (a) Velocity field, (b) vorticity , (c) current density and (d) induced magnetic field for $Ha = 100$ where $Re = 100, Re_m = 1$.

CHAPTER 5

CONCLUSION

The main purpose of this thesis is to present the use of boundary element method as a satisfactory numerical approach for solving the boundary value problems governed by transient partial differential equations. The BEM is implemented in two categories as considering the fundamental solutions depending on time and space, and space variables only. The first approach is the time-domain BEM whereas the second one uses fundamental solution of Laplace equation considering all the other terms as inhomogeneity (DRBEM).

Chapter 2 contains the numerical solutions of diffusion, convection-diffusion and scalar wave equations by using the boundary element method with time-dependent fundamental solutions. The above mentioned equations are directly weighted by their fundamental solutions depending on time. The BEM discretization of each equation gives a square linear system of algebraic equations for obtaining the solution either on the boundary or interior nodes. Differing from other BEM applications with the fundamental solutions depending on the space variables only, the size of the final system is larger due to the discretization of both boundary and time intervals. But, the solutions are obtained at the required space points and time levels directly without the need of another numerical scheme for the time derivative discretizations. This solution procedure allow us to use large time increments due to the use of time-dependent fundamental solutions. Therefore, the error propagation by using another time integration scheme is eliminated and the stability problems are overcome to some extent. Constant element variations are assumed for the unknowns on both the boundary elements and time intervals. This way, the complexity of computations are kept as small as possible.

In Chapter 3, the time-domain BEM approach is presented for the nonlinear system of partial differential equations and the magnetohydrodynamic flow equations. The numerical technique is basically the same as constructed in Chapter 2, that is the time-dependent fundamental solution is used as a weighting function in order to obtain integral equations arising in boundary element methods. However, the treatment of the time integrals of boundary integral equations are different than the procedure used in Chapter 2. In this chapter we consider the BEM equation at each time interval separately, thus, time iteration has been built up and we take the advantage of using newly obtained solution values for the next time blocks as initials. Chapter 3 can also be considered in two parts; application to the nonlinear reaction-diffusion problems when the nonlinearity is of added type, and application to the MHD duct flow problems. The part dealing with the solution of the system of nonlinear reaction-diffusion equations displays the feasibility of the method to the nonlinear case, and also to more general regions. The proposed numerical scheme is employed to a single reaction-diffusion equation in a square. Then, applications are given for systems of nonlinear reaction-diffusion equations in circular and square regions where the latter one is the Brusselator system. The nonlinear terms are linearized during the iteration process assuming the previously obtained values as initials for the next steps. Since, the time-domain BEM is based on using the existing time-dependent fundamental solution which addresses to the whole equation, the procedure still enables one to use very small number of boundary elements, and quite large time intervals in time iterations compared to other numerical schemes. The emphasis is given on the solution of magnetohydrodynamic (MHD) duct flow problems in the second part of Chapter 3. The time-domain BEM solution procedure is tested on some convection-diffusion problems and the MHD duct flow problem with insulated walls to establish the validity of the approach. The numerical results for these sample problems compare very well with the analytical results. Then the time-domain BEM formulation of MHD duct flow problem with arbitrary wall conductivity is obtained for the first time in this thesis in such a way that the equations are solved together with the coupled boundary conditions. The use of time-dependent fundamental solution enables us to obtain numerical solutions for this problem for Hartmann number values up to 300, and for several values of wall conductivity parameter. Thus, Chapter 3 contains two of the main contributions made in the thesis.

Finally, a dual reciprocity boundary element method formulation coupled with an implicit backward difference time integration scheme is presented for solving the unsteady, laminar, viscous, incompressible fluid flow, and full magnetohydrodynamic flow equations. MHD equations here also contains induced magnetic field and electric current density as unknowns. The common nature in Navier-Stokes equations and full MHD equations is the presence of nonlinear convection terms. Also, the absence of vorticity and current density boundary values brings the difficulty in the application of BEM. Thus, the DRBEM is more suitable for treating all these nonlinear terms as inhomogeneity in the equations and solving the equations iteratively. The DRBEM makes also possible to obtain missing boundary conditions for vorticity and current density by using coordinate matrix which is the main part in the formulation. DRBEM has the advantage of using much simpler fundamental solution of Laplace equation which is easy to implement, and results in boundary integrals only. The MHD equations are the coupled system of Navier-Stokes equations and Maxwell's equations of electromagnetics through Ohm's law. We are mainly concerned with a stream function-vorticity-magnetic induction-current density formulation of the full MHD equations in two-dimensions. The stream function and magnetic induction equations which are poisson-type, are solved by using DRBEM with the fundamental solution of Laplace equation. In the DRBEM solution of the time-dependent vorticity and current density equations all the terms apart from the Laplace term are treated as nonhomogeneities. Thus, the matrix-vector forms for all equations contain standard DRBEM matrices of which are computed once and used in all the iterative process invariably. In the resulting initial value problems for the unsteady vorticity and current density equations, the time derivative terms are approximated by an implicit backward difference scheme known as Gear's scheme while the convective terms are approximated by radial basis functions used in DRBEM. The implicit Gear's scheme is an unconditionally stable finite difference approach. Thus, the necessity of small time increments is eliminated. The validity of the technique is demonstrated by first solving the Navier-Stokes equations in a square cavity of which characteristics are very well known. Then, applications are given for the full MHD flow equations, in a square cavity and in a backward-facing step. The numerical results for the square cavity problem in the presence of a magnetic field are visualized for several values of Reynolds, Hartmann and magnetic Reynolds numbers. The effect of each parameter is analyzed through stream function, vorticity, current density and magnetic induction behaviours in terms of contour values. Then, we provide the solution of the step flow problem for the velocity field, vorticity, current density and magnetic field for increasing values of Hartmann number. The solution of full MHD flow equations by using DRBEM is another original contribution obtained in the thesis.

For further studies, it can be considered to extend both the time-domain BEM and DRBEM for solving fourth order biharmonic equations. In time-domain applications the corresponding time-dependent fundamental solution has to be derived, and then applications can be given for solving Navier-Stokes equations in terms of fourth order stream function equation. For DRBEM applications, the fundamental solution of biharmonic operator is already known but the boundary-only formulation has to be obtained. This way, most of the elasticity problems which are governed by fourth order differential equations are able to be treated by boundary element schemes.

REFERENCES

[1] Su, X. and Yuan, X. *Implicit solution of time spectral method for periodic unsteady flows*, Int. J. Numer. Meth. Fluids, **63(7)**, 860-876, (2010).

[2] Makinde, O.D. and Chinyoka, T. *Numerical investigation of transient heat transfer to hydromagnetic channel flow with radiative heat and convective cooling*, Commun. Nonlinear Sci. Numer. Simul. **15**, 3919-3930, (2010).

[3] Boppana, V.B.L. and Gajjar, J.S.B. *Global flow instability in a lid-driven cavity*, Int. J. Numer. Meth. Fluids, **62(8)**, 827-853, (2010).

[4] Shang, Y. *New stabilized finite element method for time-dependent incompressible flow problems*, Int. J. Numer. Meth. Fluids, **62(2)**, 166-187, (2010).

[5] Chen, Z., Steeb, H. and Diebels, S. *A time-discontinuous Galerkin method for the dynamical analysis of porous media*, Int. J. Numer. Meth. Fluids, **30(11)**, 1113-1134, (2006).

[6] Cehlin, M. and Moshfegh, B. *Numerical modeling of a complex diffuser in a room with displacement ventilation*, Building and Environment, **45**, 2240-2252, (2010).

[7] Afsar, A.M. and Go, J. *Finite element analysis of thermoelastic field in a rotating FGM circular disk*, Appl. Math. Modell., **34**, 3309-3320, (2010).

[8] Tezduyar, E. and Sathe, S. *Modelling of fluid-structure interactions with the space-time finite elements: Solution techniques*, Int. J. Numer. Meth. Fluids, **54(6)**, 855-900, (2007).

[9] Zhu S., Demokritou, P. and Spengler, J. *Experimental and numerical investigation of micro-environmental conditions in public transportation buses*, Building and Environment, **45**, 2077-2088, (2010).

[10] Carré, G., Lanteri, L. and Loriot, M. *High performance simulations of compressible flows inside car engine geometries using the N3S-NATUR parallel solver*, Parallel Computing, **25(12)**, 1435-1458, (1999).

[11] Xue, J. *Anon-linear finite-element analysis of buckle propagation in subsea corroded pipelines*, Finite Elem. Anal. Des., **42**, 1211-1219, (2006).

[12] Toscano, R.G., Mantovano, L.O., Amenta, P.M., Charreau, R.F., Johnson, D.H., Assanelli, A.P. and Dvorkin, E.N. *Collapse arrestors for deepwater pipelines. Cross-over mechanisms*, Comput. Struct., **86**, 728-743, (2008).

[13] Brebbia, C.A., Telles, J.C.F. and Wrobel, L.C. *Boundary Element Techniques: Theory and Applications in engineering*, Springer Werlag, Berlin, (1984).

[14] Brebbia, C.A. *The Boundary Element Method for Engineers*, Pentech Press, London, (1978).

[15] Jaswon M.A., and Symm, G.T. *Integral equation methods in potential theory and elastostatics*, Academic Press, London, (1977).

[16] Cruse, T.A. and Rizzo, F.J. *A direct formulation and numerical solution of the general transient elastodynamic problem. I*, J. Math. Analysis Applic. , **22**, 244-259, (1968).

[17] Lachat, J.C. and Watson, J.O. *Effective numerical treatment of boundary integral equations: A formulation for three-dimensional elastostatics*, Int. J. Numer. Meth. Eng., **10**, 991-1005, (1976).

[18] Banerjee, P.K. and Butterfield, R. *Boundary element methods in engineering science*, McGraw-Hill, London, (1981).

[19] Banerjee, P.K. and Watson, J.O. *Developments in boundary element methods*, Elsevier Applied Science, London, (1985).

[20] Brebbia, C.A. and Dominguez, J. *Boundary Elements*, Computational Mechanics, Southampton, Boston, (1989).

[21] Kythe, P.K. *Fundamental solutions for differential operators and applications*, The Maple Press Company, York, USA, (1996).

[22] Pozrikidis, C. *A Practical Guide to Boundary Element Methods with Software Library BEMLIB*, Chapman and Hall/CRC, (2002).

[23] Gaul, L., Kögl, M. and Wagner, M. *Boundary Element Methods for Engineers and Scientists*, Springer Verlag, Berlin, Heidelberg, (2003).

[24] Brebbia, C.A., Partridge, P.W. and Wrobel, L.C. *The Dual Reciprocity Boundary Element Method*, Computational Mechanics Publications, Southampton Boston, (1992).

[25] Tezer-Sezgin, M. and Bozkaya, C. *The boundary element solution of magnetohydrodynamic flow in an infinite region*, J. Comput. Appl. Math., **225**, 510-521, (2009).

[26] Meral, G. and Tezer-Sezgin, M. *DRBEM solution of exterior nonlinear wave problem using FDM and LSM time integrations*, Eng. Anal. Boundary Elem., **34**, 574-580, (2010).

[27] Halperin, I. *Introduction to the theory of distributions*, University of Toronto Press, Canada, (1952).

[28] Rizzo, F.J. and Shippy, D.J. *A method of solution of certain problems of transient heat conduction*, AIAA J., **8**, 2004-2009, (1970).

[29] Singh, K.M. and Kalra, M.S. *Time integration in the dual reciprocity boundary element analysis of transient diffusion*, Eng. Anal. Boundary Elem., **18**, 73-102, (1996).

[30] Tanaka, M. and Chen, W. *Coupling dual reciprocity BEM and differential quadrature method for time-dependent diffusion problems*, Appl. Math. Modell., **25**, 257-268, (2001).

[31] Tanaka, M. and Chen, W. *Dual reciprocity BEM applied to transient elastodynamic problems with differential quadrature method in time*, Comput. Meth. Appl. Mech. Eng., **190**, 2331-2347, (2001).

[32] Chang, Y.P., Kang, C.S., and Chen, D.J. *The use of fundamental Green's functions for the solution of problems of heat conduction in anisotropic media*, Int. J. Heat Mass Transfer, **16**, 1905-1908, (1973).

[33] Shaw, R.P. *An integral equation approach to diffusion*, Int. J. Heat Mass Transfer, **17**, 693-699, (1974).

[34] Qiao, H. *Transient mold cooling analysis using BEM with the time-dependent fundamental solution*, Int. Commun. Heat Mass Transfer, **32**, 315-322, (2005).

[35] Carslaw, H.S. and Jaeger, J.C. *Conduction of Heat in Solids*, 2nd Ed., Clarendon Press, Oxford, (1959).

[36] Grigoriev, M.M. and Dargush, G.F. *Boundary element methods for transient convective diffusion. Part II: 2D implementation*, Comput. Meth. Appl. Mech. Eng., **192**, 4299-4312, (2003).

[37] Grigoriev, M.M. and Dargush, G.F. *Boundary element methods for transient convective diffusion. Part III: Numerical examples*. Comput. Meth. Appl. Mech. Eng., **192**, 4313-4335, (2003).

[38] Grigoriev, M.M. and Dargush, G.F. *Efficiency of boundary element methods for time-dependent convective heat diffusion at high Peclet numbers.* Commun. Numer. Meth. Eng., **21**, 149-161, (2005).

[39] DeSilva, S.J., Chan, C.L., Chandra, A. and Lim, J. *Boundary element method analysis for the transient conduction-convection in 2-D with spatially variable convective velocity*, Appl. Math. Modell., **22**, 81-112, (1998).

[40] Bozkaya, N. and Tezer-Sezgin, M. *Time-domain BEM solution of convection-diffusion type MHD equations*, Int. J. Numer. Meth. Fluids, **56**, 1969-1991, (2008).

[41] Nardini, D. and Brebbia, C.A. *A new approach to free vibration analysis using boundary elements*, Appl. Math. Modell., **7**, 157-162, (1983).

[42] Mansur, W.J. and Brebbia, C.A. *Further development on the solution of the transient scalar wave equation*, In Topics in Boundary Element Research, Brebbia CA (ed.), Springer, **2**, 87-123. (1985).

[43] Loeffler, C.F. and Mansur, W.J. *Analysis of time integration schemes for boundary element applications to transient wave propagation problems*, In BETECH' 87, Computational Mechanics Publication, Southampton, (1987).

[44] Friedman, M.B. and Shaw, R.P. *Diffraction of pulses by cylindrical obstacles of arbitrary cross section*, ASME Journal of Applied Mechanics, **29**, 40-46, (1962).

[45] Carrer, J.A.M. and Mansur, W.J. *Time-domain BEM analysis for the 2D scalar wave equation: initial conditions contributions to space and time derivatives*, Int. J. Numer. Meth. Eng., **39**, 2169-2188, (1996).

[46] Benmansour, N., Ouazar, D. and Wrobel, L.C. *Numerical simulation of shallow water wave propagation using a boundary element wave equation model*, Int. J. Numer. Meth. Fluids, **24**, 1-15, (1997).

[47] Mansur, W.J., Carrer, J.A.M. and Siqueira, E.F.N. *Time discontinuous linear traction approximation in time-domain BEM scalar wave propagation analysis*, Int. J. Numer. Meth. Eng., **42**, 667-683, (1998).

[48] Telles, J.C.F., Carrer, J.A.M. and Mansur, W.J. *Transient dynamic elastoplastic analysis by the time-domain BEM formulation*, Eng. Anal. Boundary Elem., **23**, 479-486, (1999).

[49] Carrer, J.A.M. and Mansur, W.J. *Time-dependent fundamental solution generated by a not impulsive source in the boundary element method analysis of the 2D scalar wave equation*, Commun. Numer. Meth. Eng., **18**, 277-285, (2002).

[50] Yu, G., Mansur, W.J., Carrer, J.A.M. and Gong, L. *Time weighting in time domain BEM*, Eng. Anal. Boundary Elem., **22**, 175-181, (1998).

[51] Rizos, D.C. and Zhou, S. *An advanced direct time domain BEM for 3-D wave propagation in acoustic media*, J. Sound Vib., **293**, 196-212, (2006).

[52] Nowak, A.J. and Neves, A.C. *The multiple reciprocity boundary element method*, Computational Mechanics Publications , Southampton, Boston, (1994).

[53] Adomian, G. *Solving frontier problems modelled by nonlinear partial differential equations*, Comput. Math. Appl., **22(8)**, 91-94, (1991).

[54] Wazwaz, A.M. *A reliable modification of Adomian's decomposition method*, Appl. Math. Comput., **102**, 77-86, (1999).

[55] Wazwaz, A.M. *The decomposition method applied to systems of partial differential equations and to the reaction diffusion Brusselator model*, Appl. Math. Comput., **110**, 251-264, 2000.

[56] Twizell, E.H., Gumel, A.B. and Cao, Q. *A second-order scheme for the 'Brusselator' reaction-diffusion system*, J. Math. Chem., **26**, 297-316, (1999).

[57] Liao, W., Zhu, J. and Khaliq, A.Q.M. *Differential quadrature solution of nonlinear reaction-diffusion equation with relaxation type time integration*, Numer. Meth. Part. D. E., **18**, 340-354, (2002).

[58] Ang, W.T. *The two-dimensional reaction-diffusion Brusselator system: a dual-reciprocity boundary element solution*, Eng. Anal. Boundary Elem. **27**, 897-903, (2003).

[59] Meral, G. and Tezer-Sezgin, M. *An efficient high-order algorithm for solving systems of reaction-diffusion equations*, Int. J. Comput. Math., **86**, 451-463, (2009).

[60] Dragoş, L. *Magneto-Fluid dynamics*, Abacus Press, England, (1975).

[61] Shercliff, J.A. *Steady motion of conducting fluids in pipes under transverse fields*, Proc. Camb. Phil. Soc., **49**, 136-144, (1953).

[62] Zhang, L., Ouyang, J. and Zhang, X. *The two-level element free Galerkin method for MHD flow at high Hartmann numbers*, Phys. Lett. A, **372**, 5625-5638, (2008).

[63] Neslitürk, A.İ. and Tezer-Sezgin, M. *The finite element method solution for MHD flow at high Hartmann numbers*, Comput. Meth. Appl. Mech. Eng., **194**, 1201-1224, (2005).

[64] Tezer-Sezgin, M. and Aydın, S.H. *Solution of magnetohydrodynamic flow problems using the boundary element methods*, Eng. Anal. Boundary Elem., **30**, 411-418, (2006).

[65] Bozkaya, C. *Boundary element method solution of initial and boundar value problems in fluid dynamics and magnetohydrodynamics*, Ph.D. Thesis, Middle East Technical Univeristy, (2008).

[66] Singh, B. and Lal, J. *Finite element method for unsteady MHD flow through pipes with arbitrary wall conductivity*, Int. J. Numer. Meth. Fluids, **4**, 291-302, (1984).

[67] Salah, N.B., Soulaimani, A. and Habashi, W.G. *A finite element method for magnetohydrodynamics*, Comput. Meth. Appl. Mech. Eng., **190**, 5867-5892, (2001).

[68] Seungsoo, L. and Dulikravich, G.S. *Magnetohydrodynamic steady flow computation in three dimensions*, Int. J. Numer. Meth. Fluids, **13**, 917-936, (1991).

[69] Sheu, T.W.H. and Lin, R.K. *Development of a convection-diffusion-reaction magnetohydrodynamic solver on nonstaggered grids*, Int. J. Numer. Meth. Fluids, **45**, 1209-1233, (2004).

[70] Bozkaya, C. and Tezer-Sezgin, M. *Boundary element method solution of unsteady magnetohydrodynamic duct flow with differential quadrature time integration scheme*, Int. J. Numer. Meth. Fluids, **51**, 567-584, (2006).

[71] Wrobel, L.C., Brebbia, C.A. and Nardini D. *Analysis of transient thermal problems in Beasy system.* In BETECH 86, (Editors Conor J.J and Breabbia C.A.), Computational Mechanics Publications, Southampton, 269-276, (1986).

[72] Kumamaru, H. Kodama, S. Hirano, H. and Itoh, K. *Three-dimensional numerical calculations on liquid-metal magnetohydrodynamic flow in magnetic-field inlet-region*, J. Nucl. Sci. Technol., **41(5)**, 624-631, (2004).

[73] Kang, K.S. and Keyes, D.E. *Implicit symmetrized stream function formulations of magnetohydrodynamics*, Int. J. Numer. Meth. Fluids, **58**, 1201-1222, (2008).

[74] Navarro, H.A., Cabezas-Gómez, L., Silva, R.C. and Montagnoli, A.N. *A generalized alternating-direction implicit scheme for incompressible magnetohydrodynamic viscous flows at low magnetic Reynolds number*, Appl. Math. Comput., **189**, 1601-1613, (2007).

[75] Lee, D. and Choi, H. *Magnetohydrodynamic turbulent flow in a channel at low magnetic Reynolds number*, J. Fluid Mech., **439**, 367-394, (2001).

[76] Sekhar, T.V.S., Sivakumar, R. and Ravi Kumar T.V.R. *Effect of magnetic Reynolds number on the two-dimensional hydromagnetic flow around a cylinder*, Int. J. Numer. Meth. Fluids, **59**, 1351-1368, (2009).

[77] Kumar, H. and Rajathy, R. *Numerical study of MHD flow past a circular cylinder at low an moderate Reynolds number*, Int. J. Comput. Meth. Eng. Sci. Mech., **7**, 461-473, (2006).

[78] Armero, F. and Simo, J.C. *Long-term dissipativity of time-stepping algorithm for an abstract evolution equation with applications to the incompressible MHD and Navier-Stokes equations*, Comput. Meth. Appl. Mech. Eng., **131**, 41-90 (1996).

[79] Ancona, M.G. *Computational Methods for Applied Science and Engineering: An Interactive Approach*, Rinton Press, Princeton, New Jersey, USA, (2002).

[80] John, F. *Partial Differential Equations*, Springer-Verlag, Berlin, (1978).

[81] Raamachandran, J. *Boundary and Finite Elements*, Narosa Publishing House, New Delhi, India, (2000).

[82] Weinberger, H.F. *Partial Differential Equations with Complex Variables and Transfer Methods*, Blaisdell Publishing Company, London, (1965).

[83] Morse, P.M. and Feshbach, H. *Methods of Theoretical Physics*, Mc-Graw-Hill, Newyork, (1953).

[84] Sneddon, I. *Elements of partial differential equations*, McGraw-Hill, Newyork, (1957).

[85] Chawla, M.M. and Al-Zanaidi, M.A. *An extended trapezoidal formula for the diffusion equation in two space dimensions*, Int. J. Computs. Maths. Appl., **42**, 157-168, (2001).

[86] Adomian, G. *The Diffusion Brusselator equation*, Comput. Math. Appl., **29(5)**, 1-3, (1995).

[87] DeFigueiredo, D.B. *Boundary Element Analysis of Convection Diffusion Problems*, Lecture Notes in Engineering Series, Berlin, Springer, (1991).

[88] Ninomiya, H. and Onishi, K. *Flow Analysis Using a PC*, Computational Mechanics Publications, Southampton, UK, (1991).

[89] Wrobel, L.C., Brebbia, C.A. and Nardini, D. *The Dual Reciprocity Boundary Element Formulation for Transient Heat Conduction*, Springer Verlag, Berlin, (1986).

[90] Chen, S., Tölke, J. and Krafczyk, M. *A new method for the numerical solution of vorticity-streamfunction formulations*, Comput. Meth. Appl. Mech. Eng., **198**, 367-376, (2008).

[91] Louchart, O. and Randriamampianina, A. *A spectral iterative domain decomposition technique for the incompressible Navier-Stokes equations*, Appl. Numer. Math., **33**, 233-240, (2000).

[92] Ramšak, M., Škerget, L., Hriberšek, M. and Žunič, Z. *A multidomain boundary element method for unsteady laminar flow using stream function-vorticity equations*, Int. J. Numer. Meth. Fluids, **29**, 1-14, (2005).

[93] Aydın, S.H., Neslitürk, A.I. and Tezer-Sezgin, M. *Two-level finite element method with a stabilizing subgrid for the incompressible MHD equations*, Int. J. Numer. Meth. Fluids, **62(2)**, 188-210, (2010).

CURRICULUM VITAE

PERSONAL INFORMATION

Surname, Name: Bozkaya, Nuray

Date and Place of Birth: 24 October 1981, Ankara

email: bnuray@metu.edu.tr

EDUCATION

Degree	**Institution**	**Year of Graduation**
MS	METU, Mathematics	2005
BS	Hacettepe University, Mathematics	2003
High School	Konya Atatürk Girl High School	1999

FOREIGN INSTITUTE EXPERIENCE

Institution	**Year**
Wessex Institute of Technology Southampton, UK	2007-2008

AWARDS

- **The Scientific and Technical Research Council of Turkey (TUBITAK)**
  - The Integrated Ph.D. Scholarship, 2005-2007
  - Scholarship for Master of Science, 2003-2005

WORK EXPERIENCE

Year	Place	Enrollment
2005-present	METU, Mathematics Department	Research Assistant

FOREIGN LANGUAGES

English (fluent)

PUBLICATIONS

1. N. Bozkaya, M.Tezer- Sezgin, *Time-Domain BEM Solution of Convection-diffusion-type MHD equations*, International Journal for Numerical Methods in Fluids, **56** (2008), 1969-1991.
2. N. Bozkaya, M.Tezer- Sezgin, *The time-domain BEM solution of non-linear Reaction-diffusion Equations*, (revised version is submitted to the International Journal of Computer Mathematics).
3. N. Bozkaya, M. Tezer-Sezgin, *The DRBEM Solution of Incompressible MHD Flow Equations*, (submitted to the International Journal for Numerical Methods in Fluids, revision received).

CONFERENCE PAPERS

1. N. Bozkaya, M. Tezer-Sezgin, *The DRBEM Solution of Incompressible MHD Flow Equations*, CFDSC 2009 (Computational Fluid Dynamics Society of Canada) Conference, May 2009, Ottawa, Canada.

CONFERENCE PRESENTATIONS

1. N. Bozkaya, *The boundary element method solutions of diffusion, scalar wave and convection-diffusion equations using time-dependent fundamental*

solutions, in: Book of Extended Abstracts of IABEM (International Association for Boundary Element Methods Conference) 2006, July 2006, Graz, Austuria, pp. 87-90.

2. N. Bozkaya, *The BEM Solution of Navier-Stokes Equations using time-dependent fundamental solution*, in: Book of Abstracts of NA07, 22nd Biennial Conference on Numerical Analysis, June 2007, University of Dundee, Scothland, UK, pp. 14.

3. N. Bozkaya, M. Tezer-Sezgin, *The time-domain BEM solution of non-linear Reaction-diffusion Equations*, ENUMATH 2009 (European Conference on Numerical Mathematics and Advanced Applications) Conference, July 2009, Uppsala, Sweden.

PARTICIPATION OF NATIONAL CONFERENCES

1. N. Bozkaya, *The boundary element method solutions of diffusion and scalar wave equations using time-dependent fundamental solutions*, Workshop on Numerical Methods for Differential Equations, May 2006, İzmir, Turkey.

2. ADES, The Workshop on Differential Equations, Yeditepe University, June 2008, İstanbul, Turkey.

CITATIONS: 2 (Paper 1 in publication list.)